Parthenolide in the treatment and prevention of prostate cancer

This thesis is submitted in fulfilment of the requirements of:

Doctor of Philosophy

Katherine Morel, B. Med. Sci., B. Sci. (Hons)

March 2017

Molecular Medicine and Pathology, School of Medicine,

Flinders Centre for Innovation in Cancer,

Flinders University

Contents

Figures

Tables

Declaration

I certify that this thesis does not incorporate without acknowledgement any material previously submitted for a degree or diploma in any university; and that to the best of my knowledge and belief it does not contain any material previously published or written by another person except where due reference is made in the text.

Katherine Morel

Acknowledgements

First and foremost I would like to sincerely thank Professor Pam Sykes for her guidance and support throughout my PhD. Over the course of my PhD studies Pam has taken great care in my scientific professional development, whether it be allowing me to attend international conferences, pushing me to present at student research events or giving me the opportunity to serve on university committees. Thank you for noticing my potential, giving me to opportunity to become a part of your laboratory and encouraging me to undertake a PhD in the first place. I also extend thanks to my co-supervisors Dr Rebecca Ormsby and Associate Professor Sonja Klebe for their guidance and helpful perspectives on this thesis.

The work of this thesis would be impossible without the kind and expert assistance of Professor Eva Bezak at the University of South Australia who helped to calculate dosimetry for the in vivo radiation experiments and gave up several Saturday morning sleep ins to perform animal irradiations.

Sincere thanks go to all past and present members of the laboratory (Dr Mark Lawrence, Dr Michelle Newman, Dr Linh Tran, Emma Solly, Kaylisha Suada, Soonlee Lor and Jeffrey Mak) who have assisted in various aspects of this work.

The ex vivo prostate tumour studies were conducted in collaboration with Associate Professor Lisa Butler and Dr Maggie Centenera at the South Australian Health and Medical Research Institute. Particular thanks go to Swati Irani for doing all the hands-on work involved in these studies.

I would also like to thank the Flinders Foundation and Smiling for Smiddy for providing my PhD scholarship, this work would not have been possible without their generous support. Thanks also go to Associate Professor Chris Sweeney at the Dana Farber Cancer Institute, who has not only supported this research but also supported and encouraged me as an early career researcher.

Personally, I would like to thank my parents, brothers and sister, extended family and friends for all their help, support, love and encouragement that they have provided me not only during my PhD candidature, but my entire life. Particular thanks go to Dad for his ability to make me smile with his unyielding love of the glockenspiel.

Finally, but most importantly, thank you to Stephen. Thank you for your willingness to share me with my PhD during our first years of marriage and for your unwavering love and support and your constant belief in me. This thesis and the clinical outcomes that might come from it are dedicated to you.

Abbreviations

APES	aminopropyltriethoxysilane
AR	androgen receptor
bp	base pair
BCL-2	B-cell lymphoma 2
DAPI	4',6-diamidino-2-phenylindole
DMAPT	dimethylaminoparthenolide
DNA	deoxyribonucleic acid
dNTP	deoxynucleotide triphosphate
dUTP	deoxyuridine triphosphate
EBRT	external beam radiotherapy
ECM	extracellular matrix
EDTA	ethylenediaminetetraacetic acid
EMT	epithelial-to-mesenchymal transition
GUT	genitourinary tract
Ig	immunoglobulin
IGRT	image-guided radiation therapy
IκB	nuclear factor kappa-light-chain-enhancer of activated B cells inhibitor
IKKβ	IκB kinase beta
IMRT	intensity-modulated radiation therapy
IP	intraperitoneal
IV	intravenous
JAK	Janus kinase
MET	mesenchymal-to-epithelial transition
MMP	Matrix metalloproteinase
MnSOD	manganese superoxide dismutase
NF-κβ	nuclear factor kappa-light-chain-enhancer of activated B cells
OCT	optimal cutting temperature

PB	probasin
PBS	phosphate buffered saline
PBST	phosphate buffered saline Tween-20
PCR	polymerase chain reaction
PIN	prostatic intraepithelial neoplasia
pRb	retinoblastoma protein
PSA	prostate-specific antigen
PTEN	phosphatase and tensin homolog
PTL	parthenolide
ROS	reactive oxygen species
SC	subcutaneous
SD	standard deviation
STAT	signal transducer and activator of transcription
SV40	Simian vacuolating virus-40 (or Simian Virus-40)
tAg	small T-antigen
TAg	large T-antigen
Taq	*Thermus aquaticus*
Tdt	terminal deoxynucleotidyl transferase
TRAMP	Transgenic Adenocarcinoma of the Mouse Prostate
TUNEL	terminal deoxynucleotidyl transferase-mediated dUTP nick-end labelling
3DCRT	three-dimensional conformal radiotherapy

Standard international units of measure

°C	degrees Celsius
g	gram
Gy	gray
h	hour
L	litre
m	metre
M	molar
min	minute
s	second

Indicators of magnitude

k	kilo ($\times 10^{3}$)
m	milli ($\times 10^{-3}$)
µ	micro ($\times 10^{-6}$)

Summary

Prostate cancer is the most commonly diagnosed cancer in Australian men. While significant improvements have been made in prostate therapy, there is still a need for novel treatment options, particularly for preventing and treating metastatic prostate cancer which has a very poor prognosis, and for protecting from debilitating side effects of radiotherapy, where many men suffer side effects due to damage done to healthy tissues near the prostate.

Parthenolide is a naturally occurring sesquiterpene lactone derived from the plant feverfew (*Tanacetum parthenium*) with anti-inflammatory and anti-cancer properties through pro-apoptotic action, stimulation of reactive oxygen species, inhibition of NF-κB and its downstream targets as well as many key proteins important for metastasis. *In vitro* and xenograft studies indicate that parthenolide holds promise as an anti-cancer agent and a differential radiosensitiser for prostate cancer. This thesis describes the first examination of the anti-cancer effects of parthenolide (PTL) and dimethylaminoparthenolide (DMAPT), a parthenolide analogue with increased water solubility, in an autochthonous model of prostate cancer (TRAMP, Transgenic Adenocarcinoma of the Mouse Prostate).

Treatment of TRAMP mice with DMAPT (100 mg/kg) 3 times per week significantly increased time-to-palpable tumour development by 20% and reduced metastatic spread to the lung by 95%, compared to mice treated with a water vehicle. PTL (40 mg/kg), delivered in a 10% ethanol/saline vehicle, did not slow tumour development. Unexpectedly, the ethanol/saline vehicle induced an

aggressive metastatic phenotype in the TRAMP model, in which mice developed large palpable metastatic tumours and small slow-growing primary prostate tumours. This tumour phenotype was counteracted by parthenolide (in ethanol/saline vehicle). The chronic low dose of ethanol increased expression of molecules involved in metastatic spread, MMP2, integrin β1, laminin, fibronectin and collagen IV in primary prostate tumours, all of which were reduced to baseline levels by parthenolide.

When TRAMP and C57BL/6J mice were treated with DMAPT (100 mg/kg) or PTL (40 mg/kg) prior to 6 Gy whole body X-radiation, the level of radiation-induced apoptosis observed *in vivo* was significantly reduced in normal prostate, spleen and colorectal tissue by up to 72%. Pre-treatment with DMAPT doubled the efficacy of prostate tumour cell killing. DMAPT preferentially radiosensitised regions of high grade prostatic intraepithelial neoplasia within TRAMP prostate tissues, suggesting that DMAPT may be particularly able to target regions of higher oxidative stress, as is often observed in high grade metastatic prostate cancers. When DMAPT was combined with a low conditioning dose of radiation there was evidence that this combination might be able to augment the radioprotective effects of DMAPT alone in normal tissues.

The results in this thesis provide strong evidence for DMAPT as an anti-cancer and anti-metastatic agent, as well as a differential radiosensitiser in prostate cancer. This work provides the groundwork for future clinical trials to apply DMAPT for improving cure rates and also protecting from unwanted debilitating side-effects from prostate cancer radiotherapy. The mechanisms involved in the

anti-cancer and radioprotective effects of parthenolide are not specific to prostate cancer and therefore there is the potential for its use in the treatment of other cancer types as well.

Publications and presentations arising during candidature

Publications

KL Morel, RJ Ormsby, E Bezak, CJ Sweeney, PJ Sykes, 2017, ***Parthenolide sensitises prostate tumour tissue to radiotherapy while protecting healthy tissues in vivo***, Radiation Research, vol. 187, no. 5, pp. 501-512. (Appendix E).

Published abstracts

KL Morel, RJ Ormsby, E Bezak, WD Tilley, MD Lawrence, PJ Sykes, 2013, Parthenolide as a selective radiosensitiser in the treatment and prevention of prostate cancer, BJU International 112, p. 45.

Oral presentations

KL Morel, RJ Ormsby, E Bezak, CJ Sweeney, PJ Sykes, ***Parthenolide protects healthy tissues while sensitising prostate tumours to radiotherapy in vivo***, Australasian Radioprotection Society Annual Meeting, Adelaide Convention Centre, Adelaide, South Australia, Australia, September 11th-14th 2016.

KL Morel, RJ Ormsby, E Bezak, CJ Sweeney, PJ Sykes, ***Utilising parthenolide to protect healthy tissues while sensitising prostate tumours to radiotherapy***, SA Australian Science and Medical Research Annual Meeting, Adelaide Convention Centre, Adelaide, South Australia, Australia, June 8th 2016.

KL Morel, RJ Ormsby, E Bezak, WD Tilley, CJ Sweeney, PJ Sykes, ***The dual role of parthenolide: protecting healthy tissues while sensitising prostate tumours to radiotherapy***, 14th International Workshop on Radiation Damage to DNA, Victorian Treasury Theatre, Melbourne, Victoria, Australia, March 20th-24th 2016.

Poster presentations

KL Morel, CJ Sweeney, N Cordes, PJ Sykes, ***The role of extracellular matrix signalling in the anti-metastatic mechanism of parthenolide***, 7th Barossa Meeting for Cell Signalling in Cancer Biology and Therapy, Novotel Barossa, Rowland Flat, South Australia, Australia, November 18th-21st 2015.

KL Morel, RJ Ormsby, E Bezak, WD Tilley, CJ Sweeney, PJ Sykes, ***The Yin and Yang of parthenolide: protecting healthy tissues while sensitising prostate tumours to Radiotherapy***, Radiation Research Society Meeting, Bonaventure Resort, Weston, Florida, US, September 19th-21st 2015.

KL Morel, RJ Ormsby, E Bezak, WD Tilley, PJ Sykes, ***Parthenolide concurrently radiosensitises prostate tumour tissue and radioprotects non-tumoural tissues***, Radiation Research Society Meeting, Red Rock Resort, Las Vegas, Nevada, US, September 20th-24th 2014.

KL Morel, RJ Ormsby, E Bezak, WD Tilley, PJ Sykes, ***Parthenolide as a radioprotector of non-tumoural tissues in the treatment of prostate cancer***, SA Australian Science and Medical Research Annual Meeting, Adelaide Convention Centre, Adelaide, South Australia, Australia, June 4th 2014.

KL Morel, RJ Ormsby, E Bezak, WD Tilley, MD Lawrence, PJ Sykes ***Utilising the selective radioprotective properties of parthenolide for the treatment of prostate cancer***, Lorne Cancer Conference, Mantra Lorne, Lorne, Victoria, Australia, February 13th-15th 2014.

KL Morel, RJ Ormsby, E Bezak, WD Tilley, MD Lawrence, PJ Sykes, ***Parthenolide as a selective radiosensitiser in the treatment and prevention of prostate cancer***, Prostate Cancer World Conference, Melbourne Convention and Exhibition Centre, Melbourne, Australia, August 6th-8th 2013.

KL Morel, RJ Ormsby, E Bezak, WD Tilley, MD Lawrence, PJ Sykes, ***Utilising the selective radiosensitisation properties of parthenolide in the treatment and prevention of prostate cancer***, SA Australian Science and Medical Research Annual Meeting, Adelaide Convention Centre, Adelaide, South Australia, Australia, June 5th 2013.

Chapter 1: Introduction

Cancer

Cancer is among the leading causes of morbidity and mortality worldwide. Globally, there were 14.1 million new cancer cases, 8.2 million cancer deaths and 32.6 million people living with cancer in 2012 (*Stewart & Wild, 2014; Ferlay et al., 2015*). In Australia alone it has been estimated that the annual number of newly diagnosed cancer cases is over 130,000 with a mortality rate close to 47,000 per year (*AIHW & AACR, 2012*). The number of cases of cancer diagnosed in Australia is estimated to grow with the continually aging population in the coming years and is anticipated to reach approximately 150,000 by 2020 (*AIHW, 2012*).

Hallmarks of cancer

The complexity and diversity of cancer makes it a uniquely difficult disease to understand and treat; however, in 2000, Hanahan and Weinberg (*2000*) described six distinctive and complementary underlying principles believed to be common to all cancers. These principles were subsequently updated over a decade later to include an additional four hallmarks (*Hanahan & Weinberg, 2011*), creating a final list of ten fundamental markers of cancer (Figure 1-1). Understanding the widespread applicability of these concepts is likely to be key to the development of new cancer therapies.

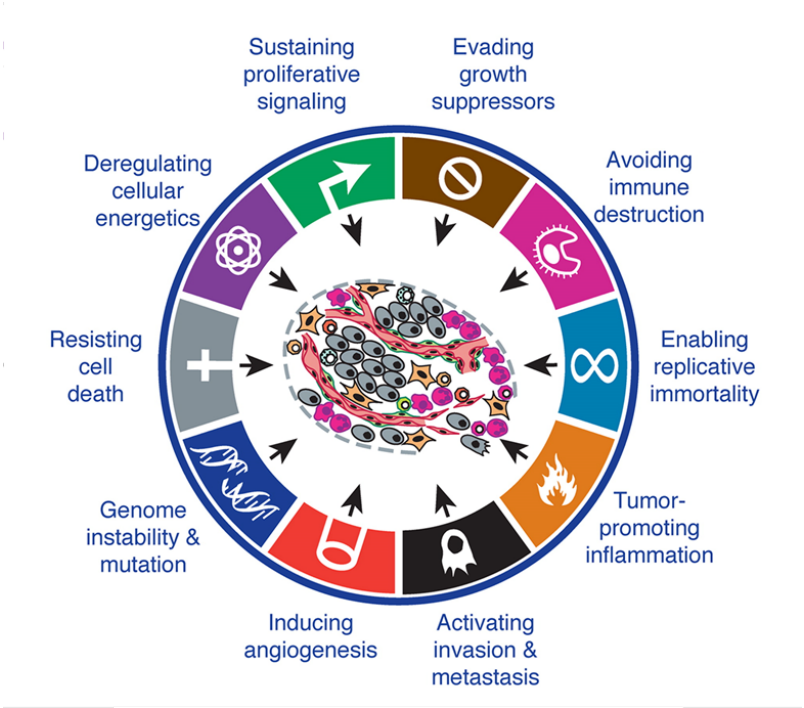

Figure 1-1: The ten hallmarks of cancer suggested by Hanahan and Weinberg

(Adapted from *Hanahan & Weinberg, 2011*)

Promotion of inflammation

One of the hallmarks of cancer is inflammation. It has long been recognised that some tumours can mirror the responses arising during normal tissue inflammation (*Dvorak, 1986*), and with the development of improved molecular markers that can more precisely identify distinct immune cell types, it has become clear that almost every cancer lesion includes immune cells in some manner (*Pages et al., 2010; Grivennikov, Greten & Karin, 2010; Pesic & Greten, 2016; Feng & Martin, 2015*). A wide range of studies into the links between inflammation and cancer progression have identified just how profoundly important immune-induced tumour-promotion (*Grivennikov, Greten & Karin, 2010; DeNardo, Andreu & Coussens, 2010; Colotta et al., 2009*). Inflammation also adds to many of the other hallmarks of cancer by providing key factors to

the tumour microenvironment to inhibit cell death, sustain and promote proliferation, facilitate angiogenesis, invasion, and metastasis, and trigger epithelial-to-mesenchymal transition (EMT) (*Landen, Li & Stahle, 2016; Clevers, 2004; Ricciardi et al., 2015*). Inflammation is evident in some tumours even during the earliest stages of cancer development and is able to foster the growth of neoplasias into fully developed cancers (*de Visser, Eichten & Coussens, 2006*). Inflammatory cells have also been shown to release stress-inducing pro-oxidant chemicals that may promote mutagenesis in nearby cancer cells, fast-tracking their progression towards increased malignancy (*Waris & Ahsan, 2006; Kamp, Shacter & Weitzman, 2011; Reuter et al., 2010*) (Figure 1-2). As such, inflammation is a significant enabling characteristic of cancer for its ability to promote other core hallmark capabilities.

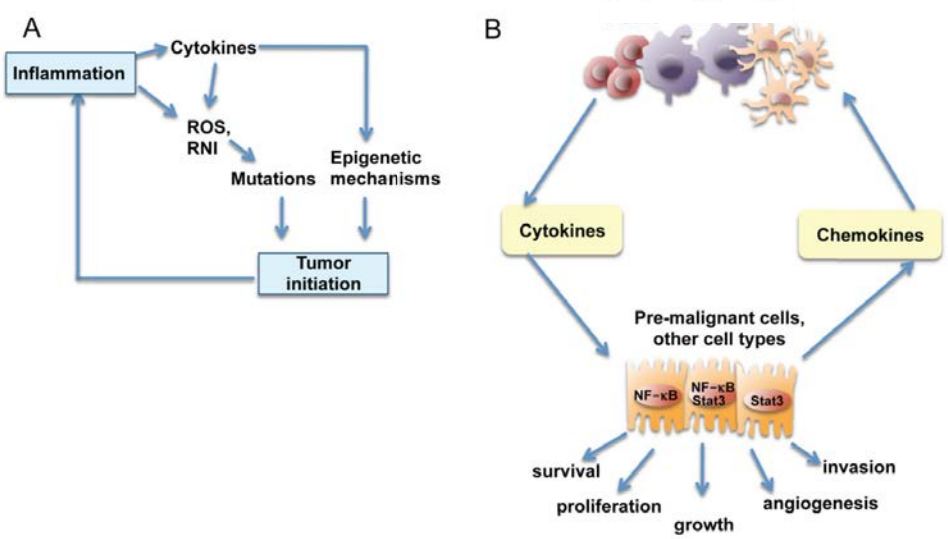

Figure 1-2: Role of Inflammation in tumour initiation and promotion

(A) Tumour initiation: reactive oxygen species (ROS) and reactive nitrogen intermediates (RNI) produced by the inflammatory response can cause mutations in nearby epithelial cells. Inflammation can also result in epigenetic changes that favour tumour initiation. Tumour-associated inflammation contributes to further ROS, RNI, and cytokine production. (B) Tumour promotion: cytokines from tumour-infiltrating immune cells activate NF-κB or STAT3 in premalignant cells to control pro-cancer processes. Within positive feed-forward loops, NF-κB and STAT3 induce production of chemokines that attract additional immune and inflammatory cells to sustain tumour-associated inflammation (taken from *Grivennikov, Greten & Karin, 2010*).

NF-κB regulates inflammatory and immune responses, as well as cell growth, by promoting related gene expression (*Baldwin, 1996; Gerondakis et al., 1998; Ghosh, May & Kopp, 1998; Pahl, 1999; Barkett & Gilmore, 1999*). These include genes that encode a wide range of cytokines and chemokines and receptors required for neutrophil adhesion and migration (*Bonizzi & Karin, 2004*). Additionally, NF-κB-activated cytokines, including TNF-α and IL-1β, are able to activate the NF-κB pathway directly, creating an auto-regulatory feedback loop that can significantly upscale inflammatory responses. NF-κB also increases iNOS and COX-2 expression, enzymes that contribute to advancing the inflammatory process (*Tak & Firestein, 2001*). NF-κB is also known to modulate survival of B-lymphocytes, cell proliferation, and ultimately the differentiation of B lymphocytes into plasma cells (*Gerondakis et al., 1998; Sen, 2006; Lucas, McAllister-Lucas & Nunez, 2004*). Additionally, NF-κB can regulate production of IL-2, which induces T lymphocyte proliferation and differentiation (*Arima et al., 1992*).

Constitutive NF-κB activation is often observed in various tumour types, including breast, prostate, and colon cancers (*Rayet & Gelinas, 1999; Wu et al., 2015; Karin et al., 2002; Van Waes, 2007*). Such dysregulation is thought to be caused by altered regulatory proteins that serve to activate signalling pathways involved in NF-κB activation. NF-κB is therefore an attractive therapeutic target for cancers where inflammation is implicated in pathogenesis.

Triggering metastasis and angiogenesis

During pathogenesis of many cancers, cells from primary tumours can escape, invade nearby tissues, and then spread to distant sites where they usually lodge and form new tumours. Despite significant research, these distant metastatic growths remain the leading cause of cancer related deaths (*Msaouel et al., 2008; Pedraza-Farina, 2006; Bogenrieder & Herlyn, 2003; Killion & Fidler, 1989*). Tumour progression towards metastasis is thought to be delineated as a stepwise and multistage process consisting of local invasion and penetration of basement membranes, entry into blood vessels, survival in the circulation, lodgement in distant organs, micrometastasis formation and metastatic colonisation (*Oskarsson, Batlle & Massague, 2014; Valastyan & Weinberg, 2011*). Almost all the events during the process are coordinated by complex pathways within tumour cells, endowing these cells with genetic or epigenetic alterations that favour survival, proliferation, dissemination and progression to distant metastasis (*Valastyan & Weinberg, 2011*) (described in Figure 1-3). Equally important for metastasis are the interactions between tumour cells and extracellular matrix (ECM) components, stromal cells, immune cells, cancer associated fibroblasts (CAFs) and many other cells, both at local and in distant sites.

Primary tumours are enriched in various cytokines, growth factors, chemokines and proteases, many of which favour the survival and proliferation of tumour cells, and impart migratory capability to them. This departure involves the EMT process whereby a subset of tumour cells within the primary tumour switches

off epithelial markers such as E-cadherin and turns on mesenchymal markers, such as vimentin, which leads to loss of cell polarity, cytoskeletal reorganisation and dissolution of adherens and tight cell junctions (*Valastyan & Weinberg, 2011; Nieto, 2013*). Tumour growth factor beta (TGF-β) is a key promoter of EMT (*Katsuno, Lamouille & Derynck, 2013*). Under certain physiological conditions, a variety of developmental signalling pathways, such as WNT and NOTCH have been shown to induce EMT. Additional signalling molecules that are thought to induce EMT include inflammatory cytokines, hypoxia through HIF-1α, and extracellular matrix (ECM) stiffness (*Y. Wu et al., 2009; Lo et al., 2007*; *Yang et al., 2004*; *Wei et al., 2015*).

EMT transcription factors, such as the SNAIL, ZEB and TWIST transcription families, respond to downstream signalling pathways by activating and coordinating the EMT process. Members of these transcription factor families block transcription of E-cadherin and downregulate tight junction proteins, providing epithelial structure support as well as regulating multiple signalling pathways via associated proteins (*Batlle et al., 2000; Comijn et al., 2001; Ikenouchi et al., 2003; Fang et al., 2011*). TWIST1 has also been shown to aid the breakdown of the basement membrane, thus promoting EMT (*Wei et al., 2015*).

During the EMT process, upregulated expression pro-EMT genes, including fibronectin, vimentin and N-cadherin, as well pro-migration cell surface proteins is commonly observed (*Porta-de-la-Riva et al., 2011; Beaty & Condeelis, 2014*). This mesenchymal shift promotes greater cell motility and contractility (*Haynes et al., 2011*), as well as increased matrix metalloproteinase (MMP) expression,

which in turn promotes ECM degradation and pro-invasive behaviour (*Leong et al., 2014; Watanabe et al., 2013*).

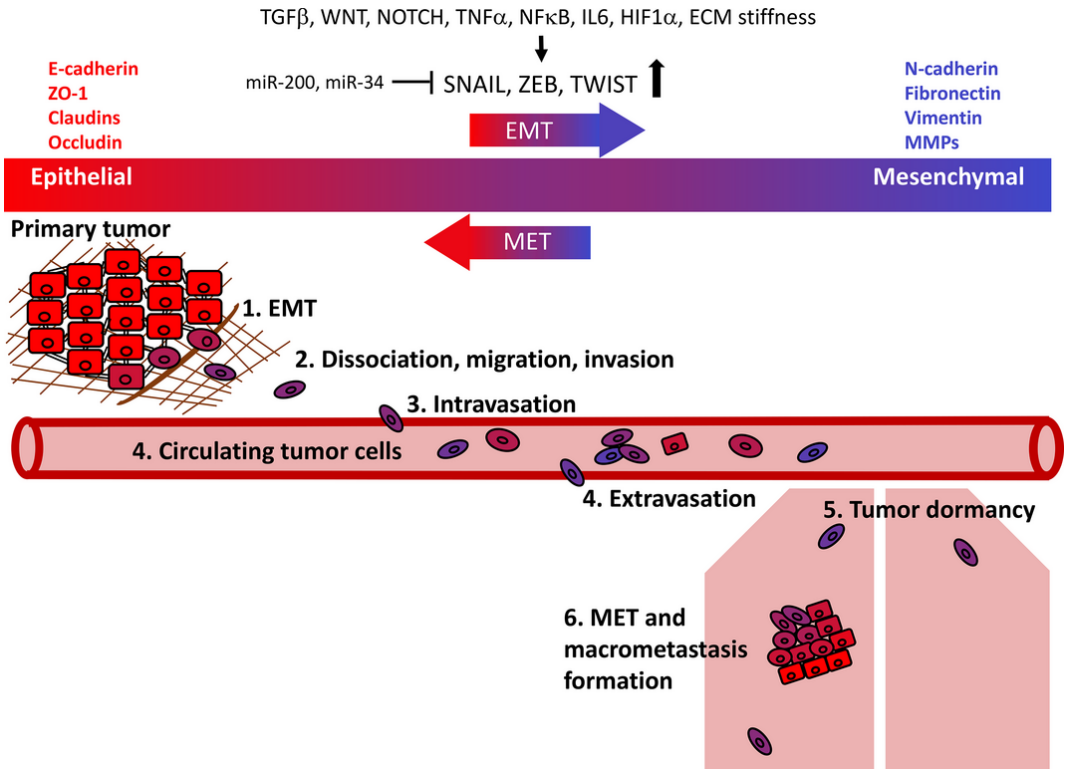

Figure 1-3: The processes of epithelial-to-mesenchymal transition and mesenchymal-to-epithelial transition

Primary epithelial tumour cells undergo EMT, acquiring the ability to disseminate, invade surrounding stroma, and intravasate into the blood vessels. Circulating tumour cells are able to survive in the circulation and ultimately extravasate to distant sites. Disseminated cancer cells can remain in a dormant state before undergoing mesenchymal-epithelial transition (MET) to proliferate and form macrometastases (taken from *Yeung & Yang, 2017*).

The EMT process is not just a pathway progressing in once direction, but is rather a multifaceted range of reversible overlapping pathways that can result in cells in existing between epithelial or mesenchymal states. This unique effect has obvious implications in tumour metastasis and is one of the major reasons that metastatic disease is such a challenge therapeutically.

Angiogenesis provides vital vascular support to tumours during cancer pathogenesis (*Bergers & Benjamin, 2003; Hicklin & Ellis, 2005*). The tumour vasculature not only delivers vital nutrients to growing tumours but provides important routes for dissemination of tumour cells. Development of blood and lymphatic endothelial cells is known to be stimulated by vascular endothelial growth factor (VEGF), which is commonly found in high levels within the tumour microenvironment (*Carmeliet, 2005*). VEGF has been shown to facilitate the intravasation process by increasing vascular permeability within tumours. Importantly, the tumour vasculature is known to be structurally abnormal. In normal vasculature, pericytes and endothelial cells share a basement membrane and have tight gap junctions that restrict capillary leakage. Tumour pericytes have been shown to only have a very loose association with the endothelial cells, which contributes to the development of intercellular gaps that provide an easy for tumour cells to escape and invade (*Xian et al., 2006; Gerhardt & Semb, 2008*). The increased leakiness cause by these loose intercellular junctions causes an increase in interstitial fluid pressure, which adds to dissemination by promoting passive tumour cell escape the stroma (*Jain, 2005*). In addition to increasing vascular permeability, VEGF has the ability to support the formation of the pre-metastatic niche by allowing micrometastases to grow and develop into macrometastases by recruiting VEGFR2-positive endothelial cell progenitors to build tumour vessel during the early stages of metastatic disease (*Kaplan et al., 2005; Ellis & Hicklin, 2008*).

Sustaining proliferation and resisting cell death

Cancer cells acquire the ability to sustain and promote proliferation. In normal cells these processes are tightly controlled through careful promotion of growth signals that allow progression through the cell cycle. This process ensures homeostatic maintenance of cell number, normal tissue architecture and function (*Hanahan & Weinberg, 2011*). Cancer cells can also dysregulate these signals to become self-sustaining (*Hanahan & Weinberg, 2011*). Cancer cells acquire an abnormal ability to sustain proliferative signalling in several ways. Firstly, by stimulating autocrine proliferation by directly upregulating production of growth factor ligands themselves (*Walsh et al., 1991*). Additionally, cancer cells can stimulate paracrine proliferation by inducing normal cells within the surrounding stroma to produce a supply of growth factors (*Cheng et al., 2008; Bhowmick, Neilson & Moses, 2004*). By increasing the concentration of key receptors on the surface of cancer cells, tumours can also render themselves hyper-responsive to low levels of growth factor ligand. Cancer cells may also constitutively activate the components of downstream signalling pathways, which removes the necessity for wait for ligand-mediated activation of these pathways.

Important negative feedback loops may also be disrupted in cancer cells. In normal cells these feedback loops provide a vital safety check that limits hyper-activated signalling pathways (*Wertz & Dixit, 2010; Cabrita & Christofori, 2008; Mosesson, Mills & Yarden, 2008*), however if these loops become disrupted it may lead to unchecked proliferation. An example of this is the Ras onco-protein,

which, when switched on subsequently switches on additional pro-growth and pro-survival genes (*Hanahan & Weinberg, 2011; Bardeesy & Sharpless, 2006*).

In addition to the ability to induce and sustain proliferative signalling, cancer cells are required to circumvent the powerful mechanisms that negatively regulate aberrant cell proliferation. Cancer cells are able to bypass key cell cycle checkpoints, which are vital for preventing aberrant cell proliferation (*Caldon, Sutherland & Musgrove, 2010; Ringshausen, Peschel & Decker, 2006*). Rb and p53 are two of the most commonly dysregulated tumour suppressors in cancer (*Ringshausen, Peschel & Decker, 2006; Sherr, 2004*). Rb protein responds to a wide range of extracellular and intracellular signals to determine whether or not cells ought to progress through the cell growth cycle, and can actively halt progression past the G_1 cell-cycle check point (*Deshpande, Sicinski & Hinds, 2005; Sherr & McCormick, 2002*). A defective Rb pathway allows cancer cells to proliferate unchecked. A key function of p53 is to regulate apoptosis in the presence of a range of cellular stressors, including but not limited to DNA damage, oxidative stress, osmotic shock, and ribonucleotide depletion (*Lakin & Jackson, 1999*; *Liu & Xu, 2011; Gambino et al., 2013; Kishi et al., 2001; Tanaka et al., 2000*). Cell cycle progression can be halted by p53 until these conditions have been normalised. When p53 is lost cell-cycle progression is able to continue despite the presence of potentially mutagenic DNA stress and damage. Although Rb and p53 have intrinsic importance, there also is evidence that both tumour suppressors form part of a greater protective network that also functions to limit inappropriate replication (*Lipinski & Jacks, 1999; Ghebranious & Donehower, 1998*).

In normal cells, apoptosis can be initiated in response to DNA damage and stress, however, cancer cells have been shown to be less sensitive to many stressors and are therefore able to limit or entirely avoid apoptosis (*Jin & El-Deiry, 2005*) (Figure 1-4). Apoptosis occurs via intrinsic and extrinsic pathways. The intrinsic pathway, which is initiated via intracellular stress, is considered to be highly important in cancer. The intrinsic apoptosis pathway can be triggered by stressors including genomic instability, growth factor deprivation, and oxidative stress, and is known to be carefully regulated by the BCL-2 family of proteins.

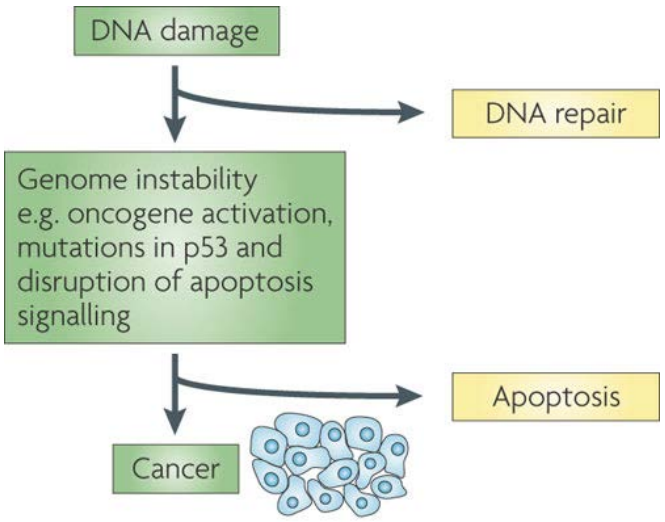

Figure 1-4: Apoptosis pathways in normal and cancer cells

To cope with DNA damage, cells have evolved a sophisticated repair system. Failure of this system leads to genomic instability, which triggers apoptosis under normal physiological circumstances. Should mutations in key apoptosis signalling proteins and oncogene activation also occur, then tumour development is a likely scenario (*taken from Colotta et. al. 2009*).

Many cancers acquire the ability to bypass the apoptotic pathway by dysregulating the BCL-2 regulatory proteins, either by upregulating BCL-2 expression or by downregulating related pro-apoptotic proteins (*Letai, 2008*). Cancer cells can further escape apoptosis by reducing the upstream stress signals that feed into and stimulate the BCL-2 pathway. For example, in a normal

situation, p53 responds to cellular stress by upregulating pro-apoptotic pathways, however, p53 can accumulate mutations that render cells less sensitive to DNA damage (*Hemann & Lowe, 2006*). Equally, in some cancer types, apoptotic resistance has been linked to inhibition of caspase-3 (*Devarajan et al., 2002; Quintavalle et al., 2013*).

NF-κB activates a number of key genes of the intrinsic and extrinsic apoptotic pathways. For example, NF-κB is known to upregulate the expression of proteins in the TNF-α signalling cascade. Research suggests that TRAF2 and TRAF6, both of which are involved in TNF-α signalling, lead to upregulation of pro-survival signalling (*Wang et al., 1998*). NF-κB also increases expression of the inhibitors of apoptosis (IAPs) proteins as well as several members of the pro-survival BCL-2 family (*Wang et al., 1998; Chen & Tu, 2002; Lee et al., 1999; Viatour et al., 2003*). The IAP proteins prevent both extrinsic and intrinsic apoptosis pathways by directly inhibiting several key effector caspases (reviewed in *Yang & Li, 2000*), while the anti-apoptotic Bcl-2 proteins antagonise and inhibit pro-apoptotic regulator proteins (reviewed in *Delbridge & Strasser, 2015*).

Additional cancer characteristics

Sustaining unchecked proliferation requires cancer cells to be able to adjust their energy production by adjusting their glucose metabolism to upregulate glucose transporters and to use alternative metabolic pathways (*Hay, 2016; Phan, Yeung & Lee, 2014*). This allows cancer cells to divert glycolytic intermediates to alternate pathways, including those required to assemble new cells (*Hanahan & Weinberg, 2011*).

Immunosurveillance is an essential process that actively inhibits the growth of neoplastic tissue in the human body. A healthy and active immune system has the ability to continuously recognise and eliminate cancer cells before they can establish and develop into a solid tumour, however, immunoediting can limit this ability (*Sherr, 2004; Vajdic & van Leeuwen, 2009*). This occurs in three key phases, namely the elimination phase, the equilibrium phase and the escape phase. During the elimination phase, the immune system activates in response to inflammatory cytokines from the cancer cells and attempts to eradicate cancer cells via cytotoxic mechanisms. In the equilibrium phase, the immune system limits growth of any cancer cells that have escaped the elimination phase, but does not completely eradicate the transformed cells, which can lead to selection of cells with mutations that increase immune resistance. Finally, cancer cells that are invulnerable to immune defences can progress into the escape phase, where the escaped cancer cells, with various genetic and epigenetic changes, continue to divide and grow (*Teng et al., 2008*).

Normal cells have an inherent cellular mechanism that limits their ability to replicate past a certain point. Cancer cells acquire the ability to bypass this protective mechanism by overexpressing telomerase (*Artandi & DePinho, 2010*). Telomerase is often only thought of in the context of maintaining telomere length, however additional functions of telomerase, namely in the promotion of tumour growth, have been recently been identified (*Hanahan & Weinberg, 2011; Artandi & DePinho, 2010*).

Genomic instability is common in many cancers, particularly in hereditary disease. Cancer can accumulate multiple mutations in order to promote tumour growth, and the unpredictable nature of these mutation events is major contributor to the heterogeneity observed in many cancer cells (*Venkitaraman, 2001; Negrini, Gorgoulis & Halazonetis, 2010*). Acquisition of these mutations is accelerated by dysregulation of normal DNA repair pathways. The 'caretaker' genes in such pathways detect genetic damage, activate DNA repair pathways, directly fix damaged DNA, and inactivate or inhibit pro-mutagenic stimuli (*Levitt & Hickson, 2002*). By downregulating these caretaker genes, cancer cells can increase the overall rate of mutations and, therefore, tumour development.

Cancer therapy

Cancer is treated in a range of ways, including surgery, chemotherapy, radiotherapy, and hormonal therapy. The choice of therapy depends of a wide variety of factors, such as the location of the tumour, the expected aggression of the disease, as well as the overall health of the cancer patient. Removing the entire cancer without harming normal, healthy tissues is the ultimate objective of treatment and can be achieved in a variety of ways. Tumour removal is often achieved by surgery, however, the invasive nature of many cancers can significantly limit the effectiveness of this method. Equally, chemotherapy and radiotherapy induce toxicity in healthy cells, resulting in unwanted side effects. Therefore, curative outcomes with some side effects can often be accepted in practice. In the case where curative therapy is not possible,

treatment of cancer can also be used to suppress the cancer to a manageable state and maintain that state to increase life expectancy, or to simply provide palliative care to improve the remaining quality of life.

Surgery

In principle, solid cancers are able to be cured if they are completely removed during surgery, but ensuring the entire tumour mass is removed can often prove difficult. In the case that a tumour has metastasised to distant sites before surgery can be carried out, complete removal of the tumour is generally impossible. Traditionally it has been considered that as cancers progress, tumours first grow at their primary site, slowly invade nearby lymph nodes, and then ultimately disseminate other parts of the body. However, even small localised tumours are increasingly being recognised as possessing metastatic potential and identification of metastatic disease following surgery is on the rise (*Smaldone et al., 2012; Klatte et al., 2008*). Surgery is often used in the treatment of breast cancer, prostate cancer, and non-small cell lung cancer. Depending on the case at hand, the purpose of surgery can be to remove just the tumour or the entire organ. Additionally, surgery can also be carried out for tumour staging, to determine the magnitude of the disease and whether or not it has metastasised. Surgery can occasionally be used for palliative therapy to help to reduce pain from complications such as spinal cord compression or bowel obstruction.

Radiotherapy

Radiation therapy utilises ionising radiation to eradicate cancer cells and reduce tumour burden. Administration of radiotherapy can occur externally, by external beam radiotherapy (EBRT), or internally, by brachytherapy. A key benefit of radiotherapy is that the effects, at least for solid for solid cancers, are generally localised to the region being irradiated. Radiotherapy kills cells by inducing DNA damage, inhibiting the ability for targeted cells to continue to grow and divide. The ultimate goal of radiotherapy is to kill the targeted cancer cells without injuring nearby normal tissues. To achieve this, radiotherapy is often delivered in multiple fractions, which allows normal to recover between doses (*Baskar et al., 2012*).

The dose of radiation used to treat tumours is entirely dependent on a range of factors. These factors include the specific radiosensitivity of the cancer being treated as well as the proximity of nearby healthy tissues that could be damaged during the process. Highly radiosensitive cancer cells, such as leukaemias and most lymphomas, are easily eradicated by modest doses of radiation (2-20 Gy), while many epithelial cancers, which are not as radiosensitive, require a significantly higher radiation dose (60-70 Gy) (*Illidge, 2011; Gerweck et al., 2006*). Some cancers, such as renal cell cancer and melanoma, are highly radioresistant and a curative dose would not be considered to be clinically safe. While radiotherapy may not be used for curative therapy in these more resistant tumours, it may still be a palliative option for metastatic disease.

A number of technological advances have improved the way that external radiotherapy is delivered. Three-dimensional conformal radiotherapy (3DCRT) and, more recently, intensity-modulated radiation therapy (IMRT) are highly precise methods of radiation delivery. In 3DCRT and IMRT the radiation beam conforms to match the shape of the tumour, which should limit the dose that nearby structures, such as the spinal cord or blood vessels, receive. The radiation dose is able to match the three-dimensional shape of the tumour by controlling, or modulating, the radiation beam's intensity. The intensity of the radiation dose is increased near the tumour mass, while the intensity is reduced near normal healthy tissues (*B. Wu et al., 2009*). In addition to advances such as IMRT, developments in medical imaging have become integral to radiation oncology, and the development of image-guided radiotherapy (IGRT) protocols have added to previous 3DCRT and IMRT technology to improve tumour targeting and healthy tissue sparing (reviewed in *Dawson & Sharpe, 2006*). Prior to IGRT, CT scan technology is used to identify tumour and healthy tissue areas, while three-dimensional soft-tissue imaging is used during therapy to track tumour motion. The increased precision and accuracy of IGRT has improved tumour killing while limiting the incidence and severity of radiation toxicity in a proportion of patients (*Dawson & Sharpe, 2006; Sterzing et al., 2011*). While, these technological advances have resulted in improved tumour targeting, reduced side effects, and better treatment outcomes than even 3DCRT, no single technology or strategy exists that is appropriate for all clinical situations. Despite significant effort to target therapy to the tumour mass alone, radiation therapy-induced side effects still occur. These adverse effects can range from relatively

manageable, such as skin irritation and burns, to very debilitating, such as fibrosis, incontinence and infertility.

Chemotherapy

Chemotherapeutic agents are designed to impede cancer cell division, thus tumour growth. While chemotherapy can be highly effective, most drugs are not specific to cancer cells and therefore target all rapidly dividing cells. Therefore, like many cancer therapies, chemotherapy has the potential to significantly damage normal tissue, which can cause significant side effects, particularly in tissues with cells that divide rapidly. Such tissues include bone marrow, the digestive tract, and hair follicles, which leads to the most common chemotherapy side effects, including myelosuppression, mucositis and alopecia. Currently, chemotherapy is most often given as multiple drug combinations, rather than as a single agent. Treating some haematological cancers can require high chemotherapeutic doses, alone or in combination with whole body irradiation, which entirely eradicates bone marrow. Bone marrow or peripheral blood stem cells collected prior to such ablative therapy, or obtained from a matched donor, enable recovery post-treatment.

As with other types of cancer therapy, the therapeutic outcome of chemotherapy depends a range of factors, including the specific type of tumour. The outcomes of therapy can range from being entirely curative, most commonly in leukaemia (*Freedman, 2012*), to being relatively limited, such as in some brain tumours (*Rampling, James & Papanastassiou, 2004*), to being pointless in others, as is the case for many skin cancers (*Neville, Welch & Leffell,*

2007). Chemotherapeutic drugs can also be delivered as a neoadjuvant therapy prior to the major therapy, most commonly surgery. As with chemotherapy, the benefits of neoadjuvant chemotherapy can differ depending on the cancer type and stage.

Additional therapy options

Targeted therapy is currently an area of research receiving significant attention and to date has been able to significantly improve treatment of some cancer types. Targeted cancer therapy utilises agents that specifically target and deregulate the pathways involved in tumour growth and development. Targeted therapies are specifically selected because they interact with target pathways rather than simply killing cells, as is the case with standard chemotherapy. Many targeted therapy drugs inhibit enzymatic domains on overexpressed or genetically altered proteins that allow cancer cells to function (*Afghahi & Sledge, 2015*). Key examples of such drugs are imatinib and gefitinib, both of which are potent tyrosine kinase inhibitors which are used to treat some types of leukaemia, as well as lung and breast cancers (*Natoli et al., 2010*). Targeted therapy can also utilise radionuclides attached to small peptides, which are designed to target and bind to specific cells in the tumour region. The radionuclides slowly kill the cancer cell as they decay in the cell area (*Gudkov et al., 2015*). An additional form of targeted cancer therapy is monoclonal antibody therapy. This approach utilises a therapeutic antibody, which is designed to bind to and inhibit specific tumour cell surface proteins. One example of monoclonal antibodies currently in use clinically include trastuzumab, an anti-HER2/neu

antibody which is used for treatment of breast cancer (*Vogel et al., 2002*). Immunotherapy is an additional cancer therapy option, and is designed to activate and utilise an individual patient's immune system to combat tumours. Immunotherapy may use a variety of methods to induce an immune response against tumours, including administering interferons and other cytokines to induce an immune response in patients with melanoma and renal cell (*Motzer et al., 1999*; *Lizee et al., 2006*), and intravesical BCG immunotherapy for treatment of bladder cancer (*Koya, Simon & Soloway, 2006; Droller, 2001*). Cancer vaccines that can illicit specific immune responses are currently a large area of research interest, specifically for the use in treating malignant melanoma and renal cell carcinoma (*Allen & Gundrajakuppam, 2012; Yoshimura & Uemura, 2013*). One immune-stimulating vaccine-like therapy currently in clinical use is Sipuleucel-T, which is used to treat metastatic hormone-refractory prostate cancer (*Frohlich, 2012; Anassi & Ndefo, 2011*).

Stumbling blocks and limitations

While significant advances in cancer treatment have been made and several cancer types have high cure rates, there are still limitations to current therapies.

Cancer heterogeneity is an issue that can have significant repercussions for cancer therapy. Targeted cancer therapy, which works by targeting genes of proteins required for tumour cell proliferation and survival, has significantly improved patient outcomes in a wide range of solid tumour types. However, in many cases of advanced disease, it has been shown that a targeted approach can

have limited benefit despite patients being selected based on key molecular markers. In these cases, targeted therapy is either not effective, or only provides clinical benefit for a finite period of time period (*Gore & Larkin, 2011; Diaz et al., 2012*). This split in patient efficacy may be partially explained by tumour heterogeneity, where some subpopulations of tumour cells are affected while others are not. To provide more widely applicable therapies, novel drugs should be targeted to more generally applicable cancer hallmarks, rather than highly specific genetic markers, which may only apply to a small fraction of tumours.

Radiotherapy is an important treatment option for many cancers, with more than fifty percent of all cancer patients receiving radiotherapy during cancer treatment (*Moding, Kastan & Kirsch, 2013*). While radiotherapy can be very successful, the associated normal tissue toxicity and side effects can still seriously affect the quality of a patient's life (*Sanda et al., 2008; Yucel et al., 2014; Pinkawa et al., 2010*). Radiotherapy toxicity can have acute or long-term side effects and can affect patients in different ways depending on the cancer type. Adverse side effects can include, in the short-term, skin irritation, burns, fatigue and hair loss, and in the long-term, trouble swallowing (head and neck cancer), deafness (brain cancer), heart and lung disease (breast cancer) and cystitis, incontinence and proctitis (prostate cancer) (*Marks et al., 1995; Berkey, 2010; Smith et al., 2009*). While early adverse effects that occur during or just after treatment often resolve within a couple of months, the late adverse effects may not manifest until several months to several years after therapy is completed and can be permanent.

For many cancer patients, metastatic disease is a terminal illness. Although cancer death rates have declined, for the most part patients with metastatic disease have not benefited from therapeutic improvements. In many cancer types (including breast, kidney, melanoma, ovarian, prostate and uterine) patients initially diagnosed with localised disease have almost a 5-year survival incidence close to 100%, while 5-year survival incidence drops to less than 25% when patients are first diagnosed with distant metastatic disease (*Siegel, Miller & Jemal, 2016; Steeg, 2016*). Despite the clear need for anti-metastatic therapies, many recent attempts to target metastatic cancer pathways have provided mixed results. For example, one particularly disappointing set of compounds have been the SRC inhibitors dasatinib and saracatinib (*Parsons & Parsons, 2004; Summy & Gallick, 2003*). On the basis of highly positive pre-clinical data in cell lines (*Nam et al., 2005; Lee et al., 2004*) and nude mouse models (*Park et al., 2008; Yang et al., 2010; Koreckij et al., 2009*), SRC inhibition was anticipated to be a highly potent anti-metastatic therapeutic target for prostate cancer. However, in patients with refractory disease, dasatinib failed as a single anti-metastatic agent (*Twardowski et al., 2013; Yu et al., 2011; Yu et al., 2009*) and did not increase overall survival when combined with docetaxel (*Araujo, Trudel & Paliwal, 2013*). The majority of compounds identified for use with other metastatic cancers have had similar lacklustre results in the clinical trial stages, and the search for novel and effective anti-metastatic drugs is an ongoing pursuit.

The need for novel therapies

There is a significant need for novel therapies that target not just one but multiple aspects of the hallmarks of cancer. One such compound is parthenolide (PTL), which is a naturally occurring anti-inflammatory compound (Figure 1-5). Historically the most common use of PTL is as an anti-inflammatory agent, and thus the compound is perfectly suited to block tumour-promoting inflammation (*Kwok et al., 2001*). PTL acts to reduce inflammation by inhibition of the NF-κB pathway. This anti-NF-κB mechanism of PTL also acts to help reduce metastatic spread and development. PTL is able to promote cell death via multiple pathways, most notably through modulation of the BCL-2 family of proteins and subsequent activation of caspase-mediated cell apoptosis (*Zhang, Ong & Shen, 2004*). The pro-apoptotic action of PTL is due, in part, to its induction of ROS, which selectively pushes cancer cells towards intrinsic cell death pathways (Figure 1-5).

Early *in vitro* and *in vivo* work have shown that PTL holds promise not just as a chemotherapeutic but also as a modulator of tissue sensitivity to radiotherapy.

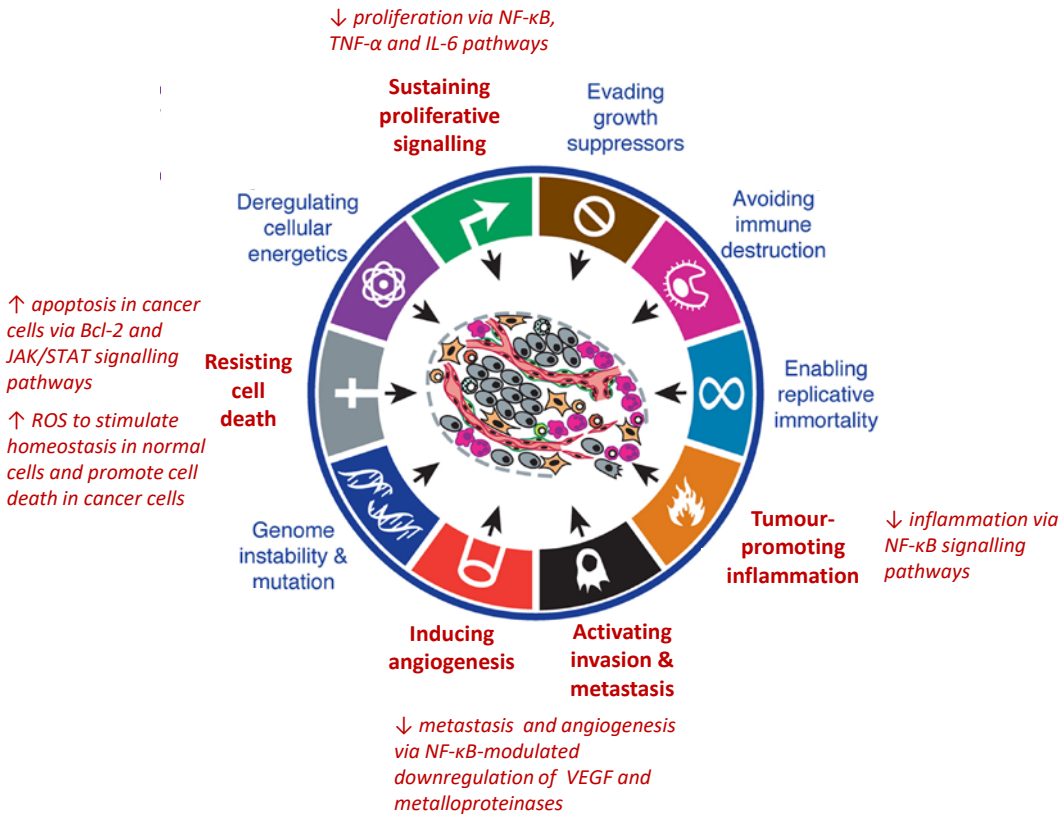

Figure 1-5: The major anti-cancer mechanisms of parthenolide target multiple hallmarks of cancer

The hallmarks of cancer, annotated with some of the major reported molecular mechanisms of parthenolide (in red) (*adapted from Hanahan & Weinberg, 2011*).

Parthenolide

Origins and chemistry

Sesquiterpene lactones plant-derived compounds that have been extensively used in herbal medicine for a variety of inflammatory diseases (*Marles et al., 1995*). PTL is a naturally occurring sesquiterpene lactone, which is commonly found in the flowers and leaves of feverfew (Figure 1-6). Native to the Balkans, the medical use of feverfew (*Tanacetum parthenium*) can be traced back to the ancient Greeks and early Europeans (*Knight, 1995*). Feverfew has been used for hundreds of years as a natural anti-inflammatory compound to treat arthritis,

asthma, dermatitis, earache, fever, headache, as well as being an anticoagulant, a digestive aid, and as treatment for depression, vertigo, and kidney stones (*Jain & Kulkarni, 1999; Vogler, Pittler & Ernst, 1998; Heptinstall et al., 1992*).

Figure 1-6: Feverfew (*Tanacetum parthenium*)

Representative images of the flower (A) and leaves (B) of the feverfew plant (taken from *Gardenia.net, 2017*)

PTL is found mostly in the superficial leaf glands, while being almost undetectable in the roots, and makes up 85% of the total sesquiterpene content (*Heptinstall et al., 1992*). Commercially available PTL (for research purposes) is extracted from the plant leaves, rather than being completely synthesised (Abcam, Sigma-Aldrich, Santa Cruz Biotechnology, Enzo Life Sciences and Cayman Chemical).

Anti-cancer effects of PTL

In addition to its powerful anti-inflammatory effects, PTL was shown to have anti-tumour properties for the first time in 1973 (*Wiedhopf et al., 1973*). These properties of PTL have been accredited to its ability to inhibit nuclear factor

kappa B (NF-κB), which was initially discovered in 1997 (*Bork et al., 1997*), and then further examined by studying the many steps in the NF-κB signalling pathway (*Garcia-Pineres et al., 2001; Hehner et al., 1999; Kwok et al., 2001; Zhang et al., 2005*). Despite being identified as a tumour inhibitory agent as early as 1973, it was only after the patenting of PTL for its use in cancer prevention in 2005 (*Nakshatri & Sweeney, 2005*) that significant research was directed towards the molecular mechanisms behind these anticancer properties. One of the more recent discoveries about PTLs anti-cancer mechanism, has been the insight into the drugs ability to radiosensitise tumour tissues while conversely increasing radioresistance of normal healthy tissues (*Sun et al., 2007; Sun et al., 2010; Watson et al., 2009; Mendonca et al., 2007; Xu et al., 2013*). This has the clinical potential to help reduce the radiation-induced side effects of radiotherapy. The potential that PTL holds in a clinical setting is limited by the significant hydrophobicity of the compound, thus limiting the oral bioavailability of the drug in blood plasma (*Schneider-Stock et al., 2012; Mathema et al., 2012; Kreuger et al., 2012; Pajak, Orzechowski & Gajkowska, 2008*).

Parthenolide analogues

PTL has been shown to have high potency against a variety of cancer types; however, PTL's limited bioavailability is a significant restriction for its use in a clinical setting. Studies have been successful in identifying PTL derivatives with greater water solubility without loss of potency (*Crooks, Jordan & Wei, 2006*). Altering the α-methylene or the endocyclic alkene functional groups (highlighted in Figure 1-7a) has been found to reduce PTL activity (*Neelakantan et al., 2009; Nasim & Crooks, 2008; Peese, 2010*). However, conjugation of aromatics (*Nasim*

& Crooks, 2008), or aliphatic amines (*Neelakantan et al., 2009*) to the α-methylene produces analogues with comparable efficacy and increased hydrophilicity. One such analogue is dimethylamino-parthenolide (DMAPT) (Figure 1-7b), which has been shown to kill 93% of primary acute myeloid leukaemia cells (*Neelakantan et al., 2009*).

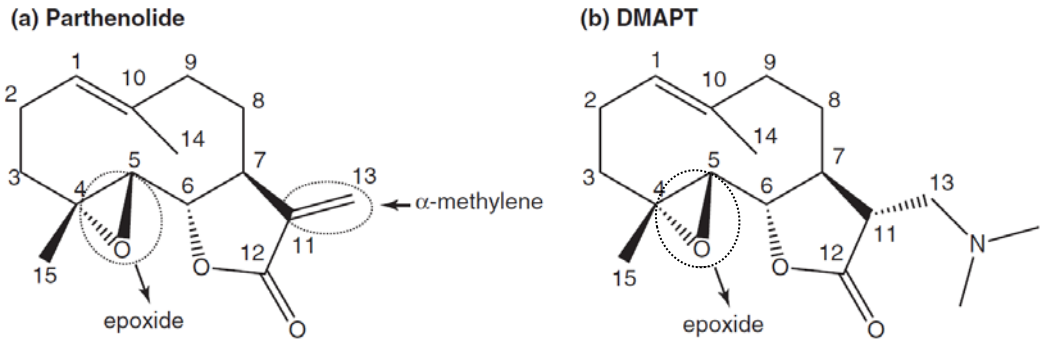

Figure 1-7: Comparison of PTL and DMAPT chemical structures

PTL (a) has epoxide and α-methylene functional groups, DMAPT (b) retains the epoxide functional group, but the α-methylene is replaced by an amine group

The development of the hydrophilic analogue DMAPT has helped to unlock the therapeutic potential of PTL by increasing plasma concentrations after oral dosing, while still maintaining acceptable toxicology in animal studies (*Guzman et al., 2007*).

Mechanisms of action of PTL

The current postulated mechanisms of PTL's ability to sensitise cells to extrinsic apoptosis signals include inhibition of the NF-κB pathway, inhibition of transcriptional activity of STATs, and the resulting transcriptional downregulation of several pro-survival genes (Figure 1-8). Additionally, inducing

oxidative stress and the resulting mitochondrial dysfunction promotes intrinsic apoptosis in cancer cells (Figure 1-8).

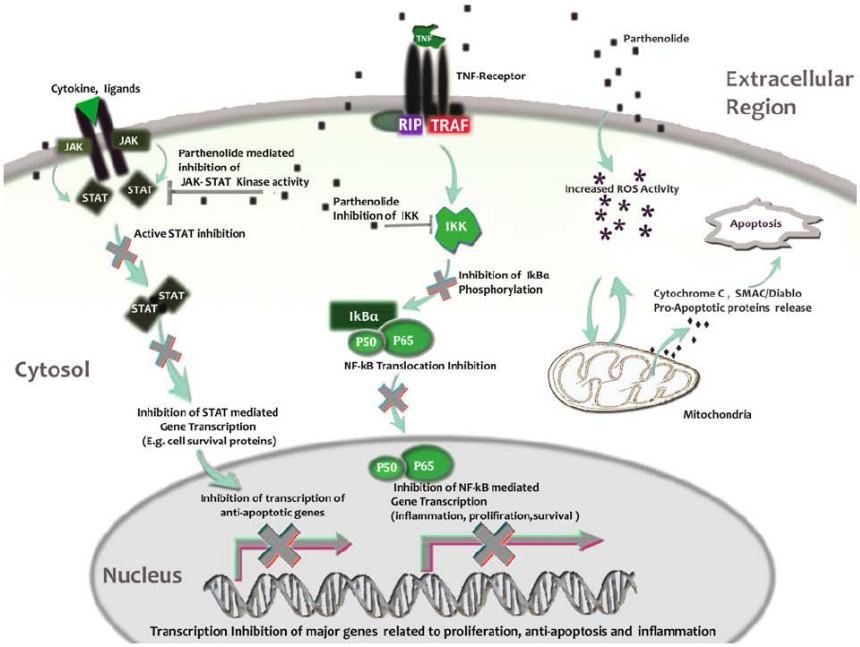

Figure 1-8: A basic model of parthenolide-mediated anti-cancer and anti-inflammatory activities

Parthenolide-mediated inhibition of NF-kB, STAT's transcriptional activity, and resulting downregulation of multiple anti-apoptotic gene transcription results in sensitisation of cells to extrinsic apoptotic signals. In addition, induction of oxidative stress and the cascade of reactions leading to mitochondrial dysfunction leads to activation of intrinsic apoptosis in cancer cells. (taken from *Mathema et al., 2012*)

Inhibition of NF-κB by PTL

PTL is a well-known NF-κB inhibitor, most likely due modulation of several different points along the NF-κB signalling pathway (Figure 1-8). Many NF-κB inhibitors are antioxidant compounds, however the structure of PTL does not promote free radical scavenging (*Bork et al., 1997*). Quantitative studies of NF-κB DNA-binding affinities across more than one hundred sesquiterpene lactones, including PTL, have been able to correlate inhibition of NF-κB with the amount of alkylating centres but not with lipophilicity (*Siedle et al., 2004*). In particular, the

presence of an α-methylene-γ-lactone (Figure 1-7a) was found to be the most important requirement for NF-κB inhibition (*Siedle et al., 2004*). In another study, 6 different PTL derivatives were utilised to identify that differences in derivative polarity could affect NF-κB inhibitory potential (*Dell'Agli et al., 2009*). The compounds with greater polarity, bearing hydroxyl functional groups, were found to be superior inhibitors of NF-κB-driven transcription (*Dell'Agli et al., 2009; Ghantous et al., 2010*).

The best studied mechanism by which PTL supports NF-κB inhibition is by directly binding to key NF-κB subunits (Figure 1-8). NF-κB is a protein complex that controls transcription of DNA in response to varying cellular stimuli. The α-methylene functional group of PTL (Figure 1-7) acts to alkylate cysteine-38 in the p65/NF-κB subunit (*Garcia-Pineres et al., 2001*). Sesquiterpene lactones lacking the α-methylene group lack anti-inflammatory properties *in vitro* and *in vivo* and are unable to inhibit NF-κB even at increasing concentrations (*Bork et al., 1997; Kwok et al., 2001*). The hypothesis of α-methylene-mediated cysteine-38 alkylation is reinforced by studies utilising cell lines with mutated p65/NF-κB lacking cysteine-38, which were found to nullify the ability of PTL to inhibit NF-κB (*Garcia-Pineres et al., 2001*).

PTL can also inhibit the IκB kinase (IKKβ) complex (Figure 1-8), which phosphorylates NF-κB inhibitors IκBα and IκBβ, ultimately promoting their degradation. Direct inhibition of IKKβ by PTL occurs through alkylation of cysteine-179, leading to downstream stabilisation IκBα and IκBβ. In cell lines where cysteine-179 was absent, IKKβ sensitivity toward PTL was

eliminated (*Kwok et al., 2001*) In addition to altering IKKβ sensitivity to PTL, cysteine-179 dysfunction is known to downregulate NF-kB-regulated cell survival and proliferative proteins and increase sensitivity of tumour cells to chemotherapeutic agents (*Gupta et al., 2010*). Given its importance as a critical player in the inflammatory pathway, the multi-subunit IKKβ complex may represent a very attractive target for pharmaceutical intervention.

JAK-STAT inhibition by PTL

Proteins from the signal transducer and activator of transcription (STAT) family are extracellular transcriptional factors that facilitate a wide range of biological functions, including cellular proliferation, differentiation and apoptosis (*Meyer & Vinkemeier, 2007*). Normally, phosphorylation of STAT tyrosine is short lived; however, consistent tyrosine-phosphorylation of STATs is has been reported in many cancer cell lines and human tumours (*Bromberg, 2002*). Constitutively activated STATs have been observed in numerous cancer types, including leukaemia, breast cancer, and prostate cancer (*Endo, Toyota & Imai, 2004; Sheen-Chen et al., 2007; Ferrajoli et al., 2006; Tam et al., 2007*). Recent research has shown that PTL-mediated inhibition of Janus kinase (JAK) proteins (Figure 1-8) inhibits activity of STAT proteins, which in turn help to modulate the effects that PTL elicits on death receptors (*Carlisi et al., 2011*). Resistance to TNF-related apoptosis-inducing ligand (TRAIL)-mediated apoptosis is often reported in cancer cells (*Zhou et al., 2008*). PTL has been found to increase the number of R1, R2, and R3 TRAIL receptors (*Guzman et al., 2005*) and induce an extrinsic apoptotic pathway in colorectal cancer cells (*Kim et al., 2015*). Inhibition of IL-6 expression,

mediated by PTL, is also thought to be related to the downregulation of STAT3 through Tyr705, resulting in the prevention of translocation of STAT into the nucleus (*Sobota et al., 2000*).

Increased ROS activity by PTL

Imbalances between ROS induction and the ability of cells to remove reactive intermediates or fix the subsequent damage can lead to a shift to a pro-oxidative state (*Tapia, 2006*). The intracellular redox state occurs as a careful balance between oxidative stress and endogenous thiol buffering systems, incorporating non-protein molecules, for instance glutathione (GSH), as well as many protein thiols, including thioredoxin. Studies have shown that the redox status of cells plays an important role in survival and cell death (reviewed in *Hampton & Orrenius, 1998*). The ability to upregulate production of ROS is a major mechanism of the pro-apoptotic ability of PTL (*Juliana et al., 2010; Nakshatri, Rice & Bhat-Nakshatri, 2004*). Because ROS levels are innately elevated in cancer cells, only very minimal pro-apoptotic activity is observed in normal cells (*Steele et al., 2006; Herrera et al., 2005;* reviewed in *Hampton & Orrenius, 1998*). PTL activity has been linked to the reaction of the α-methylene-γ-lactone functional group (Figure 1-7a) with glutathione or cysteine thiol groups of target molecules (*Winterbourn & Hampton, 2008*). These redox reactions have the ability to act as a biological switch for signalling downstream cascades (*Winterbourn & Hampton, 2008; Lee, Cha & Kim, 2000*). The added oxidative stress induced by PTL appears to have a wider range of inhibitory and pro-apoptotic effects on tumour cells (*Pajak, Orzechowski & Gajkowska, 2008*). Studies show that PTL increases ROS

levels in prostate cancer (PC3) cells through activation of NADPH oxidase, which subsequently promotes a range of reactions involving the P3K/Akt pathway and FOXO3a. This ultimately leads to inhibition of manganese superoxide dismutase and catalase, both of which are key antioxidant enzymes (*Sun et al., 2010*). It has been shown that PTL promotes ROS-mediated apoptosis in leukaemia cells to illicit an anti-cancer effect (*Zunino, Ducore & Storms, 2007*). In colorectal cancer cell lines, PTL-induced oxidative stress activates intrinsic cell death pathways, which in turn leads to degeneration of the mitochondrial membrane and an upregulation of pro-apoptotic proteins (*Zhang, Ong & Shen, 2004*). In addition to these findings, a study into human gastric cancer has shown that PTL-mediated mitochondrial damage results in the release of cytochrome c into the cytosol, which consequently controls expression of BCL-2 family proteins and activates caspase-mediated cell apoptosis (*Zhao, Xu & Li, 2009*).

P53 activation by PTL

The p53 protein is crucial in multicellular organisms, where it regulates the cell cycle and, thus, functions as a tumour suppressor. To elicit an effective and timely response to stimuli such as genotoxic stress, the cellular concentration and transcriptional activity of p53 are tightly maintained. PTL is known to target and activate p53 cellular functions via ubiquitination of MDM2 (*Gopal, Chanchorn & Van Dyke, 2009*). Although research has indicated that p53 activation is likely to be involved in PTL's anti-cancer mechanism (*Dey, Tergaonkar & Lane, 2008; Kawasaki et al., 2009; Dinarello, 1998*), a recent study of the complimentary action of PTL in melanoma cells when given in

combination with doxorubicin found that although PTL was able to reduce constitutive and doxorubicin-induced NF-κB activity, it had no effect on p53 (*Wozniak et al., 2013*). This may indicate that p53 is not essential for the tumour-killing action of PTL. This finding is supported by studies into the radio-sensitisation of prostate cancer cell lines by PTL, which found that increased irradiation-induced cell death occurred in both p53-null (PC3) and p53-wildtype (LNCaP) prostate cancer cell lines (*Sun et al., 2007; Sun et al., 2010*). In a 2009 study, PTL was shown to inhibit constitutive and radiation-induced NF-kB binding activity and enhanced the X-ray sensitivity of PC3 cells (*Watson et al., 2009*). It was proposed that the suppression of radiation-induced NF-kB activity by PTL led to X-ray sensitisation through inhibition of split-dose repair in the p53 null cells. Although p53 activation may not be essential for the anti-cancer effect of PTL, recent studies have found that phosphatase and tensin homolog (PTEN) accentuates this anti-cancer effect, and this action may modulate p53 expression though targeting the PTEN/Akt/MDM2/p53 pathway (*Di Fiore et al., 2013; Sun et al., 2007*).

Selective targeting of cancer stem cells by PTL

Cancer heterogeneity results in multiple subpopulations of cells within and between tumours. One of the many cell subpopulations is known as cancer stem cells (CSC) or tumour-initiating cells. CSCs are tumour cells that possess characteristics associated with normal stem cells, specifically the ability to self-renew and to generate mature cancer cells through differentiation (*Valent et al., 2012*). Generally speaking, CSCs are rare and proliferate more slowly than other

more differentiated cancer cells, but they are believed to establish the basis of tumours (*Valent et al., 2012; Guzman & Jordan, 2005*). CSCs could be a major factor behind resistance to chemotherapy, incomplete cancer eradication, and tumour relapse (Figure 1-9).

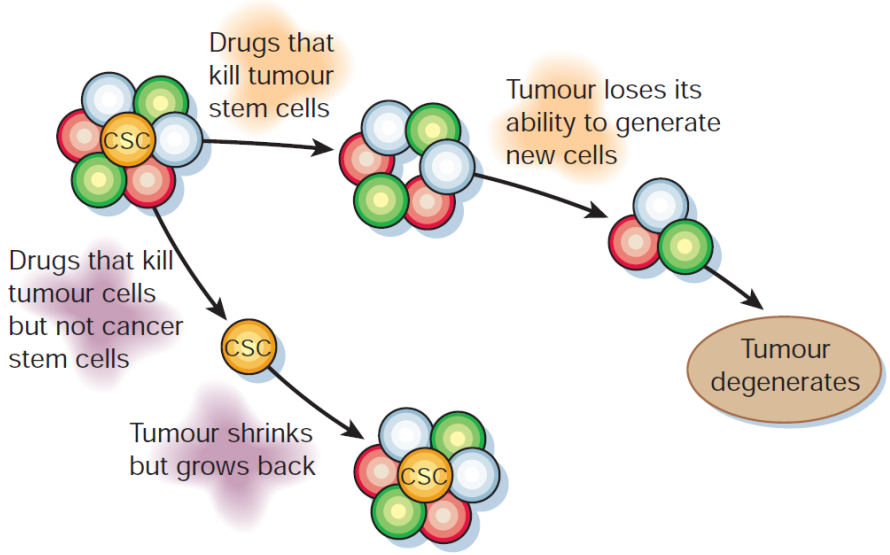

Figure 1-9: Comparison of tumour killing therapies

Comparison of conventional therapies which may shrink tumours by killing tumour cells but not cancer stem cells, and therapies targeted against cancer stem cells, which have greater potential to render tumours unable to maintain themselves or grow (taken from *Reya et al., 2001*)

PTL was shown to be the first small molecule to selectively eradicate CSCs without significantly altering normal stem cells (*Guzman et al., 2005*). This observation has been replicated in several leukaemia and lymphoma models, as well as in solid tumours (*Gunn et al., 2011; Carlisi et al., 2016; Guzman et al., 2007*). CSCs have higher NF-κB-dependent survival compared with normal stem cells, which may be one reason why PTL is able to target them so selectively (*Valent et al., 2012; Zhou & Zhang, 2008*). Interestingly, not all NF-κB inhibitors have the ability to target CSCs, which implies that the particular step along the

NF-κB pathway that is targeted during inhibition may be important to the anti-CSC response. PTL's ability to selectively target CSCs might also be linked to their ability to simultaneously activate p53 (*Dey, Tergaonkar & Lane, 2008*), by increasing DNA binding (*Kawasaki et al., 2009*) and protein levels with associated phosphorylation of serine 15 (*Guzman et al., 2005; Guzman et al., 2007*), and by inhibiting NF-κB. PTL has also been shown to inhibit several key pathways required for CSC survival, namely NF-κB, JAK/STAT, MAPK, and phosphatidylinositol-3-kinase (*Kawasaki et al., 2009; Dreesen & Brivanlou, 2007*). Drugs targeting these pathways might have complimentary effects in eliminating tumours, as has been seen in the synergy between PTL and PI3K inhibitors (*Hassane et al., 2010*). PTL has also shown preferential targeting of ABCB5-positive melanoma CSCs, which subsequently prevents chemo-resistance in melanoma (*Czyz, Koprowska & Sztiller-Sikorska, 2013; Schatton et al., 2008*). PTL has superior abilities to eradicate melanospheres, which are melanoma cells that grow as non-adherent colonies and that show *in vitro* self-renewing capacity and multipotency, compared commonly used melanoma chemotherapeutics, such as dacarbazine (*Czyz, Koprowska & Sztiller-Sikorska, 2013*).

In vitro studies

On a molecular level, PTL has been shown to alter signalling pathways to induce selective toxicity of tumour cells in several cancer types *in vitro*. The underlying molecular interactions involved in PTL's promotion of tumour-specific cell death have been mainly linked to inhibition of NF-κB and JAK/STAT signalling, and induction of JNK, as well as heightened redox stress, leading to changes in gene

expression, in particular downregulation of anti-apoptotic genes and up-regulation of pro-apoptotic genes (*Kreuger et al., 2012; Mathema et al., 2012*). The chemotherapeutic properties of PTL have been in part attributed to its impact on epigenetic mechanisms, which are commonly modified in cancer cells. Expression of histone deacetylase 1 (HDAC1) is often increased in cancer cells, which are known to be more sensitive to HDAC inhibitors than normal cells are. In several cancer types, PTL has been shown to selectively deplete HDAC1 *in vitro* without altering other HDACs (*Gopal, Arora & Van Dyke, 2007; Ghantous et al., 2012; Salisbury & Cravatt, 2008*). PTL promotes HDAC1 degradation and modifies histone structure at the p21 promoter, which results in greater p21 transcription and subsequent upregulation of cancer killing (*Gopal, Arora & Van Dyke, 2007; Ghantous et al., 2012*). Many tumours express elevated levels of DNA methyltransferases (DNMTs) DNMT1 and DNMT3b, which both contribute to tumour development by inhibiting expression of tumour suppressors. *In vitro* and *in vivo* studies in myeloid leukaemia and skin cancer, have found that PTL induces global DNA hypomethylation via inhibition of DNMT1 (*Liu et al., 2009*).

In vivo studies

A broad range of *in vivo* PTL studies have been carried out to date, these studies are briefly summarised in Appendix A. Oral dosing of PTL is significantly less effective than with other drug administration methods. Although oral PTL significantly inhibits tumour growth in some *in vivo* models, the high lipophilicity of the compound limits PTL's ability to achieve an effect proportional to the dose

administered (*Kawasaki et al., 2009*). This limitation of PTL was a major reason for the development of the water-soluble PTL analogue, DMAPT. The poor solubility of PTL restricts oral dosing of mice to a maximum of 40 mg/kg, providing a maximum plasma concentration of less than 1 µM, which is well below the ideal therapeutic plasma concentrations of 5-10 µM (*Sweeney et al., 2005*). In contrast, DMAPT has been tested *in vivo* at oral doses up to 100 mg/kg, which results in maximum plasma concentrations of 25 µM in mice and 61 µM in dogs (*Guzman et al., 2007; D. Cheng et al., 2005; Peese, 2010*). Administration by IV or IP allows a higher drug dose to be administered; however, PTL and DMAPT plasma levels following drug injection are reportedly lower than might be expected, potentially due to drug precipitation after injection (*D. Cheng et al., 2005; Dell'Agli et al., 2009*). Injecting PTL into or near by the tumour or *ex vivo* pre-treatment of tumour cells before xenograft implantation have both been proven to successfully increase drug potency. Even when DMAPT is administered orally complete eradication of tumour volumes has not been observed. PTL and DMAPT may potentially have greater benefit when delivered in combination with other drugs. It has been observed that PTL and DMAPT are not effective in all cell subpopulations present in a tumour, however, they do appear to selectively target the CSCs, which results in inhibition of metastasis and tumour cell engraftment.

Clinical trials with PTL

Clinical trials assessing the toxicity and efficacy of PTL have been limited and the majority have focused on feverfew rather than the purified active compound.

The first clinical study to assess the efficacy of feverfew against migraine began in 1985 (*Johnson et al., 1985*). The study provided evidence that feverfew taken prophylactically prevents attacks of migraine, and identified no adverse side effects, although it should be noted that many of the patients accepted into this study were already suffering from PTL's described side effects (nausea, blurred vision, fatigue) which were later described (*Curry et al., 2004*). Subsequent trials for migraine treatment identified no significant side effects (*Murphy, Heptinstall & Mitchell, 1988; Pfaffenrath et al., 2002; Diener et al., 2005*).

The first trial to examine PTL's anti-cancer ability was a Phase I clinical trial designed to examine the pharmacokinetics and toxicity of PTL delivered to cancer patients in the form of the herbal supplement feverfew (*Curry et al., 2004*). Feverfew was delivered orally, once a day in a 28-day cycle starting with a 1 mg per day dose and then escalating to daily doses of 2, 3, and 4 mg. This dosing schedule resulted in no significant toxicity, however, at these doses PTL was not detectable in plasma. It was therefore concluded that daily oral feverfew, containing up to 4 mg of PTL, while well tolerated, would not be clinically effective against cancer. It was also concluded that purification of PTL would be required to allow greater doses to be delivered for clinical applications.

PTL and DMAPT are currently in ongoing Phase I clinical trials for their ability to eradicate CSCs in AML, ALL and other blood-lymph tumours (*Gopal, Chanchorn & Van Dyke, 2009; Dittmar & Zänker, 2013; Ghantous et al., 2013*), however, published information about these trials is not yet available.

While PTL holds significant clinical promise for many cancer types, its use in the treatment of prostate cancer may be particularly beneficial, due to the slow disease progression, limited options for treating metastatic disease and common use of radiotherapy in treatment.

Prostate Cancer

Function and anatomy of the prostate

The prostate is a walnut sized mammalian organ of the male reproductive tract. It is located at the base of the bladder with the urethra running through its centre. Epithelial, solid, glandular prostatic shoots invade the peri-urethral mesenchyme, forming a complex branched ductal structure (*Schalken & van Leenders, 2003*). The glandular structures produce a proportion of the fluid comprising an ejaculate, whilst the muscular components supply some of the rhythmic contractions which aid ejaculation and close the urinary urethra, to limit contamination of the ejaculate with urine (*De Marzo et al., 2007; Shafik et al., 2006*). Secretions from the prostate gland contain a range of proteins, the three most abundant being; prostate-specific antigen (PSA), prostatic acid phosphatase (PAP) and prostate secretory protein of 94 amino acids (PSP94, also known as β-microseminoprotein) (*Weiber et al., 1990*).

The human prostate is defined through a zonal histological system (rather than a distinct lobe structure), which is based on the relationship to the ejaculatory ducts (Figure 1-10) (*Wendell-Smith, 2000; McNeal, 1968*). The zone-based division of the human prostate correlates well with the various pathologies of

the prostate. Histopathological findings of focal atrophy, prostatic intraepithelial neoplasia (PIN) and carcinoma are found in high prevalence in the peripheral zone. The transitional zone is somewhat prone to focal atrophy, PIN and carcinoma; whilst benign prostatic hyperplasia is almost exclusive to the transitional zone.

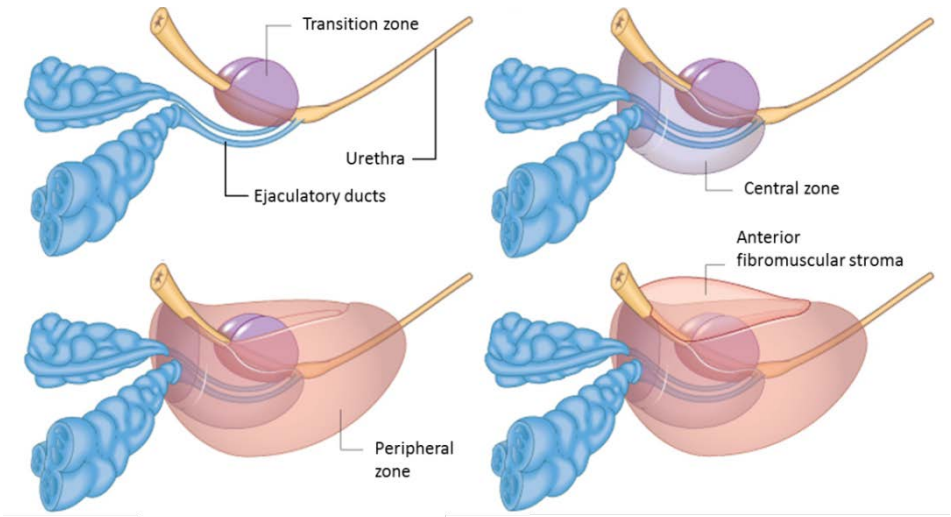

Figure 1-10: Zonal nomenclature of the human prostate, including the Transition, Central and Peripheral zones

(adapted from *Standring, 2008*).

The epithelial prostate glands are comprised of four main cell types: basal, transit amplifying, neuroendocrine and luminal epithelial cells. These cell types form two histological layers, the basal and luminal layers, which are bordered by a basement membrane of extracellular matrix; these form a barrier between the basal cells and the fibromuscular stroma (Figure 1-11). The cellular layers of the epithelium can be identified through specific marker profiles. Basal cells express cytokeratins (CK) 5 and 14 along with BCL-2 and CD44; luminal cells express CK8 and 18, the androgen receptor and PSA (*Hudson et al., 2001*). The luminal layer

of the prostate consists of tall columnar cells, is androgen dependent and responsible for the secretion of PAP, PSA and PSP94 into the seminal fluid. The basal layer contains androgen-independent cuboidal cells, and is considered to be the proliferative compartment of the prostate.

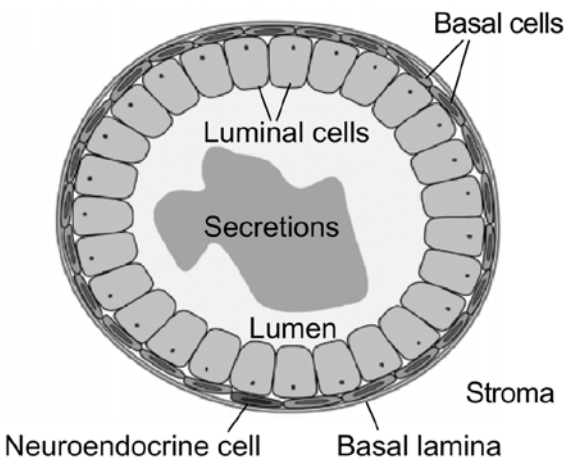

Figure 1-11: Schematic depiction of structure and cell types comprising the human prostatic duct

(taken from *Abate-Shen & Shen, 2000*)

Given the ability of the prostate to regenerate following luminal cell depletion, resulting from androgen withdrawal, the basal layer has been associated with putative stem cell populations, capable of regenerating the differentiated cells of the epithelium. Ongoing work, aimed at identifying this stem cell population and differentiating cells has complicated the traditional view that the prostate epithelium is comprised of two distinct layers. Populations of cells are being identified which express cell marker profiles which are intermediate between basal and luminal cells. Stem cells located in the basal layer give rise to the basal cells and transit amplifying cells (progenitor cells) (Figure 1-12). The transit amplifying cells, expressing both luminal and basal markers, proliferate to give

rise to luminal and neuroendocrine cells. The transit amplifying cells have also been implicated as potential cells of prostate cancer origin and may therefore prove to be an important target in improved cancer therapeutics (*Hallstrom & Laiho, 2008; Hudson, 2004; Hudson et al., 2001; Taylor, Toivanen & Risbridger, 2010*).

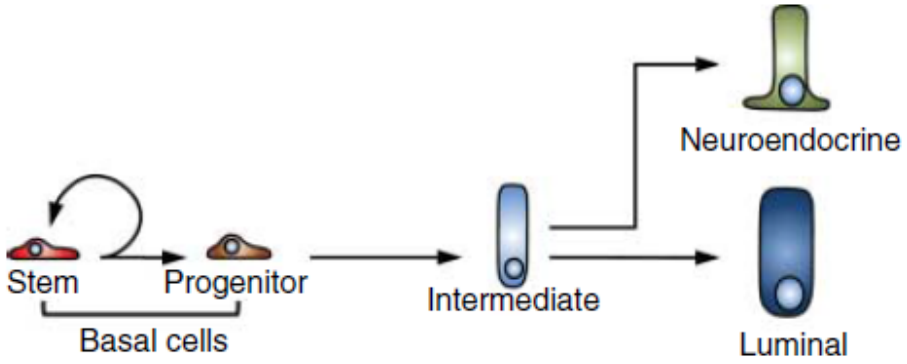

Figure 1-12: Model of differentiation hierarchy for putative prostatic stem cells

In this model, basal cells self-renew, give rise to progenitor (transit amplifying cells), followed by intermediate cells and then terminally differentiated luminal or neuroendocrine cells in a linear manner (taken from *Taylor, Toivanen & Risbridger, 2010*).

Incidence, morbidity and mortality of prostate cancer

Prostate cancer arises in the epithelial cells of the glandular prostate; adenocarcinomas of the prostate account for approximately 90% of all prostate cancer diagnoses (*Long et al., 2005*). Prostate cancer is zone specific, with approximately 70% of carcinomas arising in the peripheral zone (*McNeal et al., 1988*). Information regarding the zone of cancer origin also has prognostic value, with evidence indicating that those arising in the transitional zone have less malignant potential than those of the peripheral zone (*Greene et al., 1991*).

Most prostate cancers are relatively indolent, and may never result in a clinical expression, or when still confined to the prostatic capsule, are in most cases curable through traditional surgical and radiation treatments. However, once established, aggressive prostate cancer invades the basal lamina of the prostate gland, infiltrating the surrounding prostatic stroma. This results ultimately in metastasis, primarily to lung and bone, which has very poor prognosis (reviewed in *Abate-Shen & Shen, 2000*).

Prostate cancer is known to be associated with a range of environmental and genetic factors; however, age is the single greatest risk factor of prostate cancer. Despite only affecting men, prostate cancer is the most commonly diagnosed cancer in western countries, with over 180,000 new cases diagnosed globally each year (*Siegel, Miller & Jemal, 2016*). The pre-malignant lesions associated with prostate cancer can be identified in men in early adulthood and become much more common in men aged 30-50 year old, implying that prostate cancer has a long latency time (*Sakr et al., 1993*). Prostate cancer differs from many forms of cancer in that it is both heterogeneous and multifocal (Figure 1-13). Evaluations of prostatectomies have shown mulitfocality in the majority of cases, both in the early lesions of prostate cancer, such as PIN, and the cancer foci themselves (*Sakr et al., 1993*). This tendency to develop multifocally has been demonstrated in a variety of studies, with rates ranging from 60% to 90% (*Bastacky et al., 1995; L. Cheng et al., 2005b; L. Cheng et al., 2005a; Miller & Cygan, 1994; Arora et al., 2004*). The features of multifocality and genetic heterogeneity have led to two main hypotheses on the underlying processes

enabling these features. Firstly, the prostate has been shown to be deficient in G1/S, intra-S, and G2/M checkpoints, which allows the accumulation of genetic changes capable of driving mulitifocal and heterogeneous carcinogenic processes (*Girinsky et al., 1995; Hallstrom et al., 2007*). Secondly, the prostate is immunologically privileged, compromising immune surveillance of tumourigenesis (reviewed in *Leibovitz, Baumoehl & Segal, 2004*). Some dietary and environmental factors inherent in the Western lifestyle also appear to be a significant influence on the development of prostate cancer (*Peto, 2001; Giovannucci et al., 2007*).

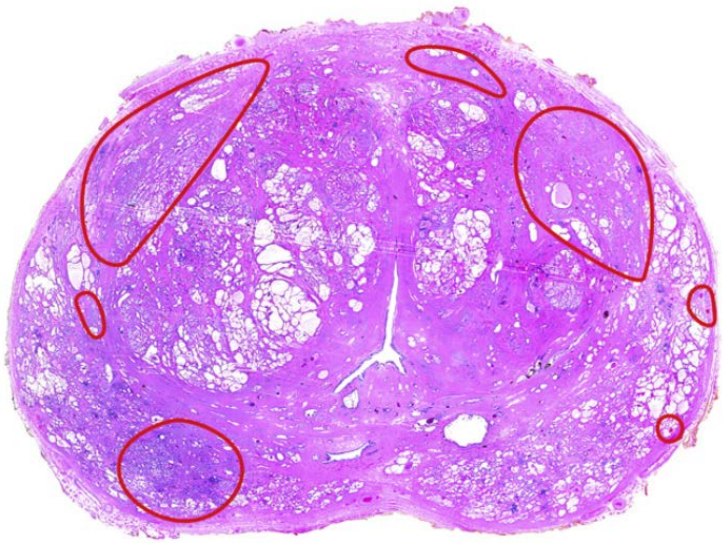

Figure 1-13: Prostate cancer multifocality

Diverse topographical distribution of different-sized tumour foci within a whole-mount prostate specimen; tumour foci are circled (in red) (taken from *Andreoiu & Cheng, 2010*)

The typical view of the histological changes which accompany the carcinogenic process of the prostate is that prostatic intraepithelial neoplasia (PIN) is the earliest recognisable stage. PIN lesions, like adenocarcinomas, are multifocal and

genetically heterogeneous, displaying some but not all the phenotypic, genotypic and biochemical markers of adenocarcinomas (*Bostwick et al., 1998;* reviewed in *Abate-Shen & Shen, 2000;* reviewed in *Schrecengost & Knudsen, 2013*). The clinical importance of this was first established by McNeal and Bostwick (*1986*) who found high grade PIN to be associated with adenocarcinomas (82% of prostates with carcinomas versus 43% of benign prostates examined harbouring PIN lesions). This information has led to the current model for the histological progression of prostate cancer; whereby a continuum of pathology exists which begins with the pre-malignant lesions (PIN) and develops through to *in situ* adenocarcinomas which invade the basal membrane and invade the local tissue resulting, ultimately, with metastasis (Figure 1-14).

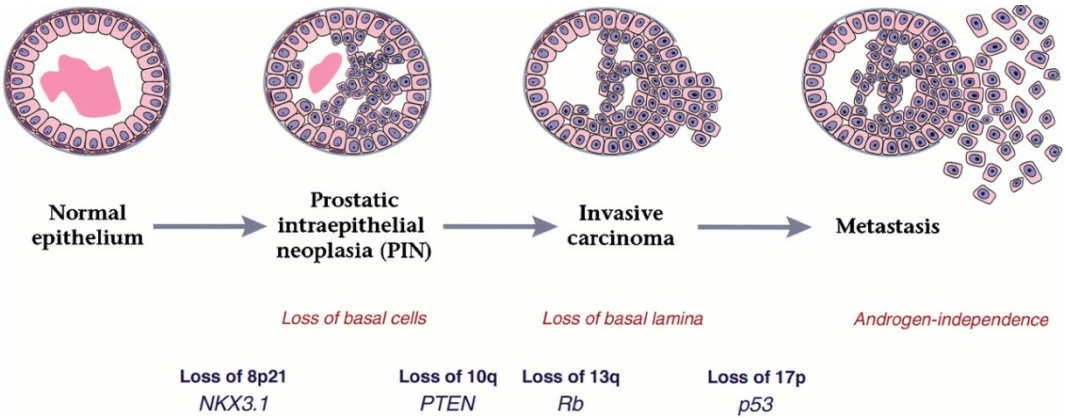

Figure 1-14: Histopathological progression of prostate cancer

Indication of the timing of common genetic mutations (NKX3.1, PTEN, Rb and p53 loss) which can occur in the prostate carcinogenesis process (taken from *Abate-Shen & Shen, 2000*).

PIN lesions can be sub-classified into different architectural patterns and grades of severity, a subject which goes beyond this brief review. However, key features include: branching and undulating luminal surfaces, basophilic glands due to

enlarged nuclei and high nuclear to cytoplasmic ratio, and epithelial hyperplasia (Figure 1-14 and Figure 1-15)(*Epstein, 2009*).

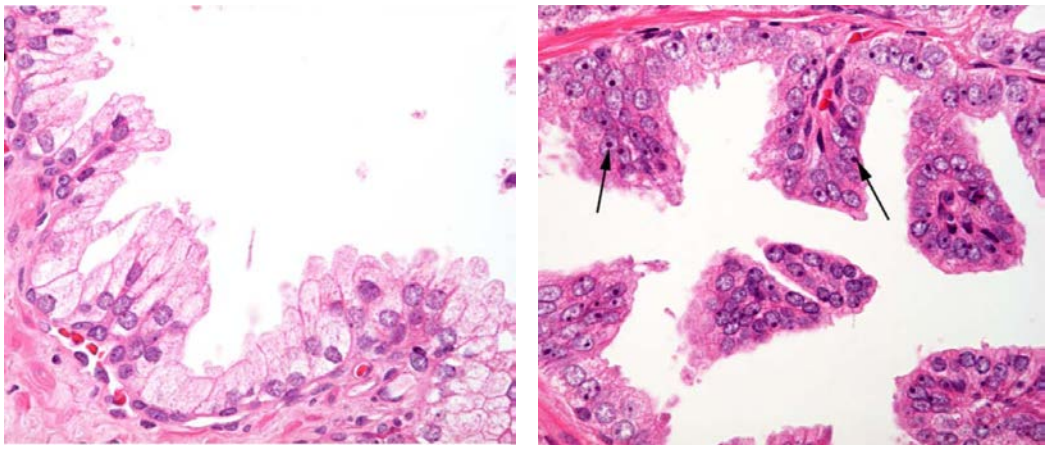

Figure 1-15: Comparison of human normal prostate epithelium and human PIN lesions

Representative images of human normal prostate epithelium (left) and human PIN lesions (right), showing enlarged nuclei (indicated by arrows), basophilia and epithelial hyperplasia (taken from *Iwata et al., 2010*)

The genetics of prostate cancer

Prostate carcinogenesis is accompanied, and driven by, a complex array of molecular and genetic changes. A variety of genetic changes (chromosomal, gene mutational and epigenetic) have been found to be associated with prostate cancer, however, no single mutational event of a tumour suppressor gene has been widely accepted as critical or required for its development (reviewed in *Hallstrom & Laiho, 2008;* reviewed in *Berger et al., 2011*).

As with many cancers there exists a familial or inherited form of prostate cancer, which predisposes an individual to develop a carcinoma. Depending on how these familial or inherited forms of prostate cancer are defined, they contribute between 5-20% of cases of disease in the population. Several genes are

implicated in prostate cancer. Based on their position within chromosomal regions that are lost with high frequency in prostate cancer, their functions, associations with other cancers, and direct evidence for mutation in prostate cancer, these include AR, TP53, Rb, PTEN and NKX3.1 (Homeobox protein Nkx-3.1). Epigenetic changes are also implicated; most notably and well-studied is the hypermethylation of CpG islands within the promoter region of GSTP1, which is strongly associated with prostate cancer and pre-malignant lesions such as PIN (*Hopkins, Burns & Routledge, 2007; De Marzo et al., 2004; Schrecengost & Knudsen, 2013; Henrique et al., 2013*). More than 40 genes have now been reported to be the targets of epigenetic silencing in prostate cancer (*Nelson, De Marzo & Yegnasubramanian, 2009*). The TMPRSS2-ERG fusion gene, which links the ERG (ETS gene-related gene) oncogenic transcription factor gene to the androgen receptor-regulated transmembrane protease serine 2 (TMPRSS2) gene, has been found in over half of prostate tumours (*Hoimes & Kelly, 2010; Leman & Getzenberg, 2009*)

Prostate cancer diagnosis

The early detection of prostate cancer is key to its management, as the prognosis for organ confined disease is much better than for metastatic disease. The most common detection methods are either direct palpation of a tumour using a digital rectal examination or indirectly through the measurement of serum PSA level. Following initial screening, needle biopsies provide the opportunity for histological analysis and combined with PSA testing can be used to confirm diagnoses, provide prognosis and direct treatment strategy.

Prostate cancer treatment

Complicating the treatment of prostate cancer is the difficulty that clinicians have in distinguishing aggressive life-threatening cancers from indolent tumours which may have little impact on patient health. Thus, evaluation of prognosis on an individual basis is clearly required to direct treatment strategy.

For many clinicians a 'wait and see' approach is advised to patients with organ confined disease, particularly in older men. The indolent nature of many cancers may be such that patients die from other causes before their prostate cancer progresses sufficiently to cause mortality or significant morbidity. Surgical intervention and radiation therapy are both recommended treatment strategies for men with relatively long life expectancies and with good prognostic indicators (such as organ-confined cancer, low PSA and low Gleason score). However, much of the choice of treatment is in negotiation with patients as there is little convincing evidence to support any particular strategy as being superior over the other (*Wilt et al., 2008;* reviewed in *Wallace et al., 2014*).

For organ-confined prostate cancer, fractionated external beam radiation is commonly applied (approximately 2 Gy fractions, to a minimum total dose of approx. 74 Gy) to the prostate (*Graham et al., 2008; Ward et al., 2014*). In palliative treatment protocols for metastatic cancer, much larger dose fractions may be used. Brachytherapy, where irradiation of tissue can be made through the internal deposition of radioactive seeds, is also another option. A range of surgical techniques are also available (laparoscopic, retropubic, perineal, robotic) which generally remove the entire prostate and attached seminal vesicles, with

the aim to remove the cancer before metastasis (*Wolf et al., 2010*). Chemotherapeutic intervention, in conjunction with the radiation and surgical interventions described, using a variety of compounds and combinations of compounds (estramustine, 5-fluorouracil, cyclophosphamide, doxorubicin, mitoxantrone, and docetaxel) have been used in treatment however, their efficacy has been limited (*Alan & Daniel, 1993; Shelley et al., 2008*).

Hormonal interventions have been used, particularly in more advanced cases, to alleviate symptoms and delay progression. The luminal epithelial cells of the prostate and up to 90% of diagnosed prostate cancers are androgen-dependent (*Heinlein & Chang, 2004*). Androgen blockade or withdrawal through castration (physical or chemical) results in initial loss of tumour bulk, pain reduction and improved PSA levels. However, ultimately an androgen-independent cancer phenotype emerges which is incurable, with time to death of approximately two years (*Hoimes & Kelly, 2010*).

The detection and treatment options outlined above have dramatically improved patient outcomes, yet, even with these advances approximately 15% of diagnosed patients will progress though to, and die of, metastatic disease (*Galsky & Vogelzang, 2010*). In addition, the high frequency and severity of side effects from prostate cancer treatment has limited effective therapy. Therefore, there is an ongoing need for research into novel treatment modalities and new approaches to prostate cancer therapy.

Models to study prostate cancer

A hierarchy can be envisioned whereby as models of prostate cancer become simpler, and more removed from the human biological process they aim to recapitulate, they become potentially less relevant. *In vitro* cell cultures must therefore be considered at the weaker end of such a hierarchy, followed by three-dimensional cell culture models, then xenografted cancer cells in living immuno-deficient hosts, and finally autochthonous animal models. Conversely, the simpler the model is in such a hierarchy, the more control that can potentially be exerted over it. Here researchers must compromise between cost, ethics, simplicity and the relevance of their chosen model to the disease processes they aim to investigate.

Cell lines are particularly suitable for addressing questions relating to events and physical interactions underlying fundamental cellular processes (such as growth, differentiation, structure and transformation) because they reduce the complexity inherent in the in vivo system. The three most widely used prostate cancer cell lines (DU-145, PC3 and LNCaP) are derived from brain metastasis, spinal and lymph node metastasis respectively, and became available in the late 1970's (*Webber, Bello & Quader, 1996*). Since then the number of available cell lines has increased, with the desire to produce lines capable of providing representative models for the various stages and molecular phenotypes of prostate cancer (for example p53 and AR mutations). Some of these new cell lines have later been found to be contaminated with other cells (such as HeLa) or derivatives of established (DU-145, PC3 and LNCaP) cell lines, rather than being

newly derived lines of prostate origin. This fact highlights the difficulty that has been found in producing prostate cancer cell line models (reviewed in *Bokhoven et al., 2003; Sobel & Sadar, 2005;* reviewed in *Wu et al., 2013*). In vitro work with cell lines has been invaluable in delineating many of the molecular pathways involved in prostate carcinogenesis and avoids many of the ethical and cost restraints which accompany animal work. However, extrapolation from in vitro studies to the in vivo situation is often questioned.

Histologically, cancer cells reside as 3D organoids in a host microenvironment, which has been shown to be pivotal to malignant progression of cancer cells (*Shekhar, Pauley & Heppner, 2003; Chung et al., 2005; Bissell, Rizki & Mian, 2003; Fidler, 2003*). This means that limited information can be gleaned from 2D *in vitro* studies. 3D culture systems for *in vitro* studies are thought to better recapitulate the microenvironment of cells, and therefore can more accurately describe the pathophysiology of cancer. A variety of 3D culture methods have been developed based on current knowledge of cellular and tissue architecture, in efforts to produce the most *in vivo*-like structures possible (reviewed in *Wang et al., 2005*). A recent 3D approach in prostate cancer research is *ex vivo* culture of biopsied human tissues, which retains the native tissue architecture, hormone responsiveness, and cell-to-cell signalling of the tumour microenvironment in a dynamic and manipulable state (*Centenera et al., 2013*). *Ex vivo* culture systems capture the structural complexity and heterogeneity of human prostate cancers in a laboratory setting, making them an important adjunct to current cell-line-based and animal-based models. In a hierarchical sense these ex vivo human

models may fall somewhere just below *in vivo* models, as they are a 3D model of true human prostate cancer, yet lack the immune system of animals or humans.

Xenograft models, where established tumour lines are propagated into immuno-deficient mice, have the advantage over cell culture of enabling investigation of angiogenesis and metastasis, using human derived cells. The major limitations of this model type rests in the advanced stage that these cell lines represent in tumourigenesis, and the absence of competent immune-response and microenvironment structure where vascular, lymphatic and stromal interactions are distorted (*Abate-Shen et al., 2008*). These limitations have even prompted the suggestion that the intermediate nature of xenograft models, between cell cultures and 'true' mouse cancer models, should result in their re-definition as 'animal culture' (*Frese & Tuveson, 2007*). Patient-derived xenograft (PDX) models, which are xenograft models developed by transplanting human tumours into immune-compromised mice, have gained popularity as a more realistic preclinical cancer model (*Rubio-Viqueira & Hidalgo, 2009; DeRose et al., 2011*). PDX models have been used for the preclinical investigation of various aspects of prostate cancer including angiogenesis, identification of castrate-resistant stem-like cells, effects of anti-androgen therapies, and interactions between tumour cells and the bone microenvironment (*Raheem et al., 2011; Gray et al., 2004; Toivanen et al., 2013*). PDX tumours have been shown to retain the majority of key genes expressed in primary tumours (*Lin et al., 2014*). PDX studies are generally accepted as more clinically relevant cell-line derived xenograft studies.

Autochthonous animal models of prostate cancer can be divided into the non-transgenic and transgenic models. Non-human prostate cancer is confined to dog and rat models (*David et al., 1998*). Canines develop spontaneous prostate cancer, with bone metastasis, that is histopathologically very similar to humans. However, disease is sporadic and incidence not well defined. An average age of 10 years to diagnosis, cost, ethical issues, along with its sporadic nature make this model relatively difficult to use (*David et al., 1998; Navone et al., 1998*).

Transgenic mouse models of prostate cancer have several advantages: they can be bred quickly, have relatively short progression times, high penetrance, and greater metastatic reproducibility over spontaneous and induced models (*Winter, Cooper & Greenberg, 2003*). Two main approaches have been used to genetically modify mice for prostate cancer induction. The first links a strong prostate-specific promoter to a viral oncogene. The earliest such model utilised the rat prostatic steroid binding protein gene promoter fused to the SV40 (Simian Vacuolating Virus-40) large T-antigen. Male mice from this model developed prostatic adenocarcinomas and female mice developed mammary tumours, indicating the promoter was sensitive to both male and female sex hormones (*Maroulakou et al., 1994*). A variety of transgenic models of this type have followed, utilising promoter elements (such as probasin, human PSA, mouse mammary tumour virus, mouse cryptin-2 gene, and fetal globulin Gγ) to drive expression of the SV40 oncogenes (reviewed in *Shappell et al., 2004; Ahmad, Sansom & Leung, 2008; Frese & Tuveson, 2007; Huss, Maddison & Greenberg, 2001; Parisotto & Metzger, 2013*). The most widely used of these

models are the TRAMP and LPB-Tag (LADY) models, which utilise two different probasin promoters and SV40 constructs.

The second transgenic model approach has been via genetic manipulation of genes implicated in human prostate cancer; germ-line mutation of tumour suppressors, enforced over-expression through fusion with prostate specific promoters, or the newer techniques of conditional activation and/or inactivation of genes through site specific recombinase activity. These models have targeted a large variety of such genes (e.g. Trp53, Rb, Pten, k-Ras, p27, Nkx3.1, c-myc, AR) (reviewed in *Ahmad, Sansom & Leung, 2008; Shappell et al., 2004; Frese & Tuveson, 2007; Parisotto & Metzger, 2013; Wu et al., 2013*).

Although no animal model completely echoes the human disease, the TRAMP model is considered to be the most well characterised autochthonous model of prostate cancer and has been selected for use in this project (*Jeet, 2010*)

The TRAMP model

The TRAMP mouse model was developed by Greenberg et al. (*1995*) and is an autochthonous prostate cancer model. The TRAMP mouse is able to reproducibly recapitulate the staged progression of human prostate cancer. TRAMP mice develop prostate cancer with 100% frequency, driven by rising androgen levels at the onset of puberty.

The TRAMP transgene is comprised of an androgen responsive rat probasin (rPB) promoter fused to the (SV40) early region containing the small and large T-antigens (tAg and TAg respectively). Transgene-induced prostate pathology in

the TRAMP is driven by the androgen dependent expression of the SV40 early genes. The large and small T-antigens have pleiotropic effects both in their normal functions in viral transmission and in the oncogenic processes they are involved in. TAg is essential for SV40 viral replication; binding the viral origin of replication to promote DNA synthesis (*Dean et al., 1987*). The best understood targets of TAg are the retinoblastoma (Rb) family of proteins and the p53 tumour suppressor protein (*Ali & DeCaprio, 2001; Ahuja, Saenz-Robles & Pipas, 2005*). Through its interaction with Rb, the large T-antigen contributes to cellular proliferation and transformation; Rb preferentially binds and sequesters the hypophosphorylated Rb form, and thereby removes the ability of Rb to inhibit Rb regulated E2F transcription factor-initiated genes.

The importance of the tumour suppressor protein p53 is highlighted by both the frequency in which it is mutated or inactivated in cancer and the observation that it is targeted by many viral oncoproteins (including the large T-antigen) (*Sankaranarayanan & Chakraborty, 1995; Lilyestrom et al., 2006*). The transcriptional activity of p53 is modulated by a wide variety of cellular stresses and results ultimately in cell cycle arrest, senescence or the instigation of programmed cell death (apoptosis) (reviewed in *Riley et al., 2008*). The large T-antigen interferes with the action of p53 by directly binding its DNA binding domain, leading to silencing of p53's transcriptional activity but stabilisation of the protein, resulting in higher cellular concentrations of p53 (*Bargonetti et al., 1992; Lilyestrom et al., 2006*). The p53-TAg interaction also obscures the domain involved in formation of p53 tetramers, with each monomer of the hexameric

TAg complex binding a single p53 molecule, as depicted in the ribbon diagram of the crystal structure (*Lilyestrom et al., 2006*).

Several criticisms can be made of the TRAMP model. Anatomically, the mouse and human prostate have key differences; the human prostate is a single structure, defined by zones, whereas the mouse (and rat) prostate is comprised of 4 distinct lobes (anterior, dorsal, lateral and ventral) (Figure 1-16). At the molecular level, inactivation of p53 and of Rb by expression of the SV40 T-antigens, is the key driver of tumourigenesis in the TRAMP model; however, the mutations of the genes encoding these protein, although common during prostate cancer progression, are rarely an initiating mutational event in human prostate cancer.

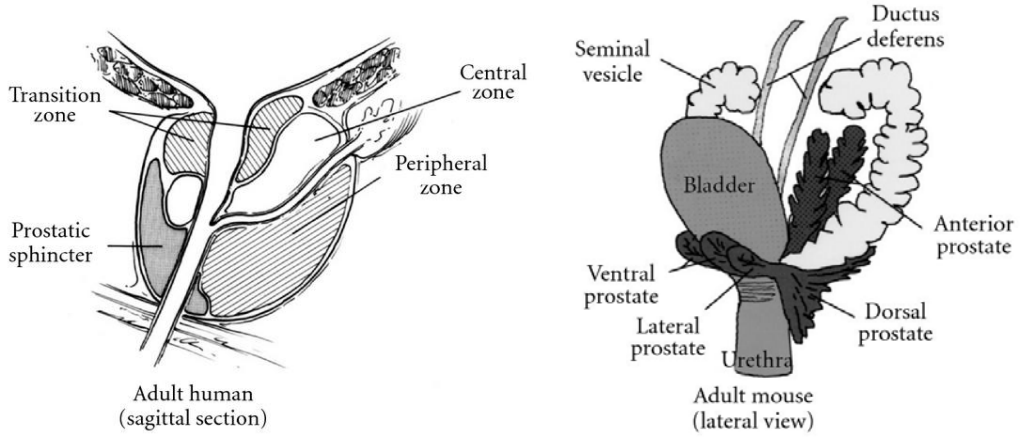

Figure 1-16: Comparison of human and mouse prostate anatomy

Schematic diagram of the human prostate (left) and mouse prostate (right) (taken from *Abate-Shen & Shen, 2002*).

Human prostate cancers are frequently found to express neuroendocrine markers with about 10% being extensively positive (synaptophysin and chromogranin A). However, prostatic neuroendocrine cancers (sometimes called

small cell carcinomas) are rare, have very poor prognosis, often present at late stage and their appearance has been associated with androgen-deprivation (*Yao et al., 2009; Zhou, Flesken-Nikitin & Nikitin, 2007*). Considerable debate over the neuroendocrine features of the TRAMP model, and the model's relevance to clinical disease has taken place over the last 10 years. Initially, the neuroendocrine features observed in the TRAMP model were recognised in advanced and poorly differentiated tumours and were thought to be a stochastic event most strongly associated with these late stage adenocarcinomas; thus, mirroring the clinical disease (*Andreas et al., 2004; Kaplan-Lefko et al., 2003*). This shift towards a neuroendocrine phenotype is still recognised with advancing stage (*Slack-Davis et al., 2009*); however, there is now extensive evidence that neuroendocrine carcinomas (small cell carcinomas) are the macroscopic tumour which is ultimately the lethal phenotype for TRAMP mice. Furthermore, the cells of origin for these tumours have been attributed (by some authors) to cells which do not arise from androgen-dependent SV40-mediated transformation of epithelial cells, undergoing a progression from PIN to adenocarcinomas (*Chiaverotti et al., 2008; Huss et al., 2007; Slack-Davis et al., 2009*). Conversely, it was recently reported that neuroendocrine carcinomas only occur in TRAMP mice following anti-cancer therapy (castration or docetaxel), a finding they attributed to more stringent criteria for neuroendocrine status and the selective pressure of these treatments (*Yao et al., 2009*). In opposition to previous studies, it was also concluded that neuroendocrine carcinomas and adenocarcinomas in the TRAMP model likely share the same progenitor cell type.

Significant progress has been made in delineating the specifics of carcinogenesis in the TRAMP model. Further work is needed to determine if the neuroendocrine phenotype reflects an inherent difference between mouse and human that predisposes the murine prostate to neuroendocrine differentiation and to ascertain what role SV40 expression may play in this process (*Abate-Shen & Shen, 2002*). The relevance of the model to human prostate cancer, given the SV40 mediated-inactivation of p53 and Rb activity and the limitations this may place on translation of work from the TRAMP model to the human disease, also requires further investigation. Even with these on-going issues, the TRAMP model still represents the most commonly used autochthonous model of prostate cancer, and has provided considerable insight into prostate carcinogenesis and response to potential therapies.

For this project an autochthonous model with an intact immune system was required to observe the 'whole-body' effect of treatments. The TRAMP model provides a staged cancer progression, which models the human disease progression, is reproducible with little inter-animal variability and high penetrance, and is able to reproduce the hormone dependence of human prostate cancer (reviewed in *Huss, Maddison & Greenberg, 2001; Jeet, 2010; Grabowska et al., 2014*).

Previous studies on parthenolide in prostate cancer

In vitro studies into PTL's anti-tumour mechanism in prostate cancer have shown that inhibition of the NF-κB pathway is a common tool for parthenolide to

radiosensitise prostate cancer cells (*Sun et al., 2010; Sun et al., 2007*). Further studies have demonstrated that PTL selectively exhibits a radiosensitisation effect on prostate cancer cells (PC3) but not on normal prostate epithelial cells (*Sun et al., 2010; Xu et al., 2013*). This radiosensitisation of cancer cells is a mechanism which is yet to be thoroughly explored outside of prostate cancer cell lines and supports the concept of using the intrinsic differences in the redox status of cancer cells and normal cells as targets for selective cancer killing.

In vivo studies into PTL's anti-cancer action in prostate cancer are limited, but have shown that PTL and DMAPT can significantly reduce prostate tumour development in xenograft models (*Kawasaki et al., 2009; Sun et al., 2010; Xu et al., 2013; Shanmugam et al., 2006; Shanmugam et al., 2010*). DMAPT has also been shown to significantly enhance radiotherapeutic ability against prostate tumours in xenograft mice, in addition to reducing radiation-induced mitochondrial damage in healthy prostate and bladder tissues. This indicates the ability of PTL and its derivatives to radiosensitise prostate tumour tissues, while increasing radioresistance in healthy cells. This thesis is the first to study the anti-cancer effects and selective radiosensitisation proterties of PTL in an autochthonous model of prostate cancer.

Aims and hypotheses

PTL has been shown to have anti-cancer properties in several cancer models *in vivo*. With respect to prostate cancer, prior work has demonstrated that PTL can reduce growth rates and induce cell death in prostate cancer cell lines but does not have the same effect on non-cancerous prostate cell lines. PTL has been shown to slow tumour development in xenograft models of prostate cancer. In order to determine if PTL holds significant promise as a prostate cancer chemo-preventive, it is important to test PTL in a cancer model where a normal prostate develops and then progresses through the different stages of tumorigenesis to become a solid tumour, as occurs in human cancer. Examining the effects of PTL on tumorigenesis in an autochthonous model of prostate cancer provides this continuum of tumour development along with the complex and changing tumour microenvironment during the different stages of carcinogenesis.

1) Aim: To determine if long-term PTL treatment can prevent or slow down prostate tumour formation.

   Hypothesis: PTL will increase time to tumour development in The TRAMP model of prostate cancer.

PTL has also been shown to increase the anti-cancer effects of radiotherapy in prostate cancer cell lines and in xenograft tumours in immune-compromised mice. In a clinical setting, both tumour and normal prostate tissue, as well as surrounding normal tissues can be damaged by radiation. The radiomodulating effects of PTL have not been examined in a model where both healthy and tumour tissues are irradiated at the same time. Cell signalling between irradiated

and unirradiated cells and a functioning immune system play key roles in radiation-induced damage and DNA repair mechanisms. Examining the selective radiosensitisation of PTL in a model of prostate cancer where the prostate is *in situ* and surrounded by normal tissues subject to collateral radiation damage will provide important pre-clinical data towards the use of PTL as a radioprotector in radiotherapy treatment.

2) Aim: To determine if PTL acts as a differential radiosensitiser during radiotherapy.

   Hypothesis: PTL will increase the tumour kill and reduce damage to normal tissues after high dose radiation in the TRAMP model of prostate cancer.

Chapter 2: Methods

Chemical purity

All chemicals used in the studies described in this thesis were reagent grade unless otherwise specified.

Mice

Ethics approval for this study was obtained from the Flinders University Animal Welfare Committee and the SA Pathology/Central Adelaide Local Health Network Animal Ethics Committee. Approval for TRAMP mouse studies was also obtained from the Flinders University Institutional Biosafety Committee (IBC) in accordance with the Australian Gene Technology Regulations, 2001. All experimental C57BL/6J mice were purchased from the Australian Animal Resources Centre (Perth, Australia). The TRAMP mouse model was originally described by Greenberg et. al. (1995). TRAMP mice contain a PB-SV40 TAg transgene which uses a probasin promoter which is switched on at puberty in the prostate and which induces high grade PIN (prostatic intra-epithelial neoplasia) and/or well differentiated prostate cancer by 16 weeks of age. Non-prostate TRAMP tissues are normal. All experimental TRAMP mice were obtained from a breeding colony in the Flinders Medical Centre Animal Facility (Bedford Park, South Australia). Clinical records were maintained for all experimental mice and a scoring matrix based on observations such as weight loss, hunching, ruffled fur and sunken eyes was used to determine when animals should be euthanised. All mice were housed in micro-isolator cages with 12 h

light/dark cycles. Food (Rat and Mouse Pellets (irradiated), Specialty Feeds, Glen Forrest, Australia, Table 2-1) and water were provided *ad libitum*.

Table 2-1: Nutritional information for Specialty Feed Rat and Mouse feed stock used in the Flinders University Animal Facility

Nutritional Parameters	*Specialty feed: Irradiated Rat and Mouse Cubes*
Crude Protein	20.0%
Crude Fat	4.8%
Crude Fibre	4.8%
Digestible Energy	14.0 MJ/kg
Ingredients	Wheat Barley Lupins Soya meal Fish meal Mixed vegetable oils Canola oils Salt Calcium carbonate Di-calcium phosphate Magnesium oxide Vitamin and mineral premix

Maintenance of the TRAMP mouse colony

TRAMP mice were originally obtained from Prof Wayne Tilley (Adelaide University). FVB and C57BL/6J mice for breeding came from breeding colonies in the Flinders Medical Centre Animal Facility. TRAMP mice were bred using hemizygous female C57BL/6J TRAMP mice (C57BL/6J-Tg(TRAMP)8247Ng) crossed to non-transgenic male FVB or C57BL/6J mice: producing both transgenic and non-transgenic offspring ((C57BL/6J-Tg(TRAMP)8247Ng × FVB)F1 or (C57BL/6J-Tg(TRAMP)8247Ng ×C57BL/6J)F1).

Breeding of experimental TRAMP mice

All experimental transgenic mice used were TRAMP × FVB F1 mice. Breeding of TRAMP mice was performed at the Flinders University School of Medicine Animal Facility where the mice were bred synchronously. Breeder pairs were 'teased' by placing the male and female in the same cage with physical separation for 3 days. On the 4th day the physical barrier was removed and breeding pairs were co-caged for 4 days to allow time for mating to occur. Females were checked twice daily and removed where a vaginal plug was observed. Using this strategy, mice in each cohort were born between 1-4 days of each other.

Screening for the TRAMP transgene

Mouse ear notches were taken at 4 weeks of age for genotype determination. DNA was extracted using an alkaline lysis method. The ear tissue was placed in a 0.5 mL tube with 75 µL of alkaline lysis buffer (10 mL sterile water, 14 µL of 50% sodium hydroxide and 14 µL of 0.5 M EDTA (pH 8)) and then heated to 95°C for 30 min, before cooling at 4°C for 15 min. Tubes were then briefly pulse centrifuged before the addition of 75 µL of 40 mM Tris-HCL and homogenisation by pipette. Samples were stored at 4°C.

The transgenic status of mice was determined by polymerase chain reaction (PCR) based on the protocol published by Hurwitz *et al. (2001)*. Briefly, the TRAMP transgene was detected using PB-1-For (located in the probasin promoter region) and TAg-Rev (located in the SV40 TAg region) primers (Appendix B: PCR Primers) to amplify a 600 bp product. The TAg primers will only

amplify product if the transgene is in the germline DNA. DNA amplifiability was determined by amplification of a 500 bp portion of the mouse β casein (MβC) gene using MβC-For and MβC-Rev primers (Appendix B: PCR primers). PCR was performed in Platinum *Taq* buffer (Invitrogen, USA), 25 mM $MgCl_2$, 10 mM dNTP (Fisher Biotech, Australia) and 1 U of Platinum *Taq* DNA polymerase (Invitrogen, USA). MβC and TRAMP primers were used at 5 and 10 pmoles/µL respectively. The cycling conditions for the PCR were 3 min at 94°C to activate the Platinum *Taq*, 40 cycles of 1 min at 94°C, 2 min at 60°C, 3 min at 72°C, with a final extension of 5 min at 72°C.

Initially a 2% agarose gel and electrophoresis was used to visualise PCR amplicon size and hence genotype. Subsequently, the MβC primer set was replaced with Mus6 + and Mus6 - (Appendix B: PCR Primers), which amplify a 370 bp region of the mouse Ig (immunoglobulin) gene, resulting in an increased size difference between the TRAMP-specific amplicon and the control amplicon, allowing detection using melt curve analysis. The PCR conditions were altered to include 10× *SYBR*® green and Mus6 primers at 100 ng/µL each. At the conclusion of the cycling conditions above, the temperature was reduced to 55°C and held for 1 min, then melt curve analysis was performed at 0.5°C increments up to a temperature of 95°C (Qiagen Rotor-Gene Q Thermal Cycler). The negative derivative of change in fluorescence was plotted as a function of temperature to discriminate between genotypes. The peak melt temperature for the control Ig amplicon is observed at 84°C and the TRAMP specific amplicon at 88°C. Positive TRAMP control DNA samples were taken from TRAMP tumour tissue, negative

controls were extracted from non-transgenic TRAMP litter-mates and C57BL/6J mice.

Administration of parthenolide to mice

PTL (Sigma-Aldrich, Castle Hill, Australia) was kept in aliquots as a stock solution at 100 mg/mL in absolute ethanol (Sigma-Aldrich) and stored at -20°C. On the day of treatment, PTL stock was diluted 10-fold to form a slurry solution in sterile saline (0.9% Sodium Chloride for Irrigation, Baxter Healthcare, Old Toongabbie, Australia). DMAPT (obtained from Dr Peter Crooks, University of Arkansas for Medical Sciences, Little Rock, USA) was stored at -20°C. On the day of treatment, DMAPT was dissolved at 20 mg/mL in sterile water. C57BL/6J or TRAMP mice were physically restrained by hand and gavaged using a 0.5 mL syringe and 20 Gauge (2.0 mm × 38 mm) straight stainless steel gavage needle. Control animals received an identical volume per weight of vehicle controls.

In vivo long-term treatment studies

For long-term studies, 6 week old male TRAMP mice were treated by oral gavage thrice weekly on a continuing basis until palpable tumour detection.

Animal monitoring and detection of palpable prostate tumours

At the time of treatment mice were assessed visually for general indications of well-being and manually for palpable prostate tumours. To assess mice for palpable tumours, animals were restrained by hand and the lower abdominal region was palpated for masses. Detection of a large palpable mass resulted in

the euthanasia of the mouse within 72 h by CO_2 asphyxiation. No palpable tumours were detected in any non-transgenic litter-mates.

Tissue excision, measurement and blood collection

The tumour, remaining genitourinary tract (GUT), para-aortic lymph nodes, testes, bladder, descending colon (including rectum), spleen, liver, kidneys, lung, brain and heart were removed. All tumours, primary prostate and distant metastatic, were weighed using benchtop digital scales. All tissues were embedded in Tissue-Tek® Optimal Cutting Temperature (OCT) cryoprotectant (Sakura® Finetek) and rapidly frozen on dry ice. Tissues were stored at -80°C for subsequent analysis. Bone marrow was isolated by flushing a single femur with 2 mL PBS and dispersing into 2 % (w/v) formaldehyde (Sigma-Aldrich) at 4°C. Blood was collected directly into EDTA/Heparin-free tubes (BDMicrotainer®) and allowed to coagulate at room temperature for between 1-4 h. The blood was centrifuged at 800 g for 15 min and the serum collected. Sera were stored at -80°C.

In vivo irradiation studies

For irradiation studies, 16 week old male TRAMP or C57BL/6J mice were treated by oral gavage three times over one week and irradiated 24 h after the final treatment.

Irradiation procedures and dosimetry

All animal irradiations were performed using either a Varian 600CD Linear Accelerator, 6MV X-ray beam, located at the Royal Adelaide Hospital or a Precision X-Ray Inc. X-RAD 320 Cabinet irradiator, located at the Flinders University School of Medicine Animal Facility.

For irradiation at the Royal Adelaide Hospital, mice were transported to and from the Flinders University School of Medicine Animal Facility inside their usual cages, in a climate controlled vehicle. The journey takes approximately 30 min in each direction. Mice were restrained in a Perspex holder (0.5 cm thick) designed for the purpose, during irradiation, or sham irradiation (described in detail in *Hooker et al., 2004*). Irradiations and dosimetry were performed by Prof. E. Bezak (Medical Radiation, School of Health Sciences, University of South Australia, Adelaide, South Australia). Irradiation was performed using a Varian 600CD Linear Accelerator, 6MV X-ray beam, for experiments where mice were administered 6 Gy. The dose-rate was 1 Gy/min, FSD (focus to skin distance) of 100 cm (Build-up 1.2 cm^3). Calibrations of dose-output were performed by Prof. E. Bezak. The calibration of the Varian 600CD Linear Accelerator was made according to the International Atomic Energy Agency's technical report on Absorbed Dose Determination in External Beam Radiotherapy (Series No. 398) (*2000*).

For irradiation at the Flinders University School of Medicine Animal Facility mice were transported to the X-ray room inside their usual cages. Mice were restrained in a Perspex holder (0.5 cm thick) designed for the purpose, during

irradiation, or sham irradiation. Irradiation was performed using a Precision X-Ray Inc. X-RAD 320 Cabinet irradiator, for experiments where mice were administered 6 Gy or 10 mGy. For 6 Gy irradiation the dose-rate was 2.2 Gy/min, with a 300 kV 13 mA beam and FSD of 62 cm. For 10 mGy irradiation the dose-rate was 16.7 mGy/min, with a 200 kV 1 mA beam and FSD of 62 cm. The dose calibration of the orthovoltage 300 kV X-ray beam produced by the X-RAD 320 was carried out according to the Institute of Physics and Engineering in Medicine and Biology (IPEMB) protocol, and were performed by Dr. T. Rutten (Medical Physicist, Royal Adelaide Hospital).

Tissue excision, measurement and prostate micro-dissection

Following irradiation, mice were euthanised by CO_2 asphyxiation at appropriate analysis time-points. The prostate, testes, bladder, descending colon (including rectum), spleen, liver, and kidneys were removed. The prostate was then weighed and photographed. All tissues were embedded in OCT (Tissue-Tek®) cryoprotectant and rapidly frozen on dry ice. Tissues were stored at -80°C for subsequent analysis. Bone marrow was isolated by flushing a single femur with 2 mL PBS and dispersing into 2 % (w/v) formaldehyde (Sigma-Aldrich) at 4°C. Prior to analysis, the prostate was thawed on ice cold PBS then dissected under a microscope into the anterior, ventral and dorsolateral lobes, and immediately re-embedded in OCT (Tissue-Tek®) cryoprotectant as individual lobes.

Ex vivo prostate tissue culture

Human ethics approval was obtained from the Adelaide University Human Ethics Committee and the Southern Adelaide Clinical Human Research Ethics Committee.

Fresh prostate cancer specimens were obtained with written informed consent from men undergoing robotic radical prostatectomy at St Andrew's Hospital, Adelaide, through the Australian Prostate Cancer BioResource. A 6 mm core of tissue was dissected into 1 mm^3 pieces and cultured in triplicate on a pre-soaked gelatin sponge (Johnson and Johnson, New Brunswick, NJ) in 24-well plates containing 500 µL RPMI 1640 with 10% FBS, antibiotic/antimycotic solution (Sigma-Aldrich, St Louis, MO), 0.01 mg/mL hydrocortisone, 0.01 mg/mL insulin (Sigma). Tissues were treated by adding vehicle or DMAPT directly into the culture medium. Tissues were cultured at 37°C for 48 h then formalin-fixed and paraffin embedded before being analysed by immunohistochemistry for the proliferative marker Ki67 and apoptosis marker cleaved caspase-3.

Haematoxylin and Eosin staining

Four micrometre sections of frozen prostate samples were cut on a cryostat (Cryocut CM1850 UV, Leica, USA) and mounted on APES (3-aminopropyltriethoxysilane) coated slides (Sigma-Aldrich, Castle Hill, Australia) (slides were coated according to the protocol described in Appendix C: Solutions). Sections were immediately fixed in formal alcohol (1:4 concentrated formalin and absolute ethanol) upon cutting and remained in fixative until staining. Slides were washed in a bath with running tap water, stained in Harris

Haematoxylin (5 min) and washed again in tap water. The haematoxylin was differentiated (process of over-staining followed by selective removal of non-specific stain, to ensure saturation of specific binding) with 1% acid ethanol and washed in tap water. Sections were blued (arrest of differentiation (by alkali) resulting in change in colour of haematein (oxidised derivative of haematoxylin) to blue hue) using lithium carbonate and washed in tap water before staining with eosin (5 sec). Slides were then washed and dehydrated serially in tap water, 3× ethanol, 2× xylene, before coverslipping with Leica CV Mount (Leica Microsystems).

Histopathology grading of TRAMP prostate tissue

Two non-consecutive sections per animal were taken from OCT embedded dorsolateral prostate and stained using haemotoxylin and eosin as described above. Slides were coded such that sections from individual mice were scored together and that the identifying mouse number and treatment were blinded to the scorer.

Sections were simultaneously scored for histopathology grade using the system described by Berman-Booty *et. al.* (*2012*). Briefly this grading scheme describes a method of determining a distribution-adjusted lesion score for which the numerical grade determined can be analysed statistically. Firstly the most severe histological lesion from seven increasing grade categories is identified, followed by an estimation of the lesion's distribution. The lesion is then assigned to an integer of 0-21: based on a score of the severity, ranging from 0-7, and each

score categorised as having a distribution of focal (1-3 isolated lesions), multi-focal (3 or more lesions, up to approximately 30% gland involvement), or diffuse (more than 30% gland involvement) (Table 2-2). Secondly the most common histological lesion is identified and assigned a lesion integer of 1-21 in the same manner as scoring the most severe lesion. The final PIN grade is obtained by adding the scores for the most severe and most common lesions together, eg most severe: 18, most common: 12, final grade: 30.

Table 2-2: Scoring matrix for determination of the adjusted lesion score from the lesion grade and distribution

Lesion grade	Distribution	Adjusted lesion score
0	Diffuse	0
1	Focal	1
1	Multifocal	2
1	Diffuse	3
2	Focal	4
2	Multifocal	5
2	Diffuse	6
3	Focal	7
3	Multifocal	8
3	Diffuse	9
4	Focal	10
4	Multifocal	11
4	Diffuse	12
5	Focal	13
5	Multifocal	14
5	Diffuse	15
6	Focal	16
6	Multifocal	17
6	Diffuse	18
7	Focal	19
7	Multifocal	20
7	Diffuse	21

Immunofluorescent detection of proteins in frozen tissue sections

Frozen tissue sections were prepared as described for Haematoxylin and Eosin staining, then fixed in 2% formaldehyde (10 min) followed by glycine washes (3 × 2 min, 0.1 M glycine) to quench unreacted aldehyde groups. Sections were washed (3 × 5 min, PBST), permeabilised (1% Triton-X100 in PBS), washed (3 × 5 min, PBST), and blocked for 1 h at room temperature (5% goat serum + 0.1% Tween-20 in PBS) before incubation with a primary antibody (Table 2-3) in 1% goat serum overnight at 4°C. Sections were washed in PBST (4 × 2 min) and incubated for 1 h at 37°C with a 1/300 dilution of Alexa Fluor® 488-conjugated goat anti-rabbit antibody (A11008, Invitrogen) in 1% goat serum. Sections were then washed in PBST (6 × 2 min) and coverslipped with Vectashield® (Vector Laboratories) containing DAPI.

For staining of TRAMP dorsolateral prostate sections, directly conjugated primary antibodies were used. When conjugated primary antibodies were used staining occurred as above, however after the primary antibody incubation sections were then washed in PBST (6 × 2 min) and coverslipped with Vectashield® (Vector Laboratories) containing DAPI.

Table 2-3: Primary antibodies and concentrations used in immunofluorescent staining protocols

Target	Conc. Used	Details	Company	Number
AR	1/200	Rabbit monoclonal anti-Androgen Receptor antibody [EPR1535(2)]	Abcam	ab133273
AR	1/100	Rabbit monoclonal Anti-Androgen Receptor antibody [EPR1535(2)] (Alexa Fluor® 488)	Abcam	ab194194
CD31	1/50	Rabbit polyclonal anti-CD31 antibody	Abcam	ab28364
Collagen IV	1/100	Rabbit polyclonal anti-Collagen IV antibody	Abcam	ab6586
Fibronectin	1/100	Rabbit polyclonal anti-fibronectin antibody (H-300)	Santa Cruz Technology	sc-9068
Integrin β1	1/100	Rabbit monoclonal anti-Integrin beta 1 antibody [EPR16895]	Abcam	ab179471
Laminin	1/100	Rabbit polyclonal anti-Laminin antibody	Abcam	ab11575
MMP2	1/100	Rabbit polyclonal anti-MMP2 antibody	Abcam	ab37150
NF-κB	1/100	Rabbit monoclonal NF-κB p65 (D14E12) XP® antibody	Cell Signalling Technology	8242
NF-κB	1/100	Rabbit monoclonal NF-κB p65 (Ser536) (93H1) (Alexa Fluor® 488 Conjugate) antibody	Cell Signalling Technology	4886
SV40 TAg	1/100	Rabbit polyclonal SV40 TAg antibody (v-300)	Santa Cruz Technology	sc-20800
γH2AX	1/100	Rabbit monoclonal phospho-Histone H2AX (Ser139) (20E3)(Alexa Fluor® 488 Conjugate) antibody	Cell Signalling Technology	9719

Dual immunofluorescent detection of protein in frozen tissue sections

Frozen tissue sections were prepared as described above, including a primary antibody and Alexa Fluor® 488-conjugated goat anti-rabbit antibody (A11008, Invitrogen). Following secondary antibody incubation, sections were washed in PBST (6 x 2 min), permeabilised (1% Triton-X100 in PBS), washed (3 × 5 min, PBST), and blocked for 1 h at room temperature (5% goat serum + 0.1% Tween-20 in PBS) before incubation with a second primary antibody (Table 2-3) in 1% goat serum overnight at 4°C. Sections were washed in PBST (4 × 2 min) and incubated for 1 h at 37°C with a 1/300 dilution of Alexa Fluor® 594-conjugated goat anti-mouse antibody (R37117, ThermoFisher) in 1% goat

serum. Sections were then washed in PBST (6 × 2 min) and coverslipped with Vectashield® (Vector Laboratories) containing DAPI.

Immunofluorescent detection of apoptosis by TUNEL in frozen tissue sections

Staining for apoptosis was carried out using the TUNEL (Terminal deoxynucleotidyl transferase dUTP nick end labelling) In Situ Cell Death Detection Kit, Fluorescein (Roche). Frozen tissue sections were prepared as described for Haematoxylin and Eosin staining, then fixed in 1% formaldehyde (30 min) followed by PBS washes (3 × 10 min), permeabilisation (1% Triton-X100, 1% Sodium Citrate dihydrate in PBS) and PBS washes (3 x 5 min). Sections were incubated with TUNEL reaction solution (45 µL TUNEL label solution, 5 µL TUNEL enzyme solution) for 1 hour at 37°C, then washed in PBS (3 x 5 min). Slides were then coverslipped with Vectashield® (Vector Laboratories) containing DAPI.

Positive controls comprised incubating control sections with 100 µL DNase solution (262.5 µL water, 16.25 µL 1M Tris, 32.5 µL BSA (10 mg/mL, Sigma-Aldrich), 13 µL DNase I (75 Kunitz units/mL, Sigma-Aldrich)) for 10 min at room temperature immediately prior to TUNEL reaction solution incubation. Negative controls comprised sections in a TUNEL reaction mix lacking the TUNEL enzyme solution.

Microscopy

Images of each tissue section were captured with the use of an external 17 megapixel digital camera (DP73; Olympus, Japan) on a BX63 Automated

Fluorescence Microscope (Olympus, Japan) and controlled by CellSens Dimensions Software (Olympus, Japan). Both Brightfield (for analysis of TRAMP pathology) and fluorescence (for analysis of apoptosis and protein expression) images were captured using the same microscope and camera. Images were stored as 8-bit TIFF (Tagged Image File Format) files. For TRAMP dorsolateral prostate pathology grading, the entire tissue section was imaged using a 20× objective lens and stitched together using CellSens Dimensions Software (Olympus, Japan) to form one large image. For analysis of spleen and prostate sections, 30 random, non-overlapping images (per mouse from two non-consecutive sections) were taken using a 20× objective lens. For analysis of colorectal sections, 50 random, non-overlapping images (per mouse from two non-consecutive sections) were taken using a 40× objective lens. Images were analysed using custom pipelines (Appendix D: CellProfiler™ pipelines). CellProfiler™ analysis pipelines were designed to identify frequency of positive cells (for apoptosis and SV40 TAg analysis) or to measure fluorescence intensity (for quantitation of protein expression).

Statistical methods

Statistical analysis of data was performed using GraphPad Prism Statistics Version 7.0 (GraphPad Inc, USA). Calculations of power and sample size were made using G*Power 3.0.10 (*Faul et al., 2007*).

Two-tailed Independent Samples T-tests were used to compare the means of two normally distributed groups. Equality of variance was assessed using the

Levene's test and normality by quantile-quantile (Q-Q) plots. Data which was not normally distributed or ordinal data, such as adjusted PIN lesion grade (0-42) was compared using the Mann-Whitney *U*-test. To assess the relationship between two sets of data, a linear regression and correlation analyses were used. For studies of time-to-palpable tumour, Kaplan-Meier analysis was performed and a survival plot generated. Distribution differences in time-to-palpable tumour between groups were compared using log-rank test (Mantel-Cox). Throughout the text and figures, means are given ± the standard deviation (SD), unless otherwise stated. All p-values less than 0.05 were considered significant.

Chapter 3: Selection and development of methods and analysis

Measures of TRAMP prostate development pathology

Measurement of weight and volume of the structures within the genourinary tract (GUT) of the TRAMP mouse are used to reflect differential rates of cancer progression. Progression can also be monitored and assessed longitudinally using imaging techniques and physical palpation of tumours.

The protocol outlined by Hurwitz *et. al.* (*2001*) was used for the removal and micro-dissection of the GUT. The GUT (including the seminiferous vesicles and drained bladder) and prostate were weighed. GUT and prostate weights were normalized to body weight, given that both body weight and organ weight can be influenced by treatment. These measures of mouse and organ weights were made using a standard calibrated balance. Variation in this measure can be introduced by variation in how the organs are removed and prepared for weighing. To limit variation, GUT and prostates were removed and weighed immediately following euthanasia, prior to excision of other organs. Micro-dissection of prostate was performed by a single individual (K. Morel).

The longitudinal study of tumour development in TRAMP mice can be made using *in vivo* imaging techniques, time-to-palpable tumour and survival itself. *In vivo* imaging of cancer development can be made using a variety of methods (ultrasound, MRI, CT scans, bioluminescence) (reviewed in *Kaijzel, van der Pluijm & Lowik, 2007*). These imaging methods require mice to be anestheticised for accurate tumour identification and it was decided that for such a long-term

study which would require regular imaging of animals, the stress to the animals would be significant. In addition, survival as an endpoint was not considered to be ethically justified. Therefore, the endpoint of time-to-palpable tumour was used to assess tumour progression longitudinally. Time-to-palpable tumour has been used extensively in TRAMP studies as a marker of tumour progression, with the average interval between palpable tumour and cancer-related death measured at 4.1 weeks (± 2.2 weeks) (*Hsu et al., 1998*).

Prostate pathology analysis methods in the TRAMP model

Pathology analysis of the TRAMP model has utilised a wide range of nomenclature, scoring matrices and methods. Early in the development of the TRAMP model a system of pathology scoring was developed analogous to the Gleason prostate pathology scoring system, which is the standard clinical prostate pathology system (*Gingrich et al., 1999; Gleason & Mellinger, 1974*). A further refined system was developed by Kaplan-Lefko *et al.* (*2003*) and is now widely used for TRAMP pathology analysis. This system defines the distribution of six tiers of pathology grade (normal, PIN, well-differentiated, moderately-differentiated, poorly differentiated, and phylloides-like lesions). While this system offers descriptive definitions and appraisal of pathology extent, it does not provide a numerical scoring system to facilitate statistical analysis. The development of a semi-quantitative pathology scoring system for the TRAMP mouse, amenable to statistical analysis, was made by Suttie *at al.* (*2003*). This system, where a numerical score is assigned based on lesion distribution and the most advanced lesion type observed, yields a distribution-adjusted lesion score

amenable to non-parametric statistical analysis. While this method is semi-quantitative, allowing statistical analysis of tissue grading, it provides a score which is only informed by the most severe lesion type and does not consider the distribution of lesser, potentially more common, grades of pathology present within a sample. A further refined TRAMP pathology grading scheme has been most recently published which, acknowledging the advantages of the statistically amenable Suttie *et al.* (*2003*) grading method, also generates a numerical distribution-adjusted lesion score (*Berman-Booty et al., 2012*). To further refine the grading system, the scheme outlined by Berman-Booty *et al.* (*2012*) incorporates not only the most severe lesion and its distribution but also the distribution of the most common lesion, to give a single distribution-adjusted lesion score representative of the whole prostate tissue section.

For this thesis, it was determined that the Berman-Booty *et al.* (*2012*) method of tissue grading would provide the most informative assessment of TRAMP prostate pathology.

Development of image analysis methods

Platform choice and general approach

In order to assess endpoints within mouse tissue sections, an objective, repeatable and sensitive methodology was sought. Automated computer-assisted image analysis provides these capacities along with the ability to quantitatively, and in a high throughput manner, measure multiple parameters.

There are many available image analysis platforms, both proprietary and freely available. In determining the system most suitable; cost, user-control and minimal computer programming requirements were essential. CellProfiler™ is an open-source, freely available image analysis platform designed specifically for biologists. Developed at the Broad Institute of MIT and Harvard, the software is modular in nature and does not require a detailed knowledge of computer programming, although individual modules can be modified and tailored to specific functions or the code itself can be accessed and modified. It also offers the capacity to integrate with the popular image analysis program ImageJ (NIH). Using CellProfiler™, in combination with immunofluorescent techniques, analysis pipelines for apoptosis and protein expression analysis were developed. A general approach for analysis of fluorescence microscopy images was developed here (Figure 3-1) and was adapted for each fluorescence endpoint independently.

As methods were developed, various aspects of the analysis methodology were validated and optimised.

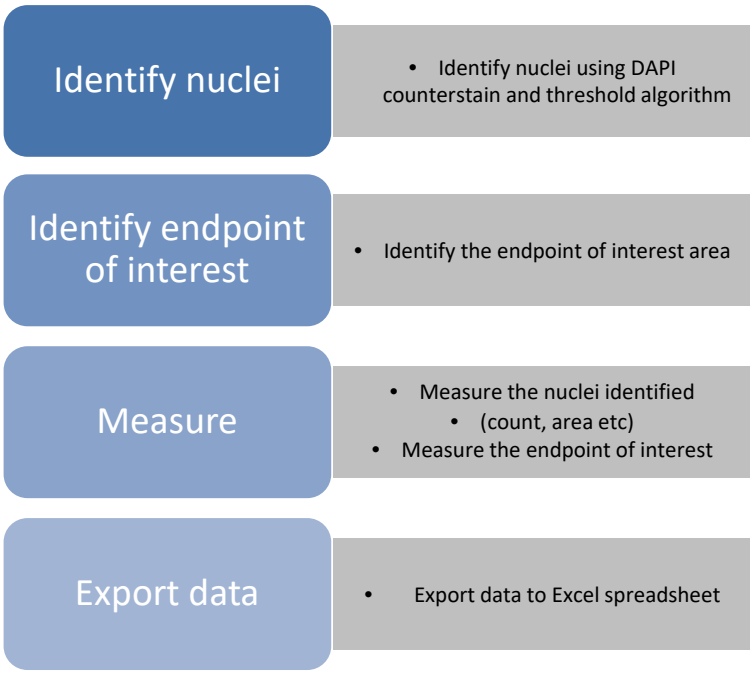

Figure 3-1: General outline of the approach used for image analysis using CellProfiler™

The basic CellProfiler™ analysis approach, developed for the measurement of endpoints within fluorescent images. For analysis of nuclear localised endpoints the nuclei area identified in step 1 was used to mask the image containing the endpoint of interest.

Development of an automated analysis for apoptosis within frozen mouse tissue sections

Numerous marker and methods for analysis of apoptosis are available. Methods, such as flow cytometry or mRNA expression analysis of apoptosis related genes, which are not amenable to *in situ* analysis, were not considered. Common *in situ* methods for analysis of apoptosis include detection of caspase-3, annexin V and nick end labelling. For analysis of apoptosis in mouse tissues, the fluorescein *in situ* cell death detection kit (Roche Diagnostics) was selected for use, given its robust nature. This kit utilises the TUNEL reaction in which the Tdt enzyme labels the free 3' hydroxyl termini of DNA (which are present during apoptosis) with

fluorescein-labelled dUTPs. Cells undergoing apoptosis were labelled with fluorescein and nuclei were counterstained with DAPI (Figure 3-2).

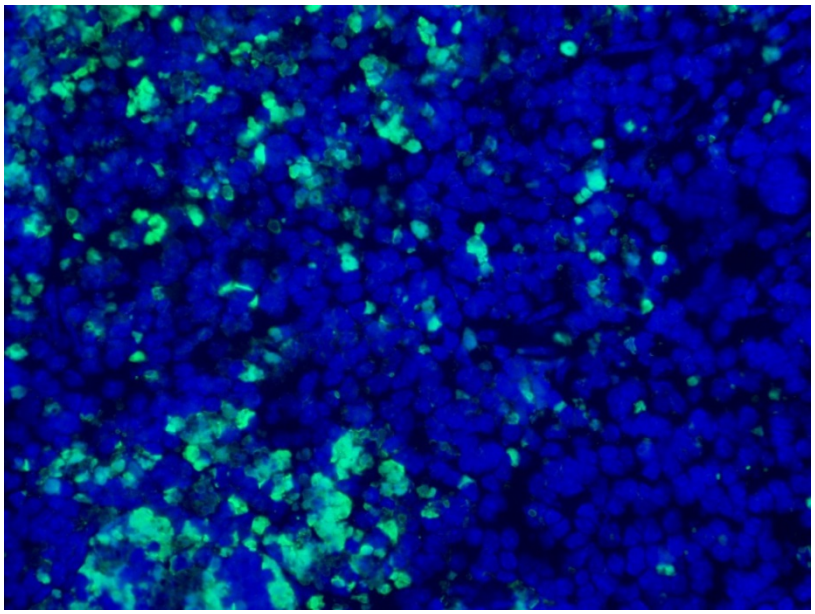

Figure 3-2: Representative TUNEL staining of C57BL/6J spleen following 6 Gy irradiation

Representative false-coloured image of TUNEL staining in C57BL/6J spleen sections 6 h after exposure to 6 Gy X-irradiation. TUNEL staining labels DNA nick-ends with fluorescein (green) and nuclei are counterstained with DAPI (blue).

Using CellProfiler™, an analysis method was constructed based on the outline given in Figure 3-1, and optimised using archival TRAMP and C57BL/6J spleen tissue. The animals used in this optimisation study were 12-16 weeks old and received either sham or 6 Gy X-irradiation.

The first step of the CellProfiler™ pipeline is to detect the nuclei from the DAPI image, which was carried out using the Otsu Global thresholding algorithm. This method measures the intensities of the pixels in the whole image and calculates a threshold using total mean and variance. Based on this threshold value each pixel is set to either 0 or 1 (i.e. background or foreground). While this method of

thresholding worked well for images that were mostly covered with cells, it was less effective in images with large regions of blank space, such as in non-tumour prostate tissues (Figure 3-3). It was determined that where there were limited objects in the images, the automatic threshold tended to be calculated as unreasonably low, resulting in a haloing effect around positive cell areas and false positive regions in the background.

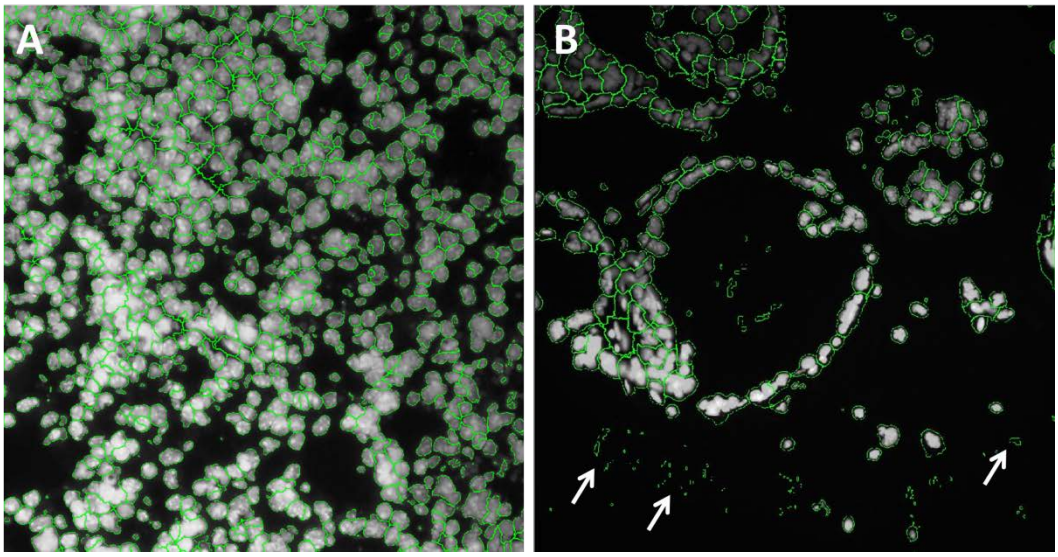

Figure 3-3: Otsu Global-based identification of cell nuclei by CellProfiler™ from the DAPI image channel

A) Representative image of accurate cell identification (A) and poor cell identification (B), where many of the cells have a haloing effect and there are false-positive regions in the background (white arrows).

To help improve the analysis, a lower limit on the threshold was included in the Otsu Global algorithm as a precaution in case the automatically calculated threshold is set too low. This lower limit was determined empirically by manually measuring the mean pixel intensity of approximately 10,000 cells to identify the normal pixel intensity range for all cells (Figure 3-4). Using this additional threshold setting CellProfiler™ identification of nuclei was significantly improved.

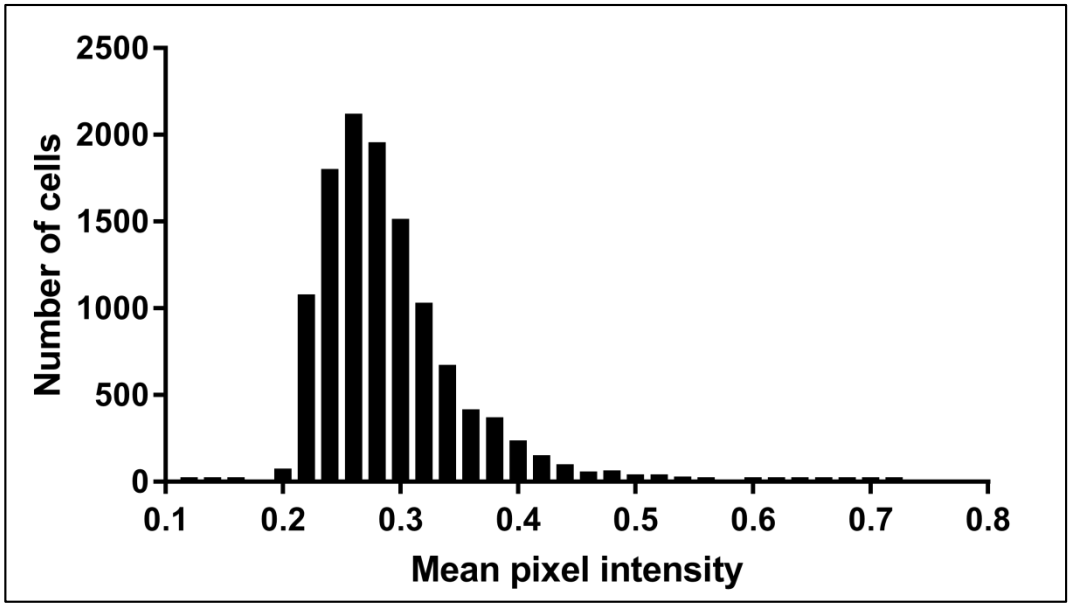

Figure 3-4: Pixel intensity histogram of DAPI-stained nuclei

The majority of nuclei were determined to have a pixel intensity greater than 0.2. This intensity was then used to set a CellProfiler™ threshold for more accurate nuclei detection in subsequent pipeline analyses.

In this initial study it was also noted that the segmentation of individual nuclei by CellProfiler™ varied significantly depending on the tissue type and thickness of individual sections. In spleen tissues and regions of high grade PIN and adenocarcinoma in prostate tissues, cells were packed too densely for the analysis software to identify individual cells, resulting in an analysed cell count significantly lower than the true value. To overcome this issue the segmentation of individual nuclei was rejected in favour of identifying total nuclei area and total apoptotic area, above a defined pixel intensity threshold. These areas were then used to calculate the apoptosis frequency as a percentage of total DAPI area. Where required for some analyses, an estimated cell count was calculated from the total DAPI pixel area based on mean pixel area of known cell types.

Determining the area of TUNEL staining, within the identified nuclei areas was also made using the Otsu Global algorithm with a set pixel intensity threshold. As with the nuclei identification, thresholds were determined empirically based on the staining within an experiment and kept constant through analysis of a single experiment. Changing the intensity threshold used to determine TUNEL-positive area from one set of images to the next has the obvious effect of altering the mean area, however the differences between individual animals within each experiment remained largely unaffected and different experiments were never directly compared without re-staining and imaging of tissues.

This optimisation finalised the CellProfiler™ apoptosis analysis pipeline (Figure 3-5) which was subsequently used for analysis of apoptosis in C57BL/6J and TRAMP prostate (Figure 3-6) and spleen tissue (Figure 3-7).

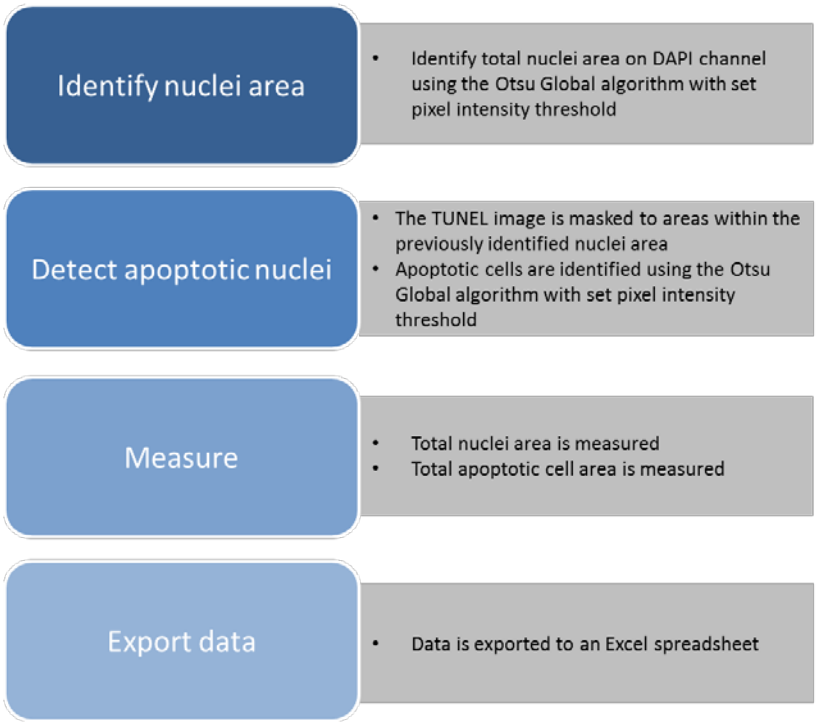

Figure 3-5: Outline of optimised analysis of apoptosis from TUNEL-stained tissue sections using CellProfiler™

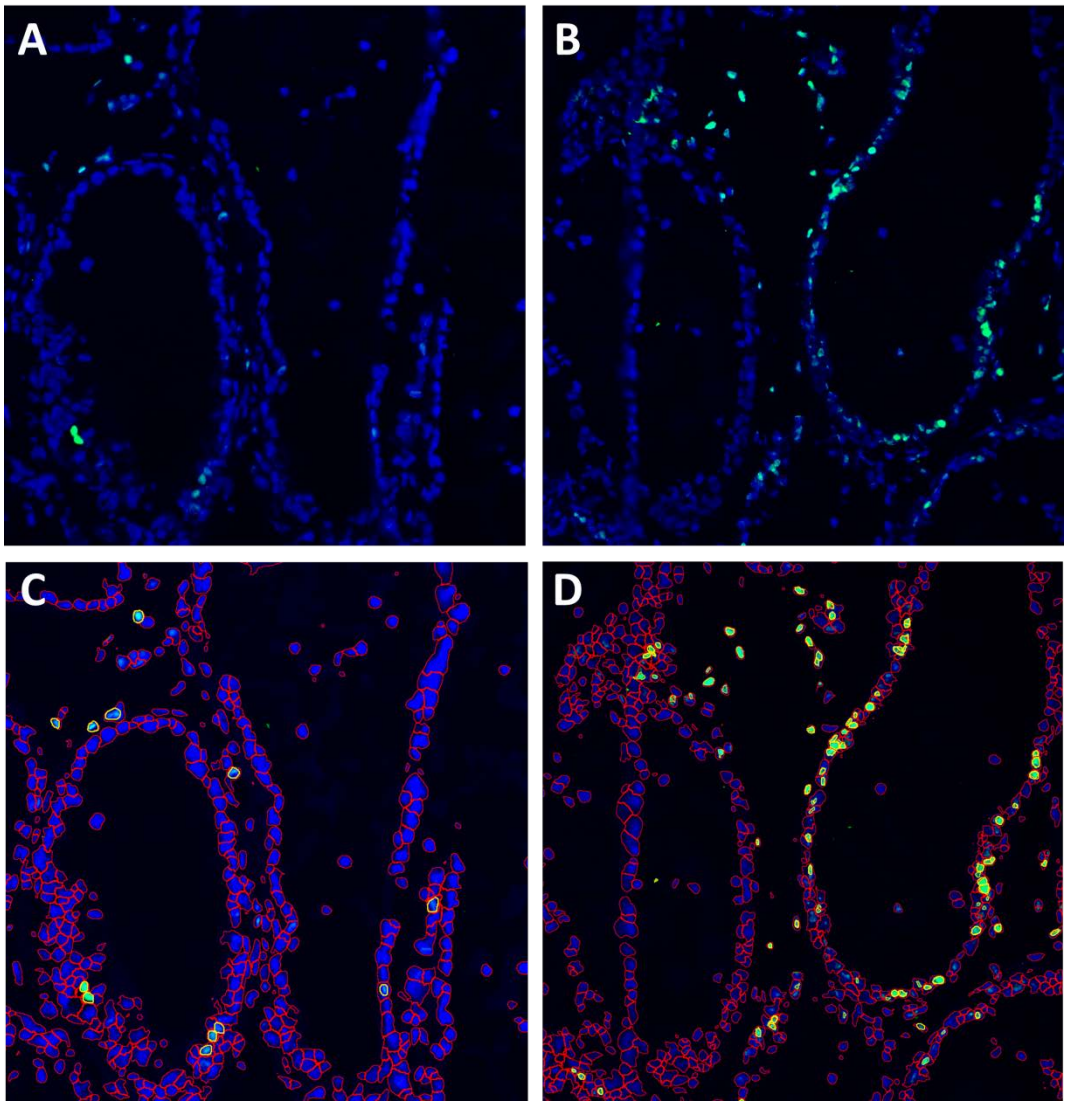

Figure 3-6: CellProfiler™ analysis for apoptosis in C57BL/6J dorsolateral prostate

Representative false-coloured image highlighting apoptosis (green) and cell nuclei (blue) in (A) sham and (B) 6 Gy-irradiated C57BL/6J dorsolateral prostate. CellProfiler™ identification of nuclei area (red outline) and apoptotic area (yellow outline) in (C) sham and (D) 6 Gy-irradiated C57BL/6J dorsolateral prostate.

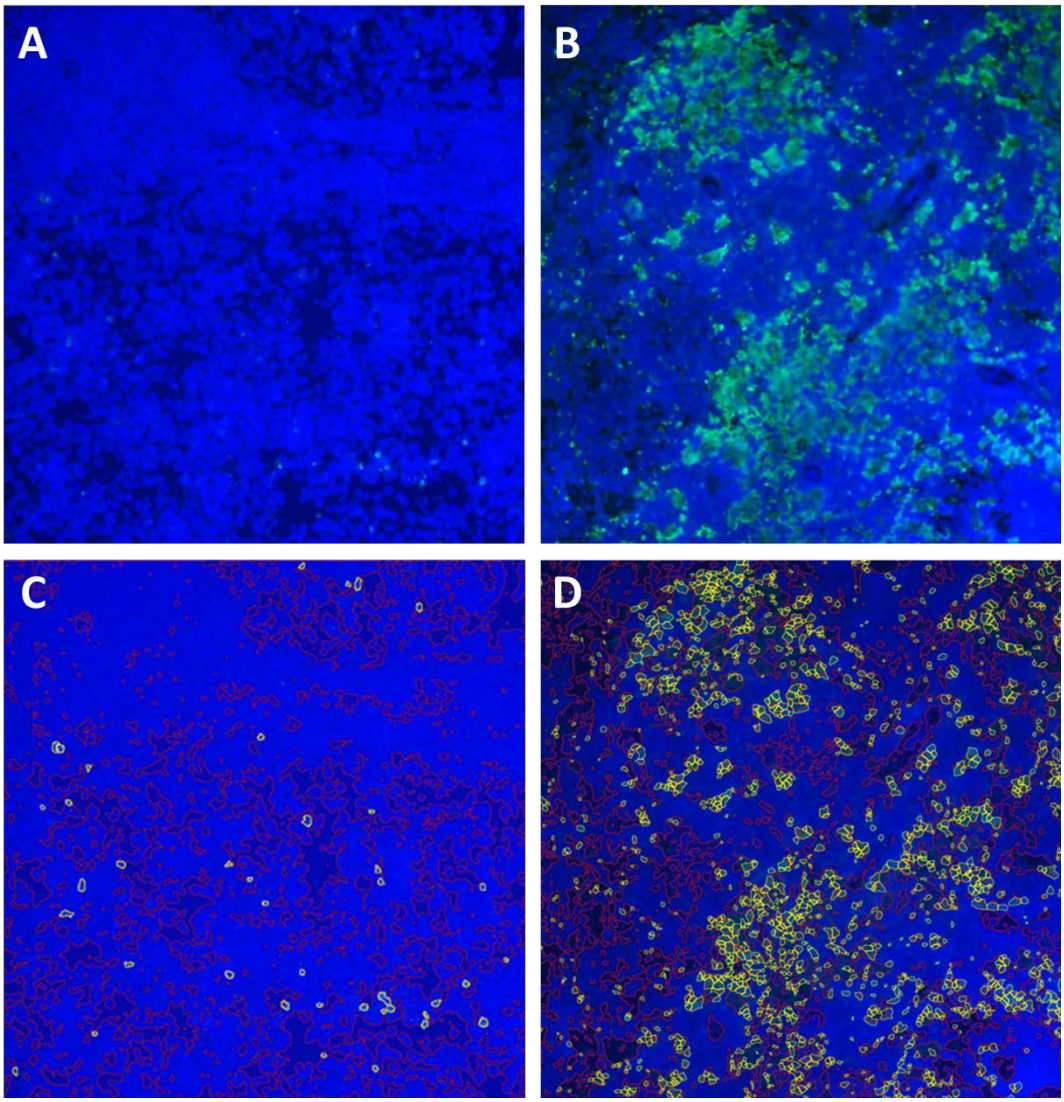

Figure 3-7: CellProfiler™ analysis for apoptosis in C57BL/6J spleen

Representative false-coloured image highlighting apoptosis (green) and cell nuclei (blue) in (A) sham and (B) 6 Gy-irradiated C57BL/6J spleen. CellProfiler™ identification of nuclei area (red outline) and apoptotic area (yellow outline) in (C) sham and (D) 6 Gy-irradiated C57BL/6J spleen.

Following the initial development of an apoptosis pipeline and using the optimised analysis method, the number of fields required to reliably determine an apoptotic frequency was established. A running mean was established from the cumulative frequency of apoptotic area to nuclei area, with successive fields. With increasing field number this frequency becomes more stable and empirically it was determined that approximately 30 fields at 20 x (objective) magnification provided the best representative apoptotic frequency for both spleen and dorsolateral prostate analysis (Figure 3-8). Analysis of fewer than 30 fields per animal would not be able to provide a representative apoptotic value, while using more than 35 fields would not significantly alter the mean frequency.

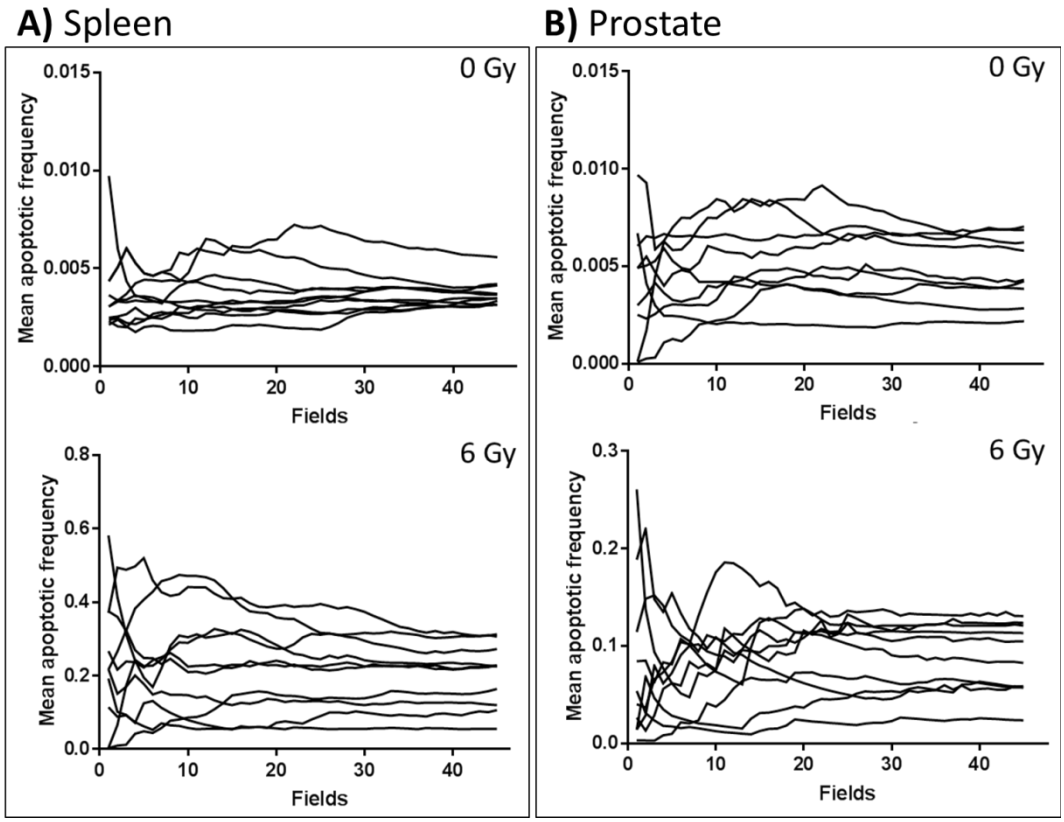

Figure 3-8: Cumulative apoptotic frequency in C57BL/6J tissues

Cumulative apoptotic frequencies in un-irradiated and irradiated C57BL/6J (A) spleen and (B) dorsolateral prostate tissue sections with increasing fields examined.

TUNEL staining in the TRAMP mouse prostate

While numerous studies have used TUNEL staining to identify apoptotic cells in TRAMP prostate tissues, it has recently been reported that widespread false-positive signal may occur in frozen TRAMP prostate tissues (*Lawrence et al., 2013a*). The false-positive signal, which was not observed in prostate tissues of non-transgenic litter-mates, co-localised with large SV40 TAg expression and was apparent in several different commercially available kits. (*Lawrence et al., 2013a*). This staining issue reportedly increases with age in TRAMP mice, with false-positive staining observed to be infrequent in young TRAMP mice (6 weeks old) but becoming more diffuse in the dorsolateral prostates of older (16 weeks old) mice. Given that the tissues examined in this thesis were all to be from mice 17 weeks of age or older, it was determined that TUNEL staining would be inappropriate to use to identify apoptosis in TRAMP prostate sections.

To confirm the observation that TUNEL staining may result in false positive results in TRAMP prostate tissues, several dorsolateral prostate tissue sections from TRAMP mice bred for the experiments in this thesis were examined for evidence of abnormal staining. False-positive TUNEL staining was observed in a large proportion of the TRAMP prostate sections inspected (Figure 3-9A). As was also described by Lawrence et al (*2013a*), this false-positive staining was not observed in the prostate tissues of non-transgenic mice (Figure 3-9B).

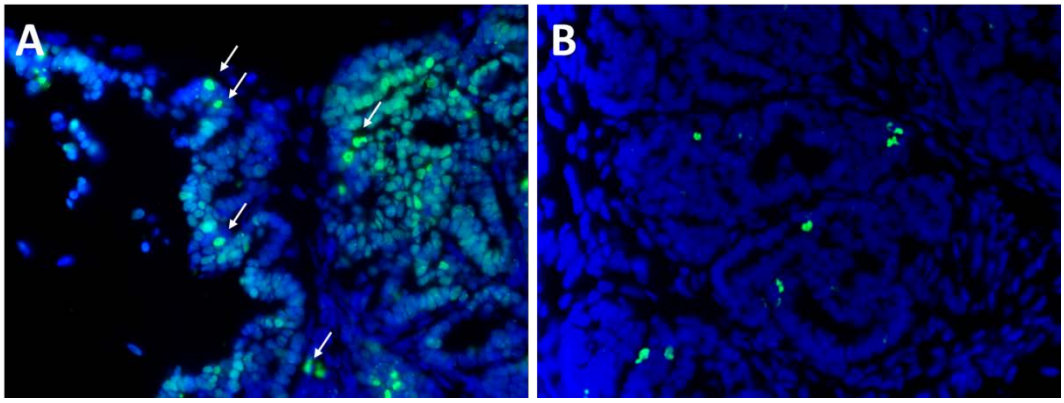

Figure 3-9: False-coloured fluorescence images of false-positive TUNEL staining in TRAMP mice

TUNEL staining in frozen dorsolateral prostate tissues from 17 week old TRAMP mice. Nuclei are counterstained with DAPI (blue) and TUNEL fluorescein signal (green). False-positive TUNEL staining is prevalent in the dorsolateral prostate of (A) TRAMP mice but not in (B) non-transgenic litter-mates. Potential instances of true apoptotic cells in TRAMP prostate are indicated with white arrows.

The modified histone variant γH2AX was selected as a potential alternate staining method for analysis of apoptosis in TRAMP dorsolateral prostates. Histone γH2AX is most widely used as a marker of DNA repair kinetics, however it is also known to accompany apoptotic DNA fragmentation (*Rogakou et al., 2000*) resulting in pan-nuclei γH2AX staining in cells undergoing apoptosis, which is easily identifiable over viable foci containing cells (*Simonsson et al., 2008; Lawrence et al., 2013a*).

Dual tissue staining using TUNEL and γH2AX was carried out in frozen dorsolateral prostate sections from untreated 17 week old TRAMP mice to assess the use of γH2AX to identify apoptotic cells *in situ*. Pan-nuclei γH2AX staining allowed clear identification of single apoptotic cells, which co-localised with bright TUNEL-stained nuclei, presumed to be instances of specific apoptosis amongst the false-positive TUNEL staining (Figure 3-10). Given the specificity of

the pan-nuclei γH2AX staining, this was subsequently used for apoptosis analysis in TRAMP dorsolateral prostate sections for all experiments throughout this thesis.

High resolution confocal images were used for apoptosis detection using γH2AX; images for analysis were taken using a 40x objective lens, using a standard epifluorescence microscope. While γH2AX foci were still able to be observed in the γH2AX-stained nuclei (particularly in irradiated tissues) (Figure 3-11) this did not affect the ability of CellProfiler™ to identify apoptotic cells.

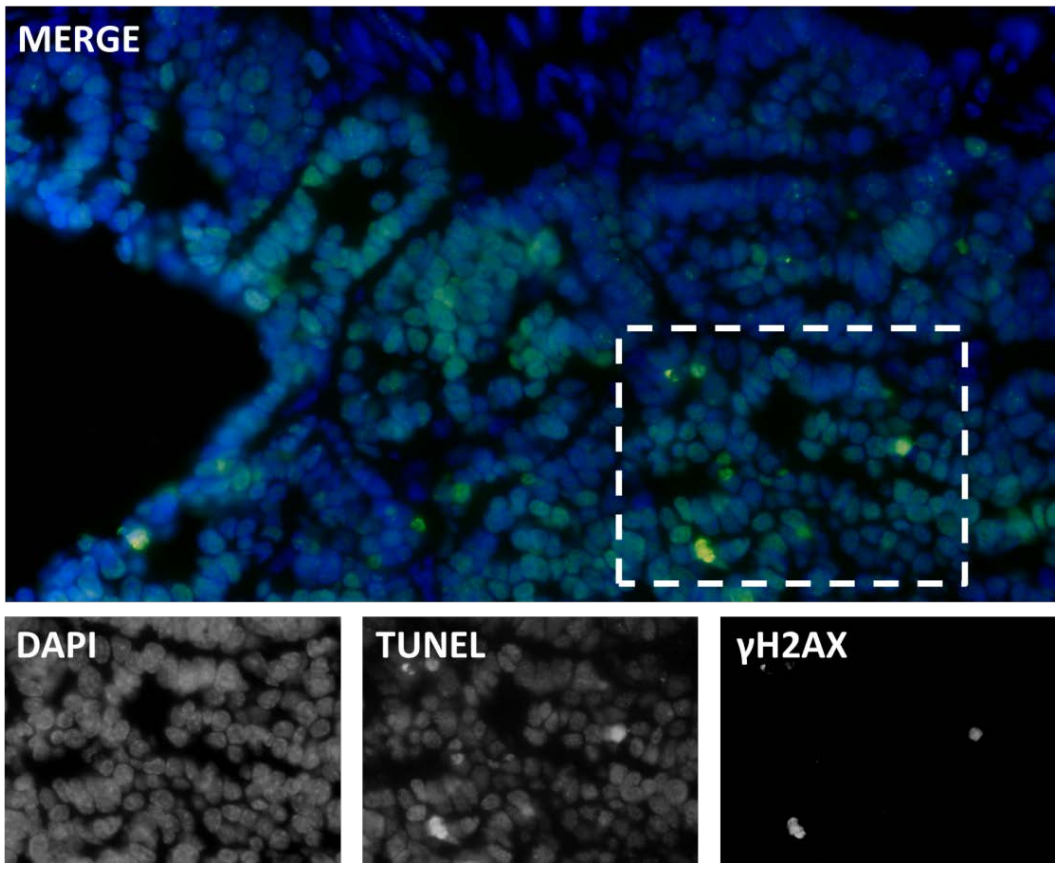

Figure 3-10: Comparison of TUNEL and pan-nuclei γH2AX staining in TRAMP dorsolateral prostate tissue.

False-coloured fluorescence images comparing TUNEL (green) and γH2AX (red) staining in 17 week old TRAMP dorsolateral prostate sections, nuclei counter-stained with DAPI (blue). Positive apoptotic cells can be observed amongst false-positive TUNEL staining, and co-localise with pan-nuclei γH2AX staining, creating a bright yellow signal in the pseudo-coloured merged image.

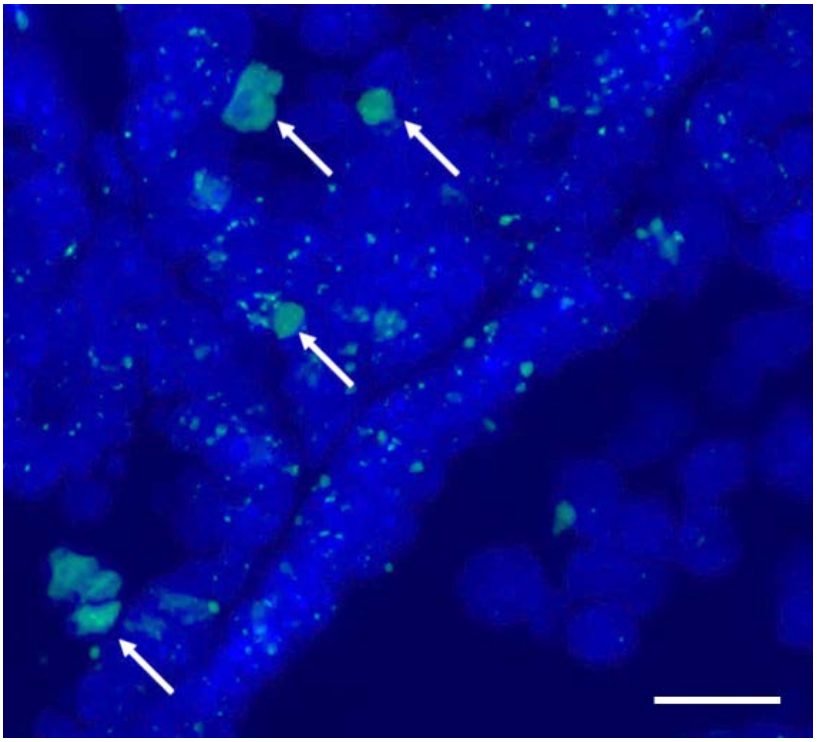

Figure 3-11: Apoptosis detection in 6 Gy-irradiated TRAMP mouse prostate by pan-nuclei γH2AX staining

False-coloured imaged of γH2AX (green) stained nuclei (blue). Apoptotic cells are indicated by arrows, and small γH2AX foci can be observed in surrounding nuclei. Scale bar 10 µm.

The CellProfiler™ pipeline was modified to eliminate γH2AX signal based on the size of the objects detected. As was the case with estimating upper and lower limits on cell pixel intensity, mean cell area was determined by measuring the area of approximately 10,000 cells, which allowed a mean range of cell area to be established (Figure 3-12). This cell area range was added to the CellProfiler™ pipeline during identification of γH2AX-positive objects, eliminating objects outside of this area range and only identifying apoptotic cells (Figure 3-13).

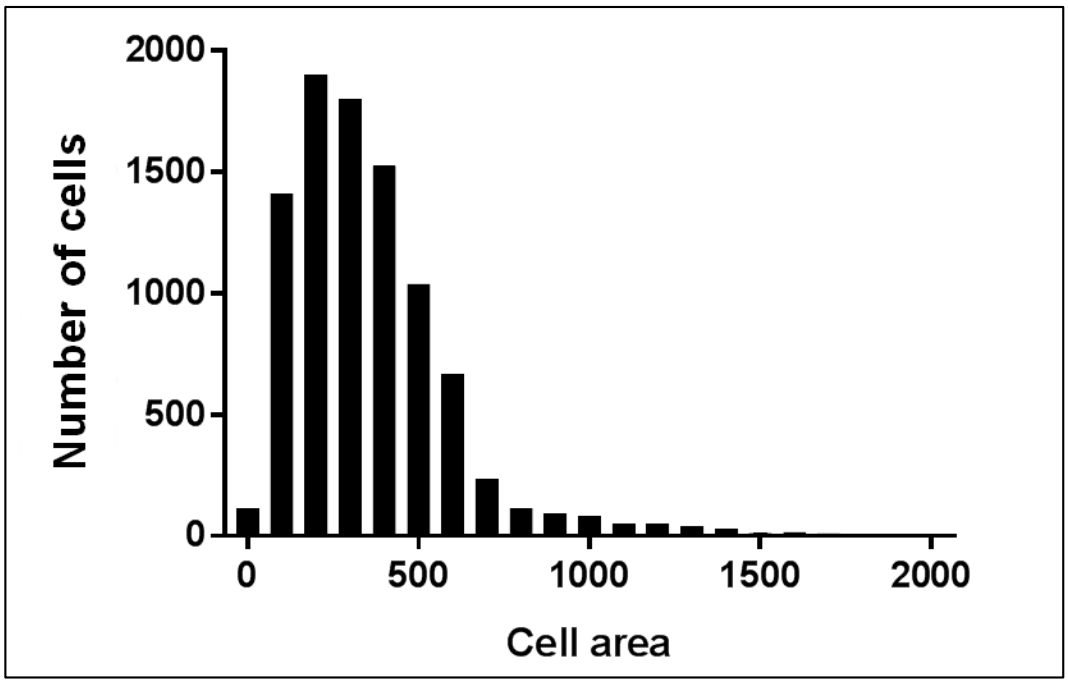

Figure 3-12: TRAMP prostate cell area histogram of DAPI-stained nuclei

Most nuclei have a pixel area between 100 and 600 pixel^2. This cell area range was then used to set a CellProfiler™ threshold for more accurate detection of apoptotic nuclei in the pipeline analysis.

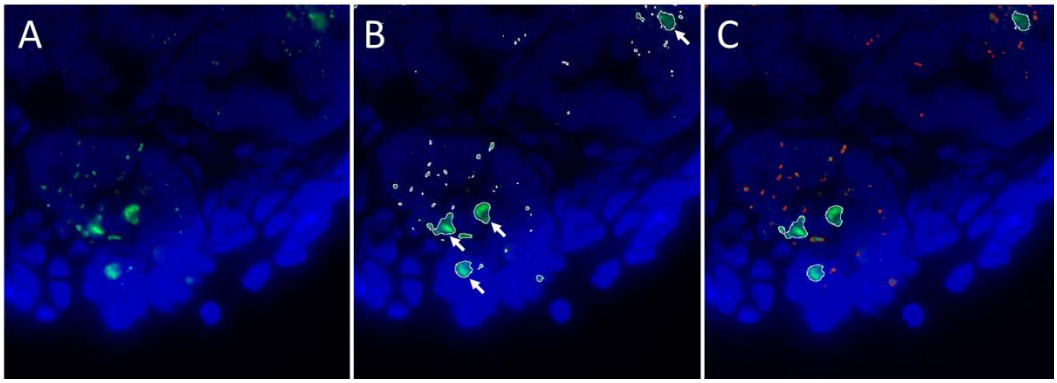

Figure 3-13: Filtering of cells stained with γH2AX in TRAMP prostate tissue sections

A) γH2AX signal (green) and DAPI stained nuclei (blue). B) Positive γH2AX objects identified by the CellProfiler™ pipeline including both apoptotic cells (indicated by arrows) and smaller γH2AX foci. C) Positive γH2AX objects filtered based on size by CellProfiler™ to differentiate apoptotic cells (white outline) from γH2AX foci (red outlines)

Following analysis of TRAMP prostate tissues using γH2AX, a further consideration for optimum apoptosis analysis became apparent. In TRAMP dorsolateral tissues stained with a primary antibody and labelled with a fluorescent secondary antibody there was significant non-specific staining that was present in regions surrounding prostate glands (Figure 3-14).

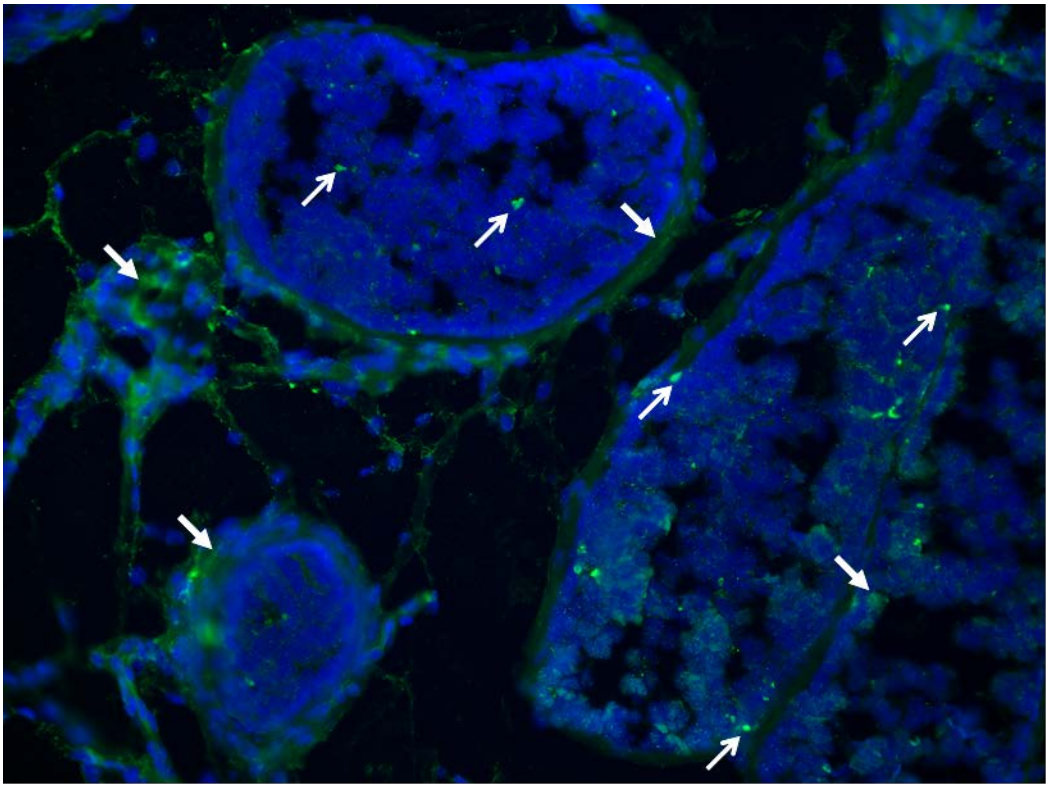

Figure 3-14: Representative image of non-specific staining present in the majority of TRAMP prostate tissues

In TRAMP prostate tissues stained using a fluorescent secondary antibody, non-specific signal is apparent in regions around the prostate glands. Apoptotic cells (examples are indicated by open arrows) are still observable amongst the non-specific staining (examples are indicated by closed arrows) but cannot be detected using an automated pipeline analysis.

While the apoptotic cells were still able to be observed amongst the non-specific staining, automated analysis was unable to be used for accurate analysis of apoptosis. In tissue sections with low apoptotic frequencies these true apoptotic cells were able to be counted manually, however this was not possible in

irradiated tissue sections where the frequency was significantly increased. To overcome this issue, the staining protocol for TRAMP prostate tissues was modified to use a primary antibody pre-conjugated to a fluorescent tag. This eliminated the need for incubation with a secondary antibody and reduced the non-specific staining to almost zero, allowing automated apoptosis analysis with the CellProfiler™ pipeline.

Development of an automated analysis for protein expression

For further analysis of data from some experiments the quantification of protein expression was required. Many methods of protein expression measurement exist, the most common being Western Blotting. However, for these studies there was often severely limited tissue available for protein extraction analysis, which meant that Western Blotting was not a viable option. Given these experiments only required measurement of relative protein expression (changes compared to a single control value) rather than absolute quantification of protein expression, modified immunofluorescent analysis methods were considered to provide relative quantitative data. A modified version of the basic CellProfiler™ pipeline (Figure 3-1) was used for quantification of relative protein expression (Figure 3-15).

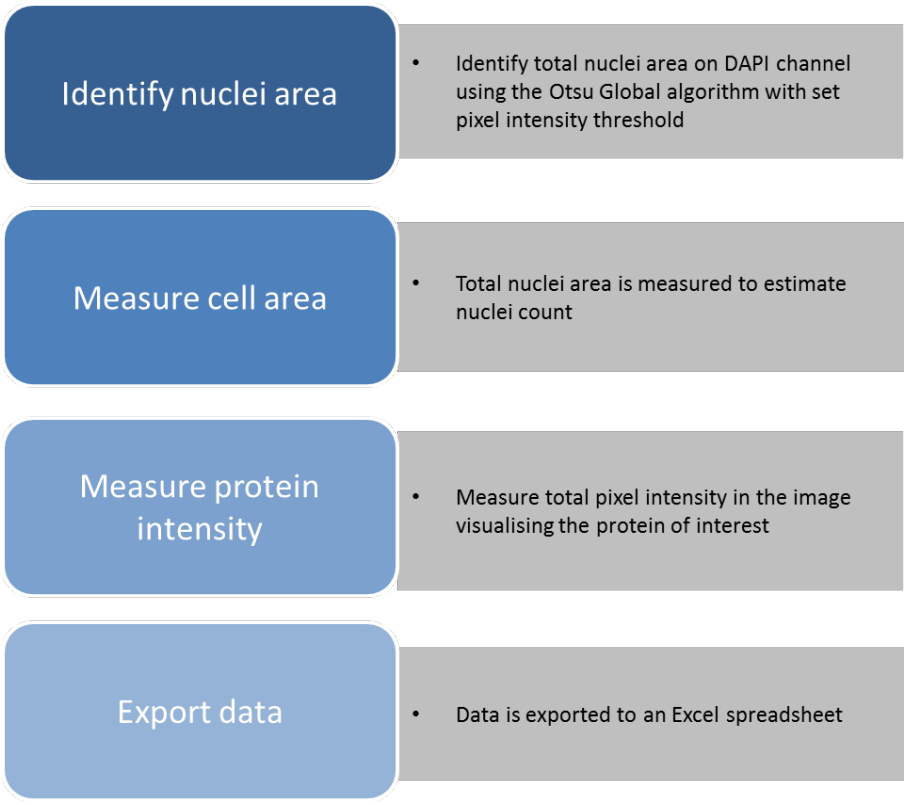

Figure 3-15: Outline of optimised method for measurement of total protein expression from stained tissue sections using CellProfiler™

Tissue sections were stained with the primary and secondary antibodies of choice and imaged in the same manner as for apoptosis analysis. Nuclei area was identified as per the pipeline used for analysis of apoptosis, and the total pixel intensity in the image visualising the protein of interest was measured. For measurement of nuclear-specific protein expression, the identified nuclei area was used to mask the image visualising the protein of interest, ensuring that only expression in the nuclei regions was measured, for measurement of non-nuclear proteins, this masking step did not occur. The nuclei area was used to estimate a nuclei count and a final measurement of fluorescence intensity was calculated per nuclei (Figure 3-16). The fluorescence intensity per nuclei in individual tissue

sections could then be compared to the intensity of a control tissue to provide a fold-change in protein expression (Figure 3-17).

This method of protein expression quantification is not without its limitations. The nature of immunofluorescent staining is that there are slight differences in staining and imaging from one experiment to the next. To ensure that this did not affect the results, tissue sections from within single experiments were imaged at the same time, to limit any fading of fluorescent signal that could artificially reduce measurement of fluorescence intensity in the images. If analysis of tissues from previously analysed experiments were required to be pooled together, the tissue sections were re-stained and imaged to reduce any inter-experiment staining variations.

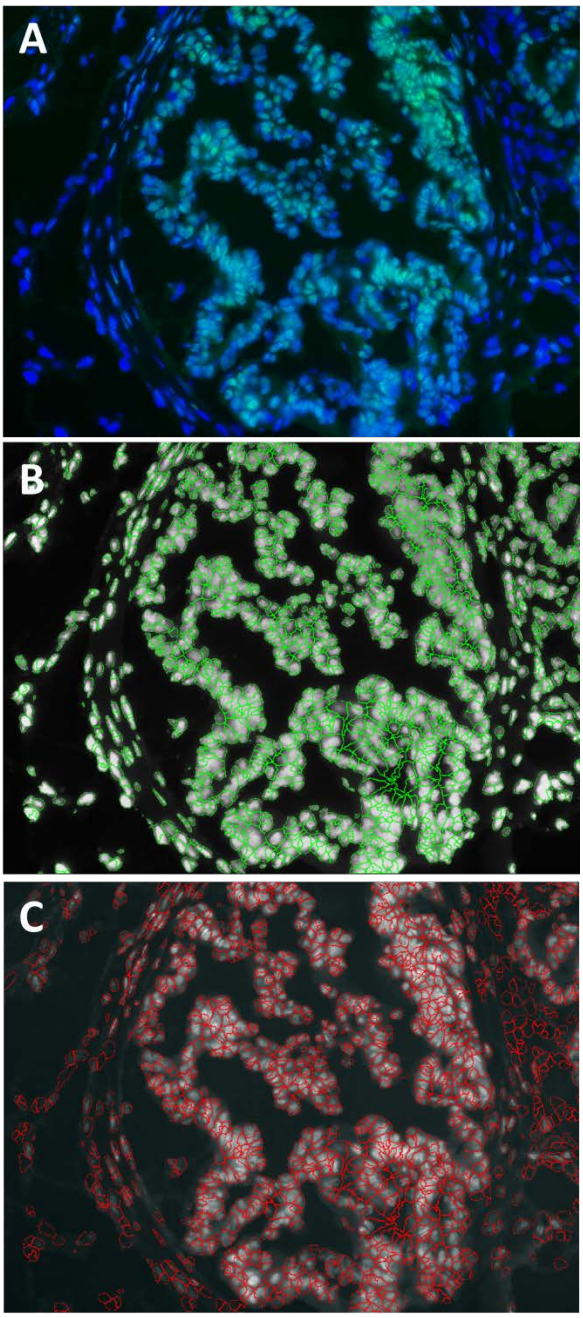

D

Measurement	Value
Nuclei area occupied	829204
Estimated nuclei count (from area)	1478
Total protein fluorescence intensity	101724
AR fluorescence intensity per nuclei	68.83

Figure 3-16: Representative measurement of nuclear-specific protein expression in TRAMP dorsolateral prostate from immunofluorescent images

(A) False-coloured image depicting AR expression in TRAMP dorsolateral prostate, (B) identification of nuclei area from DAPI image, (C) masking of AR-protein image from nuclei area and D) final analysis measurements identifying nuclei area occupied, estimated nuclei count, total AR fluorescence intensity in nuclei regions and AR fluorescence intensity per nuclei.

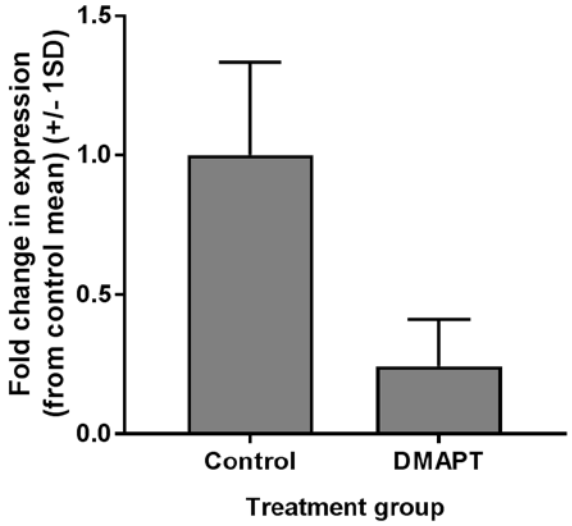

Fluorescence intensity per nuclei								
Control	44.8	104.7	81.1	102.6	75.2	40.1	62.1	98.1
DMAPT	16.1	10.1	42.1	25.1	30.1	9.2	5.1	10.1

Fold change in expression (from control mean)								
Control	0.59	1.38	1.07	1.35	0.99	0.58	0.82	1.29
DMAPT	0.21	0.13	0.55	0.33	0.40	0.12	0.07	0.13

Figure 3-17: Quantification of fold-change in NF-κB protein expression in C57BL/6J dorsolateral prostate tissue sections

Relative quantification of protein expression changes is determined from the fluorescence intensity per nuclei calculated by the CellProfiler™ pipeline

Chapter 4: The effect of parthenolide on prostate cancer development in TRAMP mice

In vitro studies have demonstrated that parthenolide has anti-cancer effects on leukaemia cells (*Dai et al., 2010; Hewamana et al., 2008; Jenkins et al., 2008*). Parthenolide can preferentially inhibit growth and induce apoptosis of prostate cancer cell lines compared to normal prostate cells *in vitro* (*Sun et al., 2010*) and can inhibit prostate tumour initiating cells in mouse xenografts (*Kawasaki et al., 2009*). Despite these promising results, PTL is yet to be tested in a model of prostate cancer that more closely follows the human disease, with a non-compromised immune system, and where tumours develop initially from normal tissue in the prostate and subsequently metastasise to distant sites. Given the importance of the immune system and the multiple stages of cancer progression, testing PTL in an autochthonous model is an important step towards translation of the compound into clinical practice.

In order to investigate the ability of PTL to slow prostate tumour development in an autochthonous mouse model, six week old TRAMP mice, at the time when tumour development is starting to be initiated by the SV40-driven transgene, were treated thrice weekly with PTL by oral gavage until palpable tumours formed.

Results

Breeding of TRAMP mice and determination of transgenic status

All experimental mice came from time matings as per the previously described protocol in Chapter 3, to ensure that all mice were born within four days of each other to limit variation between animals. The transgenic status of mice was determined by PCR as previously described in Chapter 3. TRAMP positive mice exhibited PCR melt peaks at 84°C and 88°C, whereas TRAMP negative mice only exhibited a single peak at 84°C (Figure 4-1).

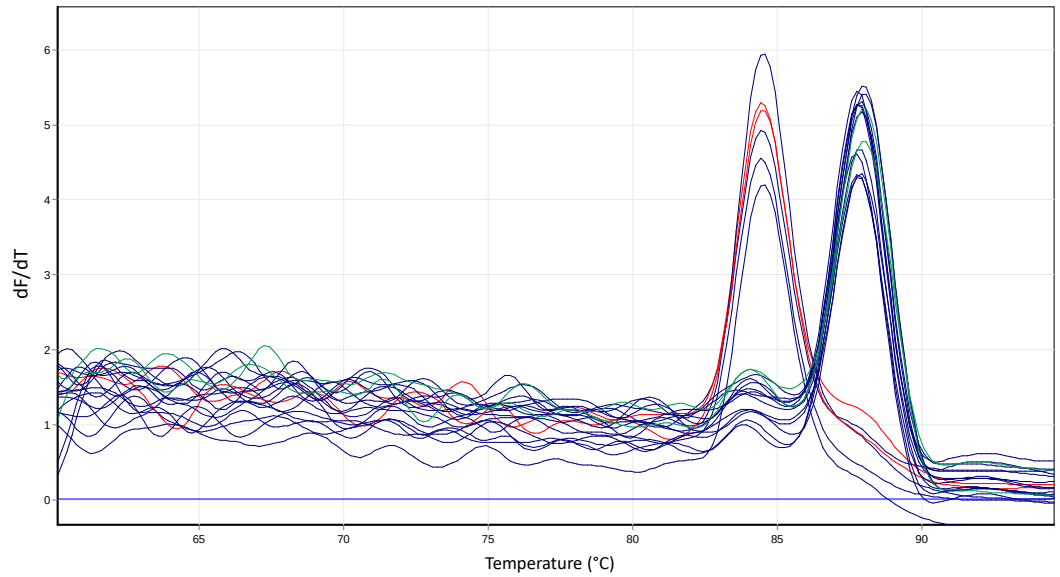

Figure 4-1: Typical melt curve analysis of TRAMP genotype

Lower temperature peak (84°C) represents control Ig amplicon melt and the upper, TRAMP specific amplicon melt temperature (88°C). Samples include a positive TRAMP control (green), negative TRAMP control (red) and a mix of unidentified experimental TRAMP samples.

A selection of non-transgenic litter-mates were kept for the extent of the animal studies to provide negative controls to ensure that the TRAMP transgene screening was accurate. None of the non-transgenic mice developed prostate

tumours (n = 18) and 100% of TRAMP mice (excluding those that were euthanised early for ethical reasons) developed prostate tumours (n = 61).

Time-to-palpable tumour studies in the TRAMP model

In order to examine the anti-cancer effects of PTL in the TRAMP model, an initial time-to-palpable tumour study was undertaken. Male TRAMP mice were delivered PTL (40 mg/kg in 10% ethanol/saline vehicle) or an ethanol/saline vehicle control three times per week by oral gavage from 6 weeks of age until palpable tumour development (up to 37 weeks of age) (Figure 4-2). Mice were weighed and assessed for palpable tumours three times per week.

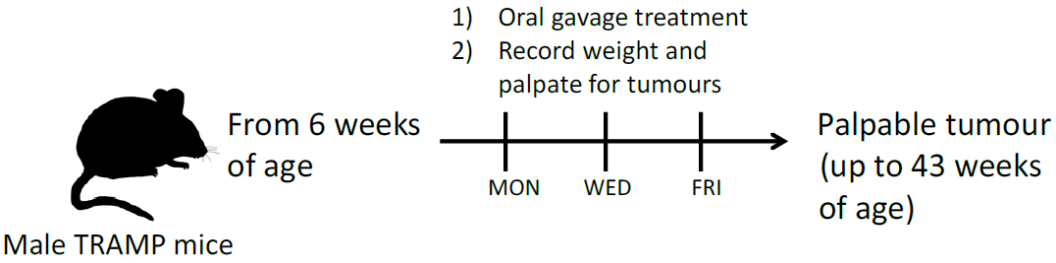

Figure 4-2: Schematic overview of treatment and assessment of mice for *in vivo* time-to-palpable tumour studies

It is reported in the literature that 100% of male TRAMP mice will develop palpable prostate tumours with some metastatic spread within 30 – 36 weeks (*Gingrich et al., 1996; Hsu et al., 1998; Greenberg et al., 1995*). In this study our data were consistent with this timeframe, with palpable prostate tumours detected in the vehicle control treatment group from 19.1 to 37.1 weeks (134 to 260 days from birth), and a median time-to-palpable tumour of 30 weeks (210 days from birth).

In this study, there was no significant difference observed in the time-to-palpable tumour between TRAMP mice treated with PTL (in 10% ethanol/saline) (171 ± 29.4 days from birth, n = 9) and mice treated with ethanol/saline vehicle control (211 ± 43.1 days from birth, n = 9) (p = 0.061, Log-Rank (Mantel-Cox), Figure 4-3).

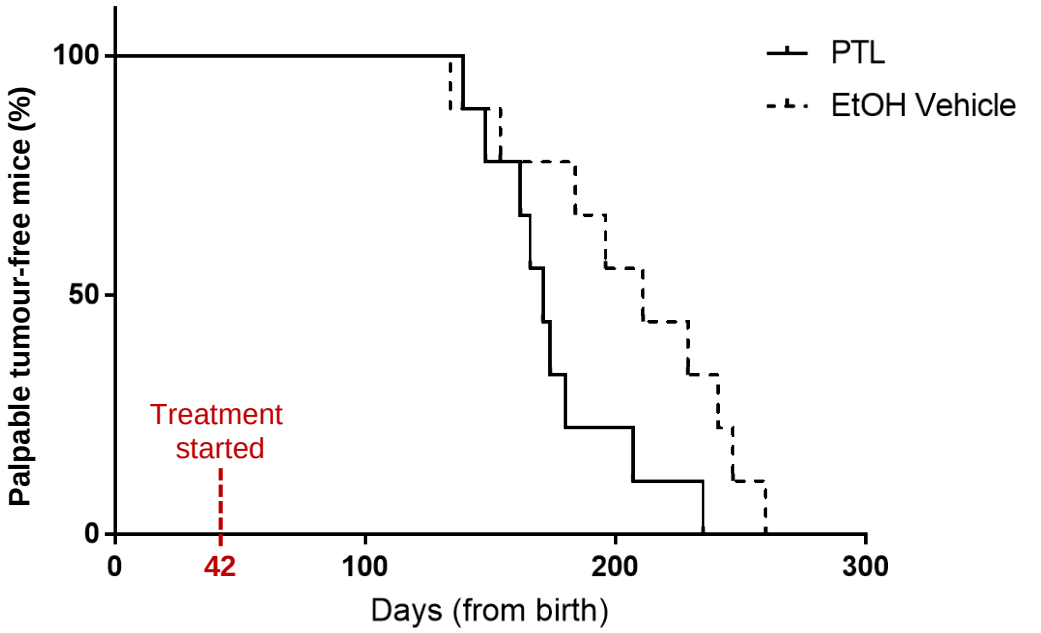

Figure 4-3: Kaplan Meier analysis of time-to-palpable tumour in TRAMP mice treated with PTL or vehicle control

TRAMP mice were treated with PTL (40 mg/kg in 10% ethanol/saline) or ethanol/saline vehicle thrice weekly by oral gavage from 6 weeks (42 days) of age, n = 9 per group, p = 0.061, Log-Rank (Mantel-Cox).

There was no significant difference in mouse weights at time of palpable tumour detection between the TRAMP mice treated with PTL (in 10% ethanol/saline), TRAMP mice treated with ethanol/saline vehicle, and untreated non-transgenic mice (p = 0.429, one-way ANOVA) (Table 4-1). Non-transgenic mice did not develop prostate tumours; therefore, weights were taken at the conclusion of

the study rather than at palpable tumour detection. Mice were weighed thrice weekly from 6 weeks of age until euthanasia; there was no significant difference in mouse growth curves between the treatment groups over the entire course of the time-to-palpable tumour study. At the time of tissue excision, prostate weight was measured and recorded as a normalised prostate weight (percentage of whole mouse weight) (Table 4-1). There was no significant difference in TRAMP mouse prostate weight at time of palpable tumour detection between mice treated with PTL (in 10% ethanol/saline) or ethanol/saline vehicle ($p = 0.258$, Mann-Whitney test). In non-transgenic mice, prostate tumours did not develop and therefore normalised prostate weights were significantly less than that of TRAMP mice.

Table 4-1: Mouse and normalised prostate weights at the time of palpable tumour detection

TRAMP status	Treatment group	Mean mouse weight (g) (±1SD)	Mean normalised prostate weight[a] (%) (±1SD)	n
Transgenic	PTL	36.7 ± 3.1	18.2 ± 3.9	9
Transgenic	Ethanol/saline	38.3 ± 5.4	11.35 ± 10.5	9
Non-transgenic	PTL	36.0 ± 4.5	0.43 ± 0.11	3
Non-transgenic	Ethanol/saline	35.3 ± 6.1	0.60 ± 0.32	3

[a]Normalised prostate weights are given as a percentage of total mouse weight at time of euthanasia.

Although there was no significant difference in time-to-palpable tumour between the treatment groups, a significant difference in TRAMP palpable tumour phenotype was detected. All mice treated with PTL (in 10%

ethanol/saline) developed the typical TRAMP tumour phenotype; a palpable prostate tumour with some smaller non-palpable metastatic tumours (Figure 4-4).

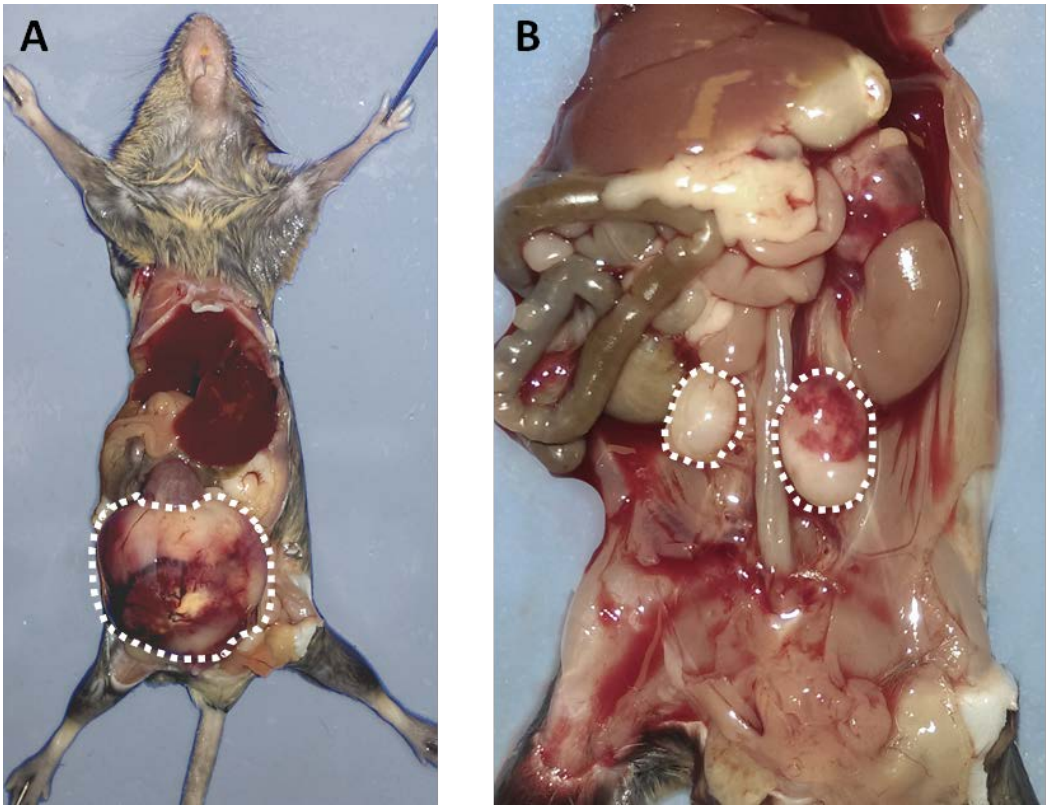

Figure 4-4: Example of typical TRAMP prostate tumour phenotype

TRAMP (A) prostate tumour, *in situ*, identified by palpation and (B) non-palpable metastatic lymph node tumours. Dotted lines outline the tumour mass, n = 54

In the ethanol/saline vehicle control treatment group, TRAMP mice were initially observed to have normal TRAMP tumour phenotypes (as per Figure 4-4); however, after 187 days of treatment (229 days since birth), mice started to develop large palpable tumours outside of the prostate (Figure 4-5A). Upon examination post-euthanasia, it was determined that these mice had very small (less than 125 mm^3) non-palpable prostate tumours (Figure 4-5B). No tumours, primary prostate or distant metastases, were identified in non-transgenic mice.

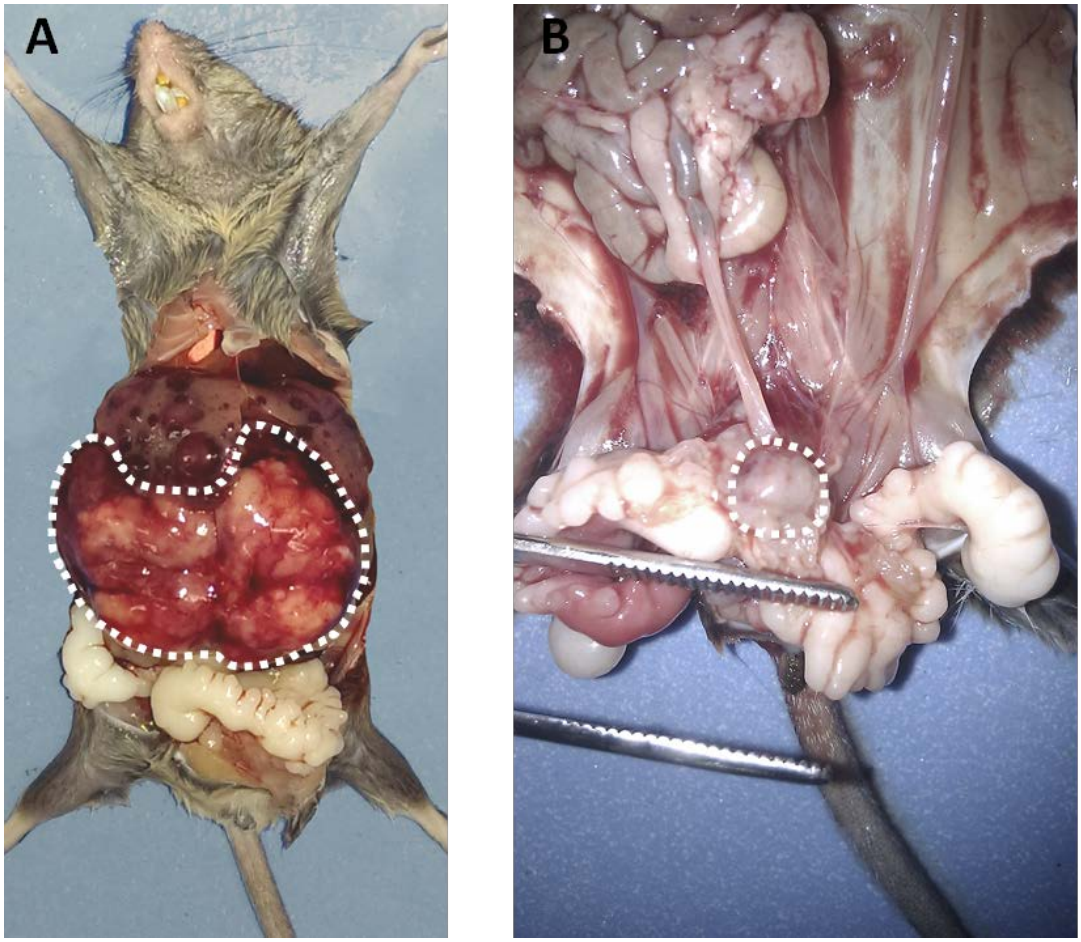

Figure 4-5: Example of the atypical TRAMP prostate tumour phenotype

Tumour phenotype detected in mice treated with ethanol/saline vehicle (n = 8) and parthenolide (in ethanol/saline) (n = 1). (A) Large metastatic tumour, *in situ*, identified by palpation and (B) non-palpable TRAMP prostate tumour attached to seminal vesicles. Dotted lines outline the tumour mass.

After the completion of the initial time-to-palpable tumour study, DMAPT, a water soluble analogue of PTL, became available and a second time-to-palpable tumour study was carried out in the same manner as the first. For this second study 6 week old TRAMP mice were treated with PTL (40 mg/kg in 10% ethanol/saline vehicle), DMAPT (100 mg/kg in sterile water), an ethanol/saline vehicle control or a water vehicle control three times per week until palpable tumour detection (up to 43 weeks).

There was a significant increase in time-to-palpable tumour detection in DMAPT treated TRAMP mice (258 ± 24.5 days from birth) compared to water control treated mice (218 ± 39.4 days from birth) (p = 0.013, Log-Rank (Mantel-Cox), Figure 4-6, Table 4-2). DMAPT increased time-to-palpable tumour detection by 40 days. The first palpable prostate tumour in the DMAPT-treated mice was detected 90 days after tumour onset in the water control-treated group (219 days from birth compared to 129 days from birth). There was no significant difference in time-to-palpable tumour between mice treated with PTL (in 10% ethanol/saline) (210.5 ± 48.8 days from birth), mice treated with ethanol/saline vehicle (228 ± 35.4 days from birth), and water vehicle treated mice (p = 0.906, Log-Rank (Mantel-Cox), Figure 4-6).

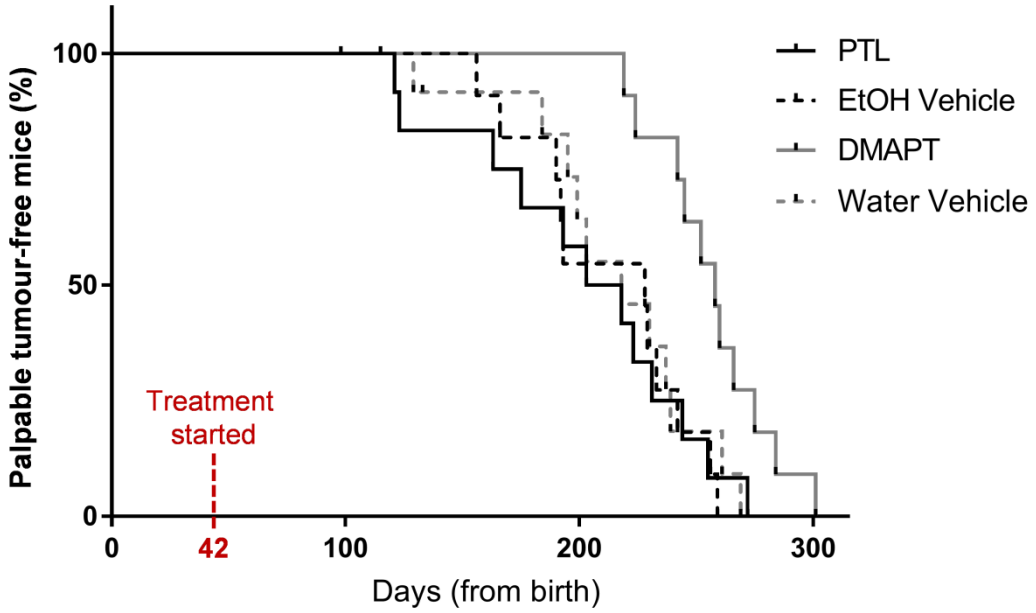

Figure 4-6: Kaplan Meier analysis of time-to-palpable tumour in TRAMP mice treated with PTL, DMAPT or vehicle controls

TRAMP mice were treated with PTL (40 mg/kg in 10% ethanol/saline), DMAPT (100 mg/kg), ethanol/saline vehicle or water vehicle thrice weekly by oral gavage from 6 weeks of age. n = 12 per group, p = 0.0164, Log-Rank (Mantel-Cox).

In this second time-to-palpable tumour study it was again observed that in TRAMP mice treated with ethanol/saline vehicle control, after 191 days of treatment (233 days from birth) mice developed palpable tumours at distant sites, with small non-palpable prostate tumours discovered upon post-euthanasia examination. One mouse in the PTL (in 10% ethanol/saline) treatment group also developed this abnormal TRAMP tumour phenotype after 230 days of treatment (272 days from birth). Only the normal TRAMP phenotype (palpable primary prostate tumours and smaller distant metastases) was observed in the water vehicle and DMAPT treatment groups.

Table 4-2: Time-to-palpable tumour statistics from PTL and DMAPT TRAMP study

Treatment group	Median palpable tumour detection time (days from birth) (±1SD)	n
PTL (40 mg/kg in 10% ethanol in saline)	210.5 ± 48.8	12
Vehicle control (10% ethanol in saline)	228 ± 35.4	12
DMAPT (100 mg/kg in water)	258 ± 24.5	12
Vehicle control (water)	218 ± 39.4	12

At the time of palpable tumour detection there was no significant difference in mouse weights between the PTL (in 10% ethanol/saline), ethanol saline vehicle, DMAPT (in water) or water vehicle treatment groups ($p = 0.537$, one-way ANOVA, Table 4-3). There was also no significant difference in mouse weights between the different treatment groups over the course of the time-to-palpable tumour study.

Table 4-3: Mouse and normalised prostate weights at the time of palpable tumour detection

TRAMP status	Treatment group	Mean mouse weight (g) (±1SD)	Mean normalised prostate weight[a] (%) (±1SD)	n
Transgenic	PTL (40 mg/kg in 10% ethanol in saline)	38.1 ± 3.5	16.5 ± 6.2	12
Transgenic	Vehicle control (10% ethanol in saline)	34.5 ± 6.2	12.4 ± 8.8	12
Transgenic	DMAPT (100 mg/kg in water)	36.1 ± 4.3	16.7 ± 1.6	12
Transgenic	Vehicle control (water)	35.2 ± 7.3	15.5 ± 4.3	12
Non-transgenic	Untreated	33.7 ± 6.4	0.37 ± 0.23	12

[a]Normalised prostate weights are given as a percentage of total mouse weight at time of euthanasia.

The PTL (in ethanol/saline) and ethanol/saline vehicle treatment groups from the two time-to-palpable tumour studies were subsequently pooled and analysed together (Figure 4-7,

Table 4-4). The median time-to-palpable tumour in the pooled PTL (in 10% ethanol/saline) and ethanol/saline vehicle treatment groups was 180 days and 219.5 days respectively, and did not differ significantly from baseline (water vehicle) palpable tumour detection time (p = 0.425, Log-Rank (Mantel-Cox)), as was also observed in the individual time-to-palpable tumour studies. Between the two separate studies, the only significant difference was the time-to-palpable tumour curves between the ethanol/saline vehicle and PTL (in ethanol/saline) treatment groups. In the first study, although there was no

significant difference in median time-to-palpable tumour, there was a reasonable gap between the Kaplan Meier curves of the two groups (Figure 4-3). In the second study, there was again no difference between the median time-to-palpable tumour between the two groups, however the curves are much closer together (Figure 4-6). This difference in the curves is likely to be due to the palpation methods used to detect tumours in the TRAMP mice. In the initial study, expecting only palpable tumours to develop in the prostate, palpation of mice was initially carried out on the lower abdominal area of the mice. This meant that large metastatic tumours were not detected in the mice until they reached quite a large size and could be identified visibly. In the second study, in expectation of tumours outside of the prostate, the mice were palpated all over their bodies to ensure that tumours were identified in a timely manner. This change in palpation technique is likely to have helped to detect distant site palpable tumours in the ethanol/saline vehicle treatment group at a slightly earlier time point than in the initial study. All subsequent analysis of tissues from these two time-to-palpable tumour studies has been carried out using data from the combined studies.

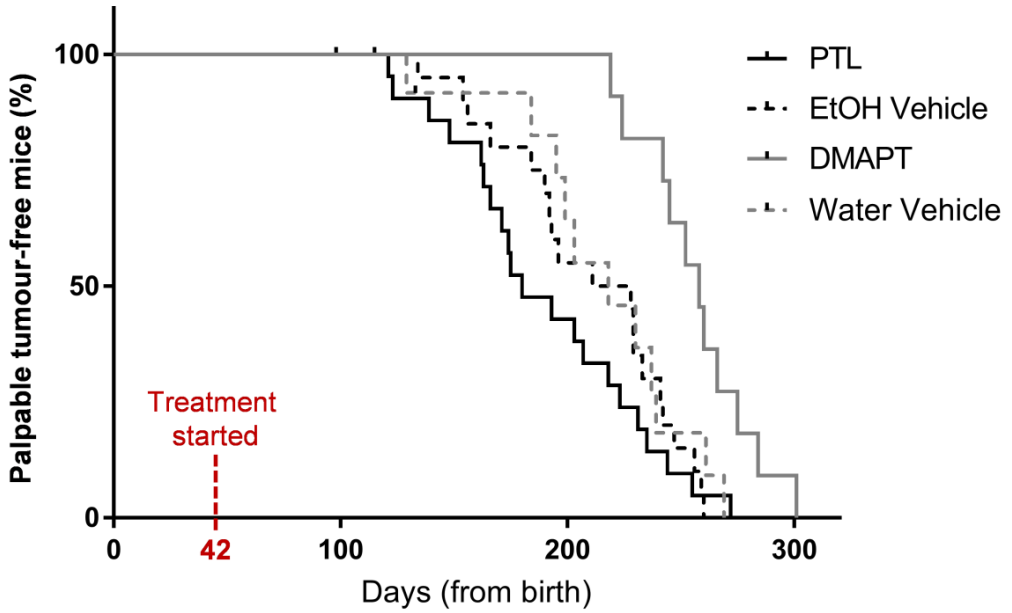

Figure 4-7: Kaplan Meier analysis of the combined time-to-palpable tumour TRAMP studies

n = 12-21 per group, p = 0.0013, Log-Rank (Mantel-Cox).

Table 4-4: Survival statistics from the combined TRAMP time-to-palpable tumour studies

Treatment group	Median palpable tumour detection time (days from birth) (±1SD)	n
PTL (40 mg/kg in 10% ethanol in saline)	180 ± 42.8	21
Vehicle control (10% ethanol in saline)	219.5 ± 38.1	21
DMAPT (100 mg/kg in water)	258 ± 24.5	12
Vehicle control (water)	218 ± 39.4	12

Ethanol and PTL/DMAPT-induced changes to TRAMP tumour burden

Given the unexpected differences in TRAMP tumour phenotypes identified in the time-to-palpable tumour studies, a more detailed examination of the differences between tumours identified in the different treatment groups was undertaken.

As previously described, a change in the tumour phenotype of TRAMP mice was observed in the ethanol/saline vehicle-treated group after 187 days of treatment (229 days from birth), where large palpable metastatic tumours (Figure 4-5A) became the first tumours detected in mice. During post euthanasia examination, small non-palpable prostate tumours (Figure 4-5B) were discovered in all mice with palpable metastatic tumours. The small non-palpable prostate tumours consisted of both adenocarcinoma and PIN tissue, while the phenotypically large palpable prostate tumours were almost entirely adenocarcinoma (Figure 4-8A). This abnormal metastatic tumour phenotype was also observed in one PTL (in 10% ethanol/saline)-treated mouse, after 230 days of treatment (272 days from birth).

The large palpable metastatic tumours identified at distant sites were analysed immunohistochemically for SV40 TAg to confirm prostatic origin (Figure 4-9). In all cases SV40 TAg staining in tumour tissue confirmed prostatic origin (n = 9) (Table 4-5); healthy spleen tissues in these mice were negative for SV40 TAg. After 212 days of treatment, one mouse treated with ethanol/saline vehicle died suddenly. Necropsy identified a thoracic tumour in the chest cavity of the animal, which was deemed the cause of the death. Immunohistochemical analysis of the tumour showed positive SV40 TAg staining, confirming that this was a metastatic tumour of prostatic origin. Early in the study (≤ 72 days of treatment) two mice developed small tumours outside of the prostate; however, the tumours were not positive for SV40 TAg (Table 4-5). These mice were censored from the Kaplan Meier time-to-palpable tumour analysis.

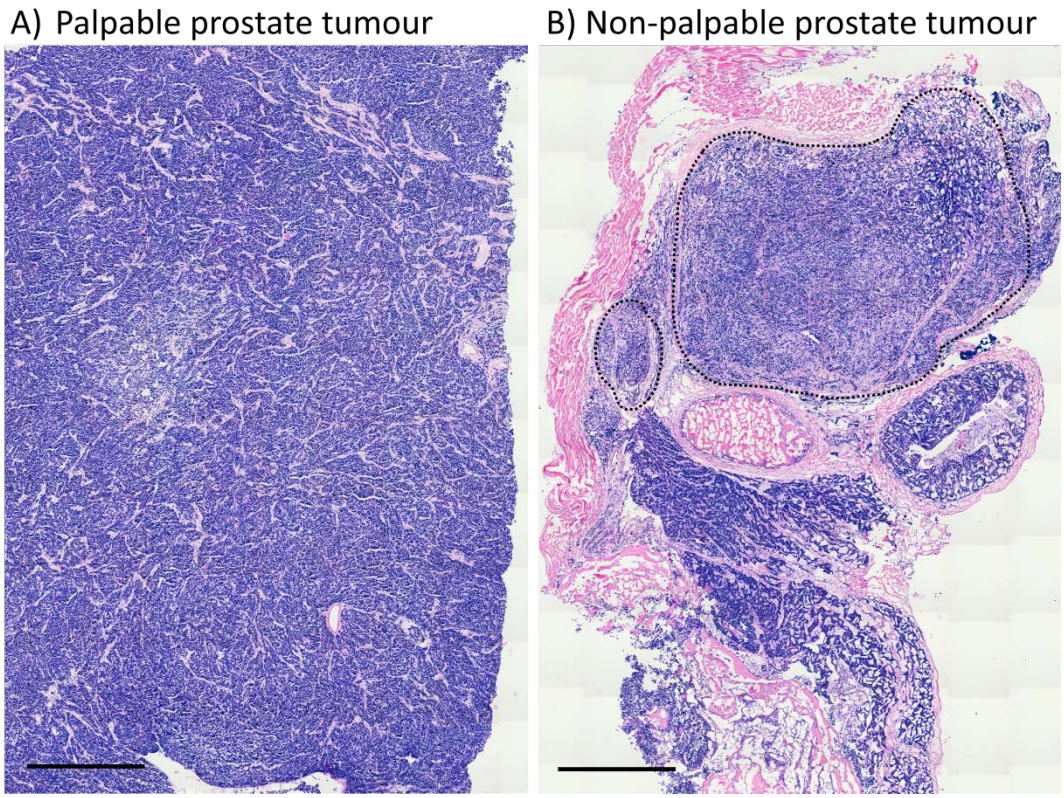

Figure 4-8: Representative TRAMP tissue pathology in palpable and non-palpable prostate tumours

Representative images of H&E staining in large palpable prostate tumours (A) and non-palpable prostate tumours (B) identified in TRAMP mice. Palpable prostate tumours consist of almost entirely adenocarcinoma, while small non-palpable tumours are a mixture of adenocarcinoma and PIN tissue (regions of adenocarcinoma in the non-palpable prostate tumour are outlined with a dashed line). Scale bar 500 µm.

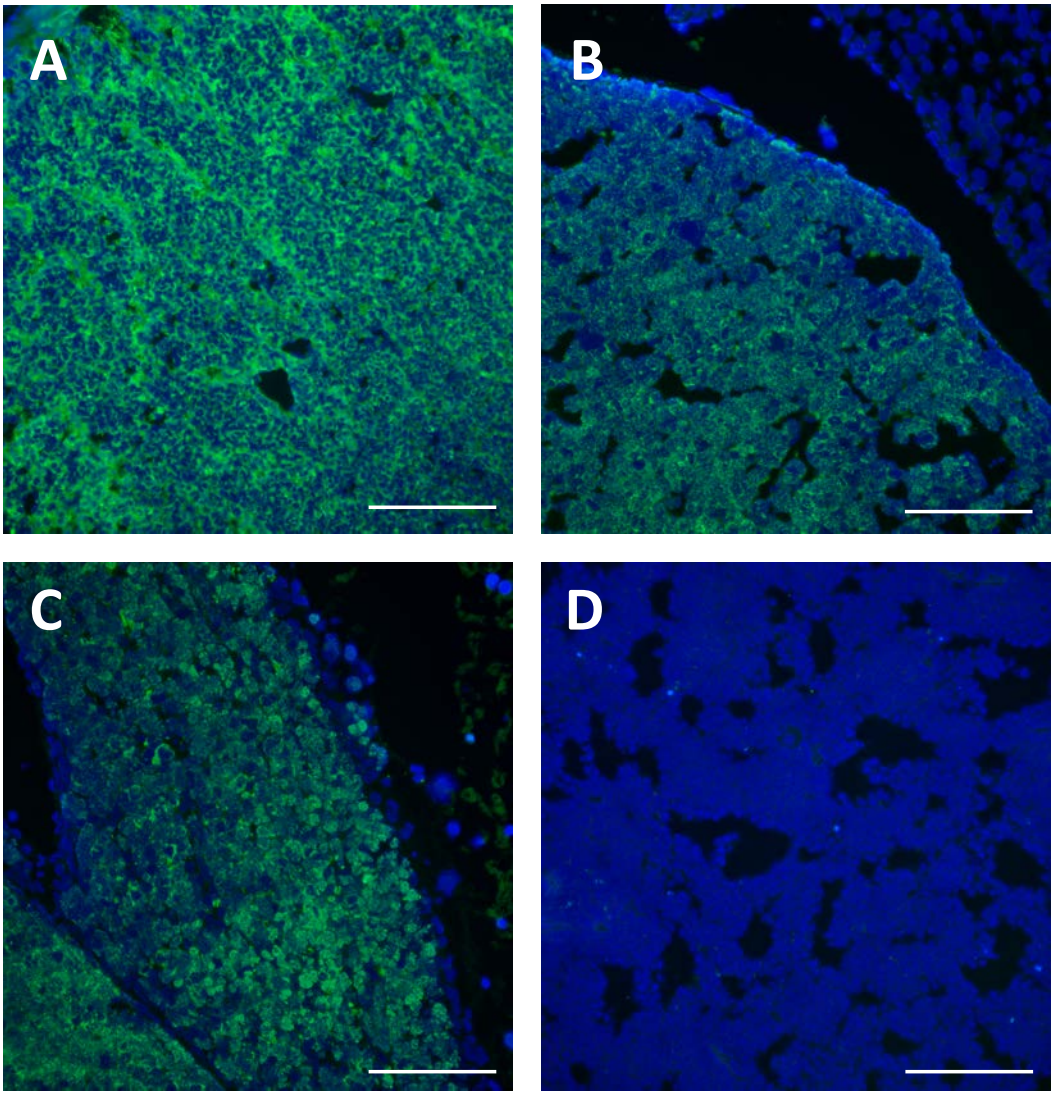

Figure 4-9: SV40 TAg staining in tumour and normal TRAMP tissues

Representative false-coloured images of TRAMP tissues stained for SV40 TAg (green) and DAPI (blue) to confirm prostatic origin in (A) primary prostate tumour, (B) palpable metastatic liver tumour, (C) metastatic kidney tumour and (D) normal spleen control tissue. Scale bar 50 µm.

Table 4-5: SV40 TAg status of tumours identified in TRAMP mice without palpable primary prostate tumours

Treatment group	Treatment length (days)	Cause of euthanasia	SV40 tumour status
EtOH/saline	54	Rapid weight loss - brain tumour	Negative
DMAPT	72	Small palpable tumour – thoracic lymph node	Negative
EtOH/saline	187	Palpable tumour - liver	Positive
EtOH/saline	191	Palpable tumour - liver	Positive
EtOH/saline	193	Palpable tumour - liver	Positive
EtOH/saline	198	Palpable tumour - kidney	Positive
EtOH/saline	200	Palpable tumour - seminal vesicle	Positive
EtOH/saline	205	Palpable tumour - liver	Positive
EtOH/saline	212	Sudden death – thoracic tumour	Positive
EtOH/saline	217	Palpable tumour - liver	Positive
EtOH/saline	218	Palpable tumour – peri-aortic lymph node	Positive
PTL	224	Palpable tumour - liver	Positive

All macroscopic tumours were excised from the mice and weighed prior to tissue embedding. As was the case for prostate weight, metastatic tumour burden was normalised to total mouse weight and has been presented as a normalised percentage of total mouse weight (Figure 4-10). At the time of palpable tumour detection, primary prostate tumour burden was not significantly different between water vehicle (15.5% ± 4.34), DMAPT (16.7% ± 1.62) and PTL in ethanol/saline (17.3% ± 5.16) treatment groups (Figure 4-10A). Although the ethanol/saline vehicle treatment group did not have a significantly reduced mean primary prostate tumour burden (12.8% ± 9.3) compared to the water

vehicle control ($p = 0.137$, Mann-Whitney test), there was a proportion of mice with clearly reduced primary tumour burden. TRAMP primary prostate tumour burden in ethanol/saline vehicle treated mice was significantly lower than in the PTL in ethanol/saline treatment group ($p = 0.0057$, Mann-Whitney test). Metastatic tumour burden was significantly increased in ethanol/saline vehicle control treated mice (8.03% ± 8.71) compared to all other treatment groups; water vehicle (1.12% ± 0.61, $p = 0.0043$), PTL in ethanol/saline (1.61% ± 1.74, $p = 0.012$), DMAPT (0.81% ± 0.32, $p = 0.0001$) (Mann-Whitney test) (Figure 4-10B). Metastatic burden in PTL in ethanol/saline and DMAPT treatment groups did not significantly differ from water vehicle-treated mice ($p = 0.16$). Despite the differences in tumour phenotypes, there was no significant difference in mean total tumour burden between the treatment groups (Figure 4-10C, one-way ANOVA, $p = 0.074$); water vehicle (16.5% ± 4.53), DMAPT (17.5% ± 1.67), ethanol/saline vehicle (21.5% ± 4.65) and PTL in ethanol/saline (19.1% ± 4.42).

Time-to-palpable tumour in the TRAMP mice varied significantly in all treatment groups, with a difference of 180 days between the first and last palpable tumours detected. Both primary prostate tumour burden and metastatic tumour burden within each mouse at the time of euthanasia are plotted for comparison on the same graph in Figure 4-11. There was no significant difference in primary prostate or metastatic tumour burdens with increasing treatment time in water vehicle, DMAPT and PTL (in ethanol/saline) treatment groups, with the exception of the final mouse in the PTL (in ethanol/saline) treatment group which developed a palpable metastatic tumour. However, the pattern of primary

prostate vs metastatic tumour burdens in ethanol/saline vehicle treated mice clearly highlights the sudden change that occurs in tumour phenotype after approximately 180 days of treatment with ethanol/saline vehicle (Figure 4-11C).

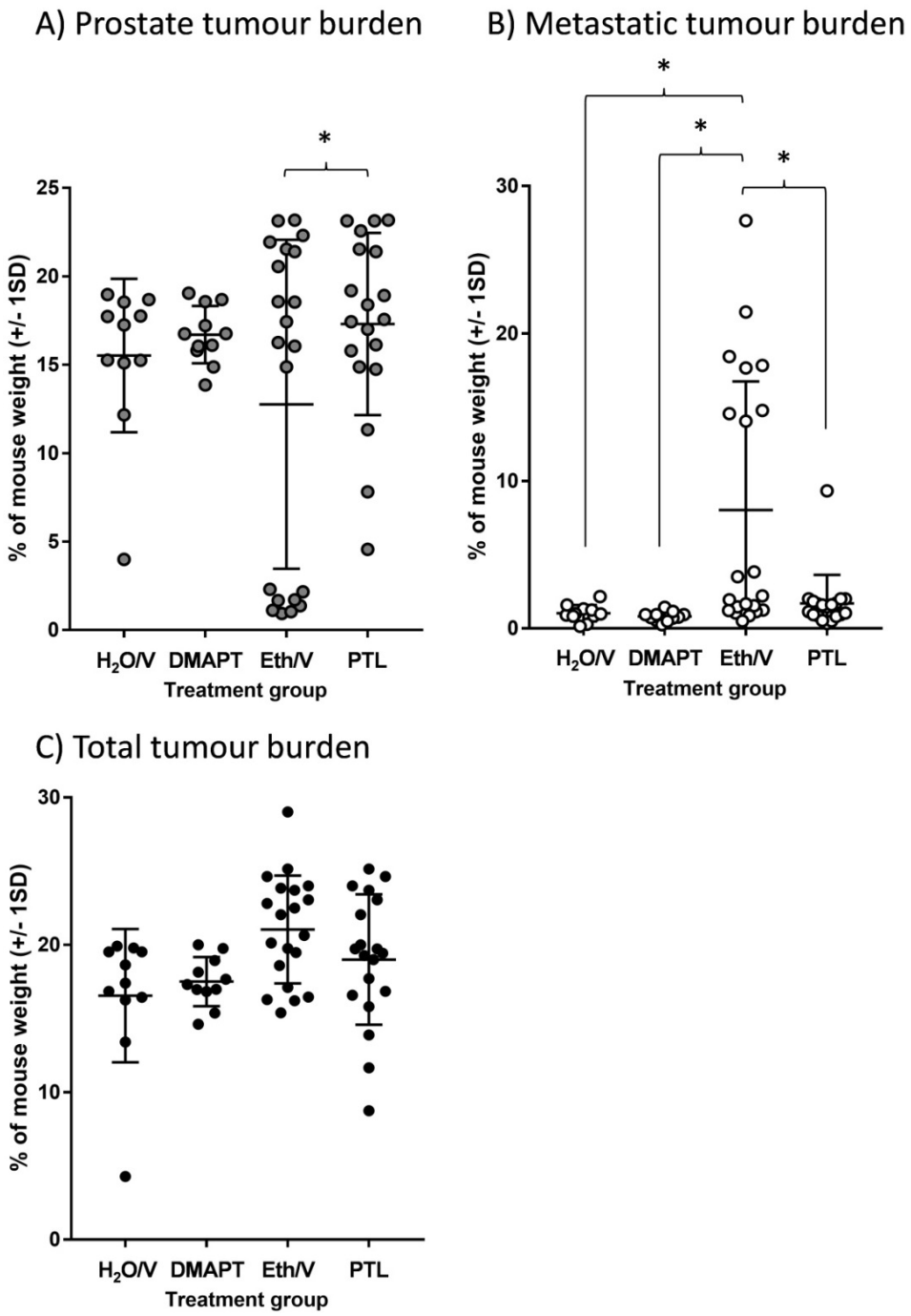

Figure 4-10: Tumour burdens as a percentage of total weight in TRAMP mice

Tumour burden in TRAMP mice treated with water vehicle (H_2O/V), 100 mg/kg DMAPT, 10% ethanol/saline vehicle (Eth/V), or 40 mg/kg PTL (in ethanol/saline). (A) Primary prostate tumour burden, (B) metastatic tumour burden, and (C) total tumour burden across all treatment groups. *$p < 0.05$, n = 11-20 mice per treatment group.

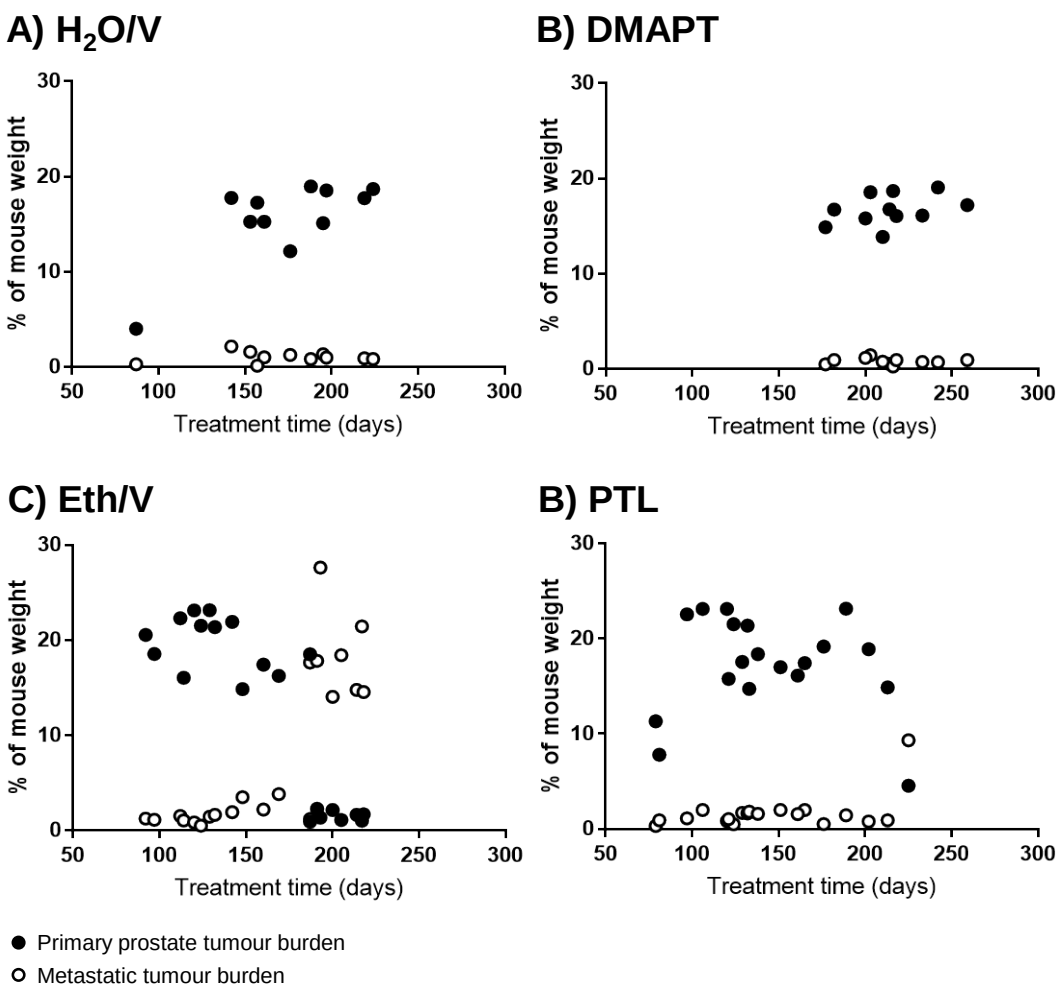

Figure 4-11: Individual TRAMP mouse tumour burdens at time of euthanasia.

Paired primary prostate tumour burden (●) and metastatic tumour burden (○) for each individual mouse, normalised to individual mouse weight, in TRAMP mice treated with (A) water vehicle (H_2O/V), (B) 100 mg/kg DMAPT, (C) 10% ethanol/saline (Eth/V), or (D) 40 mg/kg PTL (in ethanol/saline). For each mouse, both the primary prostate tumour burden and metastatic tumour burden have been plotted at the same treatment time on the x-axis (which was at the time of euthanasia). *$p < 0.05$, n = 11-20 mice per treatment group

Primary prostate tumours were stained for AR in order to investigate potential changes in AR expression due to the ethanol/saline vehicle that may result in a shift to a pro-metastatic phenotype in the TRAMP mice. Immunoreactivity of AR in the primary TRAMP prostate tumours was significantly lower than that of TRAMP prostate tissues with moderate to high grade PIN, and did not significantly differ from the negative control (Figure 4-12). SV40 TAg expression

was examined in TRAMP primary prostate tumours as a potential surrogate marker of AR expression, however the variation within treatment groups was high and no significant difference was observed (Figure 4-13).

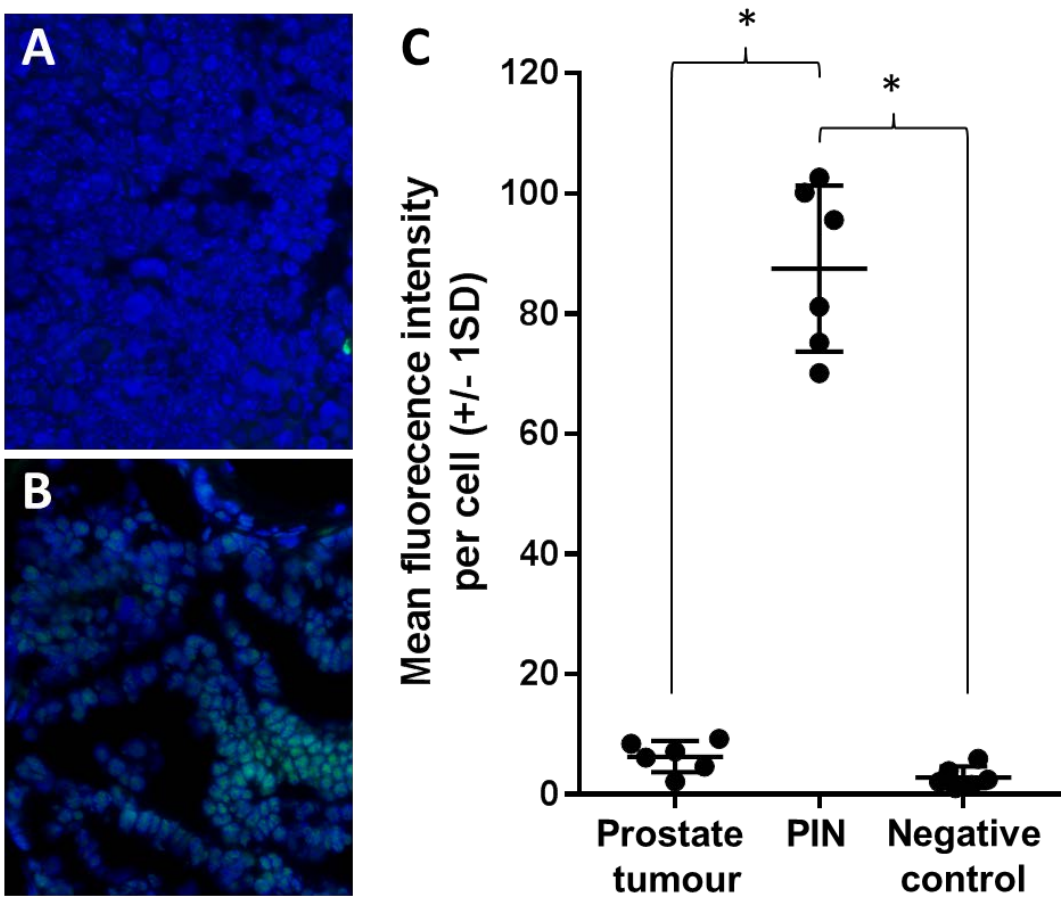

Figure 4-12: Comparison of AR staining in untreated TRAMP prostate tumour and PIN tissues

Representative false-coloured images of AR staining in (A) primary prostate tumour tissue and (B) moderate grade PIN tissue, in TRAMP mice. (C) Mean fluorescence intensity per cell measured in untreated TRAMP mice, comparing immunoreactivity in primary prostate tumours, moderate grade PIN tissue and negative control (secondary antibody only), n = 6, * $p < 0.05$.

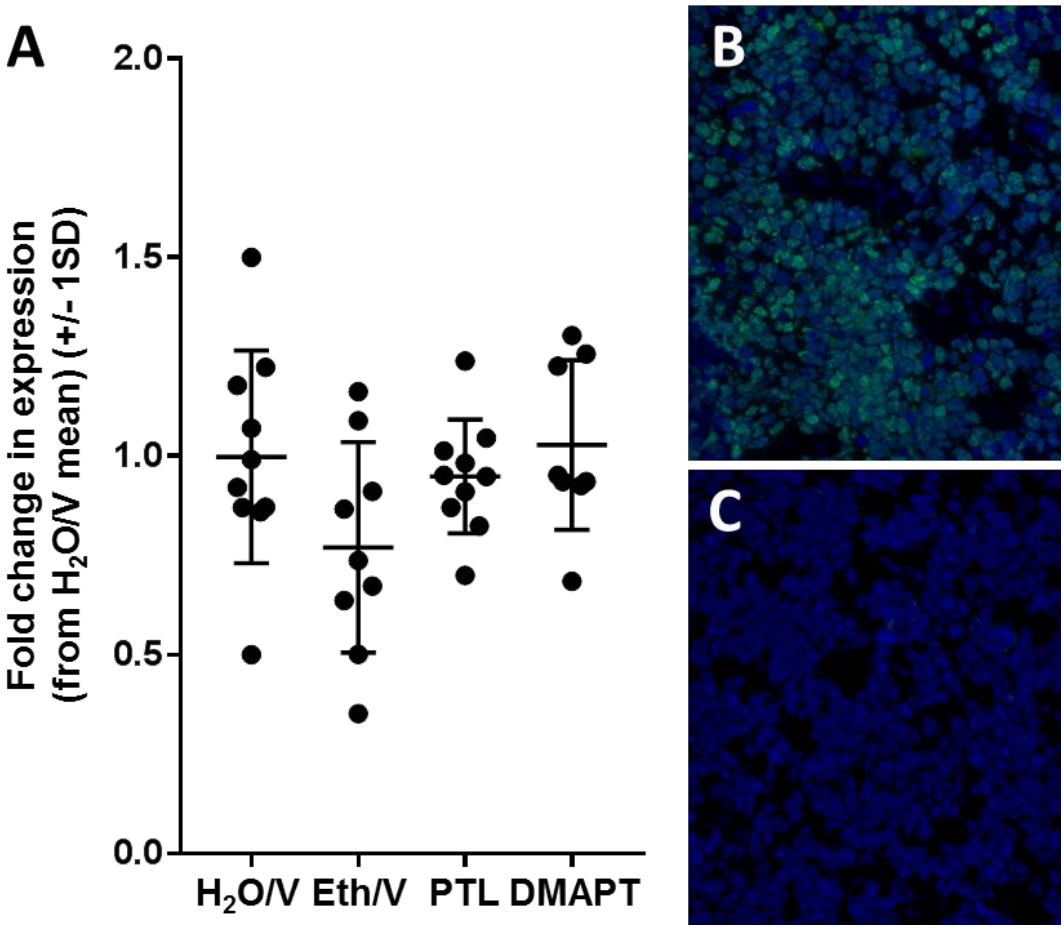

Figure 4-13: Fold changes in SV40 TAg expression in treated TRAMP primary prostate tumours

(A) Fold changes in expression (from water vehicle (H_2O/V)) in primary tumours from TRAMP mice treated with water vehicle, 10% ethanol/saline vehicle (Eth/V), 40 mg/kg PTL (in ethanol/saline), or 100 mg/kg DMAPT, n = 9-10 mice per treatment group. Representative false-coloured images of (B) positive SV40 TAg staining and (B) negative control staining in TRAMP primary prostate tumours.

While none of the TRAMP mice developed abnormal palpable metastatic tumours in the lung, it is a well described site of metastasis in the TRAMP model (*Hsu et al., 1998; Hurwitz et al., 2001; Gingrich et al., 1996*). Lung tissues were sectioned, stained using routine H&E protocols, and examined microscopically for evidence of metastatic spread. It was immediately apparent that there were significant differences in the extent of metastatic spread to the lungs of TRAMP

mice in different treatment groups (Figure 4-14). Lung tissues were subsequently analysed for SV40 TAg to confirm that the metastases were of prostatic origin and to quantify microscopic metastatic lesions within the lung sections (Figure 4-15)

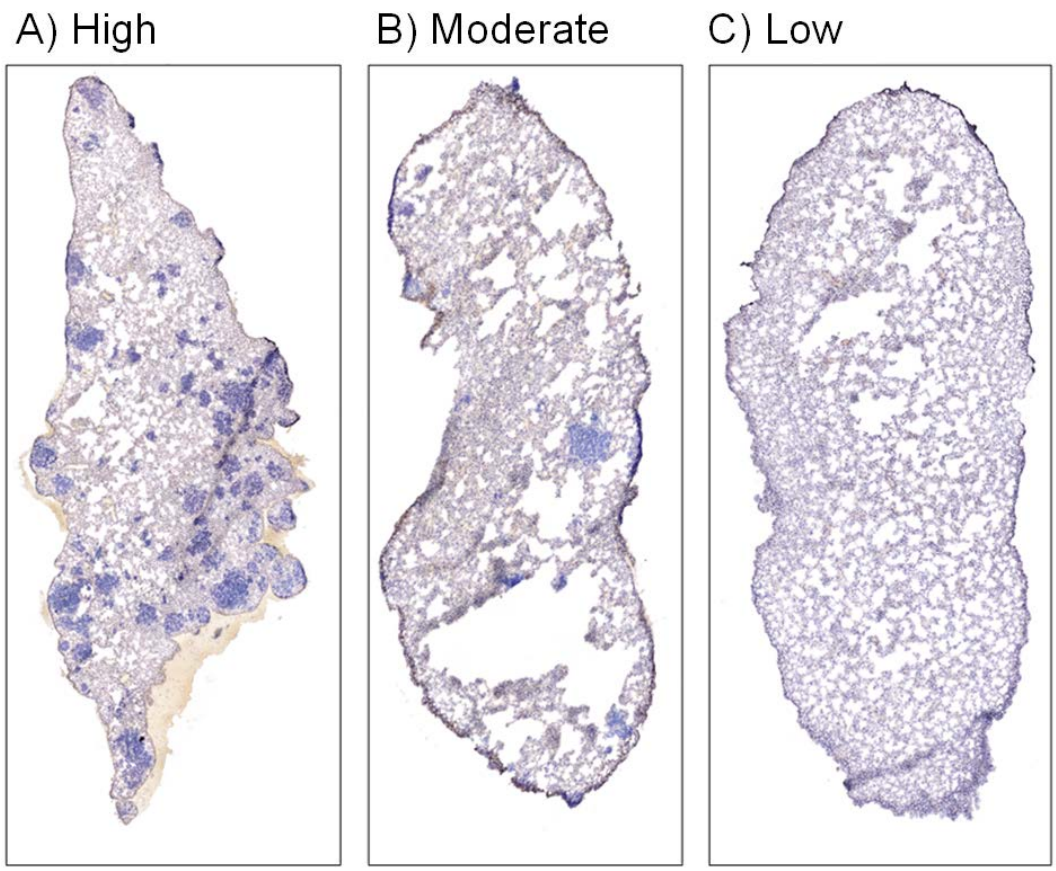

Figure 4-14: Metastatic lesions in the TRAMP lung

Representative images of (A) high, (B) moderate and (C) low levels of metastatic lesions in whole TRAMP lung tissues stained with haematoxylin. Metastatic lesions contain more densely packed cells and can be identified as dark blue-stained regions in the tissue section.

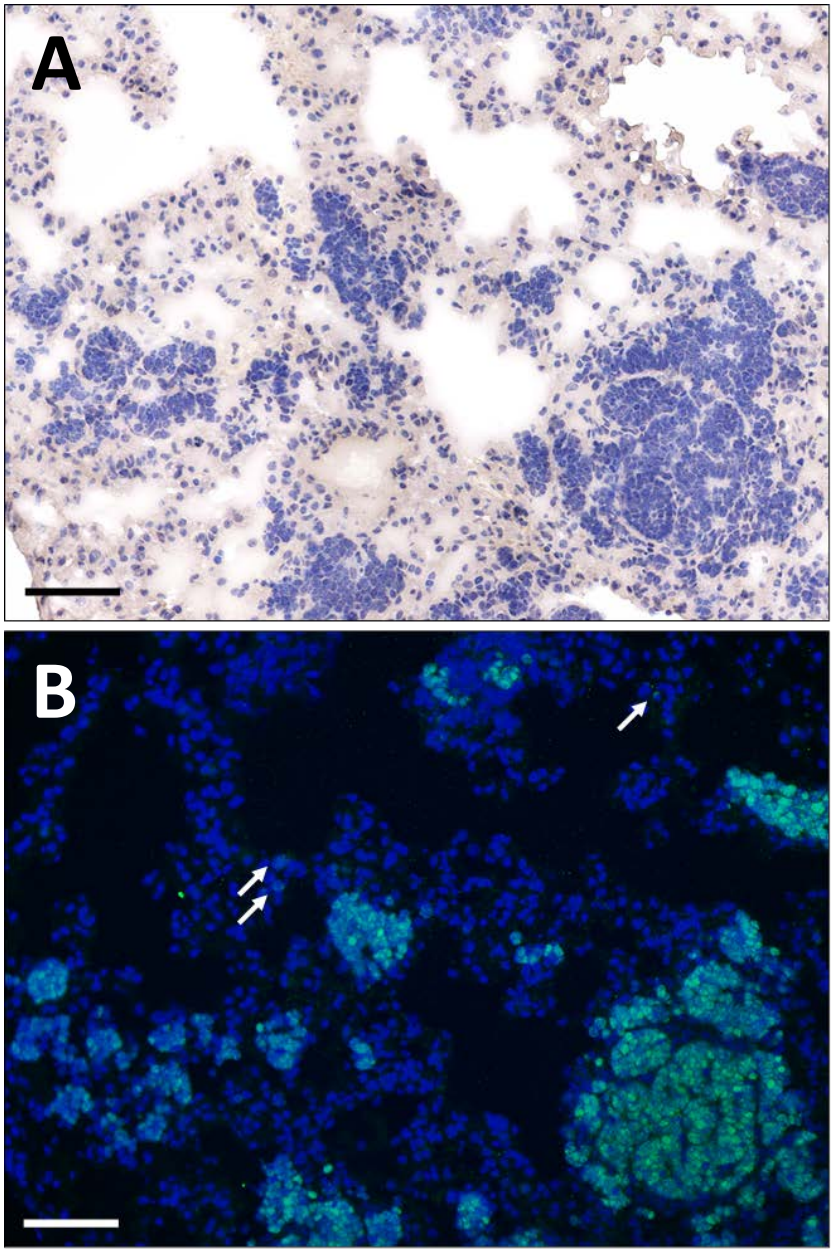

Figure 4-15: Identification of microscopic metastatic lesions in TRAMP lung by SV40 TAg staining

Consecutive sections of TRAMP lung tissue containing microscopic metastases identified by H&E staining (A) and confirmed by immunofluorescent staining for SV40 TAg (B). Most metastatic cells are present as larger lesions, however there are some single metastatic cells (identified with arrows) present in the tissue sections. Scale bar 50 µm

In the images of SV40 TAg stained lung tissue, microscopic metastatic lesions were identified as clusters of 10 or more metastatic cells. The number of microscopic metastatic lesions in ethanol/saline vehicle-treated mice (9.93 lesions ± 7.2 per mm^2) was significantly increased compared to baseline levels in water vehicle-treated mice (1.47 ± 1.29 lesions per mm^2) (574% increase, p = 0.001) (Figure 4-16). PTL (in ethanol/saline) treatment significantly reduced metastatic lung lesions (0.78 ± 1.09 lesions per mm^2) compared to the ethanol/saline vehicle-treatment group (92.1% reduction, p = 0.0002). Treatment with DMAPT significantly reduced the number of metastatic lung lesions (0.077 ± 0.12 lesions per mm^2) compared to the water vehicle treatment group (94.8% reduction, p = 0.0004) and 60% of DMAPT-treated mice had no identified metastatic lesions.

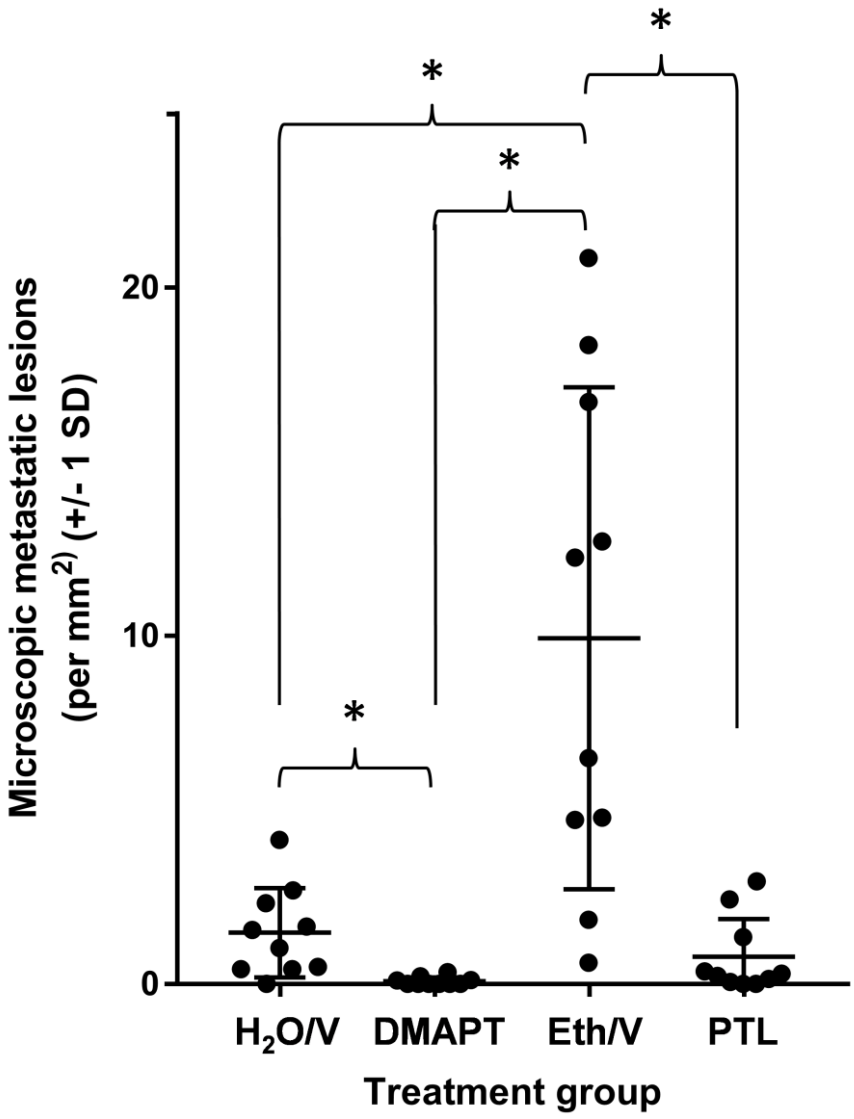

Figure 4-16: Microscopic metastatic lesions in TRAMP lung tissues

Metastatic lung lesions (clusters of ≥ 10 metastatic cells) per mm^2 in TRAMP mice treated with water vehicle (H_2O/V), 100 mg/kg DMAPT, 10% ethanol/saline vehicle (Eth/V), and 40 mg/kg PTL (in ethanol/saline), * $p < 0.05$, n = 10.

Modulation of pro-metastatic pathways by ethanol and PTL/DMAPT in TRAMP primary tumours

In addition to examining the changes to TRAMP tumour burden induced by the different treatment groups, analysis of primary prostate tumours from all treatment groups was undertaken to investigate pathways that may result in a more aggressive metastatic tumour phenotype. A panel of five proteins (collagen IV, fibronectin, laminin, MMP2 and integrin β1), all of which are known to be important for the metastatic process, were analysed for changes in expression.

Primary prostate tumour sections were analysed for protein expression using immunofluorescence, with fluorescence intensity per nuclei used as a marker of expression. In the primary prostate tumours of ethanol/saline vehicle-treated TRAMP mice, expression of collagen IV (Figure 4-17), fibronectin (Figure 4-18), laminin (Figure 4-19), MMP2 (Figure 4-20) and integrin β1 (Figure 4-21) were significantly increased above baseline (water vehicle-treated) levels (collagen IV: 1.65 fold increase, $p = 0.015$; fibronectin: 1.31 fold increase, $p = 0.016$; laminin: 1.49 fold increase, $p = 0.023$; MMP2: 2.05 fold increase, $p = 0.045$; integrin β1: 1.66 fold increase, $p = 0.009$). PTL treatment returned collagen IV, laminin, MMP2 and integrin β1 expression to baseline levels ($p < 0.05$), compared to ethanol control-treated mice. In DMAPT-treated mice, expression of laminin and MMP2 was significantly reduced in primary prostate tumours compared to baseline levels (laminin: 0.52 fold reduction, $p = 0.031$; MMP2: 0.49 fold reduction, $p = 0.015$) (Figure 4-19 and Figure 4-20).

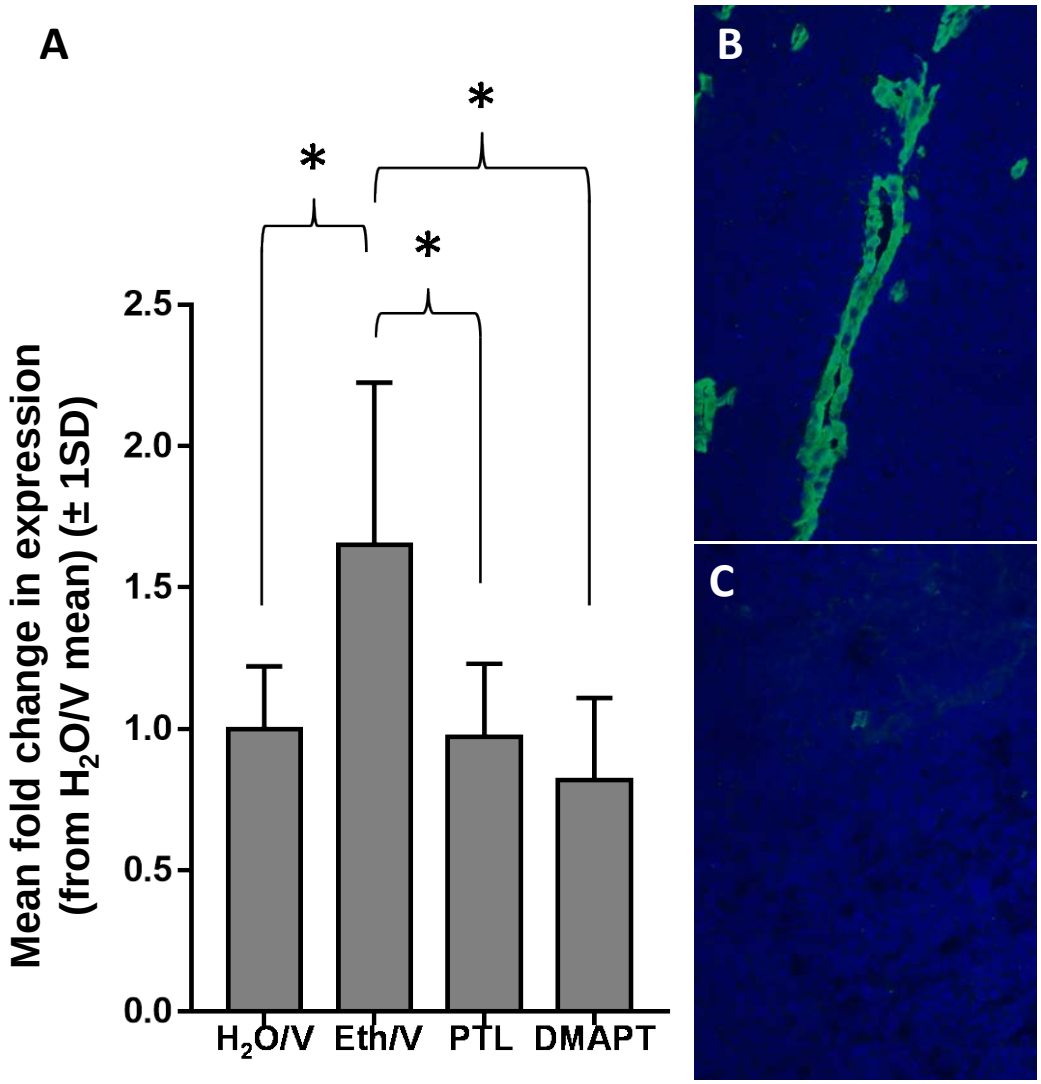

Figure 4-17: Fold changes in collagen IV protein expression in treated TRAMP primary prostate tumours

(A) Fold changes in expression (from water vehicle (H_2O/V)) in tumours from TRAMP mice treated with 10% ethanol/saline vehicle (Eth/V), 40 mg/kg PTL (in ethanol/saline) or 100 mg/kg DMAPT. *$p < 0.05$, n = 9-17 mice per treatment group. Representative images of (B) positive control and (C) negative control staining in TRAMP primary prostate tumours.

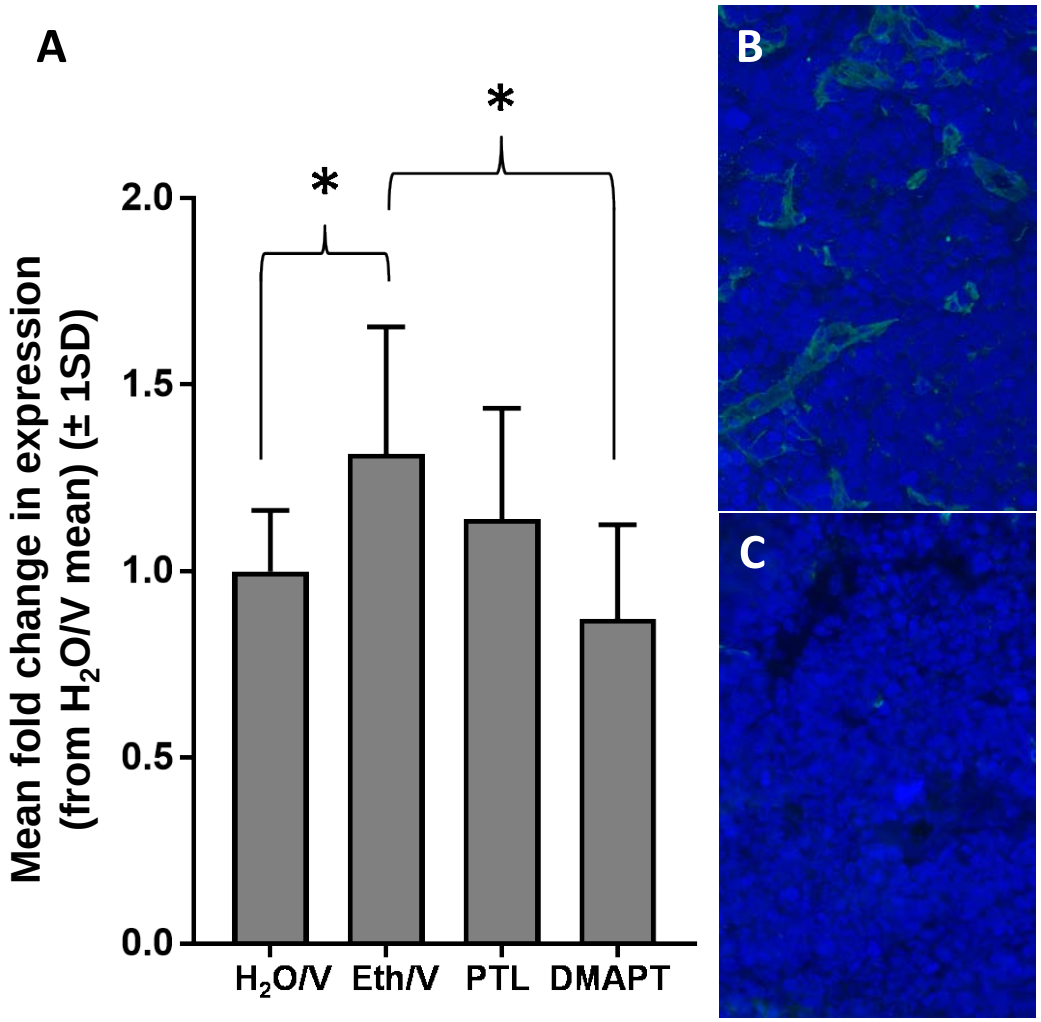

Figure 4-18: Fold changes in fibronectin protein expression in treated TRAMP primary prostate tumours

(A) Fold changes in expression (from water vehicle (H_2O/V)) in tumours from TRAMP mice treated with 10% ethanol/saline vehicle (Eth/V), 40 mg/kg PTL (in ethanol/saline) or 100 mg/kg DMAPT. *$p < 0.05$, n = 9-17 mice per treatment group. Representative images of (B) positive control and (C) negative control staining in TRAMP primary prostate tumours.

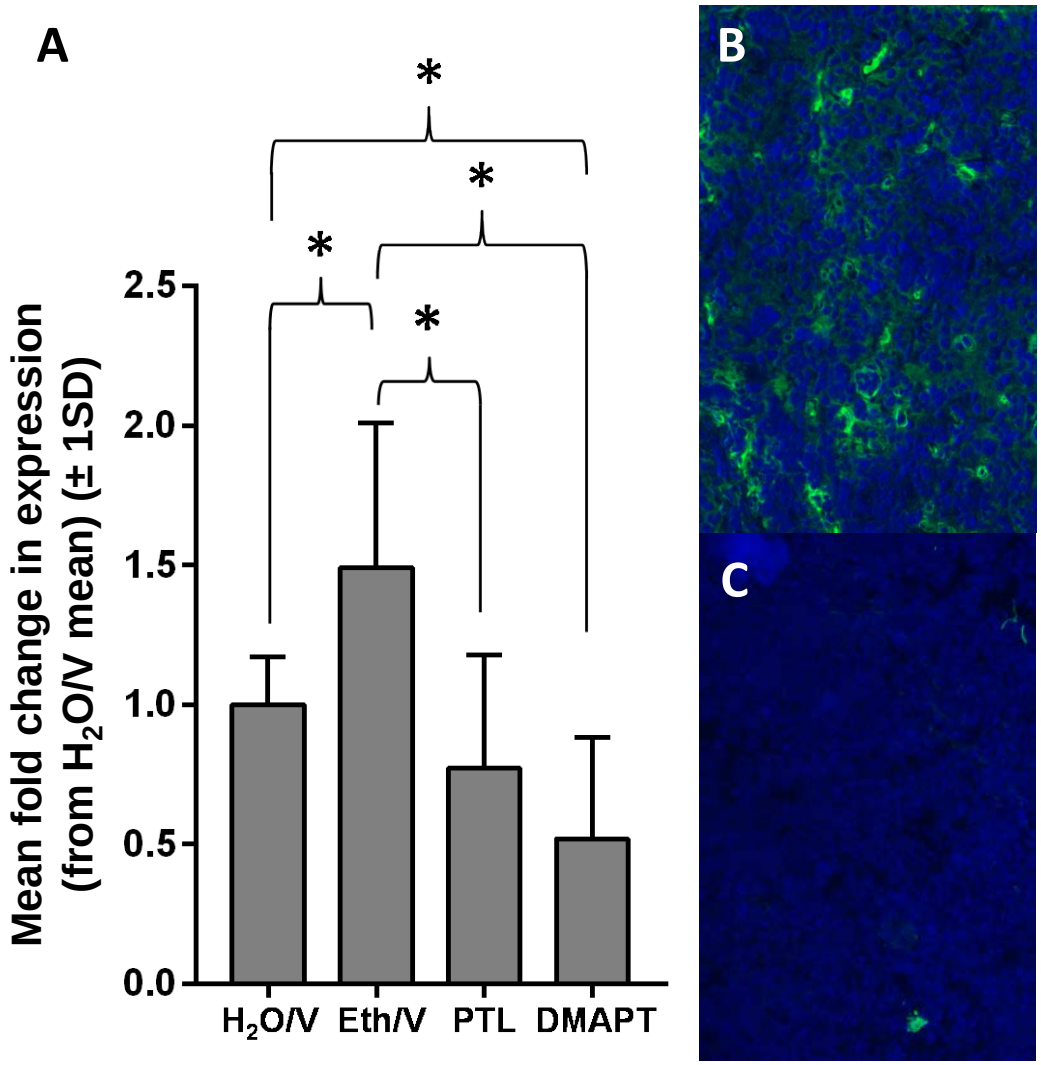

Figure 4-19: Fold changes in laminin protein expression in treated TRAMP primary prostate tumours

(A) Fold changes in expression (from water vehicle (H_2O/V)) in tumours from TRAMP mice treated with 10% ethanol/saline vehicle (Eth/V), 40 mg/kg PTL (in ethanol/saline) or 100 mg/kg DMAPT. *$p < 0.05$, n = 9-17 mice per treatment group. Representative images of (B) positive control and (C) negative control staining in TRAMP primary prostate tumours.

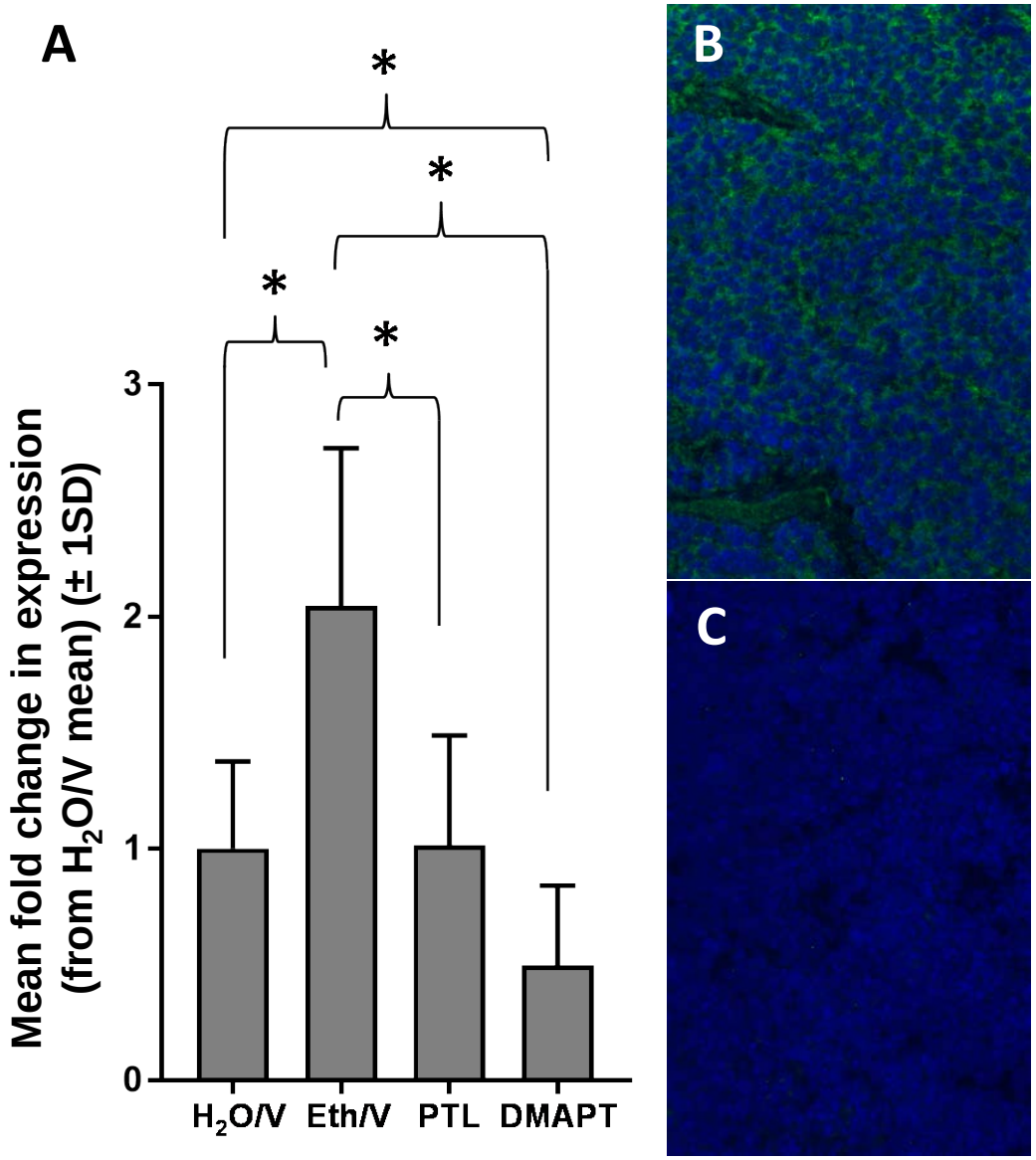

Figure 4-20: Fold changes in MMP2 protein expression in treated TRAMP primary prostate tumours

(A) Fold changes in expression (from water vehicle (H_2O/V)) in tumours from TRAMP mice treated with 10% ethanol/saline vehicle (Eth/V), 40 mg/kg PTL (in ethanol/saline) or 100 mg/kg DMAPT. *$p < 0.05$, n = 9-17 mice per treatment group. Representative images of (B) positive control and (C) negative control staining in TRAMP primary prostate tumours.

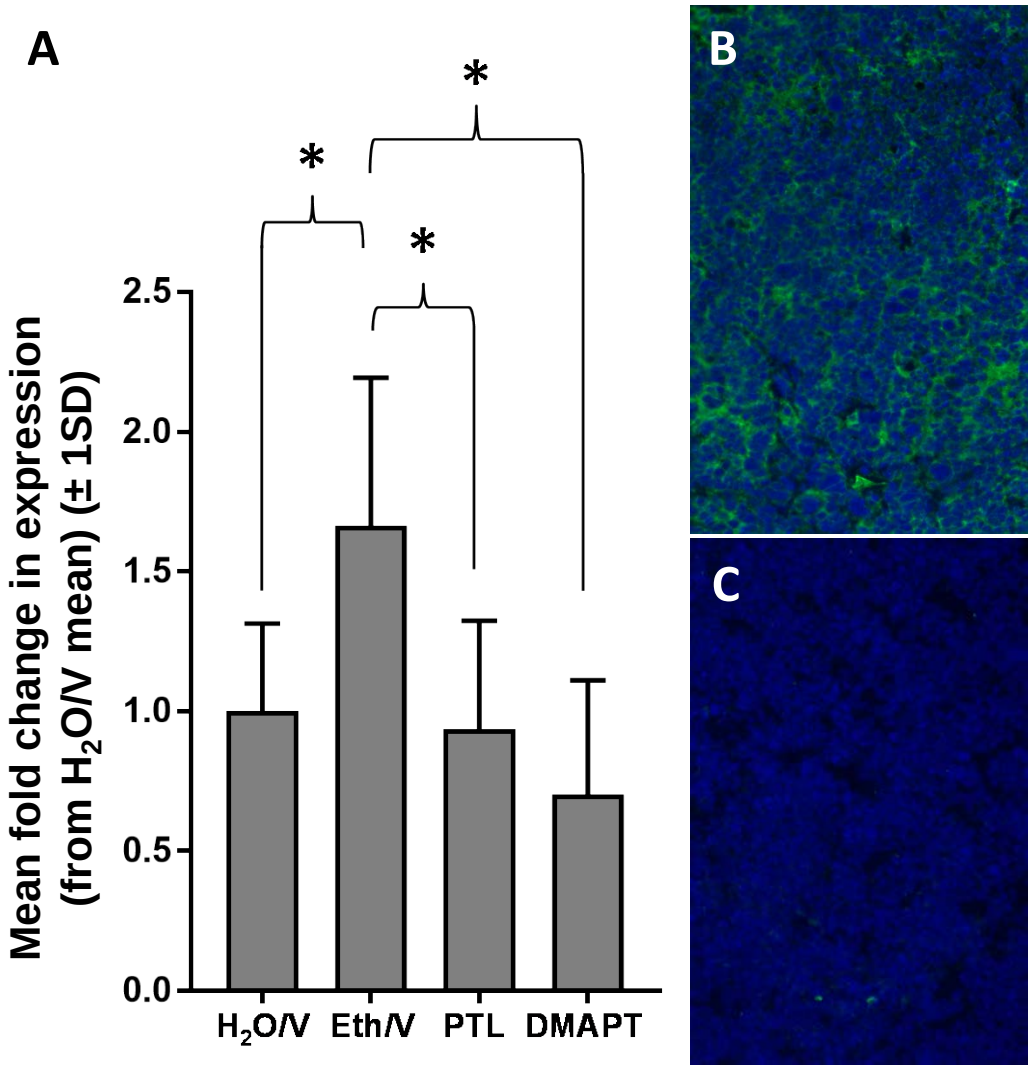

Figure 4-21: Fold changes in Integrin ß1 protein expression in treated TRAMP primary prostate tumours

(A) Fold changes in expression (from water vehicle (H_2O/V)) in tumours from TRAMP mice treated with 10% ethanol/saline vehicle (Eth/V), 40 mg/kg PTL (in ethanol/saline) or 100 mg/kg DMAPT. *$p < 0.05$, n = 9-17 mice per treatment group. Representative images of (B) positive control and (C) negative control staining in TRAMP primary prostate tumours.

In primary prostate tumours, collagen IV staining showed strong expression in the basement membrane of vessels (Figure 4-22). This collagen IV staining identifies a very different, fragmented structure to that of the vascular basement membrane in primary prostate tumours of the ethanol vehicle-treated TRAMP mice (Figure 4-22C), compared to the structure of the vascular basement membrane in other treatment groups.

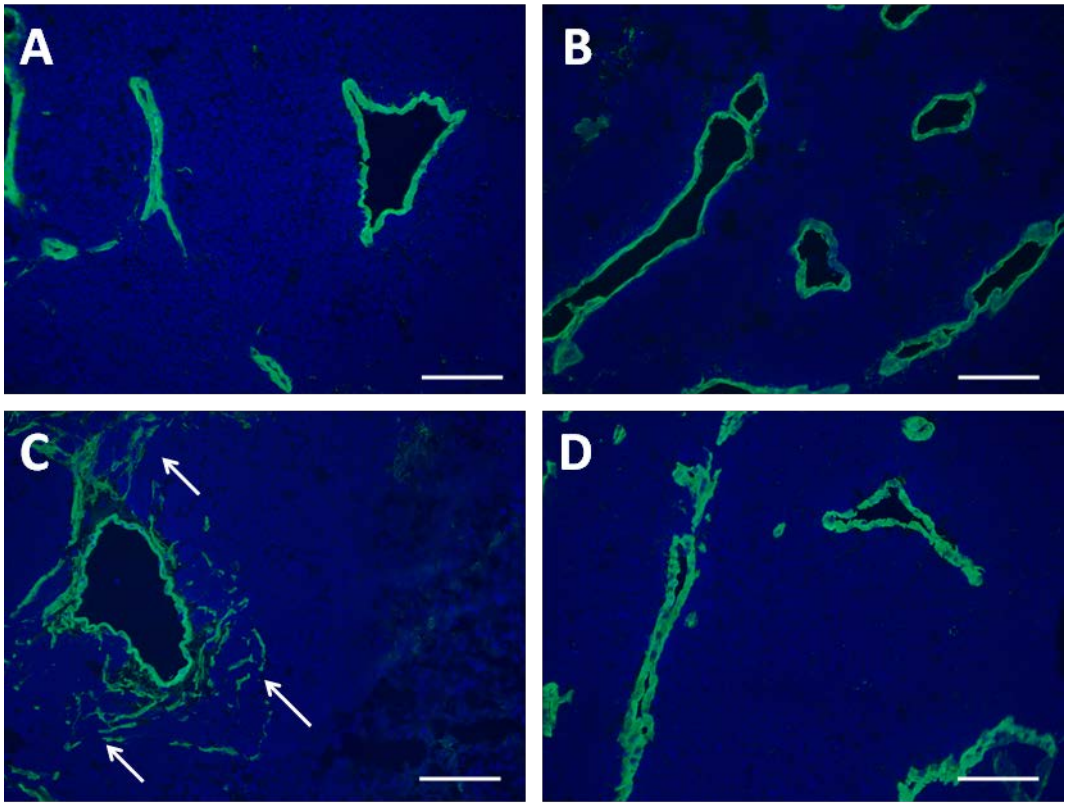

Figure 4-22: Collagen IV staining around vessels in treated TRAMP primary tumours

Representative vascular staining in tumours from TRAMP mice treated with (A) PTL (40 mg/kg in 10% ethanol/saline), (B) DMAPT (100 mg/kg in water), (C) ethanol/saline vehicle and (D) water vehicle 3 x per week until palpable tumour detection. Collagen IV staining in the ethanol treatment groups demonstrates a more fragmented and less rigid vascular basement membrane structure (representative regions indicated with arrows) compared to the other treatment groups.

To check if the collagen IV staining was identifying vascular areas only, dual staining was carried out with CD31 to identify vessels within tissue sections (Figure 4-23). Co-localisation of collagen IV and CD31 within tissue sections of primary prostate tumours revealed that while a large portion of the collagen IV staining was localised within the vessel walls, there was no co-localisation with CD31 in the more fragmented regions typically observed in the tumours of ethanol/saline vehicle-treated mice. This may indicate there is some level of ethanol-induced breakdown or fragmentation of collagen in primary prostate tumours, which is likely to allow greater escape of tumour cells and ultimately invasion to distant sites.

CD31 staining was also used to measure vascular area within the TRAMP prostate tumours. Vascular area was measured as the percentage of CD31-positve area in the total nuclei area (Figure 4-24). Vascular area in the primary prostate tumours was significantly higher in mice treated with the ethanol/saline vehicle (8.3 ± 3.7 %) compared to all other treatment groups (5.3 ± 2.4 %, 4.7 ± 1.6 % and 4.4 ± 2.6 %, in water vehicle, PTL and DMAPT treatment groups respectively, $p < 0.05$) (Figure 4-25)

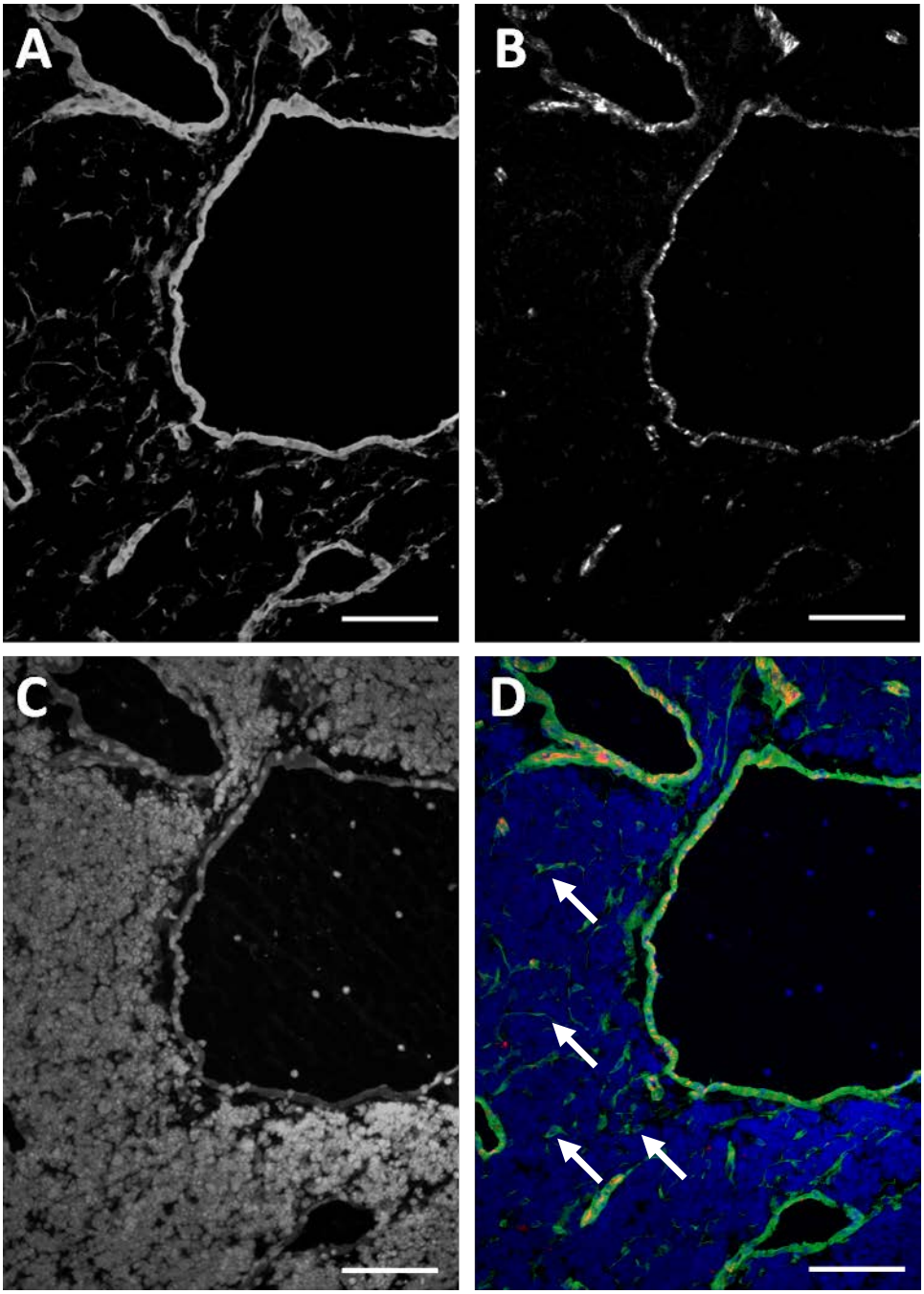

Figure 4-23: Co-localisation of collagen IV and CD31 in treated TRAMP prostate tumour vasculature

Representative images of co-localisation of vascular markers in TRAMP primary prostate tumours treated with 10% ethanol/saline vehicle 3 x weekly until palpable tumour formation. (A) Collagen IV, (B) CD31, (C) DAPI, and (D) false-coloured merged image with collagen IV (green), CD31 (red) and DAPI (blue), representative instances of fragmented regions of collagen IV-only immunoreactivity marked by white arrows. Scale bar 50 µm.

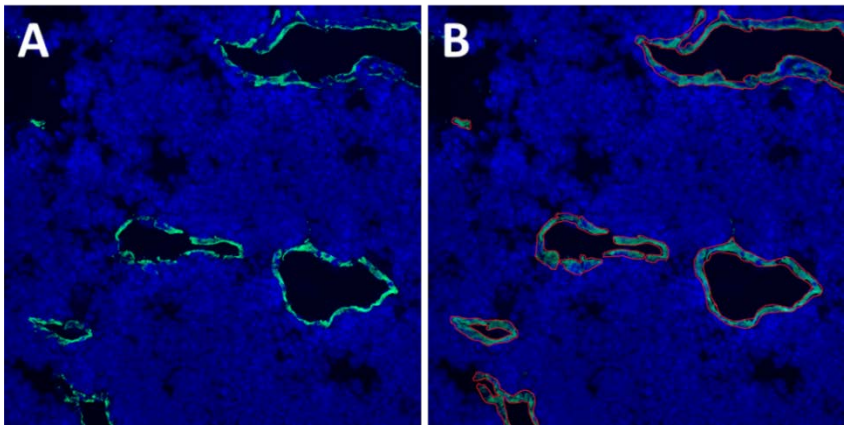

Figure 4-24: Identification of CD31-positive area in TRAMP primary prostate tumours

(A) Representative images of false-coloured images of CD31 (green) immunoreactive regions and DAPI-stained nuclei (blue) within treated TRAMP primary prostate tumours. (B) CellProfiler identification of CD31-positive area (red outlines), which was used to calculate vascular area as a percentage of total nuclei area.

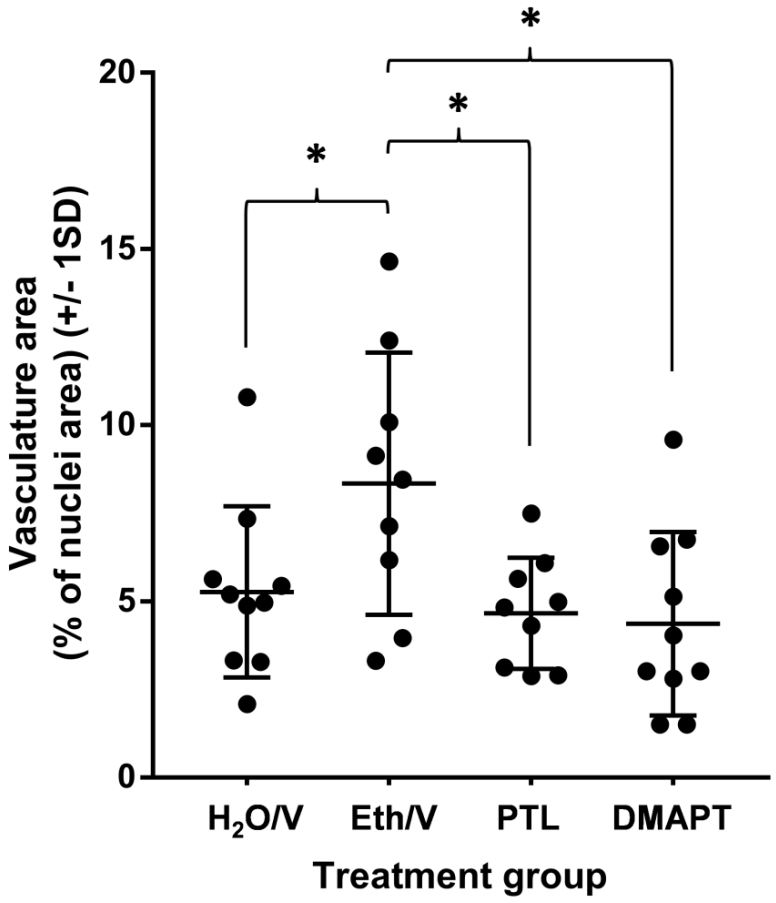

Figure 4-25: Percentage of vascular area in treated TRAMP primary prostate tumours

Vascular area (as a percentage of total nuclei area) in primary tumours from TRAMP mice treated with water vehicle (H_2O/V), ethanol/saline vehicle (Eth/V), 40 mg/kg PTL (in ethanol/saline) or 100 mg/kg DMAPT. *$p < 0.05$, n = 9-10 mice per treatment group.

Anti-cancer effects of DMAPT in prostate tumour explants

Human prostate tumour explant culture studies were undertaken in order to further examine the anti-cancer effects in a model that more closely recapitulates the genetic heterogeneity of human disease.

Fresh prostate cancer specimens were cut into small tissue pieces and cultured in triplicate on a pre-soaked gelatin sponge in the presence or absence of DMAPT (6 µM, 12 µM or 24 µM) for 48h. The tissues were then analysed by immunohistochemistry for the proliferative marker Ki-67 and apoptosis marker cleaved caspase-3. The culturing and immunohistochemical staining of prostate tumour tissues was carried out in collaboration with Associate Professor Lisa Butler and the Prostate Cancer Research Group at the South Australian Health and Medical Research Institute (Adelaide, South Australia). Analysis of stained tissue sections was carried out at Flinders University.

There was no significant difference in proliferation between the water vehicle (2.68 ± 1.5 %), 6 µM DMAPT (1.39 ± 0.69 %), 12 µM DMAPT (1.08 ± 0.86 %) and 24 µM DMAPT (1.68 ± 0.71 %) treatment groups; however, there was a trend towards decreased proliferation in the DMAPT-treatment groups (Figure 4-26C). There was also no significant difference in apoptosis between tissues treated with water vehicle (1.95% ± 1.1), 6 µM DMAPT (4.06% ± 2.3), 12 µM DMAPT (4.15% ± 2.4) or 24 µM DMAPT (2.52% ± 1.8), but again there was a trend towards increased apoptosis with DMAPT treatment (Figure 4-27C). The most pronounced changes in apoptosis and proliferation were observed before and after culturing of the explant tissues in the absence of DMAPT (Figure 4-28 and

Figure 4-29 respectively). Ki-67 staining was notably reduced (47.8 % reduction, p = 0.065, Figure 4-26C) and cleaved caspase-3 staining was increased (5961.5 % increase, p = 0.028, Figure 4-27C) in explant tissues after 48 hours of culturing. In addition to changes in proliferation and apoptosis before and after tissue culturing, there was an observable difference in tissue structure with a clear loss of glandular structure in the prostate tissue sections after 48 hours of culturing. This loss of structure made differentiating normal tissue from regions of prostate tumour tissue difficult at times.

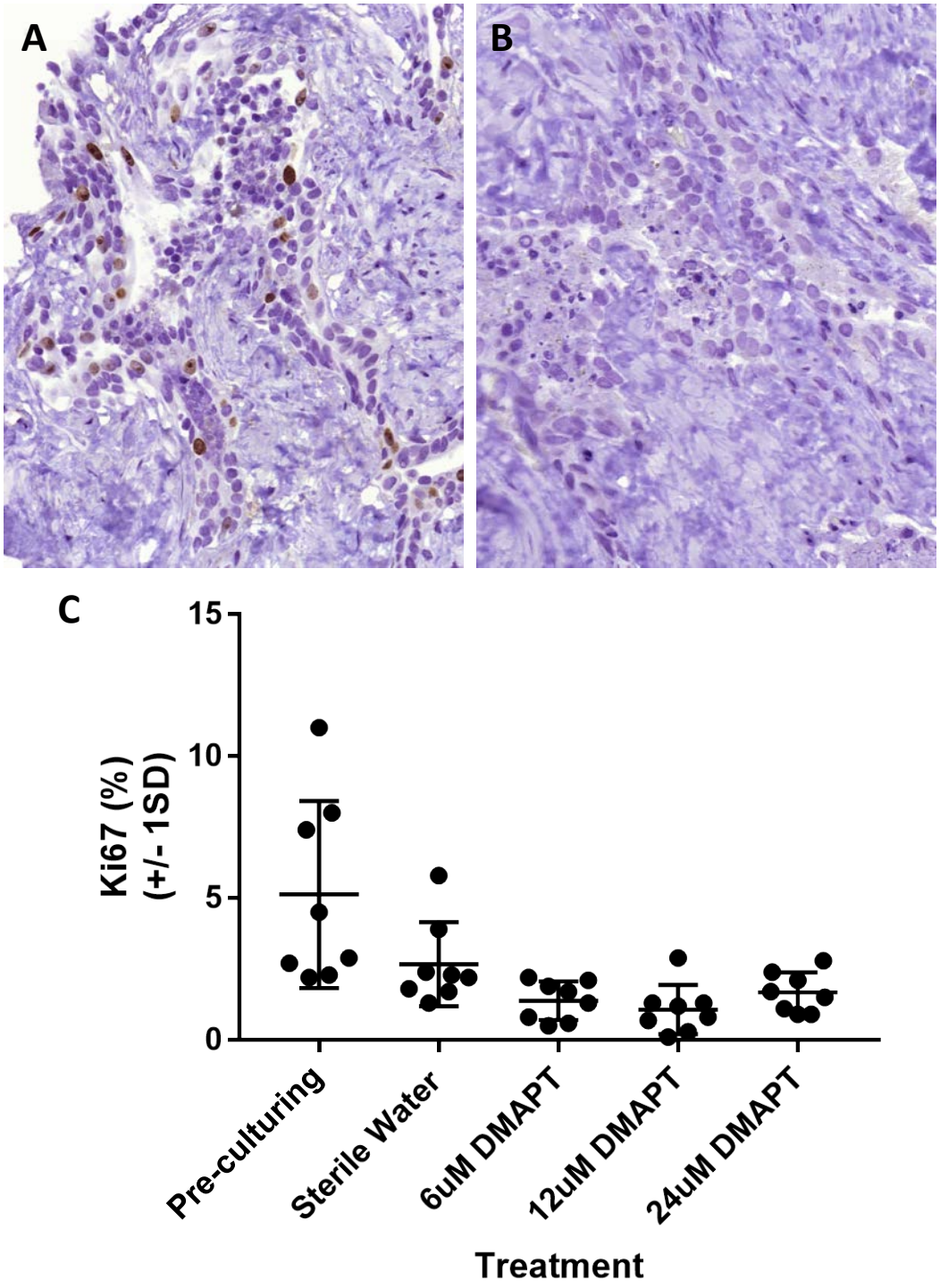

Figure 4-26: Proliferation in treated human prostate tumour explant tissue sections

Representative images of (A) high and (B) low Ki-67 staining in treated human prostate tumour explant tissues. (C) Percentage of proliferation (Ki67 positive cells) from total prostate epithelial cells in explant tissue sections, with analysis carried out prior to culturing, or after 48 h of treatment with sterile water, 6 µM, 12 µM or 24 µM DMAPT, n = 8.

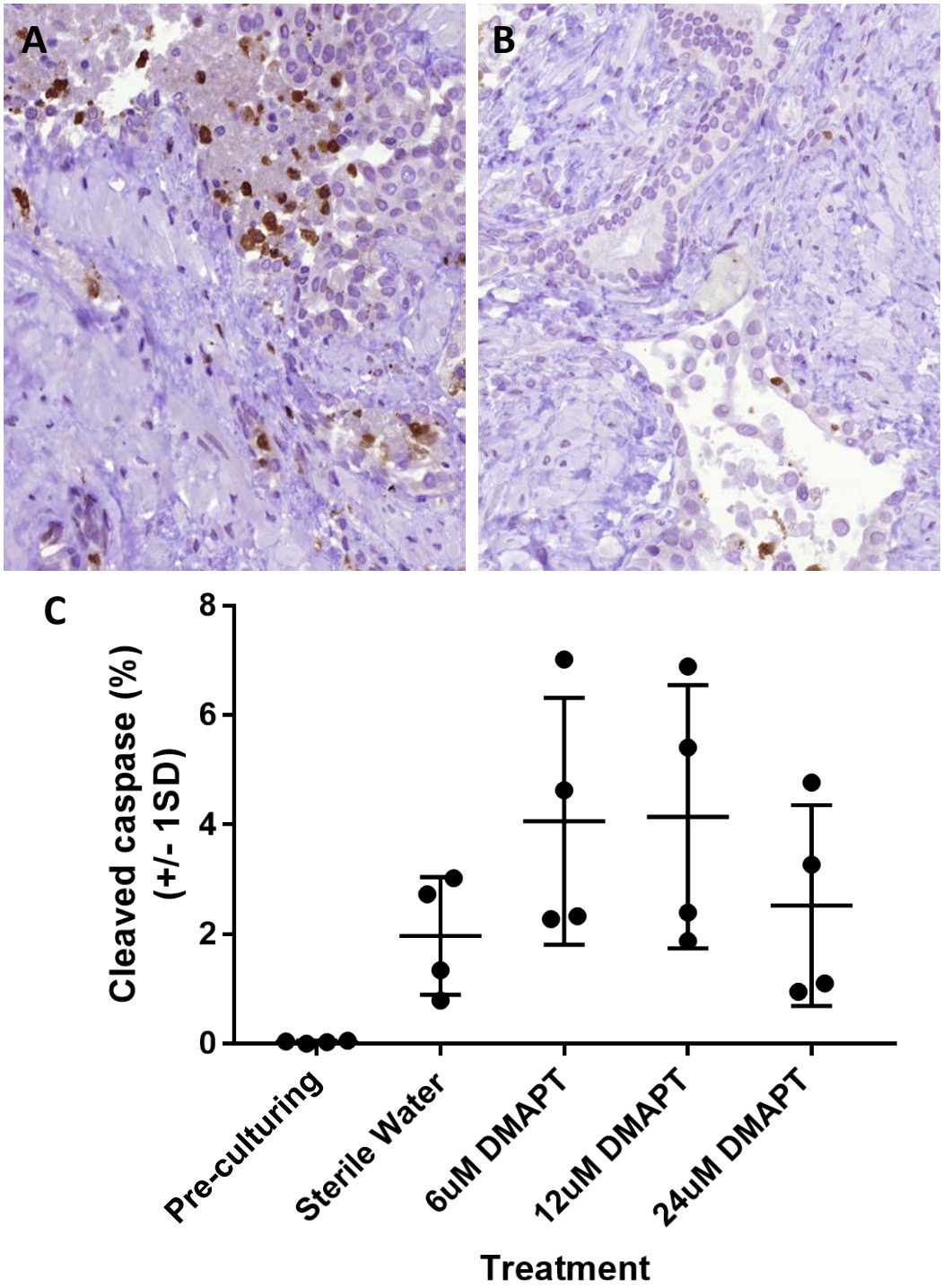

Figure 4-27: Apoptosis in treated human prostate tumour explant tissue sections

Representative images of (A) high and (B) low cleaved caspase-3 staining in treated human prostate tumour explant tissues. (C) Percentage of apoptosis (cleaved caspase-3 positive cells) from total prostate epithelial cells in explant tissue sections, with analysis carried out prior to culturing, or after 48 h of treatment with sterile water, 6 µM, 12 µM or 24 µM DMAPT, n = 4.

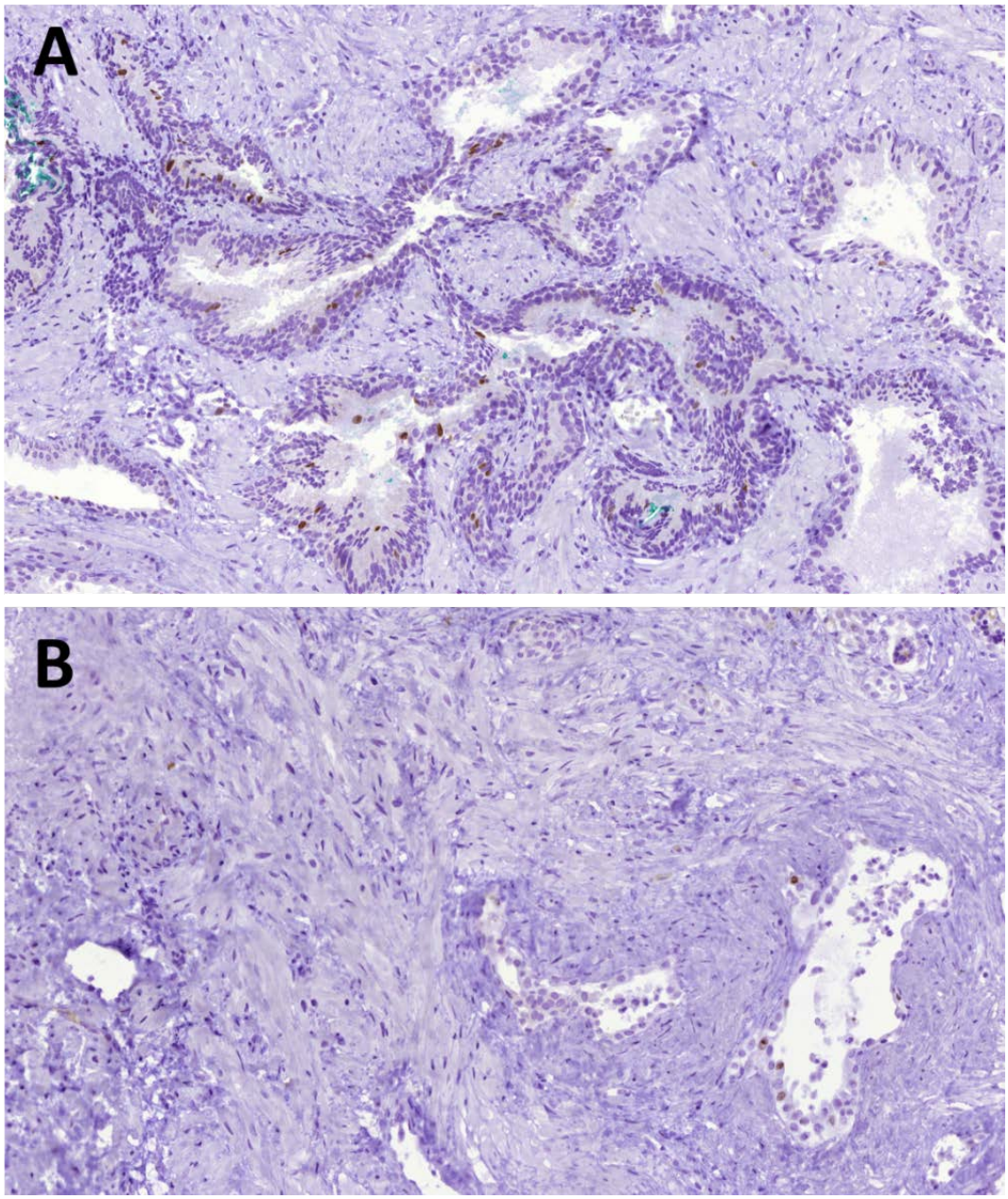

Figure 4-28: Ki-67 staining in human prostate tumour explant tissue sections before and after culturing

Representative images of Ki-67 staining in untreated human prostate tumour explant tissue sections (A) before culturing and (B) after 48 h of culturing. After culturing, tumour structure is significantly altered and Ki-67-positive cells are reduced.

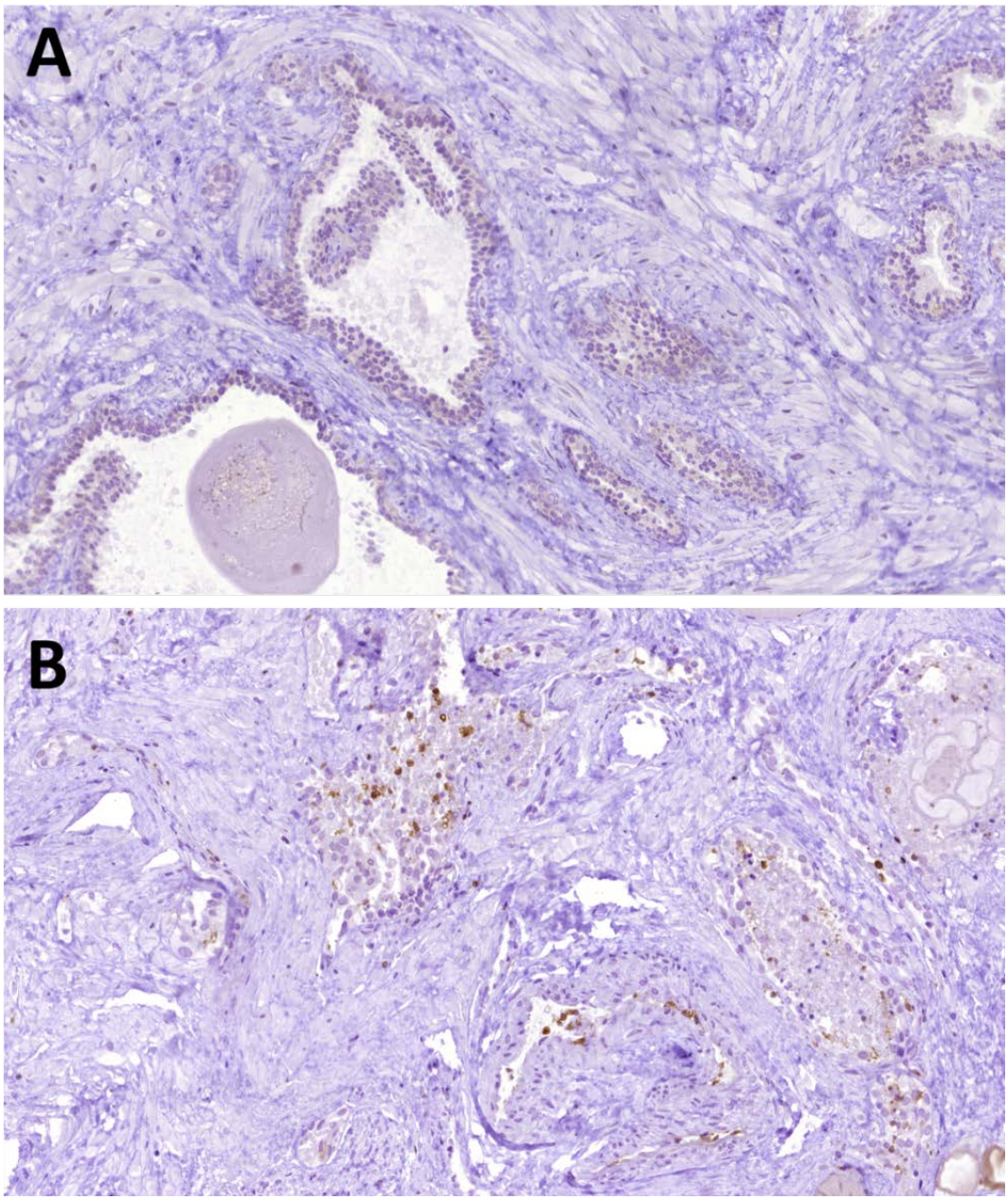

Figure 4-29: Cleaved caspase-3 staining in human prostate tumour explant tissue sections before and after culturing

Representative images of cleaved caspase-3 staining in untreated human prostate tumour explant tissue sections (A) before culturing and (B) after 48 h of culturing. After culturing, tumour structure is significantly altered and cleaved caspase-3-positive cells are increased.

Discussion

The aim of these experiments was to study the ability of PTL and DMAPT to slow tumour growth in an autochthonous model of prostate cancer. Of the two drugs, only DMAPT significantly delayed time-to-palpable tumour in the TRAMP model. PTL, which was delivered in a 10% ethanol/saline vehicle, did not slow tumour development in TRAMP mice compared to vehicle control treatment groups. This inability to significantly alter tumour latency may be due to low plasma concentration of PTL compared to DMAPT. The poor solubility of PTL restricts dosing of mice to a maximum of 40 mg/kg, providing a maximum plasma concentration of less than 1 µM, which is well below ideal therapeutic plasma concentrations of 5-10 µM (*Sweeney et al., 2005*), while DMAPT dosed at 100 mg/kg results in a maximum plasma concentration above 10 µM (*Guzman et al., 2007*). While the dosing restrictions of PTL may help to explain a reduced anti-cancer effect compared to DMAPT, it was surprising that no significant difference in time-to-palpable tumour compared to vehicle controls was observed, especially given the significant decrease (27% reduction) in xenograft tumour growth observed by Kawasaki et al. (*2009*) using 40 mg/kg of PTL in an ethanol/saline vehicle. This suggests that there are other factors playing a role in the lack of response than just dosing concentration alone. Additionally, it was found that the ethanol/saline vehicle induced NF-κB expression, potentially counteracting one of the main mechanisms of action of PTL and DMAPT. Analysis of primary prostate tumours and liver tissues from this study found that NF-κB expression was upregulated in the ethanol/saline vehicle control group compared to the water vehicle treatment group (E. Solly, Flinders University,

personal communication). High doses of alcohol have previously been reported to upregulate NF-κB expression *in vitro* and *in vivo* in a number of tissue types, including normal and tumour cells (*Hsiang et al., 2007; Nanji et al., 1999; Banan et al., 2007*), and consistently higher levels of NF-κB and VEGF have been reported in the liver of heavy drinkers (*Wang et al., 2015; Hill et al., 2000*). The results of this TRAMP study suggest for the first time that even low levels of ethanol are able to promote activation of NF-κB over time. This pro-inflammatory effect induced by low doses of ethanol may be masking the ability of PTL to slow prostate tumour development, making it difficult to judge the efficacy of PTL as a cancer preventive. In the xenograft study by Kawasaki et al. (*2009*) tumour development was significantly faster than was observed in TRAMP mice. The xenograft mice started with rapidly growing PC3-derived tumours, and mice were only treated for up to 106 days, compared to 252 days of treatment in the TRAMP mice. The results from the TRAMP studies indicate that the ethanol driven increase in NF-κB expression in primary prostate tumours increased with administration time (E. Solly, Flinders University, personal communication), with expression levels rising above those of water vehicle-treated mice after approximately 170 days of treatment. Therefore, it is possible that xenograft animals may not have been treated for sufficient time to produce an ethanol-induced increase in NF-κB, which could counteract the anti-cancer effects of PTL. An additional major difference between the Kawasaki *et al.* (*2009*) study and the present study is the immune status of the mice used. The pro-NF-κB effect of ethanol might be more pronounced in the presence of a fully functioning immune system in TRAMP mice, compared to immunodeficient

NOD/SCID mice used in the Kawasaki *et. al.* (*2009*) study. Members of the NF-κB transcription factor family play a critical role in innate immunity (reviewed in *Dev et al., 2011; Baeuerle & Henkel, 1994*) and therefore small changes in NF-κB activation may be less pronounced in immune-suppressed animals. Given the frequent use of ethanol as a vehicle in many drug studies, the pro-NF-κB effect of chronic low doses of ethanol requires further investigation, as it may be causing confounding effects in other studies.

Unexpectedly, it was observed that the long-term administration of low doses of ethanol (approximately 36 µL of pure ethanol per mouse per week) to TRAMP mice resulted in a significant change in tumour phenotype, from small to large aggressive metastases and from large to very small primary prostate tumours in approximately half of the ethanol/saline vehicle-treated mice. Metastatic burden was significantly increased in the ethanol/saline vehicle treatment group, compared to all other treatment groups. This ethanol-induced shift to a pro-metastatic tumour phenotype was observed in both of the two separate long-term *in vivo* studies. There is limited evidence that ethanol can increase or decrease cancer incidence depending on the tumour and again the mechanisms are still largely unknown (reviewed in *Meadows & Zhang, 2015*). The large majority of *in vivo* animal studies have investigated the relationship between high doses of ethanol and cancer incidence, rather than lower chronic doses of ethanol used in this study. A small number of studies in non-tumour murine models have examined the effect of low chronic doses of ethanol (approximately 40 to 800 µL pure ethanol per mouse per day delivered orally for 8 to 65 weeks)

(*Anderson, 1988; Anderson et al., 1992; Hackney, Engelman & Good, 1992; Kristiansen, Clemmensen & Meyer, 1990; Zariwala, Lalitha & Bhide, 1991*). No increase in tumour incidence was observed in these studies. In this thesis, the non-transgenic control mice that were administered ethanol/saline orally did not develop tumours, which is consistent the current literature. Also, there is epidemiological evidence that suggests that regular low to moderate alcohol consumption may actually reduce prostate cancer risk (*Schoonen et al., 2005*). The TRAMP results suggest that low chronic doses of ethanol are able to modulate the metastatic process in developing tumours but do not substantially increase spontaneous tumour development, which may explain why epidemiological studies found no association between low and moderate alcohol consumption and prostate cancer risk.

In the case of prostate cancer specifically, a few studies in humans have shown a potential association between heavy alcohol consumption and high-risk metastatic prostate cancer (*Dennis & Hayes, 2001; Fillmore et al., 2009; Gong et al., 2009*), and *in vivo,* there is evidence that high *in utero* exposure to ethanol increases the risk of prostate cancer incidence in male rats (*Murugan et al., 2013; Sarkar, 2015*). There are no published studies that have specifically investigated the effects of ethanol in the TRAMP model. Ethanol is commonly used as a vehicle for *in vivo* drug studies, but no TRAMP studies in the literature have used similar levels of ethanol administration to that used here. One study used low doses of ethanol administered as part of the vehicle control group in a long-term treatment protocol (*Jung-Hynes et al., 2011*), where TRAMP mice

received approximately 90 to 120 µL of 100% ethanol per mouse per day in drinking water for up to 18 weeks. This administration resulted in no reported change in TRAMP tumour phenotype or metastatic incidence. While this study may seem to contradict the results outlined in this thesis, one major difference between the two studies is the age of the mice at the start of ethanol administration. Here, TRAMP mice were administered ethanol from 6 weeks of age, while Jung-Hynes et al. (*2011*) started treatment from 16 weeks of age. At 16 weeks of age, prostate tissue in TRAMP mice will have progressed to contain moderate levels of PIN, with the occasional mouse showing signs of high grade PIN and prostatic adenocarcinoma (*Gingrich et al., 1996; Gingrich et al., 1999*). Potentially the administration of ethanol is required from the very early stages of prostate tumorigenesis to result in such a pronounced metastatic effect. Unfortunately, investigating this hypothesis was not possible during the time constraints of this thesis, as tissues from the long-term TRAMP studies were taken at the time of palpable tumour detection, which was as long as 34 weeks later than the estimated start of primary tumour initiation. By the time TRAMP primary tumours are able to be identified by palpation, many of the key tumour initiating proteins, such as AR, are unable to be easily detected in the tissue. Ideally, studies with low dose ethanol in TRAMP mice could be carried out where molecular changes to tissues are examined at several time-points over the course of tumour development. The results presented here are the first to demonstrate such a pronounced aggressive pro-metastatic effect in TRAMP mice without significant primary prostate tumour development. There has been one reported instance of 'tumour-free' metastasis in the absence of ethanol in

C57BL/6/TRAMP mice (*Gelman et al., 2014*). In that study a small number of mice, 30 weeks of age or older and with PIN-stage prostate tissue developed pulmonary metastatic lesions, suggesting that, at least in some cases, prostate metastases can derive from rare, aggressive cells that disseminate early. The metastatic lesions reported by Gelman et al. (*2014*) did not result in large palpable tumours, however the results indicate that TRAMP prostate tumour cells have the potential to escape very early in the tumorigenic process. The chronic pro-inflammatory effect of ethanol administration observed in the TRAMP studies presented in this thesis suggests that ethanol is increasing the ability of these early disseminating cells to escape and spread to distant sites.

In addition to promoting the development of large palpable metastatic tumours, the ethanol/saline vehicle treatment induced pulmonary metastatic lesions in TRAMP mice, further indicating significant upregulation of tumour spread throughout the body. Little is known about the role of ethanol in EMT and metastasis, however, it has been shown that acetaldehyde, the primary metabolite of ethanol, is associated with invasive potential by inducing expression of the matrix metalloproteinase, MMP9, via NF-kB and AP1 in human hepatocellular carcinoma cells (*Hsiang et al., 2007*). MMPs, particularly MMP2 and MMP9, play key roles in metastatic processes in many tumour types. In prostate cancer, increased expression of MMP2 is often reported in high Gleason grade tumours (*Still et al., 2000; Wood et al., 1997; Murray et al., 2012*), and expression in serum has been positively correlated with increased lymph node and bone metastasis, and poor clinical outcomes (*Gohji et al., 1998; Murray et*

al., 2012). MMP2 has also been reported to play a role in ethanol induced breast cancer cell invasion (*Aye et al., 2004*). In the TRAMP studies described here, expression of MMP2 in primary prostate tumours was significantly increased in the ethanol/saline vehicle treatment group, compared to the water vehicle treatment group, with the greatest expression observed in the small non-palpable tumours, where palpable aggressive metastatic tumours were present. Like NF-kB, MMP2 is known to play a key role in the modulation of inflammation (reviewed in *Parks, Wilson & Lopez-Boado, 2004*).

Activated MMP-2 is capable of degrading type IV collagen, the most abundant component of the basement membrane. Degradation of the basement membrane is an essential step for the metastatic progression of most cancers, including prostate cancer. Interestingly, the ethanol/saline vehicle treatment increased expression of collagen IV in primary TRAMP tumours, which was not expected given the significant upregulation of MMP2 in the tissues. However, it was observed that collagen IV expression strongly co-localised with blood vessel regions within tumour sections. This is not unusual, as it has been reported that almost 100% of vascular surfaces in tumours stain positive for collagen IV (*Baluk et al., 2003*). As protein expression in immunofluorescently stained tumour sections was normalised to the tissue area examined, it was determined that the increased collagen IV expression was reflective of the increased vascularisation present in the primary tumours of TRAMP mice treated with ethanol/saline vehicle. This increased vascularisation in primary tumours where aggressive metastasis was observed, agrees with reports in the literature that ethanol can

induce NF-κB and VEGF expression in tumours (*Wang et al., 2015*), both of which play critical roles in tumour angiogenesis (*Sakurai & Kudo, 2011*). In addition to highlighting the increased vascularisation of primary tumours in the ethanol/saline vehicle-treated mice, the collagen IV staining identified regions of the vascular basement membrane that were irregular in thickness, had multiple fragmented layers, and invaded into the tumour. All of these features are consistent with the unstable or dynamic nature of tumour vessels (*Baluk et al., 2003; Nagy et al., 2009*). This increased degradation of vascular basement membrane is known to increase the leakiness of tumours and hence the possibility of tumour cells to escape and disseminate to other sites of the body (*Kelley et al., 2014; Kleinman et al., 2001; Hida et al., 1994*). These results suggest that ethanol is playing an inflammatory role in the breakdown of vascular basement membranes, this may allow cells to escape the primary tumour earlier and travel to distant sites to metastasise.

In addition to promoting collagen breakdown in the vascular basement membrane, one of the major functions of MMP2 in cancer progression is its role in ECM degradation, which allows dissemination of cancer cells from the primary tumour to distant sites throughout the body. Integrins and focal adhesion molecules can act as bridges for interactions between cells and the ECM, potentially facilitating the escape of tumour cells to distant sites (*Ganguly et al., 2013; Fornaro, Manes & Languino, 2001*). There has been one report (*Schaffert, Sorrell & Tuma, 2001*) which showed selective increases in integrin subunits and integrin signalling in hepatocytes after chronic ethanol administration but the

role of integrins in ethanol associated cancer has not been studied. Levels of β1 integrins are known to be increased in prostate cancer cells in primary prostate cancer with lymph node and bone metastases, suggesting that β1 integrin activation occurs in metastatic progression of prostate cancer (*Lee et al., 2013; Sottnik et al., 2013*). In TRAMP primary prostate tumours, expression of β1 integrin was increased in ethanol/saline vehicle-treated mice compared to water vehicle mice. As was the case with MMP2 expression, the greatest expression was observed in the small non-palpable primary tumours of mice that developed palpable metastases. Given that β1 integrin is a key transmembrane receptor for the ECM ligands fibronectin and laminin, it was not surprising that expression of these proteins was also upregulated in the primary prostate tumours of the ethanol/saline vehicle-treated TRAMP mice. Adhesion to the ECM is an important initial step for cancer cell invasion and metastasis, and high doses of ethanol have previously been shown to induce expression of fibronectin and laminin in a number of cell types and subsequently promote greater focal adhesion to the ECM (*Xu et al., 2010; Roman et al., 2005*). Additionally, fibronectin has been shown to induce expression of MMP2 in prostate cancer cells, which promotes ECM degradation and tumour inflammation (*Moroz et al., 2013*). The pro-metastatic ECM pathways are complex and the multi-directional nature of the signalling pathways makes it difficult to identify which specific molecules are directly targeted by external stimuli; however, it is clear from the analysis of TRAMP primary prostate tumours that low chronic doses of ethanol are able to alter ECM signalling to upregulate tumour escape and invasion.

The pro-inflammatory and pro-metastatic effects of chronic low doses of ethanol did not promote spontaneous tumour development and metastasis in normal mice. However, the number of mice studied was only small (n = 18) and, given the low frequency of spontaneous tumours in C57BL/6J mice, a very large number of mice would need to be studied to determine if ethanol at such low doses was playing a role. It is still to be determined if the pro-metastatic effects of ethanol observed here are specific to the TRAMP model. There are no studies in the literature suggesting that ethanol may be interfering with expression of the TRAMP transgene. There is some evidence that ethanol may inhibit AR (*Chung, 1990*), which is key to the promotion of TRAMP tumorigenesis. In poorly differentiated prostate tumours of TRAMP mice at palpable tumour stage, AR expression becomes heterogeneous, weak or absent (*Kaplan-Lefko et al. 2003; Gingrich et al. 1999*), which is suggested to be due to AR mutations that spontaneously arise in late stage TRAMP tumours and are not detected by commercial AR antibodies (*Kaplan-Lefko et al. 2003*). Unfortunately this meant that AR was not informative in the tumour tissues examined here. Ideally, future studies would include the effects of ethanol in younger TRAMP mice to determine if ethanol is altering expression of AR, and hence expression of the TRAMP transgene, during early initiation of cancer, as well as repeating the experiments performed here in other mouse models of prostate cancer to establish if the effect is TRAMP specific. If the pro-metastatic effect is not specific to the TRAMP model, it may be that while low to moderate alcohol consumption in the wider population is not a risk factor for the development of prostate cancer, it may be a risk factor for metastatic disease in men

predisposed to develop prostate cancer. Potentially epidemiological studies could be designed to examine the relationship between alcohol consumption and metastatic disease in men with a family history of prostate cancer.

Interestingly, mice that were part of the PTL treatment group received the same volume of ethanol as the ethanol/saline vehicle-treated mice but did not display the same metastatic phenotype observed in the ethanol vehicle treatment groups, with the exception of one mouse in the PTL treatment group which displayed a palpable metastatic liver tumour after 208 days of treatment (the longest treatment time of the group). PTL also reduced micrometastases in TRAMP lungs to that of baseline levels and inhibited the upregulation of proteins involved in metastatic escape and spread in primary prostate tumours. Expression of laminin, collagen IV, MMP2 and integrin β1 were all significantly reduced in the primary prostate tumours of PTL-treated TRAMP mice, compared to the ethanol/saline vehicle-treated mice. This highlights the fact that, although administration of PTL (in ethanol/saline) was unable to slow time-to-palpable tumour in TRAMP mice, PTL still had a significant anti-metastatic effect. In future studies, it would be informative to examine the effects of long-term administration of DMAPT in an ethanol/saline vehicle in TRAMP mice, to determine if ethanol also reduces the ability of DMAPT to slow prostate tumour development. Potentially the greater bioavailability of DMAPT (in ethanol/saline) would result in reduced prostate tumour development compared to PTL (in ethanol/saline), but the pro-NF-κB effect of the ethanol/saline vehicle would limit the anti-cancer response to DMAPT compared to DMAPT in water.

There have been two previous *in vivo* studies investigating the ability of DMAPT to slow prostate tumour growth, both in xenograft models (*Xu et al., 2013; Shanmugam et al., 2010*), however, the nature of xenograft models means that previous *in vivo* studies have tended to examine the therapeutic ability of PTL and DMAPT, rather than their chemo-preventive potential. Short-term treatment (IP once daily for five days) of 10 mg/kg DMAPT was unable to significantly reduce growth of PC3 tumours in NCRNU (nu/nu) male mice (*Xu et al., 2013*). Longer-term treatment (oral gavage once daily for up to 88 days) of 100 mg/kg DMAPT significantly reduced PC3 tumour volume by 75% (*Shanmugam et al., 2010*). While this level of tumour impairment is impressive, the experiments were carried out in female athymic mice. Given the important role of androgen in prostate cancer, these results in female mice may be less representative of the human male cancer. In the studies presented in this thesis, long-term treatment (oral gavage thrice weekly for up to 259 days) of 100 mg/kg DMAPT (delivered in a water vehicle) was able to significantly delay prostate tumour development in male TRAMP mice, extending time to palpable prostate tumour detection by more than 41 days. This represents a 20% time delay in tumour development compared to water control-treated mice, and is the first study to show that DMAPT delays tumour onset in an autochthonous model of prostate cancer, supporting the use of DMAPT as a cancer preventive. Effective chemoprevention with other compounds in the TRAMP model has previously been shown to translate successfully into patient outcomes. For example, daily oral dosing of TRAMP mice with green tea polyphenols was shown to increase tumour free survival by 52% and identified that administration of green tea

polyphenols might be beneficial in the early stages of prostate cell transformation but not once tumours were already established (*Gupta et al., 2001*). Subsequently, a clinical trial was carried out with men identified with pre-malignant high grade PIN lesions. Daily oral treatment with green tea polyphenols for one year resulted in a reduction in prostate cancer diagnosis (from 53% to 11%) (*Brausi, Rizzi & Bettuzzi, 2008; Bettuzzi et al., 2006*). The reduction in tumour growth observed with thrice weekly DMAPT treatment was less pronounced than that of the daily green tea polyphenol treatment in TRAMP mice. Both DMAPT and green tea have low toxicity, therefore a daily oral dosing regimen of DMAPT is possible and may provide a greater delay in tumour development than was observed in the thrice weekly dosing studies presented in this thesis. In other cancer types the reported efficacy of DMAPT as a chemo-therapeutic against tumour growth differs significantly. In bladder, breast and lung cancer models, 40-100 mg/kg DMAPT reportedly limits tumour growth by 35-63% (*Shanmugam et al., 2011; D'Anneo et al., 2013; Vegeler et al., 2007*), whereas in acute myeloid leukaemia and pancreatic tumour models 40-100 mg/kg DMAPT has been unable to significantly alter tumour growth (*Yip-Schneider et al., 2008; Hassane et al., 2010*). This suggests that, although the anti-cancer mechanisms of DMAPT are common to many cancer types, the chemotherapeutic response can differ between tumour types. Further studies are required to examine the chemo-preventive ability of DMAPT in other cancer types.

DMAPT significantly reduced metastasis in the lungs of TRAMP mice below that of baseline level. In 60% of mice studied, there was no evidence of metastatic spread to the lungs when DMAPT was administered. This is the first description of a DMAPT-induced reduction in metastatic prostate cancer, and is on par with some of the most pronounced anti-metastatic effects reported in TRAMP mice (*Raina et al., 2008; Singh et al., 2008*). Previous xenograft breast cancer studies have reported a 36% and 66% reduction in lung metastasis following daily treatment with PTL (40 mg/kg) (*Sweeney et al., 2005*) and DMAPT (50 mg/kg) (*D'Anneo et al., 2013*) respectively. Here lung metastasis was almost completely inhibited (95% reduction) in the TRAMP model following thrice weekly treatment with DMAPT (100 mg/kg). Further investigation is required to study the metastatic spread of TRAMP prostate tumours to tissues other than lung (such as liver, kidney and spleen), as it is highly likely that DMAPT has also reduced metastasis at other distant sites. DMAPT also significantly reduced expression of MMP2 and laminin in primary prostate tumours compared to that of water-vehicle treated mice, both of which are heavily implicated in tumour invasion and metastasis in a variety of tumour types, including prostate cancer (*Shaverdashvili et al., 2014; Mendes, Kim & Stoica, 2005; Mendes et al., 2007; Kawaguchi, 2016*).

In addition to studying the anti-cancer effect of DMAPT *in vivo*, a small study was started using a human prostate tumour explant model. While the results from this initial study look promising, the ability to study the anti-proliferative and pro-apoptotic effects of DMAPT were hindered by significantly lower than

expected baseline levels of proliferation in the tissues following culture. The expected frequency of positive Ki67 of approximately 15-40%, which is normally observed in the cultured prostate tumours (*Armstrong et al., 2016*), was not seen in the studies carried out for this thesis. The percentage of proliferation in epithelial cells of control-treated tissues was only 2.7%, approximately 6 to 15-fold lower than levels cited in the literature. The lower than expected proliferation frequency was determined to be due to a change in culture media that was used for these experiments, compared to previous studies (M. Centenera, personal communication). Changing back to the previously used culture media resulted in a higher level of baseline proliferation in cultured tumour tissues, however there was limited time to carry out repeat experiments with DMAPT. This unfortunately limited the ability to observe strong anti-proliferative effects as a result of DMAPT treatment in the human tissues. Both PTL and DMAPT have been shown to illicit strong anti-proliferative and pro-apoptotic effects in a variety of cancer cell lines at concentrations of 5-25 µM (*Shanmugam et al., 2011; Song et al., 2014; Carlisi et al., 2011; D'Anneo et al., 2013*), therefore it seems likely that in future human prostate explant culture studies, DMAPT will demonstrate some ability to reduce proliferation and increase apoptosis and that the responses may be correlated with clinical molecular markers.

Given that the most life-threatening aspects of the oncogenic process are invasion and metastasis, these data highlight the potential for DMAPT as a promising novel therapeutic in prostate cancer, due to its ability to slow down prostate cancer development and its potent anti-metastatic properties. The

mechanisms involved in the anti-cancer effect of DMAPT are not specific to prostate cancer and therefore it seems likely that DMAPT may also be a useful therapeutic for other cancers, particularly those where metastatic disease is common.

Chapter 5: Modulation of radiosensitivity by parthenolide and low dose radiation

Radiotherapy is widely used in cancer treatment, however the benefits can be limited by radiation-induced damage to neighbouring healthy tissues. Previous literature has demonstrated that PTL is able to selectively enhance radiosensitivity of prostate cancer cells with reduced damage to normal prostate epithelial cells *in vitro* (*Sun et al., 2010; Xu et al., 2013; Sun et al., 2007*). *In vivo*, PTL has been shown to radiosensitise human prostate cancer PC3 cell derived tumours in nude mice (*Xu et al., 2013*), however, these abilities are yet to be demonstrated in autochthonous models of prostate cancer. During radiotherapy, patients are not only exposed to high therapeutic doses of radiation but can also receive low doses of radiation during CT imaging protocols. Such exposures are becoming increasingly common with the use of image guided radiotherapy. Low doses of radiation, like PTL, have been shown to induce an adaptive response to protect healthy tissues from subsequent high dose radiation-induced damage. The mechanism of low dose radiation-induced radioprotection occurs via different pathways than PTL. Therefore, the combination of PTL and low dose radiation has the potential to be utilised to improve radiotherapy by killing more tumour cells and less normal cells.

Here, the effects of PTL and low dose radiation on healthy and tumour tissue radiosensitivity in the TRAMP model have been examined. Experiments were carried out according to the protocols outlined in Figure 5-1.

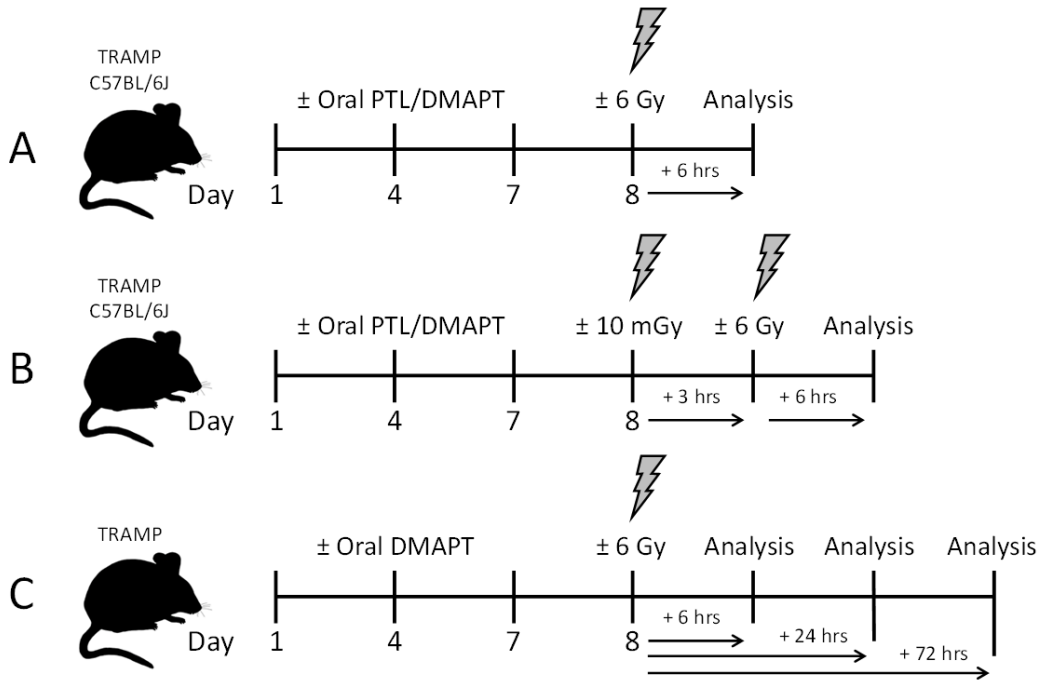

Figure 5-1: Schematic overview of treatment and irradiation protocols for *in vivo* studies

Overview of short term (A) high dose and (B) low dose (B) radiotherapy studies, and (C) temporal high dose radiotherapy studies.

Results

Parthenolide protects healthy tissues from radiation damage when delivered alone or in combination with a conditioning low dose of radiation

In preliminary experiments, C57BL/6J and TRAMP mice were treated as per the protocol described in Figure 5-1A to determine if PTL could protect from apoptosis induced by a high dose of radiation in normal tissues, and to determine if normal tissues responded differently in the different strains of mice. Across all experiments baseline apoptosis frequency in normal tissues did not differ significantly between C57BL/6J and TRAMP strains (n = 12-26); mean baseline apoptosis frequency in both mouse strains was 0.0041 (± 0.0023 SD) in

normal dorsolateral prostate, and 0.0074 (± 0.0036 SD) in normal spleen, with mean baseline of 0.53 (± 0.17 SD) apoptotic cells per crypt in normal colorectal tissues. When analysed 6 hours after exposure to 6 Gy, the mean apoptosis frequency increased 31-fold to 0.13 (± 0.035 SD) in normal dorsolateral prostate (n = 23), and 29-fold to 0.21 (± 0.027 SD) in normal spleen (n = 67), with mean apoptotic cells per crypt increasing 11-fold to 5.81 (± 0.54 SD) in normal colorectal tissue of C57BL/6J mice (n = 67). PTL (40 mg/kg) induced a partial protection from 6 Gy radiation-induced apoptosis in normal C57BL/6J dorsolateral prostate (34.5% reduction, p = 0.002), and spleen (17.3% reduction, p = 0.041) tissues and in normal TRAMP spleen tissues (31.4% reduction, p = 0.01) 6 hours post-irradiation (Figure 5-2). Radiation-induced apoptosis was not significantly reduced by PTL in normal colorectal tissues of either mouse strain.

C57BL/6J mice were treated as per the protocol described in Figure 5-1B to determine if a 10 mGy conditioning dose of radiation could add to PTL-induced reduction of apoptosis following 6 Gy in normal tissues (Figure 5-3). A dose of 10 mGy alone induced a significant increase in apoptosis (489.5% increase, p = 0.017) in spleen (Figure 5-3B); but not in prostate or colorectal tissues (Figure 5-3A and 5-3C) when analysed 9 hours post-irradiation. In the absence of PTL, the 10 mGy conditioning dose induced a radio-adaptive response when delivered 3 hours before a 6 Gy high dose in the dorsolateral prostate (28.4% reduction in apoptosis, p = 0.045), compared to the sham conditioning dose plus 6 Gy exposure (Figure 5-3A). There was also a trend towards an adaptive response in normal spleen tissue (15.8% reduction in apoptosis, p = 0.084) (Figure 5-3B). PTL

decreased apoptosis in sham treated dorsolateral prostate (28.7 % reduction, $p = 0.048$) and reduced 6 Gy-induced apoptosis in the presence and absence of a 10 mGy conditioning dose in spleen and prostate ($p < 0.05$), however a 10 mGy dose did not significantly add to PTL-induced protection from apoptosis ($p > 0.05$).

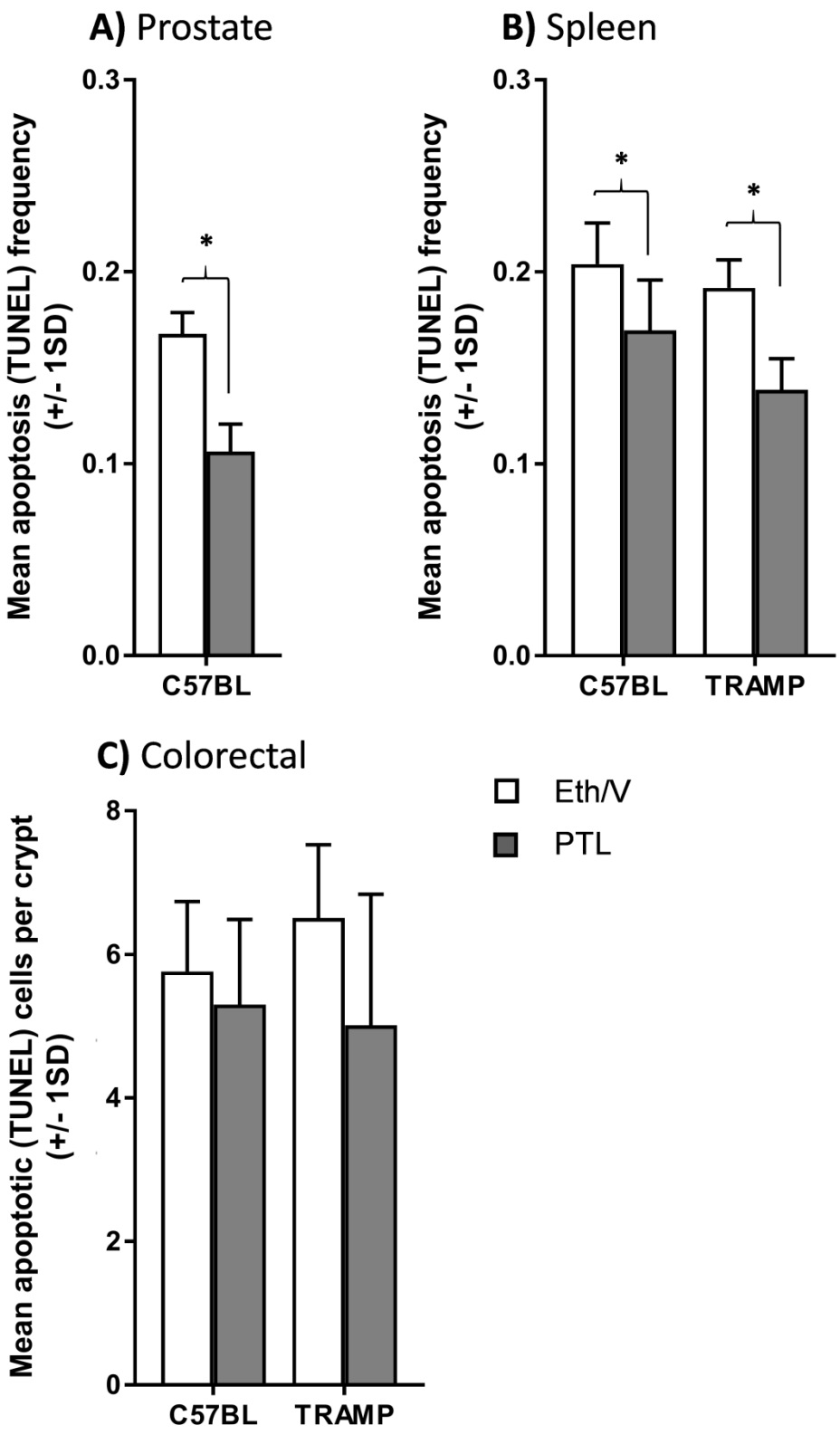

Figure 5-2: Apoptosis in normal C57BL/6J and TRAMP tissues following treatment with PTL and 6 Gy X-radiation exposure

Mean apoptosis (±1SD) in normal C57BL/6 (A) dorsolateral prostate, and normal C57BL/6J and TRAMP (B) spleen and (C) colorectal tissues following 3x40 mg/kg PTL (in 10% ethanol/saline) or ethanol/saline vehicle control (Eth/V) treatments over 1 week, with exposure to 6 Gy whole body X-irradiation 24 h after the final treatment. *$p < 0.05$, $n = 5$-15.

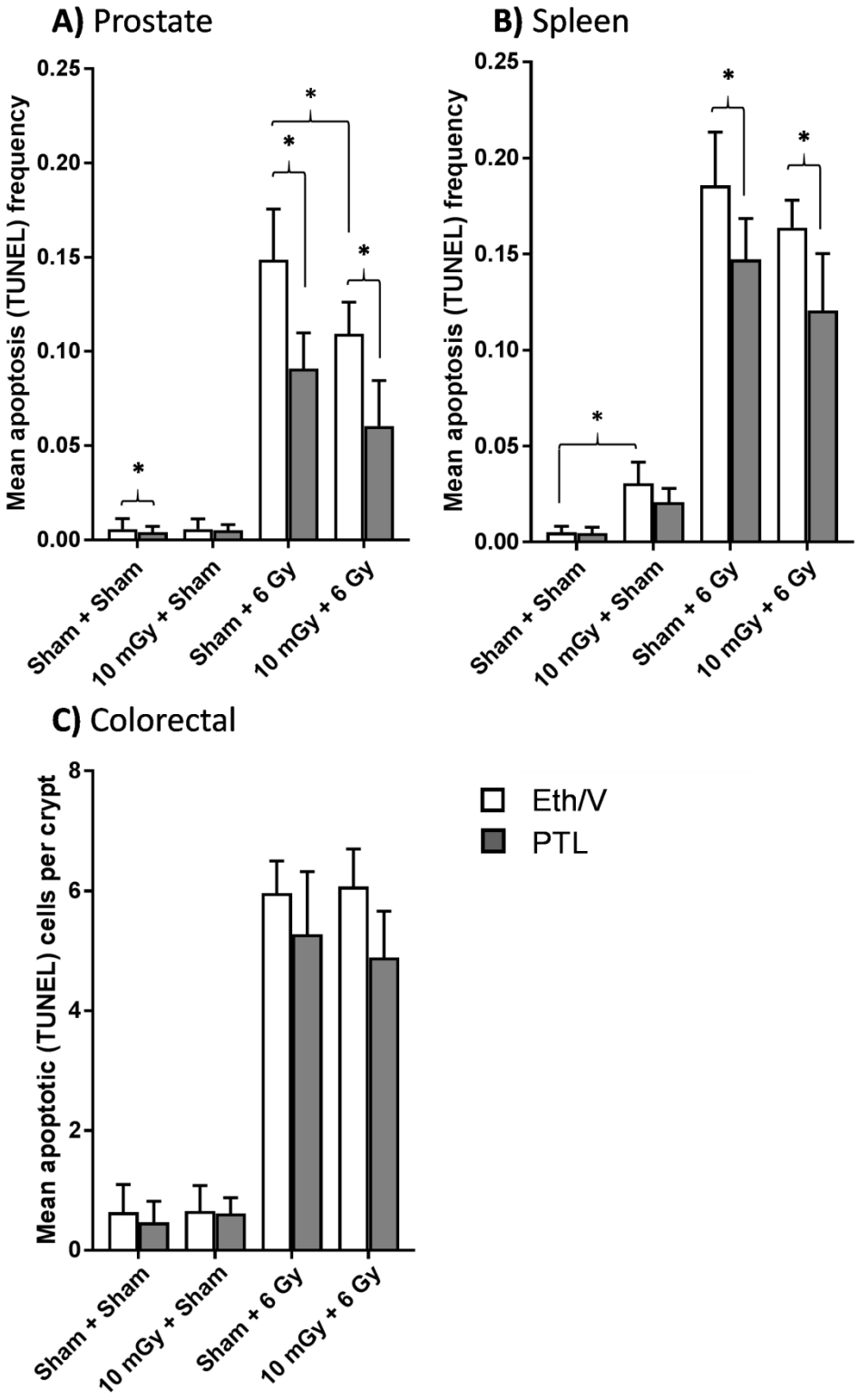

Figure 5-3: Apoptosis in normal C57BL/6J tissues following treatment with PTL and combinations of sham, 10 mGy and 6 Gy X-radiation exposure

Mean apoptosis (±1SD) in normal C57BL/6 mouse (A) dorsolateral prostate, (B) spleen and (C) colorectal tissue following 3x40 mg/kg PTL (in ethanol/saline) or 10% ethanol/saline vehicle control (Eth/V) treatments over 1 week, with combinations of exposure to sham, 10 mGy and 6 Gy whole body X-irradiation 24 h after the final PTL treatment. *$p < 0.05$, $n = 6$.

Comparison of radioprotection using PTL and DMAPT

Midway through the experiments for this thesis DMAPT, a PTL analogue with increased solubility and bioavailability, was made available for use in these studies. The efficacy of DMAPT as a radioprotector of healthy tissues was compared with PTL in C57BL/6J mice (Figure 5-4). DMAPT (100 mg/kg) significantly increased radioprotection from 6 Gy induced apoptosis in healthy C57BL/6J mouse dorsolateral prostate (71.7% reduction, $p = 0.026$), spleen (48.2% reduction, $p = 0.0001$) and colorectal tissues (38.0% reduction, $p = 0.0002$) (Figure 5-4), compared to the radioprotection provided by PTL (40 mg/kg) (dorsolateral prostate: 41.4% reduction, $p = 0.045$; spleen: 29.5% reduction, $p = 0.011$; colorectal: 15.7% reduction, $p = 0.0674$). Compared to PTL, DMAPT increased radioprotection in dorsolateral prostate, spleen and colorectal tissues by a further 1.6 – 2.4 fold.

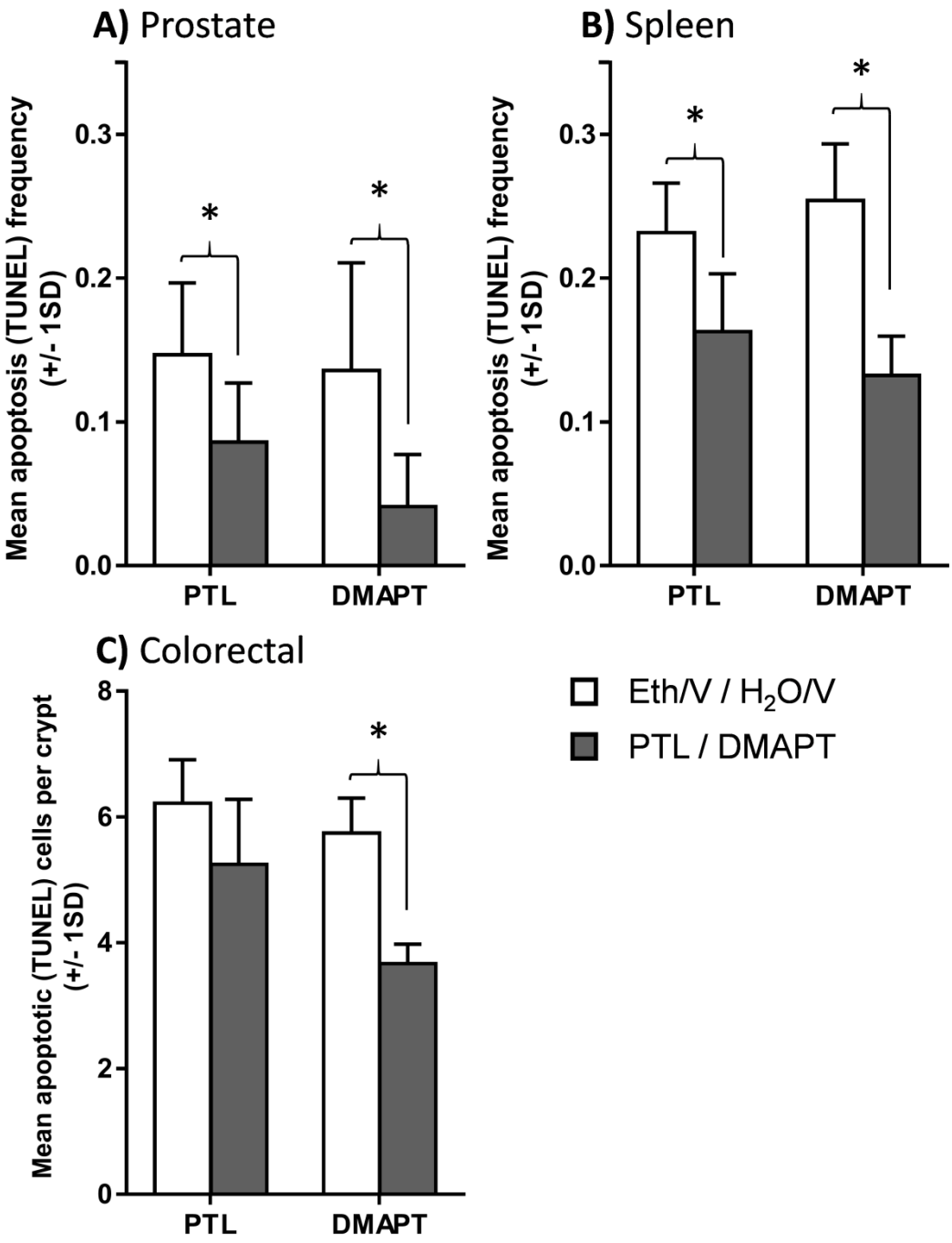

Figure 5-4: Comparison of apoptosis levels in normal C57BL/6J tissues following treatment with PTL or DMAPT and 6 Gy X-radiation exposure

Mean apoptosis (±1SD) in C57BL/6J mouse (A) dorsolateral prostate, (B) spleen and (C) colorectal tissues following 3x 40 mg/kg PTL (in ethanol/saline), 100 mg/kg DMAPT, 10% ethanol/saline vehicle control (Eth/V) or water vehicle control (H_2O/V) treatments over 1 week, followed by 6 Gy whole body X-irradiation 24 h after the final drug treatment, *$p < 0.05$, $n = 6$.

In order to compare the radio-protective effects of PTL and DMAPT with NF-κB expression, protein expression was measured in dorsolateral prostate tissues from C57BL/6J mice treated with PTL (in ethanol/saline), DMAPT and respective vehicle controls. A large proportion of NF-κB staining in the dorsolateral prostate tissues was cytoplasmic, however some staining was present in the nuclei (Figure 5-5). Activation of the NF-κB pathway triggers proteasomal IκB degradation and enables active NF-κB transcription factor subunits to translocate to the nucleus and induce target gene expression. Therefore, NF-κB expression in the dorsolateral prostate tissues was only measured within nuclei areas (identified by DAPI staining) to capture changes in active NF-κB expression. Expression was measured as mean pixel intensity per nuclei, and has been represented as a fold-change in expression from the water vehicle mean (Figure 5-6). There was no significant difference in dorsolateral prostate NF-κB expression between the water vehicle and ethanol/saline vehicle treatment groups ($p = 0.89$). PTL (in ethanol/saline) did not significantly alter NF-κB expression compared to the water or ethanol/saline vehicle controls ($p = 0.26$), however there was a trend towards decreased expression compared to both vehicle control treatment groups (0.73 fold-change in NF-κB expression compared to water vehicle). Mice treated with DMAPT had significantly reduced NF-κB expression in dorsolateral prostate tissues compared to those treated with water vehicle ($p = 0.013$) and ethanol/saline vehicle ($p = 0.0063$).

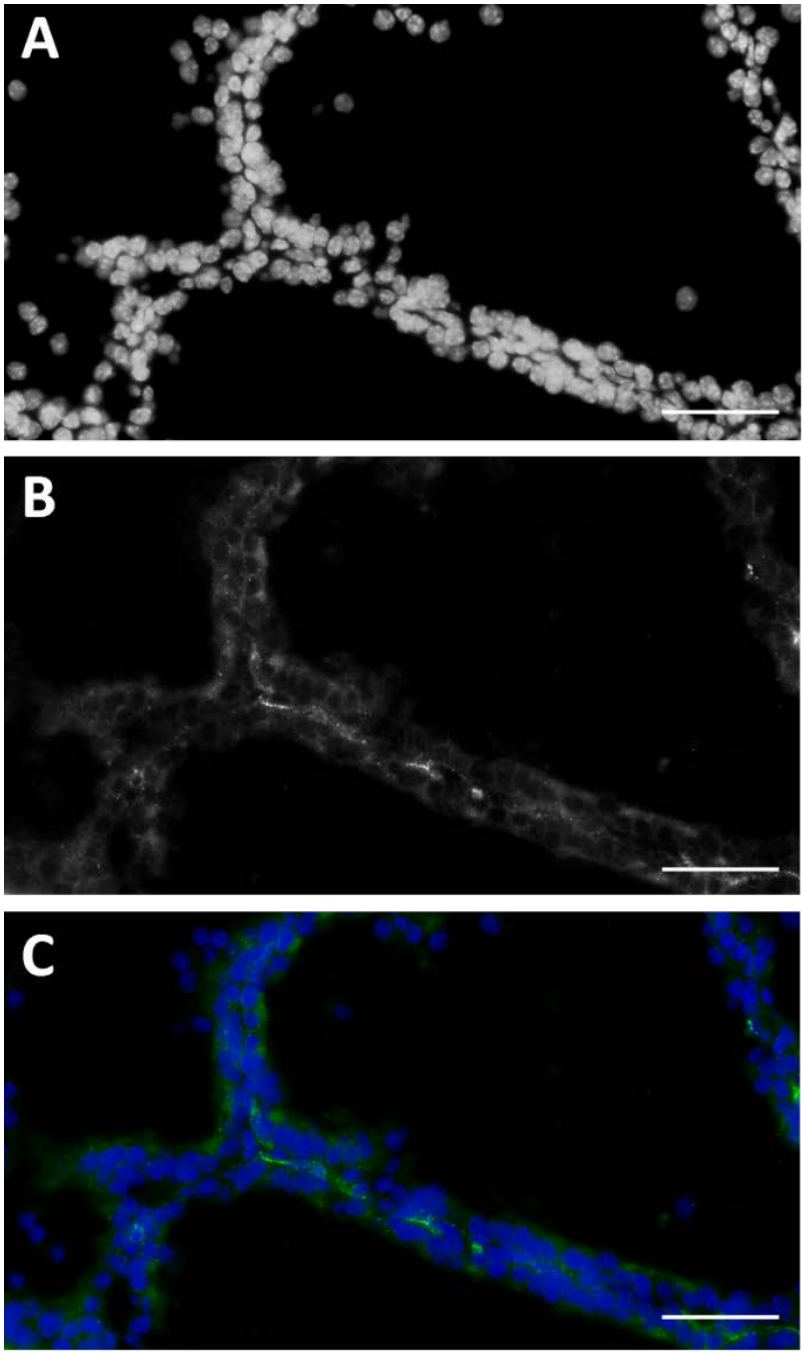

Figure 5-5: NF-κB staining in C57BL/6J dorsolateral prostate tissues

Representative images of NF-κB staining in C57BL/6J dorsolateral prostate tissues. Individual images of DAPI staining (A) and NF-κB staining (B), and false-coloured merged image (C) with NF-κB (green) and DAPI (blue). Scale bar 50 µm.

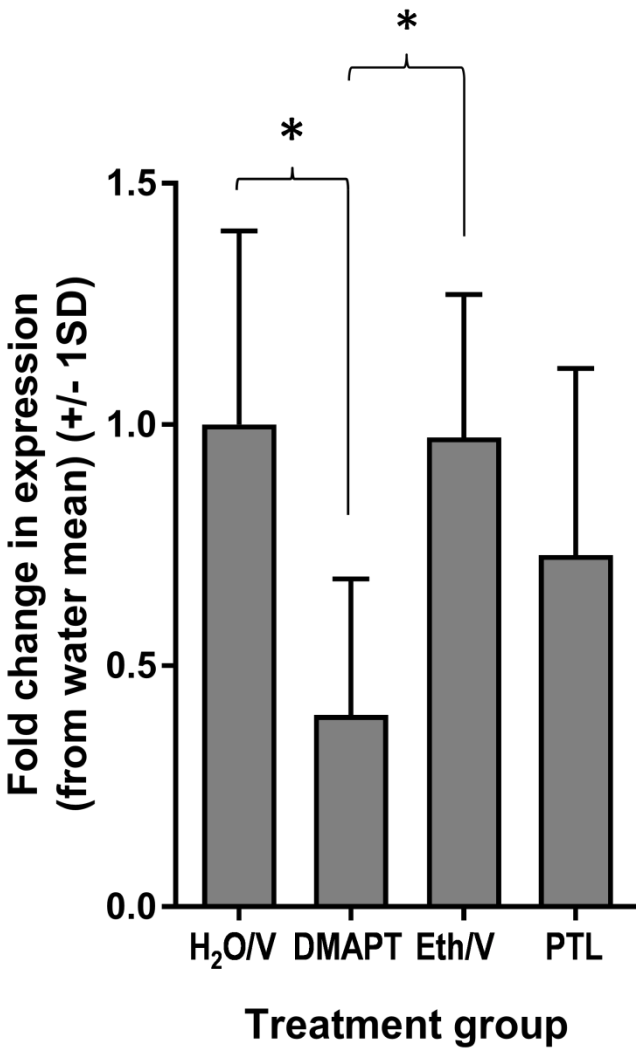

Figure 5-6: Fold changes in NF-κB protein expression in treated C57BL/6J dorsolateral prostate

Fold changes in expression (from water vehicle) in dorsolateral prostate tissues from C57BL/6J mice treated with 10% ethanol/saline vehicle (Eth/V), 40 mg/kg PTL (in ethanol/saline), water vehicle (H_2O/V) or 100 mg/kg DMAPT, *$p < 0.05$, $n = 6$ mice per treatment group.

DMAPT radioprotects healthy tissues while sensitising prostate tumour tissue to radiation induced damage

To examine the effect of DMAPT and low dose radiation on healthy and tumour tissue radiosensitivity, TRAMP mice were treated as per the protocol described in Figure 5-1B. TRAMP mice were treated with DMAPT and 6 Gy X-irradiation in the presence or absence of a 10 mGy conditioning dose (Figure 5-7). In the absence of DMAPT, a 10 mGy conditioning dose delivered 3 hours prior to the high dose reduced 6 Gy-induced apoptosis in normal TRAMP spleen (13.6 % reduction, $p = 0.047$) (Figure 5-7B), compared to animals that received a sham conditioning dose. In normal TRAMP spleen and colorectal tissues, DMAPT reduced 6 Gy-induced apoptosis in the presence and absence of a 10 mGy conditioning dose, compared to vehicle control-treated mice (Figure 5-7B and Figure 5-7C). In the TRAMP model, most prostates are in the mid-stages of tumour development by 16 weeks of age. Across all experiments ($n = 26$ mice), mean apoptosis frequency in TRAMP dorsolateral prostate was 0.012 (± 0.0046 SD) at baseline and increased 11-fold to 0.1344 (± 0.053 SD) following 6 Gy exposure ($n = 51$ mice). DMAPT increased radiation-induced apoptosis in TRAMP prostate tissues in the absence and presence of a 10 mGy conditioning dose (81.9% increase, $p = 0.02$; 135.0% increase, $p = 0.0024$ respectively) (Figure 5-7A). In the absence of DMAPT, there was no significant difference in apoptosis in TRAMP prostate PIN tissue with or without a 10 mGy conditioning dose.

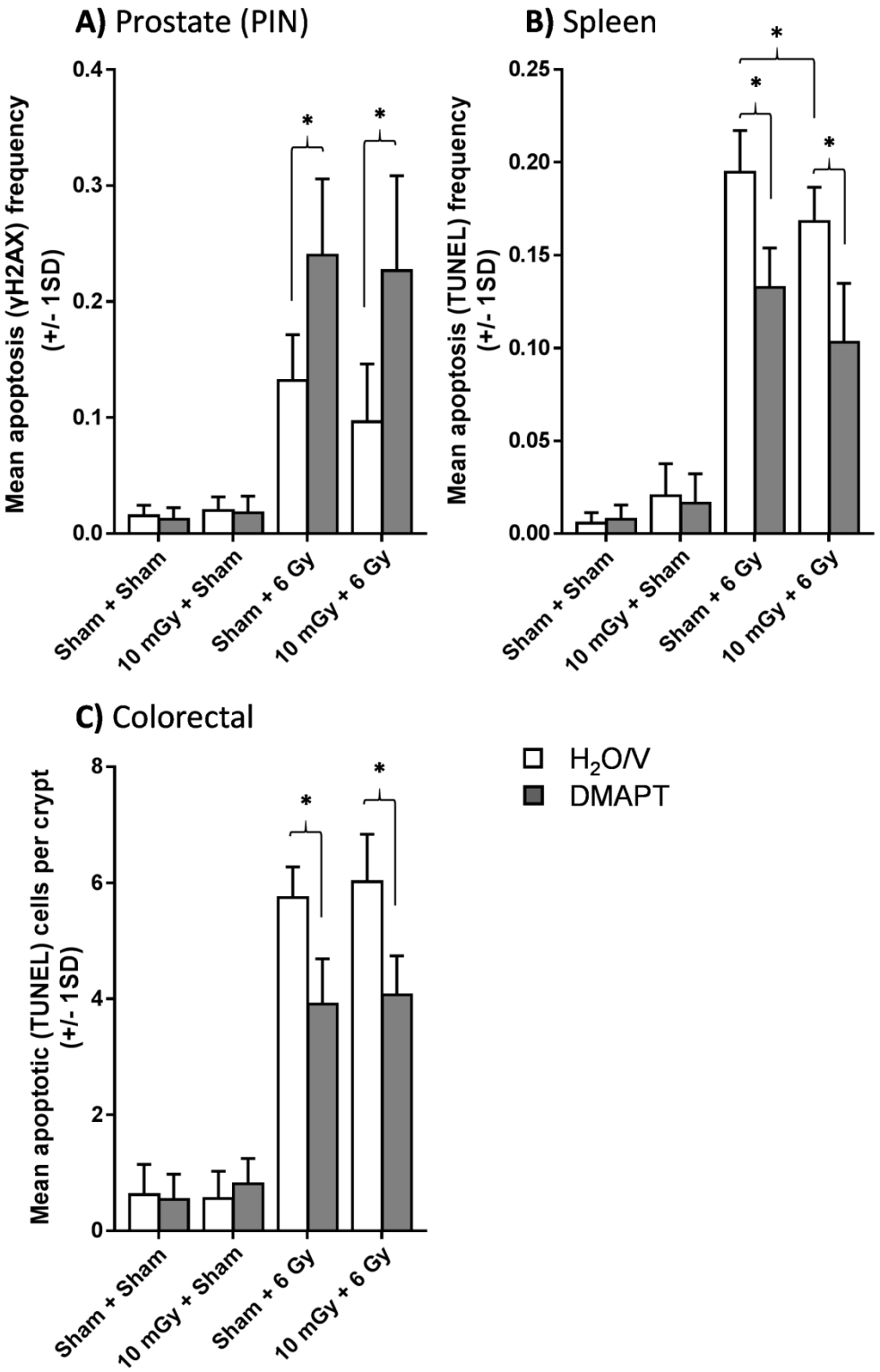

Figure 5-7: Apoptosis in normal and tumour TRAMP tissues following treatment with DMAPT and combinations of sham, 10 mGy and 6 Gy X-radiation exposure

Mean apoptosis (±1SD) in TRAMP (A) dorsolateral prostate, (B) spleen and (C) colorectal tissues following 3x 100 mg/kg DMAPT or water vehicle control (H_2O/V) treatments over 1 week, followed by sham, 10 mGy or 6 Gy whole body X-irradiation (alone or in combination) 24 h after the final DMAPT treatment. Error bars 1SD, *$p < 0.05$, n = 11-14.

Differential radiosensitisation from DMAPT in TRAMP tissues persists beyond the initial phase of apoptosis

In temporal studies, TRAMP mice were treated as per the protocol described in Figure 5-1C. In the absence of radiation, apoptosis in spleen, colorectal and dorsolateral prostate tissue was not significantly different between treatment groups and did not significantly alter across the different time points ($p > 0.05$, ANOVA with Turkey's multiple comparisons test) (Figure 5-8). In TRAMP dorsolateral prostate (Figure 5-8A), significant augmentation of 6 Gy-induced apoptosis was observed in the DMAPT treated mice at 6 hours post-irradiation (119.4 % increase, $p = 0.0018$) compared to vehicle-treated mice. An increase in apoptosis was still present 18 hours later in the DMAPT-treated group (107.2 % increase, $p = 0.048$) and apoptosis levels returned to baseline frequency by 72 hours. In colorectal tissues (Figure 5-8B), a reduction in 6 Gy-induced apoptosis was observed 6 and 24 hours post-irradiation (34.6% reduction, $p = 0.0034$ and 55.6% reduction, $p = 0.0002$) respectively compared to the vehicle control-treated mice. By 72 hours, apoptosis returned to baseline levels.

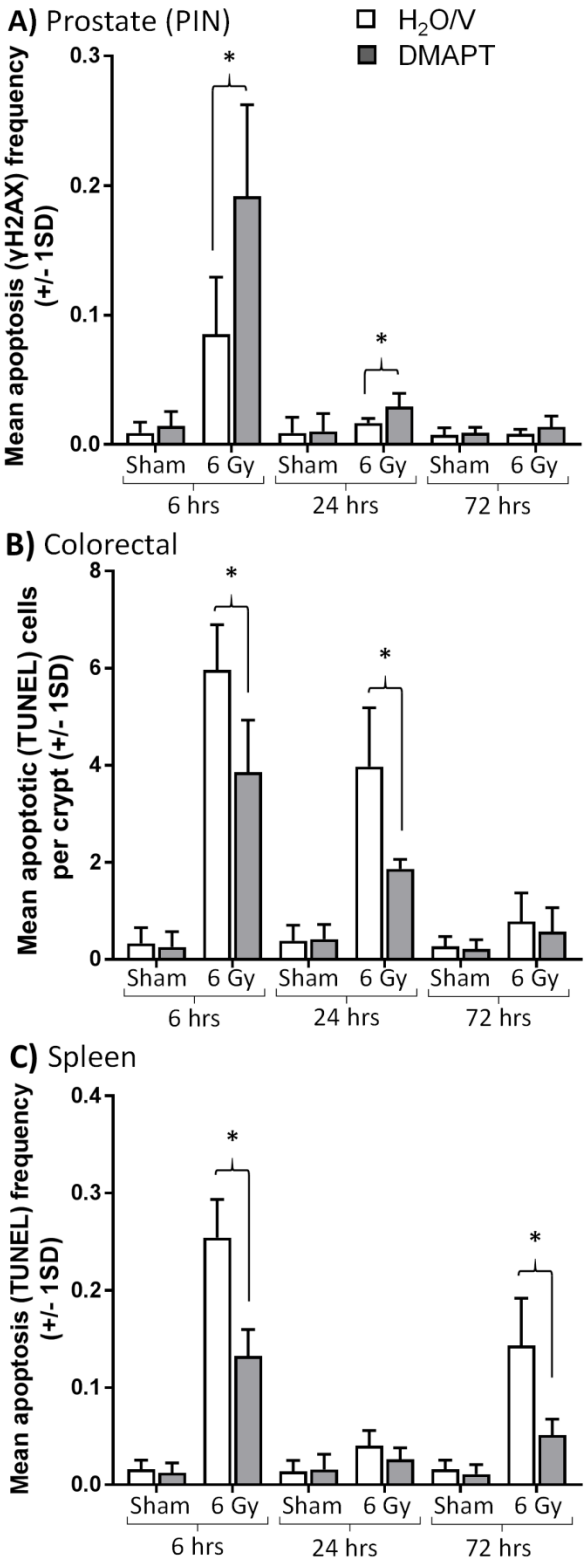

Figure 5-8: Temporal changes in apoptosis in normal and tumour TRAMP tissues following treatment with DMAPT and 6 Gy X-radiation exposure

Mean apoptosis (±1SD) in TRAMP (A) dorsolateral prostate, (B) colorectal tissues and (C) spleen following 3x 100 mg/kg DMAPT or water vehicle control (H_2O/V) treatments over 1 week, with exposure to a 6 Gy or sham irradiation, and tissues analysed at 6, 24 and 72 h post-irradiation. *$p < 0.05$, n = 5-15.

In TRAMP spleen (Figure 5-8C), radioprotection was observed in DMAPT treated mice 6 hours (40.1% reduction, p = 0.021) and 72 hours (64.3% reduction, p = 0.0001) post-irradiation. The apoptosis observed at 6 hours was largely follicular in both the DMAPT and vehicle control-treated groups exposed to 6 Gy, and had returned to baseline levels by 24 hours. At 72 hours there was an increase in apoptosis in the 6 Gy vehicle-treated mice, but not in DMAPT treated mice. In vehicle control-treated spleens, this second wave of apoptosis was again largely follicular (Figure 5-9), however, apoptosis in DMAPT-treated spleen was mostly observed in extra-follicular red pulp regions.

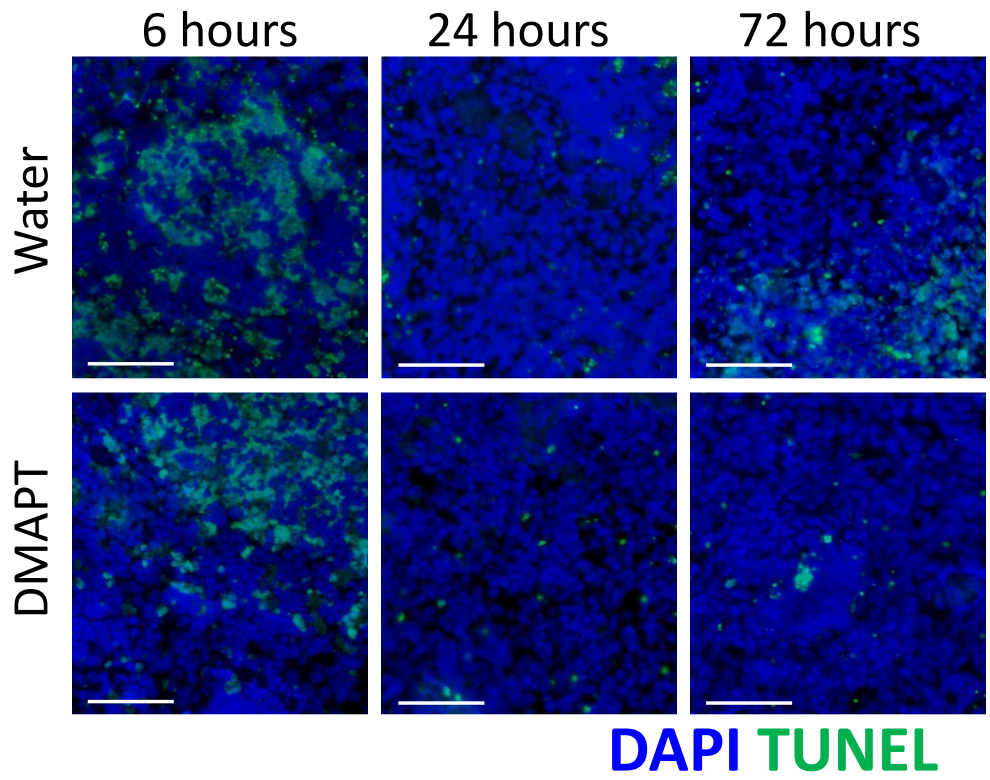

Figure 5-9: Apoptosis in TRAMP spleen tissue 6, 24 and 72 h after irradiation

Representative false-coloured images of fluorescently labelled apoptotic (TUNEL) cells in healthy spleen from TRAMP mice treated with 100 mg/kg DMAPT or water vehicle control (H_2O/V) prior to 6 Gy radiation, at 6, 24 and 72 h post-irradiation.

Enhanced radiosensitivity of TRAMP prostate tumour tissue by DMAPT is greater with increasing PIN grade

TRAMP dorsolateral prostates were scored for PIN grade using the method proposed by Berman-Booty et al (*2012*). This method assigns tissues a score based on both the most common lesions and the most severe lesions. By 17 weeks of age, the majority of TRAMP dorsolateral prostate tissues have developed moderate to high grade PIN (Figure 5-10).

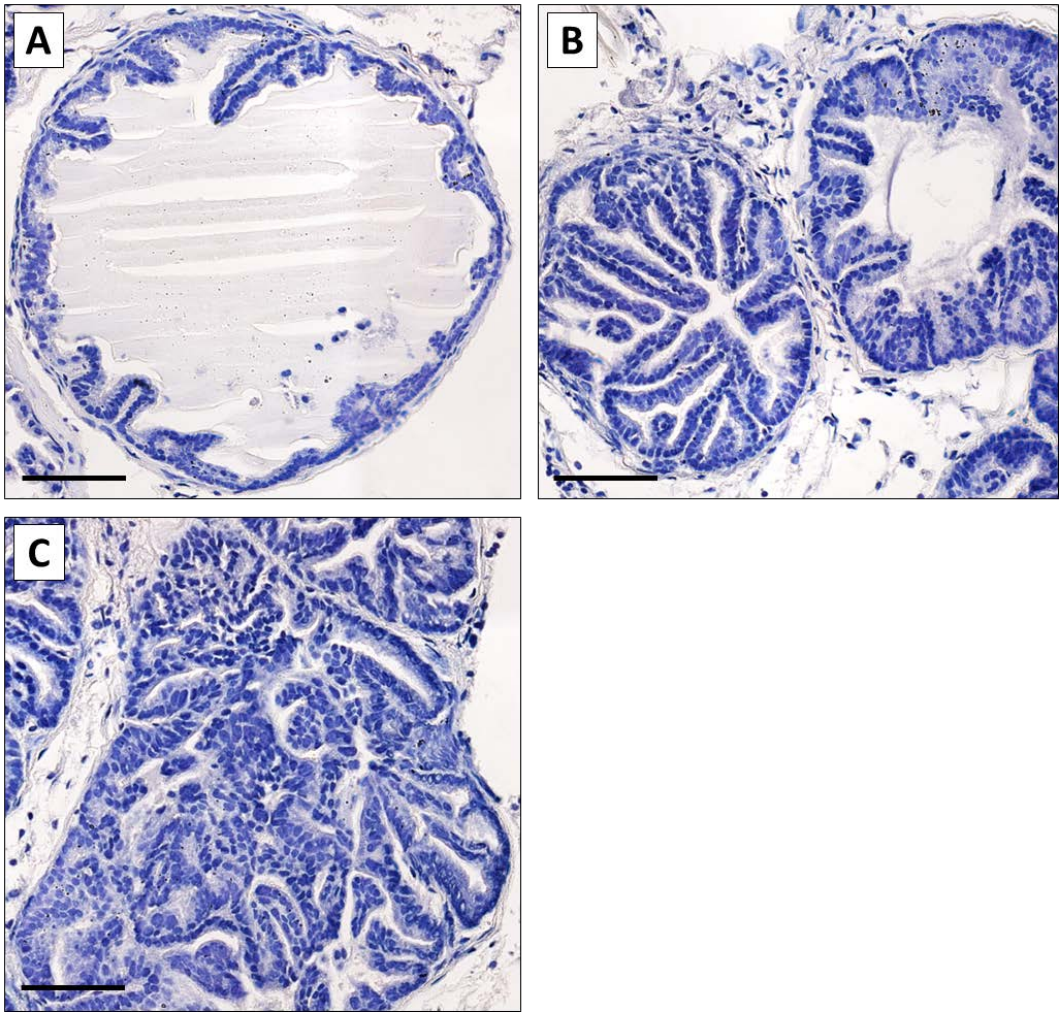

Figure 5-10: Representative morphology of TRAMP dosolaterale prostate lobes

(A) Low grade PIN, with a few areas of hyperplastic epithelium projecting into the lumen; (B) moderate grade PIN, with more prominent proliferations into the lumen; and (C) high grade PIN, where there is a mass of proliferating epithelial cells completely filling the gland (haematoxylin stain, 40x magnification, scale bar 50 µm).

When TRAMP mice were treated with PTL and 6 Gy, as per the protocol in Figure 5-1A, there was no overall significant increase in mean radiation-induced apoptosis in dorsolateral prostate of PTL-treated group compared to the vehicle control group (Figure 5-11A). However, there was a significant correlation between the amount of apoptosis induced by PTL in the presence of 6 Gy and increasing PIN grade (R^2 = 0.4037, p = 0.015) (Figure 5-11B). There was no significant correlation in apoptosis with increasing PIN grade (R^2 = 0.0104, p = 0.77) in the vehicle treated group. There was no significant difference in the distribution of individual mouse PIN grades between mice treated with PTL (18.4 ± 7.6) and mice treated with ethanol/saline vehicle control (17.8 ± 7.1) (p = 0.90) (Figure 5-12).

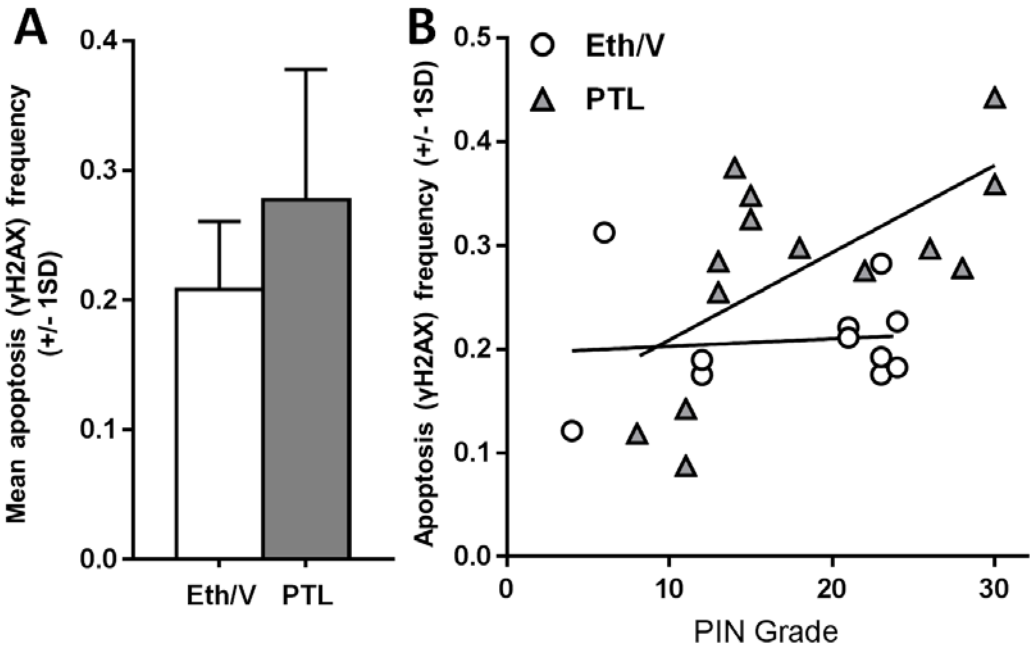

Figure 5-11: Dorsolateral prostate apoptosis frequency vs PIN grade in TRAMP mice treated with PTL

(A) Mean apoptosis (±1SD) in irradiated TRAMP dorsolateral prostates following 3x 40 mg/kg PTL (in ethanol/saline) (Eth/V) or 10% ethanol/saline vehicle control (Eth/V) treatment over 1 week, *p < 0.05, n = 12-14. (B) Apoptosis in dorsolateral prostate tissue from treated TRAMP mice plotted against PIN tumour grade.

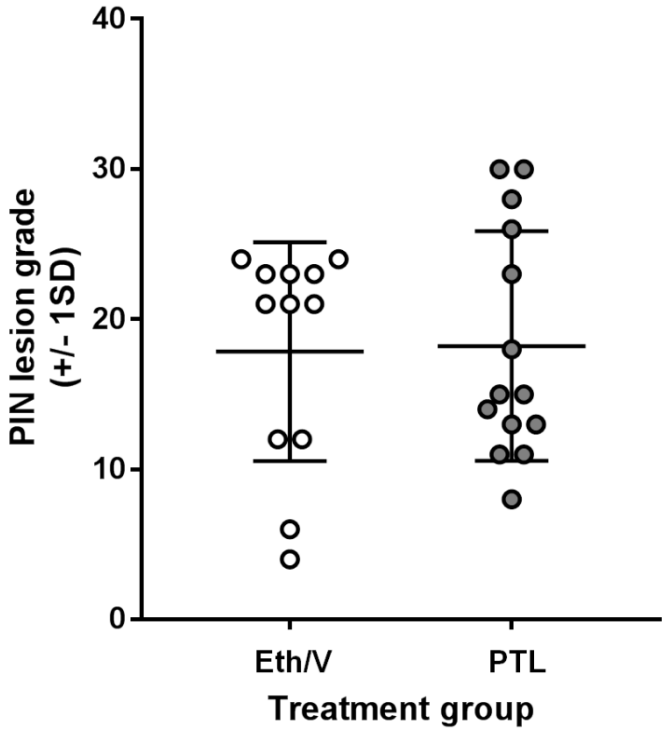

Figure 5-12: PIN lesion grade distribution in PTL-treated TRAMP tissues

Distribution of PIN lesion grade scores of individual TRAMP mice treated with 40 mg/kg PTL or 10% ethanol/saline vehicle control (Eth/V), n = 12-14.

When mice were treated with DMAPT and 6 Gy, as per the protocol in Figure 5-1A, radiation-induced apoptosis doubled in dorsolateral prostates of DMAPT-treated TRAMP mice compared to those of vehicle control-treated mice (101.3 % increase, p = 0.039) (Figure 5-13A). TRAMP dorsolateral prostates with high grade PIN development were preferentially sensitised to radiation-induced apoptosis when mice were pre-treated with DMAPT (R^2 = 0.7909, p = 0.0001), while tissues with lower grades of PIN displayed the same apoptosis frequency as those of vehicle control-treated TRAMP mice (R^2 = 0.0242, p = 0.3) (Figure 5-13B). There was no significant difference in the distribution of PIN grade of dorsolateral prostate of mice from the DMAPT (18.2 ± 5.7) and water vehicle (15.5 ± 5.0) treatment groups (p = 0.21) (Figure 5-14).

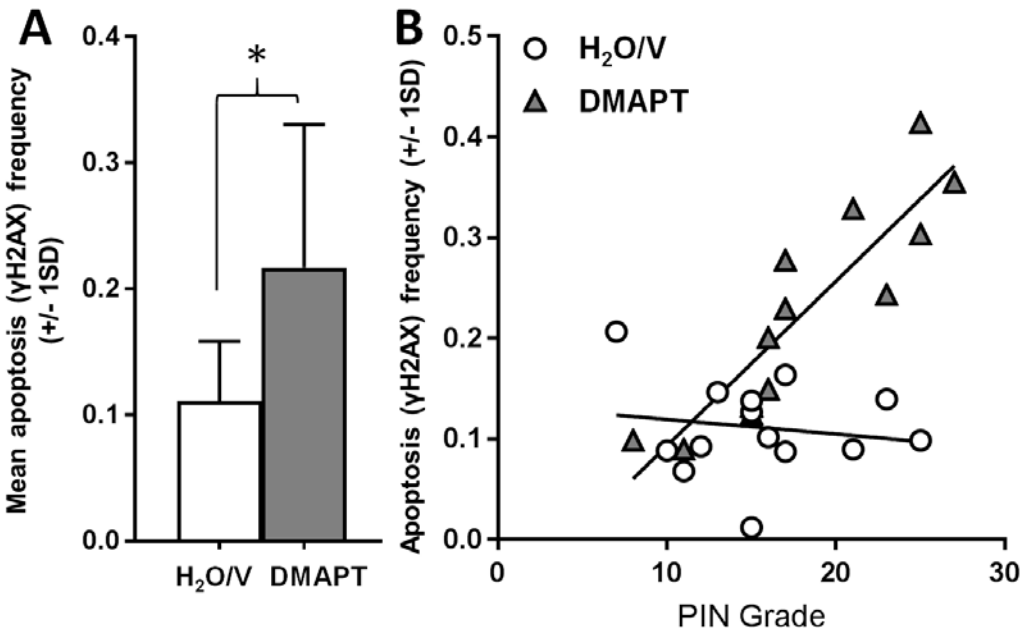

Figure 5-13: Dorsolateral prostate apoptosis frequency vs PIN grade in TRAMP mice treated with DMAPT

(A) Mean apoptosis (±1SD) in irradiated TRAMP dorsolateral prostates following 3 x 100 mg/kg DMAPT or water vehicle control (H_2O/V) treatment over 1 week, *$p < 0.05$, n = 13-14. (B) Apoptosis in dorsolateral prostate tissue from treated TRAMP plotted against PIN tumour grade.

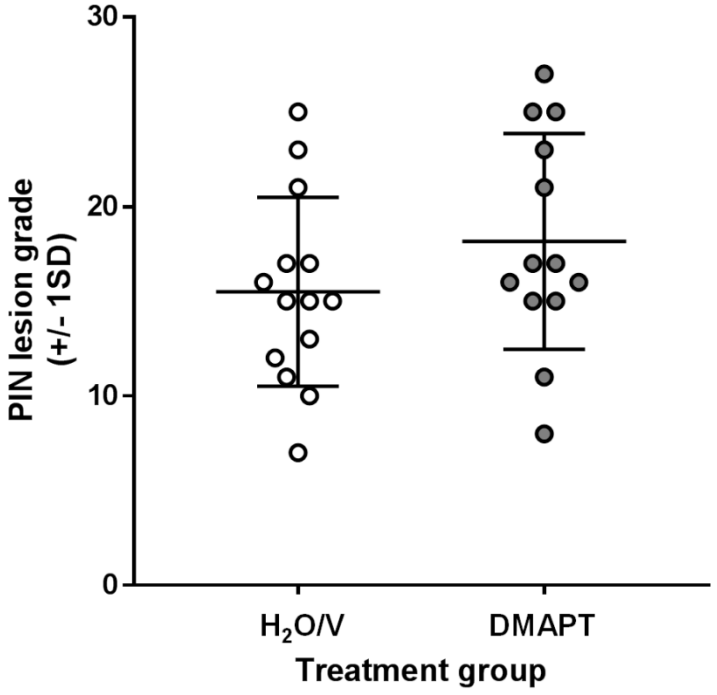

Figure 5-14: PIN lesion grade distribution in DMAPT-treated TRAMP tissues

Distribution of PIN lesion grade scores of individual TRAMP mice treated with 100 mg/kg DMAPT or water vehicle control (H_2O/V), n = 13-14

Discussion

A major limiting factor of radiotherapy is normal tissue toxicity. Prostate cancer radiotherapy can result in short-term side effects including colorectal injury which can induce diarrhoea and bleeding, while the long-term effects may include incontinence, impotence and infertility. *In vivo*, DMAPT has been shown to selectively radiosensitise human prostate cancer PC3 cell derived tumours in nude mice (*Xu et al., 2013*). Here, PTL and DMAPT were investigated to determine their ability to simultaneously protect normal tissues and sensitise prostate tumour tissues to radiation-induced cell death in TRAMP mice, which have an intact immune system and where the tumour progression within the prostate more closely mimics human prostate cancer progression. In these studies the simultaneous protection of normal tissues and radiosensitisation of TRAMP prostate tumour tissues to 6 Gy irradiation was observed, demonstrating the potential for DMAPT to be a therapeutic for prostate cancer, not only to decrease radiotherapy side effects but potentially to increase cure rate.

Significant radiosensitivity was observed in TRAMP dorsolateral prostate with moderate to high grade PIN lesions, with DMAPT doubling the frequency of radiation-induced apoptosis in these tissues. Although the TRAMP mice used here were born within 4 days of each other, TRAMP prostate tumour development progresses at different rates between individual mice, and there is a relatively wide range of PIN development between animals. This results in large variation in apoptosis frequency between animals, however it allows the effects of PTL to be observed in different stages of TRAMP prostate tumour

development. Both PTL and DMAPT preferentially increased radiosensitivity in tissues with higher grade PIN, compared to tissues with lower grades of PIN (based on lesion severity) with DMAPT showing a stronger correlation, possibly due to the higher tissue exposure with DMAPT compared to PTL. High oxidative stress levels are a hallmark of prostate cancer, and ROS levels are particularly elevated in aggressive prostate tumours compared to localised disease (*Freitas et al., 2012; Oberley et al., 2000*). Oxidative stress has been shown to increase with increasing PIN grade in TRAMP mice (*Tam et al., 2006*). PTL/DMAPT may be having the greatest effect in higher PIN grade tissue due to the presence of higher ROS-levels. PIN grade in the TRAMP model does not directly correlate with Gleason grading of human prostate cancer, however the enhanced radiosensitisation of high grade TRAMP PIN tissue may be an indicator that DMAPT could be highly effective in high grade Gleason tumours and potentially for targeted treatment of metastatic prostate cancer, which often occurs from high grade Gleason tumours and is incurable (*Humphrey, 2004*).

Not only did PTL and DMAPT enhance radiation induced apoptosis in TRAMP prostate tumour tissue, but they also protected from high dose radiation-induced apoptosis in normal tissues with DMAPT showing superior protection in normal prostate, spleen and colorectal tissue. Radioprotection in healthy tissues and radiosensitisation in tumour tissues correlated with decreased NF-κB expression, with greater inhibition of NF-κB in DMAPT-treated tissues, compared to PTL. It was surprising that the response observed in DMAPT-treated mice was not more pronounced given both the increased bioavailability of DMAPT and

that a 2.5-fold higher concentration of DMAPT was used here compared to PTL. The maximum PTL dose of 40 mg/kg, can only achieve a plasma concentration of below 1 µM (*Sweeney et al., 2005*), whereas DMAPT dosed at 100 mg/kg results in a maximum plasma concentration above 10 µM (*Guzman et al., 2007*). Although the increased dose of DMAPT did not result in a proportionately greater increase in radioprotection, it still provided a greater therapeutic effect than PTL. The ideal plasma concentration for maximum radioprotection may be somewhere between 1 and 10 µM. These results along with the increased bioavailability of DMAPT suggest that DMAPT could be a useful clinical tool for alleviating radiotherapy induced damage to normal tissue, while radiosensitising tumour tissue. Amifostine is the only radioprotector currently approved for protection of normal tissues during radiotherapy (for treatment of head and neck cancers) (*Kouvaris, Kouloulias & Vlahos, 2007*), however the effects of the drug are short-lived. More than 90% of amifostine is cleared within 6 minutes of administration and it has been shown that if radiotherapy is delivered more than 30 minutes after amifostine is administered, there may be little clinical benefit (*Buentzel et al., 2006*). The reported levels of radioprotection in response to amifostine if delivered within the restrictive timeframe (*Ormsby et al., 2014; Buentzel et al., 2006; Cassatt et al., 2003*) are similar to the results presented here with DMAPT, however DMAPT may be a more convienient radioprotector for clinical use, as here it has been shown that DMAPT can be delivered at least 24 hours before X-ray exposure. There have also been reported problems with amifostine-induced toxicity and lack of differential radiosensitivity between normal and tumour tissue (*Cassatt et al., 2003; Gu et al., 2014*), whereas DMAPT

has been shown to be highly tolerated with minimal side effects in human clinical studies (*Curry et al., 2004; Pareek et al., 2011*). The DMAPT-induced protection lasted up to 24 hours post-irradiation in normal colorectal tissues and to 72 hours in normal spleen. If these effects can be replicated in a clinical setting it may allow particularly vulnerable tissues to be spared from damage while having the added benefit of increasing tumour killing efficacy. Further *in vivo* analysis of late stage radiation damage to rectum and bladder, such as fibrosis, would help to determine whether long-term protection of these particularly vulnerable tissues is possible using DMAPT. Long term studies would also allow observation of tumour progression following DMAPT treatment and high-dose radiation.

In all experiments, endogenous apoptosis frequencies observed in TRAMP and C57BL/6J prostate, spleen and colorectal tissues were all in the range previously described in the literature (*Lawrence et al., 2013b; Ormsby et al., 2014; West et al., 2009*). In the absence of radiation, PTL and DMAPT did not modulate endogenous apoptosis in the normal tissues except for in one experiment with PTL where a significant reduction in apoptosis was observed in the dorsolateral prostate of C57BL/6J mice, but not in spleen or colon, 30 hours after the final drug treatment was delivered. PTL may be protecting a small number of cells which would normally proceed to apoptosis by inducing antioxidant responses. Given that apoptosis is a normal homeostatic mechanism that acts to maintain healthy cell populations, the clinical significance of this reduction below baseline apoptosis frequency is unclear. The same dose of PTL that was delivered to

C57BL/6J mice in this study has previously been delivered to NOD/SCID mice thrice weekly for up to 106 days without any reported negative health effects that could be attributed to a reduction in apoptosis (*Kawasaki et al., 2009*). There were also no non-tumour effects from PTL (thrice weekly treatment for up to 224 days) observed in long-term mouse studies carried out for this thesis. Further studies are required to determine if PTL is actually protecting from endogenous apoptosis, as it would have been expected that DMAPT would induce a similar or superior reduction in apoptosis, and this was not observed in the experiments here.

In addition to high therapeutic radiation doses, low doses of radiation are commonly received by patients prior to and during radiotherapy in the form of imaging CT scans. Low conditioning doses of radiation in the dose range of imaging CT scans have been shown to induce protection from effects of subsequent high doses of radiation for a wide range of biological endpoints including apoptosis *in vivo* (*Ito et al., 2007; Okazaki, Ootsuyama & Norimura, 2007; Yu, Liu & Ju, 2010*). There was a general trend towards greater radioprotection in normal tissues that received PTL/DMAPT in combination with a 10 mGy dose of X-rays 3 hours prior to the 6 Gy dose compared to those that received PTL/DMAPT prior to 6 Gy alone. Although the magnitude of PTL/DMAPT-induced radioprotection from 6 Gy-induced apoptosis was greater when mice were also exposed to 10 mGy, there was no significant difference in apoptosis frequency in tissues of mice treated with PTL/DMAPT and 6 Gy in the presence or absence of 10 mGy. If there is an additive protective effect, it is

small. In the absence of PTL/DMAPT, a 10 mGy dose induced a radioadaptive response in normal prostate and spleen in some experiments, with trends towards an adaptive response in others. Similar adaptive responses for apoptosis have been described in a number of mouse studies (*Ito et al., 2007; Okazaki, Ootsuyama & Norimura, 2007; Yu, Liu & Ju, 2010*). Here, a dose of 10 mGy alone induced a significant increase in apoptosis in C57BL/6J spleen but not in TRAMP spleen, although in both cases 10 mGy induced a protection from high dose radiation induced apoptosis, indicating a radioadaptive response. There has only been one previous report of increased apoptosis after exposure to 10 mGy alone and that was at 6 hours after *in utero* exposure of C57BL/6 embryos (*Saha et al., 2014*).

Beneficial radioadaptive effects in normal tissues in the context of radiotherapy have been well described in the literature, however there are very few studies describing tumour responses to low dose radiation. Recently radioadaptive protection of tumours has been reported in vivo (*Grdina et al., 2013*). If low doses of radiation induce a radioadaptive response in tumours, the efficacy of radiotherapy could be compromised in an image guided radiotherapy scenario. Here, a 10 mGy dose of X-irradiation did not induce an adaptive response in TRAMP prostate PIN tissue, nor did the low conditioning dose affect the ability of DMAPT to radiosensitise the TRAMP prostate PIN tissue. Further studies are required to determine if the radiation doses and timing of the conditioning image dose and the radiotherapy dose play a role in the ability to radioprotect tumour tissue. Transgene-induced prostate pathology in the TRAMP model is

driven by androgen dependent expression of SV40, which contains the large and small T-antigens. The large T-antigen in the transgene interferes with the action of p53 by directly binding its DNA binding domain, silencing p53's transcriptional activity (*Greenberg et al., 1995*). The radioadaptive response is known to be p53-dependant (*Okazaki, Ootsuyama & Norimura, 2007*) and therefore may not be observable in TRAMP prostate tissues. Adaptive response studies in a model with functioning p53 are required to determine if PTL/DMAPT can counteract any potential radioadaptive responses in tumours which possess functional p53.

In order to ensure that the DMAPT-induced radioprotection from apoptosis observed 6 hours post-irradiation in normal tissues was not simply due to a delay in radiation-induced apoptosis, temporal studies were performed on TRAMP mice treated with DMAPT and 6 Gy X-irradiation. There was no delayed induction of apoptosis in DMAPT-treated spleen and colorectal tissue where protection compared to control-treated mice was not observed, and radioprotection was maintained up to 24 hours in colorectal tissue and 72 hours in spleen. This suggests that DMAPT is providing protection via reduced apoptosis in the normal tissues, rather than delaying the apoptotic response. In normal TRAMP spleen, by 24 hours post-irradiation, apoptotic frequency was reduced to almost baseline levels both in the presence and absence of DMAPT. Unexpectedly, a second wave of apoptosis was observed at 72 hours post-irradiation in the vehicle control mice, which was significantly inhibited in the DMAPT-treated mice. There are reports in the literature of delayed waves of radiation-induced apoptosis without significant investigation into the underlying

mechanism; however several reports are correlated with reduced p53 expression within tissues (*Komarova et al., 2000; Vavrova et al., 2003*). Komarova et. al. (*2000*) showed that in γ-irradiated spleen, DNA-damage-induced apoptosis begins in regions with high levels of p53 mRNA expression, while a slower induction of radiation-induced apoptosis was observed in regions with lower p53 mRNA expression. Regardless of the underlying mechanism of action, our results indicate that DMAPT protects normal tissues from a late induction of apoptosis. Importantly, in TRAMP dorsolateral prostate DMAPT-induced radiosensitisation was observed up to 24 hours post-irradiation, with apoptosis levels returning to baseline frequency by 72 hours. This demonstrates that the radiosensitising effects of DMAPT last for a significant period of time post-irradiation, which is likely to prove useful in a clinical setting if radiosensitisation of tumours continues to occur up to 24 hours after a radiotherapy dose has been delivered.

In the present study, single whole body doses of radiation were used as a proof-of-principle to determine the potential of PTL/DMAPT as a radioprotector of normal cells whilst radiosensitising tumour cells. In future studies, the role of DMAPT as a radioprotector during multiple fractionated radiation doses targeted to the region of the tumour should be investigated to closely mirror current clinical radiotherapy protocols for prostate cancer.

Chapter 6: Summary and Conclusions

The purpose of the work described in this thesis was to perform pre-clinical studies to determine the ability of PTL and DMAPT to both slow prostate tumour growth and to increase prostate tumour radiosensitivity while protecting normal tissues during radiotherapy; thus providing a potential non-toxic therapeutic that could act as both a chemo-preventive and a differential radiosensitiser.

Parthenolide and prostate cancer development in the TRAMP model

Despite intensive investment in improving early detection, prostate cancer often escapes timely detection and, while there has been a slow decline in the number of prostate cancer-related deaths over the last decade, mortality remains relatively high (*AIHW & AACR, 2014*). Health care costs of prostate cancer, both to the individual and to the wider community, result in a significant financial burden that is only expected to grow with an aging population (*Cronin et al., 2016; Stone et al., 2005; Mariotto et al., 2011*). Even in cases of successful therapy, the treatment is associated with long-term and pervasive side-effects on patients, and resistance to therapy can develop over time (*Kroon et al., 2016; Antonarakis et al., 2014*). A proactive alternative to treating prostate cancer is to prevent or delay its occurrence and progression prior to symptomatic malignancy. This may serve to help address the issues of growing healthcare costs and increasing number of patients. This type of chemo-preventive approach would ideally utilise well-tolerated and inexpensive agents to inhibit cancer initiation or earliest dysfunction in initiated cells to reduce the risk of

cancer development in otherwise healthy individuals, or to treat individuals with a premalignant or latent disease to stop disease progression (*Vemana et al., 2014; Sandhu et al., 2013*). Prostate cancer is a disease that is highly suited to chemoprevention for many reasons. Carcinogenesis in the prostate is considered to be the result of a protracted multistep molecular process affecting numerous pathways (*Mazaris & Tsiotras, 2013; Corn, 2012; Gonzalgo & Isaacs, 2003*). This molecular pathogenesis may result in precursor lesions such as atypical small acinar proliferation and PIN lesions, which can develop many years before the detection of cancer and can often represent well-defined, potentially high-risk target populations that would benefit from primary chemoprevention (*Epstein & Herawi, 2006*). In addition to a prolonged molecular pathway of carcinogenesis, prostate cancer has a protracted latent disease state, as well as an increasing incidence with age (*Sakr et al., 1996; Powell et al., 2010; Stamatiou et al., 2006*). Such a long latency period between the development of prostate cancer and its eventual clinical manifestation makes it a prime target for chemoprevention. While some candidate therapies for prostate cancer chemoprevention have been trialled in humans, most notably finasteride (*McConnell et al., 1998; Thompson et al., 2003*), dutasteride (*Andriole et al., 2010*) and selenium (*Clark et al., 1998; Klein et al., 2011*), results have been mixed and positive clinical outcomes have been limited. Green tea, which has shown promise as a chemo-preventive in TRAMP mice and in a small scale human trial, is still currently undergoing large scale confirmatory clinical trials (*Brausi, Rizzi & Bettuzzi, 2008*). New approaches to prostate cancer chemo-prevention are therefore still required.

PTL has been shown to be well tolerated clinically and has been studied *in vivo* in xenograft models of a wide variety of cancer types (*Y. Liu et al., 2008; D'Anneo et al., 2013; Kim et al., 2013; S.L. Kim et al., 2012; Gao, Zhang & Guo, 2010; Shanmugam et al., 2011; Vegeler et al., 2007*). Prostate tumour development during treatment with PTL has only been investigated in three *in vivo* studies, all using xenograft mice (*Kawasaki et al., 2009; Shanmugam et al., 2010; Shanmugam et al., 2006*). These studies were all based on the chemo-therapeutic potential of PTL and confirmed the ability of PTL to slow, but not completely inhibit, prostate tumour growth.

To examine the chemo-preventive potential of PTL, TRAMP mice were treated with PTL or DMAPT until palpable tumours developed. PTL, which was delivered in a 10% ethanol in saline vehicle, did not slow prostate cancer development in the TRAMP model. It was determined that the low doses of ethanol from the vehicle control were inducing NF-κB and counteracting the anti-cancer effect of PTL. Contrary to the results of the experiments carried out for this thesis, the Kawasaki et al. (*2009*) study, which used immunocompromised NOD/SCID mice, showed that PTL, also delivered in a 10% ethanol/saline vehicle, was able to significantly delay prostate tumour development by 27%. In the xenograft model, the same volume of ethanol did not have the same counteractive effect on PTL, which may be due to interactions with the immune system in the TRAMP mice or due to the length of treatment time, which was significantly less in the NOD/SCID study. This difference in tumour development between studies in

xenograft and TRAMP mice highlights the need to run studies in more than one type of *in vivo* model before moving into clinical trials.

DMAPT is the most commonly used water soluble PTL derivative. In the studies presented in this thesis, TRAMP mice were treated with DMAPT (dissolved in water), or PTL (in an ethanol/saline vehicle). Unlike PTL, long-term treatment of DMAPT (delivered in a water vehicle) was able to significantly delay TRAMP prostate tumour development compared to control mice. This is the first report that DMAPT delays tumour onset and progression in an autochthonous model of prostate cancer, indicating that it shows significant promise as a prostate cancer preventive. This is a particularly impressive result given that the TRAMP model is considered a rapid and aggressive model of prostate carcinogenesis (*Grabowska et al., 2014*). These results demonstrate the potential clinical benefit of DMAPT as a prostate cancer chemo-preventive further supporting translation of DMAPT into human clinical trials.

Parthenolide and metastasis in the TRAMP model

DMAPT not only slowed prostate tumour growth in the TRAMP model, but the data presented in this thesis clearly demonstrate an additional strong anti-metastatic ability. For the overwhelming majority of cancer patients, a diagnosis of metastatic disease indicates terminal illness. Although cancer death rates have declined, for the most part patients with metastatic disease have not benefited greatly from therapeutic improvements. Despite the clear need for anti-metastatic therapies, the most recent attempts to target metastatic

pathways in prostate cancer have provided mixed results. One particularly disappointing set of compounds have been the SRC inhibitors dasatinib and saracatinib (*Parsons & Parsons, 2004; Summy & Gallick, 2003*). On the basis of highly positive pre-clinical data in cell lines (*Nam et al., 2005; Lee et al., 2004*) and nude mouse models (*Park et al., 2008; Yang et al., 2010; Koreckij et al., 2009*), SRC inhibition was anticipated to be a highly potent anti-metastatic therapeutic target for prostate cancer. However, in patients with refractory disease, dasatinib failed as a single anti-metastatic agent (*Twardowski et al., 2013; Yu et al., 2011; Yu et al., 2009*) and did not increase overall survival when combined with docetaxel (*Araujo, Trudel & Paliwal, 2013*). Not only does this highlight the need for novel anti-metastatic therapies, but it again shows the need to test these therapies in tumour models that more closely recapitulate the complexities of the human disease, such as autochthonous animal models and human tissue culture models, prior to commencing trials in humans.

The results in this thesis provide the first evidence that DMAPT reduces prostate cancer metastasis *in vivo*. Here, administration of DMAPT to TRAMP mice reduced metastatic lesions in the lung compared to a water vehicle control, and significantly reduced expression of pro-metastatic proteins, MMP2 and laminin in primary prostate tumours. MMP2 is a well-established mediator of tumour invasion and metastasis by breaking down connective tissue barriers (*Lokeshwar, 1999*). Inhibition of MMP2 is known to result in reduced prostate cancer metastasis, not only by reducing the capability of cancer cells to escape but also to lodge and grow at a distant site (*Chen et al., 2015; Shay, Lynch & Fingleton,*

2015). By systematically targeting pro-inflammatory and pro-metastatic pathways, DMAPT is able to significantly reduce invasive disease. Given the current difficulty of treating metastatic prostate cancer, DMAPT may be able to improve disease survival by reducing metastatic spread. Because changes in MMP2 and laminin are not specific to prostate cancer, there is the possibility for DMAPT to be used to limit metastatic spread in other cancer types as well. This is supported by reports in the literature of anti-metastatic activity of DMAPT and PTL in other tumour models, including breast (*D'Anneo et al., 2013; Burnett et al., 2015*), bone, pancreas (*Yip-Schneider et al., 2008; Yip-Schneider et al., 2013b; Yip-Schneider et al., 2013a*), and lung cancer (*Song et al., 2014; Shanmugam et al., 2011*).

Ethanol and metastasis in the TRAMP model

An unexpected observation of this study was that TRAMP mice receiving the 10% ethanol in saline vehicle developed a highly aggressive form of metastatic prostate cancer, which was only apparent after almost 200 days of treatment. In these animals, metastatic tumours were identified by palpation, while primary prostate tumours were small and tissues had only partially progressed to adenocarcinoma. Metastatic lesions develop at distant sites from disseminating cancer cells that can progress to tumour masses immediately or can remain dormant (*Sosa, Bragado & Aguirre-Ghiso, 2014*). Metastasis-initiating cells are most commonly thought to originate from a subpopulation present in fully progressed, invasive tumours. However, it has recently been reported that early

dissemination of metastatic cells can occur in breast cancer before any apparent primary tumour masses are detected (*Hosseini et al., 2016; Harper et al., 2016*). This early dissemination of metastatic cells has previously been reported once in the TRAMP model (*Gelman et al., 2014*). The results presented in this thesis provide the first description of ethanol-induced aggressive metastatic tumours originating from TRAMP prostate tumour cells that are likely to have spread during the early stages of primary tumour development.

There is strong evidence that chronic alcohol use increases the risk of cancers of the mouth, pharynx, larynx, oesophagus, bowel, liver and breast and the risk is related to amount of consumption (*WCRF, 2007*); however, there is very little evidence that implicates ethanol as a risk factor in prostate cancer (reviewed in *Meadows & Zhang, 2015*). Many of these pro-cancer associations are based on moderate to heavy drinking. It is not clear that chronic lower alcohol consumption is a risk factor, but given the large proportion of the population that consumes alcohol on a regular basis, it is essential to understand the role of low chronic ethanol consumption in carcinogenesis. The exact mechanism by which ethanol increases cancer risk is not known, however alcohol consumption affects many aspects of the innate and adaptive immune system which play a role in tumour formation (reviewed in *Molina et al., 2010*). Analysis of primary prostate tumour tissues from the TRAMP mice in the present study identified a significant increase in NF-κB expression with increasing administration time in TRAMP mice treated with the 10% ethanol in saline vehicle, which was not observed in the PTL (in ethanol/saline) treatment group (E. Solly, Flinders

University, personal communication). This observation is supported by reports in the literature of increased NF-κB signalling and metastatic spread following ethanol exposure in several cancer types (*Wang et al., 2015*) and may explain why PTL, which inhibits NF-κB, was such a potent inhibitor of the aggressive metastatic phenotype observed in the TRAMP mice. The link between inflammation and cancer is well documented (*Mantovani et al., 2008; Coussens & Werb, 2002*). Several inflammatory diseases, including inflammatory bowel disease, increase the risk of cancer. Conversely, in tumours that are epidemiologically unrelated to overt inflammatory conditions (such as breast cancer), the activation of oncogenes can orchestrate the production of inflammatory molecules and the recruitment of inflammatory cells. In the tumour microenvironment, inflammatory cells and molecules influence almost every aspect of carcinogenesis, especially the ability of tumour cells to metastasise (*Mantovani et al., 2008*). The pro-NF-κB effect of chronic low doses of ethanol was almost entirely counteracted by PTL, which acts primarily to inhibit the NF-κB signalling pathway as well as to reduce pro-metastatic signalling of integrins and extra-cellular matrix proteins.

There is significant evidence that AR expression may also play a role in prostate cancer metastasis (*Levesque et al., 2009; Feng et al., 2016; Y.N. Liu et al., 2008*). Unfortunately, the constraints of a time-to-palpable tumour study and the nature of the AR expression in the TRAMP model, whereby AR expression is almost entirely reduced in adenocarcinoma tissue compared to PIN tissue, made it difficult to assess the effect of low chronic doses of ethanol on AR signalling in

primary tumour and metastasis development. Ideally this long-term TRAMP study would be repeated with tissues taken for examination and analysis at various time-points throughout tumour development, rather than only at palpable tumour time. The molecular changes in the prostate that result in increased invasion and slowing of primary tumour growth are likely to occur when both high grade PIN and some adenocarcinoma tissue are present simultaneously, and would be the best time to pinpoint the cardinal changes that lead to differences in palpable tumour phenotypes.

It is not known if low dose ethanol administration is pro-metastatic in the TRAMP model alone, or if it is a true risk factor for human prostate cancer. To help clarify this effect, similar animal studies will need to be carried out using alternate models of prostate cancer, where tumours develop at different rates and tumorigenesis is driven by different molecular mechanisms. If it eventuates that this is a TRAMP-specific effect, these data will be an important consideration for prostate cancer studies using the TRAMP model. As many drugs are dissolved in ethanol prior to administration for *in vivo* studies, it will be important to recognise that using such a vehicle for an extended period of time in TRAMP mice will have a pro-inflammatory effect and may result in increased metastasis. While this may be considered a drawback, this pro-metastatic effect may also provide a unique opportunity to study aggressive metastatic prostate cancer *in vivo*. If the pro-metastatic effect of chronic low doses of ethanol is not limited to the TRAMP model, the implications for human cancer may be highly significant. The doses of ethanol used in this study (1.2 mL/kg/week) were in the

range of the average alcohol consumption per capita in Australia (0.93 – 2.5 mL/kg/week, based on an average population weight of 75 kg) (*Livingston & Dietze, 2016; ABS, 2015*). Given that these doses of alcohol are regularly consumed by the general public, and epidemiology studies have not identified a significant risk for such low doses, it seems unlikely that consuming this volume of alcohol alone would be enough to induce such a pronounced pro-metastatic response. TRAMP mice are predisposed to tumour development and tumorigenesis is being driven at a fast pace in the animals (*Greenberg et al., 1995; Gingrich et al., 1999; Gingrich et al., 1996*), while prostate cancer in most men is generally considered a slow developing disease. The difference in rate of disease progression between TRAMP and human prostate carcinogenesis may be one reason why a low dose of ethanol has such a pronounced effect in the animals. This raises the question of whether low doses of ethanol may increase risk of metastatic disease in men predisposed to prostate cancer or the small number of men that present with a more rapid prostate cancer onset. A major barrier to prostate cancer survival is the progression to metastatic disease, therefore understanding the role that low doses of ethanol may play in metastatic disease could help to improve overall prostate cancer survival rates.

Parthenolide and high dose radiation in the TRAMP model

The results presented in this thesis show that DMAPT holds significant promise for use in conjunction with radiotherapy for prostate cancer. External beam radiotherapy is delivered to approximately 48% of cancer patients at least once

during their cancer treatment (*Barton et al., 2014*). Prostate cancer has been recorded as the principal diagnosis for one-quarter of all men who receive radiotherapy (*AIHW, 2016*). Prostate cancer radiotherapy, while effective at ablating cancer cells in many cases, can result in short-term side effects, including colorectal injury which can induce diarrhoea and bleeding, and long-term side effects, including incontinence, impotence and infertility. In these studies both PTL and DMAPT were shown to protect healthy tissues from damage while sensitising prostate tumour tissues to radiation-induced apoptosis in TRAMP mice. As was observed in the time-to-palpable tumour studies, the increased water solubility and bioavailability of DMAPT makes it the drug of choice for clinical use as an adjunct to prostate cancer radiotherapy.

Men with localised low to moderate-risk prostate cancer who are treated with external-beam radiotherapy have overall survival rates above 90% (*Heidenreich et al., 2014; Strom et al., 2014*). Despite the high success of radiotherapy for localised disease, normal tissue toxicity still occurs and remains a limiting factor in the treatment of prostate cancer. The close proximity of the bladder, urethra, testis, colon and rectum to the prostate makes these organs particularly vulnerable to side-scatter radiation resulting in long-term side-effects. Approximately 10% of patients experience urinary and bowel problems including urinary incontinence and faecal urgency, bloody stools and rectal pain up to two years after treatment and nearly 40% of patients have ongoing sexual dysfunction (*Sanda et al., 2008*). These symptoms persist for many years and adversely impact the quality of life of the many patients who survive after

treatment (*Resnick et al., 2013; Yeoh et al., 2012*). Based on the intimate relationship between prostate tumours, normal prostate and surrounding tissues and surrounding critical structures it is unlikely that technological advances alone will be able to completely limit damage to healthy tissues. Chemical radioprotectors that can be administered systemically to protect healthy tissues on a molecular level appear likely to be the best option for further reducing normal tissue damage and limiting side effects. Rectal sucralfate is the only radioprotector to have been evaluated in a double-blind placebo-controlled study for prostate cancer but was not found to be effective (*O'Brien et al., 2002*). Not only has DMAPT been shown to be an effective radioprotector of healthy colorectal tissue *in vivo*, it also sensitises tumour cells, particular promoting cell death in more advanced prostate tumour tissue. DMAPT has previously been shown to be highly tolerated with minimal side effects clinically and the experimental results of studies for this thesis have shown that beneficial effects of DMAPT can be observed when the drug is administered 24 hours prior to high dose radiation exposure, which allows more flexibility around drug dosing prior to radiotherapy. For high-grade localised prostate tumours, there is reduced therapeutic benefit from radiotherapy as a monotherapy and reportedly overall survival may even decrease following radiation treatment compared to other therapies (*Degroot et al., 2013; Hoffman et al., 2013*). In a number of clinical trials, external beam radiotherapy (in the ranges of 65–70 Gy) for high-risk localised disease resulted in 10-year failure rates greater than 75% (*Bolla et al., 2010; Pilepich et al., 2005; Horwitz et al., 2008*). While monotherapy provides a low success rate, radiotherapy combined with adjuvant chemotherapy, such as

docetaxel, has shown significant benefit in increasing 5-year survival estimates in patients with high-grade localised prostate tumours (*Heidenreich et al., 2014; Kibel et al., 2007; Marshall et al., 2014*). Unfortunately, these therapeutic benefits often come with added normal tissue toxicity. The low toxicity of DMAPT, as well as the ability to selectively target higher grade prostate tumour tissue in TRAMP mice, indicate that there may be a significant use for the drug in combination with radiotherapy to improve cure rates for these high-risk tumours without the toxicity of currently used adjuvant therapies.

Additionally, there may be a role for DMAPT to play following radiotherapy, to limit relapse or metastatic spread. Biopsy-proven relapse of local disease following radiotherapy is reported in 19-65% of patients (*Zelefsky et al., 1998; Nilsson, Norlen & Widmark, 2004*), due in part to intrinsic resistance of a proportion of tumour cells to conventional radiotherapy doses. Tumour recurrence following localised prostate cancer treatment often indicates an increased risk of metastatic spread, and therefore therapeutic options must carefully balance the onset of metastatic disease with avoidance of overtreatment (*Zietman et al., 2005; Kolodziej, 2014*). DMAPT has been demonstrated as a potent anti-metastatic agent with low toxicity, therefore continued systemic administration of the drug after completion of a course of radiation therapy may preventive relapse or limit metastatic spread, thus increasing overall cure rates.

Parthenolide and low dose radiation in the TRAMP model

Prostate cancer patients receiving IGRT, receive both high and low doses of radiation during their treatment. Radiotherapy is commonly delivered in daily fractions after the tumour is imaged by a low dose CT scan just prior to the therapeutic dose to better target the tumour and to spare normal tissues. Low 'conditioning' doses of radiation are known to result in reduced genetic damage in normal cells, decreased tumour incidence and increased tumour latency (*Day et al., 2006; Mitchel et al., 2003; Olivieri, Bodycote & Wolff, 1984*). The exact mechanism of the radio-adaptive response is not fully understood, but it is known that p53, ROS, NFκB and MnSOD play a role, all of which are known to be modulated by PTL. This implies that PTL may act like a chemical form of the low dose radio-adaptive response. Although the protection induced by PTL and low dose radiation might be similar, it is likely that the exact mechanism by which it occurs is different, due to the p53-dependent nature of the radio-adaptive response and the p53-independence of PTL (*Ahmed & Li, 2008; Grdina et al., 2015; Lall et al., 2014; Tang & Loke, 2015*). The results presented in this thesis indicate that PTL and low dose radiation may be able to be combined to provide additive protection in healthy tissues. Here the time between the low priming dose (10 mGy) and the high challenge dose (6 Gy) was chosen as 3 hours, as adaptive responses have been observed for a wide range of biological endpoints within this time period. The timing between radiation doses has been used here as a proof-of-principle, however in the clinic there is only a very small window of time (less than 5 mins) between a CT scan dose and a therapeutic dose. Adaptive responses usually require a time interval of at least 30 minutes between the low

dose and the high dose, but have are known to last up to 24 hours after the low conditioning dose is delivered (*Mitchel et al., 2002; Blankenbecler, 2010*). Therefore, although a CT scan is unlikely to protect from the therapeutic dose delivered a few minutes later in a radiotherapy scenario, it is possible that the effects of the low dose will last until the following day when a second high therapeutic dose is delivered during a fractionated dosing protocol, and where a reduction in damage might be observed. Here no significant additive protection from apoptosis was observed where PTL/DMAPT and a single dose of 10 mGy were delivered prior to a single dose of 6 Gy, however, this does not mean that a radioadaptive response has not played a role. If PTL/DMAPT and a low dose of radiation were to be delivered prior to multiple fractionated higher doses delivered over a number of days, there may be cumulative additive protection that is not observable after a single dose alone.

The low dose radio-adaptive response has conventionally been considered to only be active in normal cells and that tumour cells are no longer responsive to low adapting doses of radiation, however, it has been demonstrated that low doses of radiation can elicit an adaptive response in tumour cells as well involving increased expression of survivin, an apoptosis inhibiting protein (*Grdina et al., 2013*). This creates an issue for IGRT where the image dose may be protecting tumour tissue and therefore having a significant effect on clinical outcomes. In contrast, it has been shown that PTL suppresses survivin in cancer cell lines (*Kim et al., 2010*), which suggests that while PTL/DMAPT may induce low dose radiation-like protection in healthy tissues, the same protection does

not occur in tumour tissues. Furthermore, PTL/DMAPT may be able to counteract tumour protection induced by low dose radiation, given its potent ability to radiosensitise tumour tissues. Although the studies presented in this thesis did not observe low dose radiation-induced tumour protection, this may be partly due to the timing between low and high doses, or the lack of p53 in TRAMP prostate tumours, which is known to be important for the low dose adaptive response. Further studies in p53-positive prostate tumour models are likely to be required to fully elucidate this effect.

Parthenolide as a multistage and broad-range cancer therapy

One of the significant benefits of DMAPT as a cancer therapeutic is that the mechanisms involved in the anti-cancer and radiation modulating effects of the compound (NF-κB inhibition, JAK/STAT inhibition and oxidative stress modulation) are not limited to prostate cancer (*Kansanen et al., 2013; Leinonen et al., 2014; Taguchi, Motohashi & Yamamoto, 2011*). NF-kB transcription factors play a crucial role in oncogenesis (*Staudt, 2010*), and are aberrantly activated in a wide range of human cancers, which promotes survival and malignancy by upregulating anti-apoptotic genes (*Staudt, 2010; DiDonato, Mercurio & Karin, 2012*). In numerous cancer-derived cell lines or in a primary tumours, STATs, especially STAT-3, are persistently tyrosine phosphorylated (*Bromberg, 2002*), and constitutive activation of STATs is common in a variety of cancer types, including leukaemia, multiple myeloma, breast cancer, prostate cancer, and colorectal cancer (*Endo, Toyota & Imai, 2004; Sheen-Chen et al., 2007; Ferrajoli*

et al., 2006; Tam et al., 2007). High levels of ROS are known to cause significant damage to cell structures and functions and may induce somatic mutations and neoplastic transformation (*Khandrika et al., 2009; Fang, Seki & Maeda, 2009*). Cancer initiation and progression of multiple cancer types has been linked to oxidative stress by increasing DNA mutations or inducing DNA damage, genome instability, and cell proliferation (*Visconti & Grieco, 2009*). The ability of DMAPT to target a variety of pathways common to many types of cancer makes it a promising candidate for cancer prevention and treatment in a wide range of cancers.

In conclusion, the results presented here provide strong pre-clinical evidence that DMAPT significantly slows prostate tumour development and is a potent anti-metastatic agent. When delivered prior to radiation, DMAPT was able to reduce cell death in healthy cells during radiotherapy while also increasing prostate cancer killing particularly in more advanced pathology stages of prostate cancer, providing the potential to increase cure rates. Analysis of primary prostate tumours identified important molecules involved in the mechanism of DMAPT's selective anti-cancer mechanisms, which support the potentially broader application of DMAPT for a number of different cancer types. Also, this is the first report of induction of an aggressive metastatic TRAMP mouse phenotype following chronic low doses of ethanol, which sets the groundwork for future investigations to determine the role of ethanol in early dissemination of prostate cancer cells and development of distant metastases.

Appendix A: Summary of *in vivo* PTL cancer studies

Cancer type	Drug dose	Treatment	Tumour methodology	Animal model	Anti-tumour effects	Reference
Acute myeloid leukaemia	7.5 µM PTL	*Ex vivo* pre-treatment before cell implantation, 18 h	Primary AML cells injected IV	NOD/SCID mice	↓ tumour development by > 80%	(*Guzman et al., 2005*)
	5 µM DMAPT; 100 mg/kg DMAPT	5 µM: *ex vivo* pre-treatment before cell implantation 100 mg/kg: Mice: oral gavage, single dose Dogs: oral gavage and IV, 1 x daily for 3–12 days	Primary AML cells injected by IV in mice. Canine leukaemia cells injected by IV	NOD/SCID mice; Dogs diagnosed with CD34+ leukaemia	↓ tumour development by >80%, when cells were pre-treated before implantation ↑ activation of Nrf2 stress response and γH2AX ↓ proportion of $CD34^+$cells in dogs treated IV or orally for 3–12 days	(*Guzman et al., 2007*)
	10 µM PTL	*Ex vivo* pre-treatment before tumour cell implantation, 24 h	Primary AML cells injected IV	NOD/SCID mice	↓ development of AML tumours	(*Kim et al., 2010*)
	4 mg/kg PTL; 10 mg/kg PTL	Treatment A: IV, single 10 mg/kg dose Treatment B: IP, 5 x 4 mg/kg over 7 days Both treatments started after tumours reached 100–200 mm^3	MV4-11 cells injected SC	Athymic nu/nu mice	Treatment A: ↓ global hypomethylation by 30% Treatment B: ↓ tumour growth by 37% ↓ DNMT1 expression	(*Liu et al., 2009*)
	100 mg/kg DMAPT	IP, 3 x daily for 21 days	Primary AML cells injected IV	NOD/SCID mice	Reduced tumour burden only when combined with PI3K/mTOR inhibitors	(*Hassane et al., 2010*)
	10 µg/kg PTL	IP, treatment started when tumour volume reached 100–300 mm^3, administered every 2 days for 16 days	THP-1 cells injected SC	Athymic BALB/c nude mice	↓ tumour growth by 27% ↑ apoptosis ↓ Bcl-2 and cyclin D1 expression ↓ NF-κB expression	(*Wang et al., 2012*)
	2.5 µM PTL	*Ex vivo* pre-treatment before cell implantation, 24 h	CD34+ primary AML cells injected in femur	NOD/SCID mice	Only ↓ tumour development when combined with dipeptidyl peptidase inhibitor	(*Spagnuolo et al., 2013*)
Acute lymphoblastic leukaemia	10 µM PTL; 40 mg/kg PTL	10 µM: *ex vivo* pre-treatment before cell implantation, 20–24 h 40 mg/kg: 9 treatment started after cell engraftment > 5%, 1 x daily for 9 days	Primary B-ALL and T-ALL cells injected IV	NSG mice	↓ tumour development by > 80% ↑ survival in all animals ↓ NF-κB	(*Diamanti et al., 2013*)
Bladder	100 mg/kg DMAPT	Oral gavage, treatment started 1–7 days post-tumour implantation, 2 x daily for up to 60 days	UMUC-3 cells injected SC	Athymic nude mice	↓ tumour growth by 60% ↑ p21 expression ↓ TRAF-2 expression	(*Shanmugam et al., 2011*)
Bone	1 mg/kg PTL	IP, IV, 1 x daily for 17 (IV model) or 25 (SC model) days	LM8 cells injected SC or IV	C3H mice	PTL ↓ lung metastasis when injected on same day as tumour cells ↓ NF-κB and VEGF	(*Kishida, Yoshikawa & Myoui, 2007*)
	1 mg/kg PTL	IP, 1 x daily for 10 days	W256 cells injected directly into the heart	W256 rats	↓ size of bone lesions by up to 75% ↓ tumour size ↓ trabecular bone loss	(*Idris et al., 2009*)

Cancer type	Drug dose	Treatment	Tumour methodology	Animal model	Anti-tumour effects	Reference
Brain	10 mg/kg PTL	IP, 1 x daily for 22 days	U87MG cells injected into the brain	Athymic BALB/c mice	↓ tumour volume by 24% ↓ microvessel density ↓ VEGF and MMP-9 expression	(*Nakabayashi & Shimizu, 2012*)
Breast	40 mg/kg PTL	Oral gavage, Metastasis model: tumours removed after 42 days, 1 x daily treatment for 45 days. Orthotopic model: tumours left *in situ*, treatment started 14 days after implantation and continued 1 x daily for 28 days	TMD231 cells injected into mammary fat pad	Athymic nude mice	Metastasis model: ↑ survival from 34% to 64% ↓ NF-κB expression ↓ metastatic lung deposits Orthotopic model: ↓tumour growth by 25% ↓ serum levels of IFNγ and TNFα	(*Sweeney et al., 2005*)
	10 mg/kg PTL	IV, 1 x on 5th and 1 x 8th day post-tumour implantation, mice euthanised after 18 days	MCF-7 cells injected SC	BALB/c nude mice	↓ tumour volume by 65%	(*Liu et al., 2008*)
	50 mg/kg DMAPT	Oral gavage, 1 x daily, treatment started when tumours reached 200 mm^3	MDA-MB231 cells injected SC	Athymic Fox1 mice	↓ tumour volume by 48% ↑ survival time from 12 days to 28 days	(*D'Anneo et al., 2013*)
Colon	4 mg/kg PTL	IP, treatment started 5 days post-tumour implantation, 3 x weekly, for 23 days	HT-29 cells injected SC	Athymic nude mice	↓ tumour volume by 44% ↓ angiogenesis ↑ apoptosis	(*S.L. Kim et al., 2012*)
	2.5 mg/kg PTL	IP, treatment started 5 days post-tumour implantation, 3 x weekly, for 23 days	SW620 cells injected SC	Athymic nude mice	↓ tumour volume by 19%	(*Kim et al., 2013*)
Kidney	3 µg/mouse PTL; 10 mg/kg PTL	3 µg/mouse: peritumour injection, 3 x weekly for 6 weeks 10 mg/kg: oral gavage, once daily for 6 weeks	OUR-10 cells injected SC	Athymic nude mice	↓ tumour volume by up to 65% ↓ NF-κB, Bcl-xL, IL-8, VEGF, Cox-2 and MMP-9 expression	(*Oka et al., 2007*)
Liver	4 mg/kg PTL	IP, 3 x weekly, for 2 weeks	Thioacetamide injected IP	Sprague–Dawley rats	↓ liver fibrosis ↓ α-smooth muscle actin ↓ TGF-β1 expression ↓ portal inflammation and lobe degeneration	(*I.H. Kim et al., 2012*)
Lung	40 mg/kg DMAPT	Oral gastric lavage, 5 x weekly for 32 weeks	BOP injected SC	Syrian golden hamsters	↓ tumour diameter by up to 35%	(*Vegeler et al., 2007*)
	5 mg/kg PTL	IP, treatment started 2 weeks post-tumour implantation, 3 x weekly, for 4 weeks	A549 cells injected SC	Athymic nude mice	↓ tumour growth only when combined with Taxol ↓ NF-κB expression	(*Zhang et al., 2009*)
	5 mg/kg PTL	IP, 3 x weekly for 4 weeks	H460 cells injected into the trachea	Athymic nude mice	↑ mean survival from 95 to 133 days ↓ phosphorylated IκBα and p65/NF-κB expression	(*Gao, Zhang & Guo, 2010*)
	100 mg/kg DMAPT	Oral gavage, treatment started 1–7 days post-tumour implantation, 2 x daily up to 60 days	A549 cells injected SC or IV	Athymic nude mice	↓ tumour growth by 63% ↑ p21 expression ↓TRAF-2 expression	(*Shanmugam et al., 2011*)

Cancer type	Drug dose	Treatment	Tumour methodology	Animal model	Anti-tumour effects	Reference
Mesenchyme	5 µM PTL	*Ex vivo* pre-treatment before tumour cell implantation, 6 h	Luciferase-expressing MSCs injected into ventricle cavity of colon SW480 mice xenografts	Athymic BALB/c mice	PTL-treated MSCs did not accumulate at tumour sites	(*Uchibori et al., 2013*)
Pancreas	Up to 40 mg/kg DMAPT	Oral gastric lavage, BxPC3 cells: 1 x daily for 37 days MiaPaCa-2: cells 1 x daily for 43 days	BxPC3 or MiaPaCa-2 cells injected SC	Athymic nude mice	No significant inhibition of tumour growth ↓ NF-κB	(*Yip-Schneider et al., 2008*)
	Up to 40 mg/kg DMAPT	Oral gastric lavage, 1 x daily for 32 weeks	BOP injected SC	Syrian golden hamsters	↓ tumour growth by 63% ↓ NF-κB	(*Yip-Schneider et al., 2008*)
	5 µg/mouse PTL	Injected into tumour, treatment started 24 h post-tumour implantation, 2 x weekly for 22 days	PANC-1 cells injected SC	Athymic nude mice	↓ tumour growth by 20%	(*Wang et al., 2009*)
Pituitary	8.7 mg/kg PTL	SC, treatment started 7 days post-tumour implantation, 1 x daily for 14 days	AtT20 cells injected SC	BALBc nu/nu mice	↓ tumour growth only when combined with dehydroepiandrosterone	(*Taguchi et al., 2006*)
Prostate	40 mg/kg PTL	Oral gavage, treatment started 14 days post-tumour implantation, 1 x daily for 36 days	CWR22Rv1 cells injected SC	Athymic nude mice	↓ tumour growth only when combined with docetaxel ↓ bFGF- and VEGF-induced angiogenesis ↓ TRAF1 expression	(*Shanmugam et al., 2006*)
	40 mg/kg PTL	Oral gavage, 3 x weekly for 106 days	DU145 cells injected SC	NOD/SCID mice	↓ tumour incidence by 50% at day 85 ↑ tumour latency period from 61 to 77.5 days	(*Kawasaki et al., 2009*)
	100 mg/kg DMAPT	Oral gavage, treatment started 7 days post-tumour implantation, 1 x daily for 88 days	CWR22Rv1 or PC3 cells injected SC	Female athymic nude mice	↓ tumour growth by 75% ↓ TRAF-2 expression ↑ phospho-cJUN	(*Shanmugam et al., 2010*)
	10 mg/kg DMAPT	Oral gavage, single dose prior to 3 Gy irradiation, 1 x daily for 5 days	PC3 cells injected SC	NCRNU nu/nu mice	↓ tumour growth after DMAPT alone and DMAPT + fractionated IR ↓ mitochondrial damage in healthy prostate and bladder tissues	(*Xu et al., 2013*)
Skin	1 mg/mouse PTL	Food pellets, treatment started, 1 x daily, 1 week before UVB exposure, for 24 weeks	UVB exposure	SKH-1 mice	Delayed tumour onset from 13 to 18 weeks ↓ number of large and ↑ number of small tumours ↓ UVB-induced epidermal thickness	(*Won et al., 2004*)
	0.25 mg/kg PTL	IP, 1 x daily for 12 days after UVB exposure	UVB exposure	DBA/2 mice	↓ epidermal and melanocyte hyperproliferation by up to 45%	(*Tanaka et al., 2005*)
	0.25 mg/kg PTL	IP, every other day for 10 days, stopping either upon tumour implantation or continued for 10 more days when tumours became palpable	JB6P+ cells injected SC	NMRI-Nu mice	↓ tumour volumes by up to 63% ↑ p21 expression ↓ p65 and cyclin D1 expression	(*Ghantous et al., 2012*)
Stomach	4 mg/kg PTL	IP, treatment started 24 h post-tumour implantation, 1 x daily for 21 days	MKN-45-P cells injected IP	BALBc nu/nu mice	↓ proportion of peritoneal nodules by approximately 30% No effect on survival, except in combination with paclitaxel	(*Sohma et al., 2011*)

Abbreviations: IP, intraperitoneal; IV, intravenous; SC, subcutaneous (*adapted from Ghantous et al. 2013*)

Appendix B: PCR Primers

PB-1-For: 5'- CCG GTG GAC CGG AAG CTT CCA CAA GTG CAT -3'

TAg-Rev: 5'- CTC CTT TCA AGA CCT AGA AGG TCC A -3'

MβC-For: 5'- GAT GTG CTC CAG GCT AAA GTT -3'

MβC-Rev: 5'- AGA AAC GGA ATG TTG TGG GAG T -3'

Mus6 +: 5'- GTT CTA GAC ATT GGT TCT ACT C -3'

Mus6 -: 5'- CAC CTA TTC CAT GTT GCA ACT TC -3'

Appendix C: Solutions

PBS

0.1 M phosphate buffered saline (PBS) solution was prepared by adding 80 g of NaCl, 2 g of KCl, 14.4 g of Na_2HPO_4, and 2.4 g of KH_2PO_4 to 1 litre of Milli-Q water, and adjusting pH to 7.4 at 25°C

0.1M PBS was diluted 1:10 in Milli-Q water for use in immunohistochemistry. Final concentration when diluted: NaCl 0.137 M: KCl 0.0027 M: Na_2HPO_4 0.0101 M: KH_2PO_4 0.00176 M.

High salt PBS

High salt PBS was prepared by the addition of 0.4 moles of NaCl per litre of PBS

Aqueous formaldehyde preparation

Stock formaldehyde fixative (4%) was prepared by heating PBS to 57°C on a heating block, 4 g of paraformaldehyde per litre was added and dissolved by stirring. Fixative was stored at 4°C and diluted for use as needed,

Tris-HCl

1 M Tris-HCl solution was prepared by adding 121.1 g of Tris base to 800 ml of Milli-Q water, and adding concentrated HCl to adjust the pH to 7.4 at 25°C. 1 M Tris-HCl solution was diluted as required in Milli-Q water.

APES coated slides

2% (v/v) aminopropylethoxysialne (APES) in absolute ethanol was prepared. Glass sliders were immersed for 10 s, rinsed for 10 s in absolute ethanol, rinsed for 10 s in running tap water, and then sensed for 10 s in distilled water before drying at 37°C overnight.

Appendix D: CellProfiler™ pipelines

All CellProfiler™ pipelines were performed using Python based CellProfiler™ version 2.2.0. (*Carpenter et al., 2006*)

Table A-0-1: CellProfiler™ pipeline for the analysis of apoptosis in spleen, by area of total DAPI staining occupied by TUNEL-positive cells in fluorescence images

Order	Module	Parameters	Input
	Input modules		
1	Images	Filter images?	Images only
2	Metadata	Extract metadata? Metadata extraction method Metadata source Extract metadata from	Yes Extract from file/folder names File name All images
3	NamesAndTypes	Assign a name to File does contain Name to assign these images Select the image type Set intensity range from File does contain Name to assign these images Select the image type Set intensity range from	Image matching rules _C0001.tif DAPI Greyscale image Image metadata _C0002.tif Alexa488 Greyscale image Image metadata
	Analysis modules		
4	GreyToColor	Select a color scheme Select image to be colored red Select image to be colored green Select image to be colored blue Name the output image Relative weight for the green image Relative weight for the blue image	RGB Leave this blank Alexa488 DAPI MergedColour 1 1
5	IdentifyPrimary Objects	Select the input image Name the primary objects to be identified Typical diameter of objects, in pixel units (Min,Max)	DAPI Nuclei 10-30

		Discard objects outside of the diameter range?	No
		Discard objects touching the border of the image?	No
		Threshold strategy	Global
		Thresholding method	Otsu
		Two-class or three-class thresholding?	Three classes
		Minimize the weighted variance od the entropy	Weighted variance
		Assign pixels in the middle intensity class to the foreground or the background?	Foreground
		Select the smoothing method for thresholding	Automatic
		Threshold correction factor	1
		Lower and upper bounds on threshold	0.2-1.0
		Method to distinguish clumped objects	Intensity
		Method to draw dividing lines between clumped objects	Intensity
		Automatically calculate size of smoothing filter for declumping	Yes
		Automatically calculate minimum allowed distance between local maxima	Yes
		Speed up by using lower-resolution image to find local maxima	Yes
		Retain outlines of the identified objects	Yes
		Name the outline image	NucleiOutlines
		Fill holes in identified objects?	No
		Handling of objects if excessive number of objects identified	Continue
6	IdentifyPrimary Objects	Select the input image	Alexa488
		Name the primary objects to be identified	TUNEL
		Typical diameter of objects, in pixel units (Min,Max)	10-30
		Discard objects outside of the diameter range?	Yes
		Discard objects touching the border of the image?	No
		Threshold strategy	Global
		Thresholding method	Otsu
		Two-class or three-class thresholding?	Three classes
		Minimize the weighted variance od the entropy	Weighted variance

		Assign pixels in the middle intensity class to the foreground or the background?	Background
		Select the smoothing method for thresholding	Automatic
		Threshold correction factor	1
		Lower and upper bounds on threshold	0.1-1.0
		Method to distinguish clumped objects	Intensity
		Method to draw dividing lines between clumped objects	Intensity
		Automatically calculate size of smoothing filter for declumping	Yes
		Automatically calculate minimum allowed distance between local maxima	Yes
		Speed up by using lower-resolution image to find local maxima	Yes
		Retain outlines of the identified objects	Yes
		Name the outline image	TUNELOutlines
		Fill holes in identified objects?	No
		Handling of objects if excessive number of objects identified	Continue
7	MeasureImageArea Occupied	Measure the area occupied in a binary image, or in objects?	Objects
		Select objects to measure	Nuclei
		Retain a binary image of the object regions?	No
		Measure the area occupied in a binary image, or in objects?	Objects
		Select objects to measure	TUNEL
		Retain a binary image of the object regions?	No
8	OverlayOutlines	Display outlines on a blank image?	No
		Select image on which to display outlines	MergedColour
		Name the output image	ColourOverlay
		Outline display mode	Color
		Width of outlines	1
		Select outlines to display	NucleiOutlines
		Select outline color	Red
		Select outlines to display	TUNELOutlines
		Select outline color	Yellow

9	SaveImages	Select the type of image to save	Image
		Select the image to save	MergedColour
		Select method for constructing file names	From image filename
		Select image name for file prefix	DAPI
		Append a suffix to the image file name?	Yes
		Text to append to the image name	_MergedColour
		Saved file format	tif
		Image bit depth	8
		Output file location	Same folder as image
		Overwrite existing files without warning?	No
		When to save	Every cycle
		Rescale the images?	No
		Select colormap	gray
		Record the file and path information to the saved image?	No
		Create subfolders in the output folder?	No
10	SaveImages	Select the type of image to save	Image
		Select the image to save	ColourOverlay
		Select method for constructing file names	From image filename
		Select image name for file prefix	DAPI
		Append a suffix to the image file name?	Yes
		Text to append to the image name	_ColourOverlay
		Saved file format	tif
		Image bit depth	8
		Output file location	Same folder as image
		Overwrite existing files without warning?	No
		When to save	Every cycle
		Rescale the images?	No
		Select colormap	gray
		Record the file and path information to the saved image?	No
		Create subfolders in the output foler?	No
11	ExportTo Spreadsheet	Select the column delimiter	Comma (",")
		Output file location	Default Output Folder
		Add image metadata columns to your object data file?	No
		Limit output to a size that is allowed in Excel?	No
		Representation of Nan/Inf?	NaN

		Select the measurements to export	No
		Calculate the per-image mean values for object measurements?	No
		Calculate the per-image median values for object measurements?	No
		Calculate the per-image standard deviation values for object measurements?	No
		Create a GenePattern GCT file?	No
		Export all measurement types?	Yes

Table A-0-2: CellProfiler™ pipeline for the measurement of nuclear protein expression in fluorescence images

Order	Module	Parameters	Input
	Input modules		
1	Images	Filter images?	Images only
2	Metadata	Extract metadata?	Yes
		Metadata extraction method	Extract from file/folder names
		Metadata source	File name
		Extract metadata from	All images
3	NamesAndTypes	Assign a name to	Image matching rules
		File does contain	_C0001.tif
		Name to assign these images	DAPI
		Select the image type	Greyscale image
		Set intensity range from	Image metadata
		File does contain	_C0002.tif
		Name to assign these images	Alexa488
		Select the image type	Greyscale image
		Set intensity range from	Image metadata
	Analysis modules		
4	GreyToColor	Select a color scheme	RGB
		Select image to be colored red	Leave this blank
		Select image to be colored green	Alexa488
		Select image to be colored blue	DAPI
		Name the output image	MergedColour
		Relative weight for the green image	1
		Relative weight for the blue image	1

5	IdentifyPrimary Objects	Select the input image	DAPI
		Name the primary objects to be identified	Nuclei
		Typical diameter of objects, in pixel units (Min,Max)	10-30
		Discard objects outside of the diameter range?	No
		Discard objects touching the border of the image?	No
		Threshold strategy	Global
		Thresholding method	Otsu
		Two-class or three-class thresholding?	Three classes
		Minimize the weighted variance od the entropy	Weighted variance
		Assign pixels in the middle intensity class to the foreground or the background?	Foreground
		Select the smoothing method for thresholding	Automatic
		Threshold correction factor	1
		Lower and upper bounds on threshold	0.2-1.0
		Method to distinguish clumped objects	Intensity
		Method to draw dividing lines between clumped objects	Intensity
		Automatically calculate size of smoothing filter for declumping	Yes
		Automatically calculate minimum allowed distance between local maxima	Yes
		Speed up by using lower-resolution image to find local maxima	Yes
		Retain outlines of the identified objects	Yes
		Name the outline image	NucleiOutlines
		Fill holes in identified objects?	No
		Handling of objects if excessive number of objects identified	Continue
6	MeasureImageArea Occupied	Measure the area occupied in a binary image, or in objects?	Objects
		Select objects to measure	Nuclei
		Retain a binary image of the object regions?	No
7	MeasureObject Intensity	Select an image to measure	Alexa488
		Select objects to measure	Nuclei
8	OverlayOutlines	Display outlines on a blank image?	No

		Select image on which to display outlines	MergedColour
		Name the output image	ColourOverlay
		Outline display mode	Color
		Width of outlines	1
		Select outlines to display	NucleiOutlines
		Select outline color	Red
9	SaveImages	Select the type of image to save	Image
		Select the image to save	MergedColour
		Select method for constructing file names	From image filename
		Select image name for file prefix	DAPI
		Append a suffix to the image file name?	Yes
		Text to append to the image name	_MergedColour
		Saved file format	tif
		Image bit depth	8
		Output file location	Same folder as image
		Overwrite existing files without warning?	No
		When to save	Every cycle
		Rescale the images?	No
		Select colormap	gray
		Record the file and path information to the saved image?	No
		Create subfolders in the output folder?	No
10	SaveImages	Select the type of image to save	Image
		Select the image to save	ColourOverlay
		Select method for constructing file names	From image filename
		Select image name for file prefix	DAPI
		Append a suffix to the image file name?	Yes
		Text to append to the image name	_ColourOverlay
		Saved file format	tif
		Image bit depth	8
		Output file location	Same folder as image
		Overwrite existing files without warning?	No
		When to save	Every cycle
		Rescale the images?	No
		Select colormap	gray
		Record the file and path information to the saved image?	No
		Create subfolders in the output folder?	No

11	ExportTo Spreadsheet	Select the column delimiter	Comma (",")
		Output file location	Default Output Folder
		Add image metadata columns to your object data file?	No
		Limit output to a size that is allowed in Excel?	No
		Representation of Nan/Inf?	NaN
		Select the measurements to export	No
		Calculate the per-image mean values for object measurements?	No
		Calculate the per-image median values for object measurements?	No
		Calculate the per-image standard deviation values for object measurements?	No
		Create a GenePattern GCT file?	No
		Export all measurement types?	Yes

Table A-0-3: CellProfiler™ pipeline for the measurement of total protein expression in fluorescence images

Order	Module	Parameters	Input
	Input modules		
1	Images	Filter images?	Images only
2	Metadata	Extract metadata?	Yes
		Metadata extraction method	Extract from file/folder names
		Metadata source	File name
		Extract metadata from	All images
3	NamesAndTypes	Assign a name to	Image matching rules
		File does contain	_C0001.tif
		Name to assign these images	DAPI
		Select the image type	Greyscale image
		Set intensity range from	Image metadata
		File does contain	_C0002.tif
		Name to assign these images	Alexa488
		Select the image type	Greyscale image
		Set intensity range from	Image metadata

	Analysis modules		
4	GreyToColor	Select a color scheme	RGB
		Select image to be colored red	Leave this blank
		Select image to be colored green	Alexa488
		Select image to be colored blue	DAPI
		Name the output image	MergedColour
		Relative weight for the green image	1
		Relative weight for the blue image	1
5	IdentifyPrimary Objects	Select the input image	DAPI
		Name the primary objects to be identified	Nuclei
		Typical diameter of objects, in pixel units (Min,Max)	10-30
		Discard objects outside of the diameter range?	No
		Discard objects touching the border of the image?	No
		Threshold strategy	Global
		Thresholding method	Otsu
		Two-class or three-class thresholding?	Three classes
		Minimize the weighted variance od the entropy	Weighted variance
		Assign pixels in the middle intensity class to the foreground or the background?	Foreground
		Select the smoothing method for thresholding	Automatic
		Threshold correction factor	1
		Lower and upper bounds on threshold	0.2-1.0
		Method to distinguish clumped objects	Intensity
		Method to draw dividing lines between clumped objects	Intensity
		Automatically calculate size of smoothing filter for declumping	Yes
		Automatically calculate minimum allowed distance between local maxima	Yes
		Speed up by using lower-resolution image to find local maxima	Yes
		Retain outlines of the identified objects	Yes
		Name the outline image	NucleiOutlines
		Fill holes in identified objects?	No
		Handling of objects if excessive number of objects identified	Continue

6	MeasureImageArea Occupied	Measure the area occupied in a binary image, or in objects? Select objects to measure Retain a binary image of the object regions?	Objects Nuclei No
7	MeasureImage Intensity	Select an image to measure	Alexa488
8	OverlayOutlines	Display outlines on a blank image? Select image on which to display outlines Name the output image Outline display mode Width of outlines Select outlines to display Select outline color	No MergedColour ColourOverlay Color 1 NucleiOutlines Red
9	SaveImages	Select the type of image to save Select the image to save Select method for constructing file names Select image name for file prefix Append a suffix to the image file name? Text to append to the image name Saved file format Image bit depth Output file location Overwrite existing files without warning? When to save Rescale the images? Select colormap Record the file and path information to the saved image? Create subfolders in the output folder?	Image MergedColour From image filename DAPI Yes _MergedColour tif 8 Same folder as image No Every cycle No gray No No
10	SaveImages	Select the type of image to save Select the image to save Select method for constructing file names Select image name for file prefix Append a suffix to the image file name? Text to append to the image name Saved file format Image bit depth	Image ColourOverlay From image filename DAPI Yes _ColourOverlay tif 8

		Output file location	Same folder as image
		Overwrite existing files without warning?	No
		When to save	Every cycle
		Rescale the images?	No
		Select colormap	gray
		Record the file and path information to the saved image?	No
		Create subfolders in the output folder?	No
11	ExportTo Spreadsheet	Select the column delimiter	Comma (",")
		Output file location	Default Output Folder
		Add image metadata columns to your object data file?	No
		Limit output to a size that is allowed in Excel?	No
		Representation of Nan/Inf?	NaN
		Select the measurements to export	No
		Calculate the per-image mean values for object measurements?	No
		Calculate the per-image median values for object measurements?	No
		Calculate the per-image standard deviation values for object measurements?	No
		Create a GenePattern GCT file?	No
		Export all measurement types?	Yes

Table A-0-4: CellProfiler™ pipeline for the measurement of vascular area in fluorescence images

Order	Module	Parameters	Input
	Input modules		
1	Images	Filter images?	Images only
2	Metadata	Extract metadata?	Yes
		Metadata extraction method	Extract from file/folder names
		Metadata source	File name
		Extract metadata from	All images
3	NamesAndTypes	Assign a name to	Image matching rules

		File does contain	_C0001.tif
		Name to assign these images	DAPI
		Select the image type	Greyscale image
		Set intensity range from	Image metadata
		File does contain	_C0002.tif
		Name to assign these images	Alexa488
		Select the image type	Greyscale image
		Set intensity range from	Image metadata
	Analysis modules		
4	GreyToColor	Select a color scheme	RGB
		Select image to be colored red	Leave this blank
		Select image to be colored green	Alexa488
		Select image to be colored blue	DAPI
		Name the output image	MergedColour
		Relative weight for the green image	1
		Relative weight for the blue image	1
5	IdentifyPrimary Objects	Select the input image	DAPI
		Name the primary objects to be identified	Nuclei
		Typical diameter of objects, in pixel units (Min,Max)	10-30
		Discard objects outside of the diameter range?	No
		Discard objects touching the border of the image?	No
		Threshold strategy	Global
		Thresholding method	Otsu
		Two-class or three-class thresholding?	Three classes
		Minimize the weighted variance od the entropy	Weighted variance
		Assign pixels in the middle intensity class to the foreground or the background?	Foreground
		Select the smoothing method for thresholding	Automatic
		Threshold correction factor	1
		Lower and upper bounds on threshold	0.2-1.0
		Method to distinguish clumped objects	Intensity
		Method to draw dividing lines between clumped objects	Intensity
		Automatically calculate size of smoothing filter for declumping	Yes

		Automatically calculate minimum allowed distance between local maxima	Yes
		Speed up by using lower-resolution image to find local maxima	Yes
		Retain outlines of the identified objects	Yes
		Name the outline image	NucleiOutlines
		Fill holes in identified objects?	No
		Handling of objects if excessive number of objects identified	Continue
6	MeasureImageArea Occupied	Measure the area occupied in a binary image, or in objects?	Objects
		Select objects to measure	Nuclei
		Retain a binary image of the object regions?	No
7	IdentifyPrimary Objects	Select the input image	Alexa488
		Name the primary objects to be identified	Vessels
		Typical diameter of objects, in pixel units (Min,Max)	10-200
		Discard objects outside of the diameter range?	No
		Discard objects touching the border of the image?	No
		Threshold strategy	Global
		Thresholding method	Otsu
		Two-class or three-class thresholding?	Two classes
		Minimize the weighted variance od the entropy	Weighted variance
		Select the smoothing method for thresholding	Automatic
		Threshold correction factor	1
		Lower and upper bounds on threshold	0.0-1.0
		Method to distinguish clumped objects	Intensity
		Method to draw dividing lines between clumped objects	Intensity
		Automatically calculate size of smoothing filter for declumping	Yes
		Automatically calculate minimum allowed distance between local maxima	Yes
		Speed up by using lower-resolution image to find local maxima	Yes
		Retain outlines of the identified objects	Yes
		Name the outline image	VesselsOutlines
		Fill holes in identified objects?	No

		Handling of objects if excessive number of objects identified	Continue
8	MeasureImageArea Occupied	Measure the area occupied in a binary image, or in objects? Select objects to measure Retain a binary image of the object regions?	Objects Vessels No
9	OverlayOutlines	Display outlines on a blank image? Select image on which to display outlines Name the output image Outline display mode Width of outlines Select outlines to display Select outline color Select outlines to display Select outline color	No MergedColour ColourOverlay Color 1 NucleiOutlines Yellow VesselsOutlines Red
10	SaveImages	Select the type of image to save Select the image to save Select method for constructing file names Select image name for file prefix Append a suffix to the image file name? Text to append to the image name Saved file format Image bit depth Output file location Overwrite existing files without warning? When to save Rescale the images? Select colormap Record the file and path information to the saved image? Create subfolders in the output folder?	Image MergedColour From image filename DAPI Yes _MergedColour tif 8 Same folder as image No Every cycle No gray No No
11	SaveImages	Select the type of image to save Select the image to save Select method for constructing file names Select image name for file prefix Append a suffix to the image file name? Text to append to the image name	Image ColourOverlay From image filename DAPI Yes _ColourOverlay

		Saved file format	tif
		Image bit depth	8
		Output file location	Same folder as image
		Overwrite existing files without warning?	No
		When to save	Every cycle
		Rescale the images?	No
		Select colormap	gray
		Record the file and path information to the saved image?	No
		Create subfolders in the output folder?	No
11	ExportTo Spreadsheet	Select the column delimiter	Comma (",")
		Output file location	Default Output Folder
		Add image metadata columns to your object data file?	No
		Limit output to a size that is allowed in Excel?	No
		Representation of Nan/Inf?	NaN
		Select the measurements to export	No
		Calculate the per-image mean values for object measurements?	No
		Calculate the per-image median values for object measurements?	No
		Calculate the per-image standard deviation values for object measurements?	No
		Create a GenePattern GCT file?	No
		Export all measurement types?	Yes

Appendix E: Publications arising during candidature

KL Morel, RJ Ormsby, E Bezak, CJ Sweeney, PJ Sykes, 2017, ***Parthenolide sensitises prostate tumour tissue to radiotherapy while protecting healthy tissues in vivo***, Radiation Research, vol. 187, no. 5, pp. 501-512.

RADIATION RESEARCH **187**, 501–512 (2017)
0033-7587/17 $15.00

DOI: 10.1667/RR14710.1

Parthenolide Selectively Sensitizes Prostate Tumor Tissue to Radiotherapy while Protecting Healthy Tissues *In Vivo*

Katherine L. Morel,[a,1] Rebecca J. Ormsby,[a] Eva Bezak,[b] Christopher J. Sweeney[c] and Pamela J. Sykes[a,2]

[a] *Molecular Medicine and Pathology, Flinders Centre for Innovation in Cancer, Flinders University and Medical Centre, Bedford Park, Adelaide, South Australia;* [b] *Medical Radiation, School of Health Sciences, University of South Australia, Adelaide, South Australia; and* [c] *Dana-Farber Cancer Institute, Harvard University, Boston, Massachusetts*

Morel, K. L., Ormsby, R. J., Bezak, E., Sweeney, C. J. and Sykes, P. J. Parthenolide Selectively Sensitizes Prostate Tumor Tissue to Radiotherapy while Protecting Healthy Tissues *In Vivo*. *Radiat. Res.* 187, 501–512 (2017).

Radiotherapy is widely used in cancer treatment, however the benefits can be limited by radiation-induced damage to neighboring normal tissues. Parthenolide (PTL) exhibits anti-inflammatory and anti-tumor properties and selectively induces radiosensitivity in prostate cancer cell lines, while protecting primary prostate epithelial cell lines from radiation-induced damage. Low doses of radiation have also been shown to protect from subsequent high-dose-radiation-induced apoptosis as well as DNA damage. These properties of PTL and low-dose radiation could be used to improve radiotherapy by killing more tumor cells and less normal cells. Sixteen-week-old male Transgenic Adenocarcinoma of the Mouse Prostate (TRAMP) and C57BL/6J mice were treated with PTL (40 mg/kg), dimethylaminoparthenolide (DMAPT, a PTL analogue with increased bioavailability) (100 mg/kg), or vehicle control three times over one week prior to combinations of low (10 mGy) and high (6 Gy) doses of whole-body X-irradiation. Tissues were analyzed for apoptosis at a range of time points up to 72 h postirradiation. Both PTL and DMAPT protected normal tissues, but not prostate tumor tissues, from a significant proportion of high-dose-radiation-induced apoptosis. DMAPT provided superior protection compared to PTL in normal dorsolateral prostate (71.7% reduction, $P = 0.026$), spleen (48.2% reduction, $P = 0.0001$) and colorectal tissue (38.0% reduction, $P = 0.0002$), and doubled radiation-induced apoptosis in TRAMP prostate tumor tissue (101.3% increase, $P = 0.039$). Both drugs induced the greatest radiosensitivity in TRAMP prostate tissue in areas with higher grade prostatic intraepithelial neoplasia (PIN) lesions. A 10 mGy dose delivered 3 h prior to a 6 Gy dose induced a radioadaptive apoptosis response in normal C57Bl/6J prostate (28.4% reduction, $P = 0.045$) and normal TRAMP spleen (13.6% reduction, $P = 0.047$), however the low-dose-adaptive radioprotection did not significantly add to the PTL/DMAPT-induced protection in normal tissues, nor did it affect tumor kill. These results support the use of the more bioavailable DMAPT and low-dose radiation, alone or in combination as useful radioprotectors of normal tissues to alleviate radiotherapy-induced side-effects in patients. The enhanced radiosensitisation in prostate tissues displaying high-grade PIN suggests that DMAPT also holds promise for targeted therapy of advanced prostate cancer, which may go on to become metastatic. The redox mechanisms involved in the differential radioprotection observed here suggest that increased radiotherapy efficacy by DMAPT is more broadly applicable to a range of cancer types.

INTRODUCTION

Radiotherapy is widely used in cancer treatment. Although current radiotherapy protocols can be highly effective, not all cancer cells may be killed, and damage to surrounding normal tissue is common. Damage to normal tissue can result in short and long-term complications (*1, 2*). Prostate irradiation can cause rectal damage leading to pain or bleeding in the short term, while the long-term effects may include incontinence and impotence. Significant research has been expended identifying potential radioprotector molecules to reduce the short and long-term effects of radiotherapy including amifostine (*3, 4*), Tempol (*5*), N-acetylcysteine (*6, 7*), MnSOD (*8*) and antioxidant vitamins (*9, 10*) all of which are involved in free radical scavenging, modulation of DNA repair, apoptosis and the immune system. Results of efficacy have been mixed, with problems of toxicity and lack of differential radiosensitivity between normal and tumor tissue. New radioprotectors that sensitize tumor tissue at the same time as protecting normal tissue would be ideal, thus increasing cancer kill rate and reducing unwanted side effects to normal tissue. Increasing evidence demonstrates that certain mild pro-oxidant compounds derived from natural herbal medicines might enhance radiotherapy by modulating the redox state of cancer cells to high pro-oxidant levels (*11, 12*). One such compound is Parthenolide (PTL), a major active

[1] Scholar in Training.

[2] Address for correspondence: Molecular Medicine and Pathology, Flinders Centre for Innovation in Cancer, Flinders University and Medical Centre, Bedford Park, Adelaide, South Australia; email: pam.sykes@flinders.edu.au.

ingredient derived from the traditional anti-inflammatory medicinal plant feverfew (*Tanacetum parthenium*) which belongs to the family of sesquiterpene lactones containing an α-methylene-γ-lactone moiety and an epoxide group (*13*). In addition to its anti-inflammatory effect, PTL has been shown to be highly toxic in a variety of cancer cell lines (*14–18*). Mechanistically, PTL has been shown to increase apoptosis in cancer cells through inhibition of multiple pro-survival pathways, such as NF-κB and PI3K-AKT (*11, 19*). One of the most interesting discoveries about PTL's anti-cancer mechanism has been its ability to increase radiosensitivity in tumor tissues while at the same time protecting normal cells from radiation effects. PTL can preferentially inhibit growth and induce apoptosis of prostate cancer cell lines compared to normal prostate cells *in vitro* and can inhibit prostate tumor initiating cells in mouse xenografts (*20*). Recently this differential radioprotection was shown to be mediated by a novel redox mediated modification of KEAP1 (Kelch-like ECH-associated protein 1) and Nrf2 [Nuclear factor (erythroid-derived 2)-like 2] (*18*). PTL activates NADPH oxidase in prostate cancer cell lines but not in normal cells, thus mediating intense oxidative stress in prostate cancer cells by increasing reactive oxidative species (ROS) generation and decreasing antioxidant defense capacity (*17*). Because prostate cancer cells are under higher endogenous levels of oxidative stress it is hypothesized that additional exposure to the ROS induced by PTL pushes cancer cells toward death, whereas normal cells maintain redox homeostasis through KEAP1/Nrf2 mediated adaptive oxidative responses. These results demonstrate that PTL has the potential to reduce the radiation-induced side-effects of radiotherapy while killing more tumor cells and facilitating increased radiation doses in radiotherapy.

During radiotherapy, patients are not only exposed to high therapeutic doses of radiation but can also receive low doses of radiation during CT imaging protocols. This is becoming increasingly common with the use of image guided radiotherapy. Low doses of radiation (generally below 100 mGy) given before a high dose are known to ''condition'' cells resulting in protection from a proportion of the high-dose-induced damage. This has been termed the radio-adaptive response [reviewed in (*21, 22*)]. The conditioning dose can result in reduced genetic damage (*23, 24*) and apoptosis (*25–27*) in normal cells, decreased tumor incidence and increased tumor latency (*28–30*) compared to the effects of the high dose alone. The exact mechanism of the radio-adaptive response is not fully understood, but it is known that p53 (*31*), ROS (*31, 32*), NFκB (*33, 34*), MnSOD (*35*) and several pathways in the immune system (*36, 37*) play important roles. This raises the possibility that image doses of radiation, which are usually less than 100 mGy may therefore act as a radioprotector of normal tissue. The low-dose radio-adaptive response has conventionally been considered to only be active in normal cells and that tumor cells are no longer responsive to low 'adapting' doses of radiation (*38*), however, it has been recently demonstrated that low doses of radiation can elicit an adaptive response in tumor cells as well involving increased expression of survivin, an apoptosis inhibiting protein (*39*). Importantly, it has been shown that PTL suppresses survivin (*40*). The timing between the image and radiotherapy dose is likely to be important in the ability of the image dose to protect tumor cells. This creates a dilemma for image-guided radiotherapy where the image dose may be protecting normal tissue and may therefore be reducing damaging side effects to normal tissue but at the same time be protecting the tumor and therefore reducing the efficacy of radiotherapy. Here we investigated if a low dose of radiation, in the range of conventional imaging doses, could contribute to protecting normal and tumor tissue from high-dose-induced damage, in the presence and absence of PTL and a more bioavailable analogue of PTL, dimethylaminoparthenolide (DMAPT) (*41*).

PTL has not previously been studied in mice with a normal immune system which is important for the radioadaptive response or in an autochthanous cancer model which more closely approximates cancer formation and progression in humans. The autochthanous TRansgenic Adenocarcinoma of the Mouse Prostate (TRAMP) model of prostate cancer (*42*) was used as a proof-of-principle to test whether intrinsic differences in cellular redox conditions can be used to kill tumor cells while protecting healthy cells from unwanted side effects of radiation *in vivo*.

MATERIALS AND METHODS

Preparation and Storage of PTL

PTL (Sigma-Aldrich, Castle Hill, Australia) was kept as a stock solution at 100 mg/mL in absolute ethanol and stored at –20°C. On the day of treatment, PTL stock was diluted tenfold to form a slurry in saline (0.9% Sodium Chloride for Irrigation, Baxter Healthcare, Old Toongabbie, Australia). DMAPT was obtained from Dr. Peter Crooks (University of Arkansas for Medical Sciences, Little Rock, AR) and stored at –20°C. On the day of treatment, DMAPT was dissolved at 20 mg/mL in sterile water.

Mice

Ethics approval for this study was obtained from the Flinders University Animal Welfare Committee and the SA Pathology/Central Adelaide Local Health Network Animal Ethics Committee.

C57BL/6J mice were purchased from the Australian Animal Resources Centre (Perth, Australia). The TRAMP mouse model was originally described by Greenberg *et al.* (*42*). TRAMP mice contain a PB-SV40 Tag transgene that uses a probasin promoter, which is switched on at puberty in the prostate and induces high grade PIN (prostatic intraepithelial neoplasia) and or well differentiated prostate cancer by 16 weeks of age. Nonprostate TRAMP tissues are normal. The male TRAMP mice used in this study were bred using hemizygous female C57BL/6J TRAMP mice (C57BL/ 6J-Tg(TRAMP)8247Ng) crossed to nontransgenic male FVB mice, producing both transgenic and nontransgenic F1 offspring (C57BL/6J-Tg (TRAMP)8247Ng 9 FVB). The transgenic status of mice was determined by polymerase chain reaction (PCR) using the previously published protocol by Hurwitz *et al.* (*30*). Mice were housed in micro-isolator cages with 12 h light/dark cycles. Food [Rat and Mouse

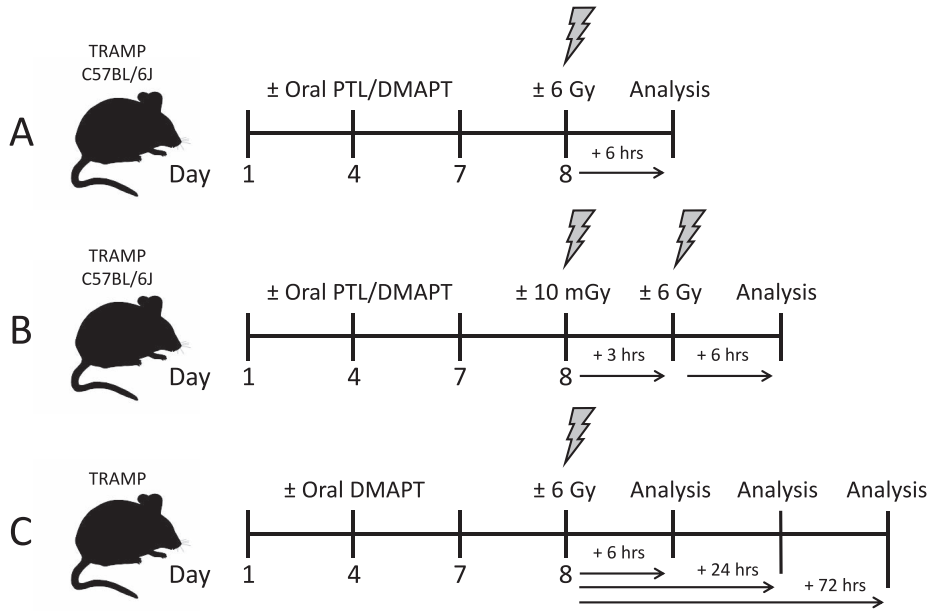

FIG. 1. Schematic overview of the PTL/DMAPT treatment and irradiation protocols. In all experiments mice received 3 doses of PTL or DMAPT on day 1, 4 and 7, and were irradiated 24 h after the last dose. Panel A: TRAMP and C57BL/6J mice received either a 6 Gy dose or sham irradiation and analysis was performed 6 h postirradiation. Panel B: TRAMP and C57BL/6J mice received either a 10 mGy dose or sham irradiation, followed by a 6 Gy dose or sham irradiation 3 h later, and tissues were analyzed 6 h postirradiation. Panel C: TRAMP mice received a 6 Gy dose or sham irradiation and analysis was performed at 6, 24 or 72 h postirradiation.

Pellets (irradiated), Specialty Feeds, Glen Forrest, Australia] and water were provided *ad libitum*. All TRAMP mice came from timed matings and were born within 4 days of each other to limit variability in tumor formation.

Treatment with Parthenolide/DMAPT and Radiation

All studies were performed on 16-week-old C57BL/6J or TRAMP mice. At this age TRAMP mice are in early stages of prostate tumor development and most prostate tissues have moderate to high levels of PIN. Mice were administered 40 mg/kg of PTL, 100 mg/kg DMAPT or vehicle controls (10% ethanol in saline or sterile water, respectively) by oral gavage 3× per week for one week. A dose of 100 mg/kg of DMAPT was selected as it is the highest safe dose tested *in vivo* (*43*). Due to the low solubility of PTL a dose of 100 mg/kg was deemed unfeasible for this study; therefore, 40 mg/kg was selected due to previous *in vivo* use (*20*). Twenty-four h after the final PTL or DMAPT treatment, mice were exposed to whole-body X irradiation. Mice were restrained in individual compartments of a 6-mm thick Perspex holder during the irradiation. Mice received either 6 Gy alone (Fig. 1A and C), 10 mGy followed by 6 Gy irradiation, sham irradiation followed by 6 Gy, or 10 mGy followed by sham irradiation, with a 3 h interval between irradiations (Fig. 1B). Irradiation was performed using either a 6 MV X-ray beam from a Varian 600CD Linear Accelerator (Varian Medical Systems, Inc., Palo Alto, CA) or 300 kV X-ray beam from a X-RAD 320 Cabinet irradiator (Precision X-Ray Inc., North Branford, CT) for experiments where mice were administered 6 Gy. Irradiation with 10 mGy was carried out using the X-RAD 320 Cabinet irradiator. The dose calibration of the Varian 600CD Linear Accelerator was made according to the International Atomic Energy Agency's technical report on Absorbed Dose Determination in External Beam Radiotherapy (series no. 398) (*44*). The dose calibration of the orthovoltage 300 kV X-ray beam produced by the X-RAD 320 was performed according to the Institute of Physics and Engineering in Medicine and Biology (IPEMB) protocol (*45, 46*). Control sham-irradiated mice underwent the same procedures as irradiated mice; however, the X-ray machines were not turned on. At the appropriate time point after X irradiation, mice were euthanized using CO_2 asphyxiation. At necropsy, full tissue panels were taken from all mice and snap frozen on dry ice in OCT cryoprotectant medium (Tissue-tek, Japan). Prior to analysis, prostates were thawed and micro-dissected in ice cold phosphate buffered saline (PBS), then immediately re-embedded in OCT. Tissues were stored at –80°C until required for analysis.

Immunohistochemistry

Frozen prostate sections (4 μm) were cut and mounted on APES-treated (3-aminopropyltriethoxysilane) (Sigma-Aldrich) glass slides. The TUNEL protocol was performed using the In Situ Cell Death Detection Fluorescein Kit (Roche Diagnostics, Germany) according to the manufacturer's instructions. Sections were dried overnight at room temperature after sectioning, fixed in 1% formaldehyde (in PBS) for 30 min, and permeabilised (1% Triton-X100/1% sodium citrate in PBS) for 10 min before application of TUNEL reagents diluted to 50% with TUNEL dilution buffer. DNase I-treated (Sigma-Aldrich) sections with label solution only (Tdt enzyme omitted) or complete TUNEL solution were used for negative and positive controls, respectively. DNase I-untreated sections were also incubated with label solution only, as a negative control. Slides were mounted with Vectashield® (Vector Laboratories) with DAPI (40,6-diamidino-2-phenylindole) and stored in the dark at 4°C. Gamma-H2AX was used as a surrogate marker for apoptosis in TRAMP prostate tissue due to high-nonspecific staining using TUNEL as described by Lawrence *et al*. (*47*). For detection of γ-H2AX, frozen sections were prepared, fixed and permeabilized as described above, then blocked for 1 h at room temperature [5% goat serum (Sigma-Aldrich) + 0.1% Tween-20 in PBS]. Sections were incubated with mouse anti-γ-H2AX antibody conjugated to Alexa Fluor® 488 (9719, Cell Signaling) at a 1/100 dilution in 1% goat

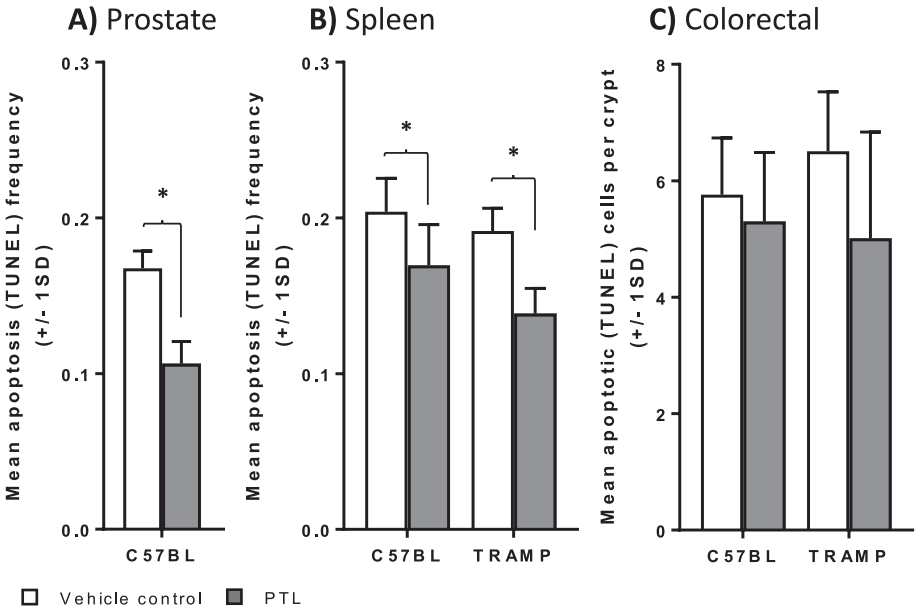

FIG. 2. Mean apoptosis (±1 SD) in (panel A) normal C57BL/6J dorsolateral prostate, and normal C57BL/6J and TRAMP (panel B) spleen and (panel C) colorectal tissue after 3× 40 mg/kg PTL or vehicle control treatments over 1 week, with exposure to 6 Gy whole-body X irradiation 24 h after the final treatment, with analysis at 6 h postirradiation. $*P < 0.05$, n = 5–15.

serum overnight at 4°C. Sections were then washed in PBST (6 × 2 min) and mounted as described above. Routine hematoxylin and eosin staining was carried out on frozen tissue sections to study prostate tissue morphology. In addition to studying prostate tissues, colorectal tissues were selected as a normal tissue for analysis given the importance of protecting the rectum and colon during prostate cancer therapy; the spleen was selected as an additional normal tissue due to its role in immune function and because the radioadaptive response has been well studied in spleen.

Image Acquisition, Processing and Analysis

Immunofluorescent images from each tissue section were captured with the use of an external digital camera (DP73; Olympus) on a BX63 Automated Fluorescent Microscope (Olympus). Thirty random fields were taken per tissue section at 20× (spleen) and 40× (colorectal and dorsolateral prostate) magnification. Images were analyzed by CellProfiler™ software to detect the number of total nuclei and apoptotic cells. In dorsolateral prostate and colorectal tissue sections CellProfiler software identified and counted individual cells from fluorescent images. For analysis of dorsolateral prostate, 30 random nonoverlapping microscope fields were analyzed to obtain a stable mean apoptotic frequency in epithelial cells. Stromal cells were not included in this analysis. For spleen, 30 random nonoverlapping microscope fields were analyzed to obtain a stable mean apoptotic frequency. Due to the density of cells in the spleen, cell counts were estimated from total cell area and apoptotic frequency measured for all spleen cells. For colorectal analysis, 50 intact crypts were counted to identify a mean number of apoptotic cells per crypt. Only epithelial cells were analyzed by this method. Statistical analyses used Graph Pad version 7 software with a significance of $P < 0.05$ used in all analyses. For comparison of two treatment groups, data were first tested for normality using a D'Agostino-Pearson test and equality of variance using an F test; when data was normally distributed with equal variance between groups a *t* test was used for analysis, where data was non-normally distributed a Mann-Whitney test was used. To assess the relationship between two sets of data, a linear regression analysis was used.

RESULTS

Parthenolide Protects Normal Tissues from Radiation-Induced Damage when Delivered Alone or In Combination with a Conditioning Low Dose of Radiation

C57BL/6J and TRAMP mice were treated as per the protocol described in Fig. 1A to determine if PTL could protect from apoptosis induced by a high dose of radiation in normal tissues, and to determine if normal tissues responded differently in the different strains of mice. Across all experiments baseline apoptosis frequency in normal tissues did not differ significantly between C57BL/6J and TRAMP strains (n = 12–26); mean baseline apoptosis frequency in both mouse strains was 0.0041 (± 0.0023 SD) in normal dorsolateral prostate, and 0.0074 (± 0.0036 SD) in normal spleen, with mean baseline of 0.53 (± 0.17 SD) apoptotic cells per crypt in normal colorectal tissues. When analyzed 6 h after exposure to 6 Gy, the mean apoptosis frequency increased 31-fold to 0.13 (± 0.035 SD) in normal dorsolateral prostate (n = 23), and 29-fold to 0.21 (± 0.027 SD) in normal spleen (n = 67), with mean apoptotic cells per crypt increasing 11-fold to 5.81 (± 0.54 SD) in normal colorectal tissue of C57BL/6J mice (n = 67). PTL (40 mg/kg) induced a partial protection from 6 Gy radiation-induced apoptosis in normal C57BL/6J dorsolateral prostate (34.5% reduction, $P = 0.002$), and spleen (17.3% reduction, $P = 0.041$) tissues and in normal TRAMP spleen tissues (31.4% reduction, $P = 0.01$) 6 h postirradiation (Fig. 2). Radiation-induced apoptosis was not significantly reduced by PTL in normal colorectal tissues of either mouse strain.

C57BL/6J mice were treated as per the protocol described in Fig. 1B to determine if a 10 mGy-conditioning dose of

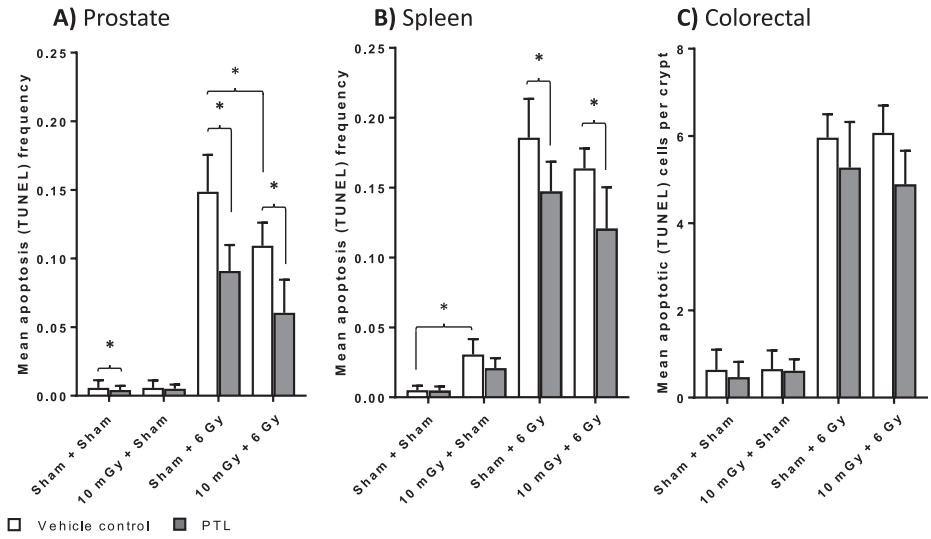

FIG. 3. Mean apoptosis (±1 SD) in normal C57BL/6J mouse (panel A) dorsolateral prostate, (panel B) spleen and (panel C) colorectal tissue after 3× 40 mg/kg PTL or vehicle control treatments over 1 week, with combinations of exposure to sham, 10 mGy and 6 Gy whole-body X irradiation 24 h after the final PTL treatment, with analysis at 6 h postirradiation. *$P < 0.05$, n = 6.

radiation could add to PTL-induced reduction of apoptosis in normal tissues after 6 Gy (Fig. 3). A dose of 10 mGy alone induced a significant increase in apoptosis (489.5% increase, $P = 0.017$) in spleen (Fig. 3B); but not in prostate or colorectal tissues (Fig. 3A and C) when analyzed 9 h postirradiation. In the absence of PTL, the 10 mGy-conditioning dose induced a radio-adaptive response when delivered 3 h before a 6 Gy high dose in the dorsolateral prostate (28.4% reduction in apoptosis, $P = 0.045$), compared to the sham-conditioning dose plus 6 Gy exposure (Fig. 3A). There was also a trend towards an adaptive response in normal spleen tissue (15.8% reduction in apoptosis, $P = 0.084$) (Fig. 3B). PTL decreased apoptosis in sham-treated dorsolateral prostate (28.7% reduction, $P = 0.048$) and reduced 6 Gy-induced apoptosis in the presence and absence of a 10 mGy-conditioning dose in spleen and prostate ($P < 0.05$), however a 10 mGy dose did not significantly add to PTL-induced protection from apoptosis ($P > 0.05$).

Comparison of Radioprotection using PTL and DMAPT

The efficacy of DMAPT (a PTL analogue with increased solubility and bioavailability) was compared with PTL in C57BL/6J mice using the protocol shown in Fig. 1A. DMAPT increased the magnitude of radioprotection from 6 Gy-induced apoptosis in normal C57BL/6J mouse dorsolateral prostate (71.7% reduction, $P = 0.026$), spleen (48.2% reduction, $P = 0.0001$) and colorectal tissues (38.0% reduction, $P = 0.0002$), compared to the radioprotection provided by PTL (dorsolateral prostate: 41.4% reduction, $P = 0.045$; spleen: 29.5% reduction, $P = 0.011$; colorectal: 15.7% reduction, $P = 0.067$) (Fig. 4). Compared to PTL, DMAPT increased radioprotection in dorsolateral prostate, spleen and colorectal tissues by a further 1.6–2.4-fold.

DMAPT Radioprotects Normal Tissues while Sensitizing Tumors to Radiation-Induced Damage

TRAMP mice were treated as per the protocol shown in Fig. 1B. TRAMP mice were treated with DMAPT and X irradiated with 6 Gy in the presence or absence of a 10 mGy-conditioning dose (Fig. 5). In the absence of DMAPT, a 10 mGy-conditioning dose delivered 3 h prior to the high-dose-reduced 6 Gy-induced apoptosis in normal TRAMP spleen (13.6% reduction, $P = 0.047$) (Fig. 5B), compared to animals that received a sham-conditioning dose. In normal TRAMP spleen and colorectal tissues, DMAPT reduced 6 Gy-induced apoptosis in the presence and absence of a 10 mGy conditioning dose, compared to vehicle-control-treated mice (Fig. 5B and C). In the TRAMP model, most prostates are in the mid-stages of tumor development by 16 weeks of age. Across all experiments (n = 26 mice), mean apoptosis frequency in TRAMP dorsolateral prostate was 0.012 (± 0.0046 SD) at baseline and increased 11-fold to 0.1344 (± 0.053 SD) after 6 Gy irradiation (n = 51 mice). DMAPT increased radiation-induced apoptosis in TRAMP prostate tissues in the absence and presence of a 10 mGy conditioning dose (81.9% increase, $P = 0.02$; 135.0% increase, $P = 0.0024$, respectively) (Fig. 5A). In the absence of DMAPT, there was no significant difference in apoptosis in TRAMP prostate PIN tissue with or without a 10 mGy conditioning dose.

Differential Radiosensitization from DMAPT in TRAMP Tissues Persists beyond the Initial Phase of Apoptosis

In temporal studies, TRAMP mice were treated as per the protocol described in Fig. 1C. In the absence of radiation, apoptosis in spleen, colorectal and dorsolateral prostate tissue was not significantly different between treatment

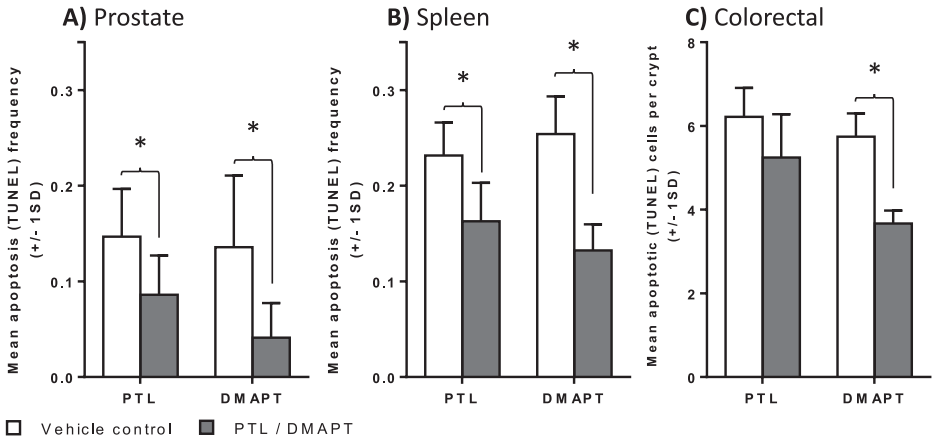

FIG. 4. Mean apoptosis (±1 SD) in C57BL/6J mouse (panel A) dorsolateral prostate, (panel B) spleen and (panel C) colorectal tissues after 3× 40 mg/kg PTL, 100 mg/kg DMAPT or vehicle-control treatments over 1 week, after 6 Gy whole-body X-irradiation 24 h after the final drug treatment, with analysis at 6 h postirradiation. $*P < 0.05$, n = 6.

groups and did not significantly alter across the different time points ($P > 0.05$, ANOVA with Turkey's multiple comparisons test) (Fig. 6). In TRAMP dorsolateral prostate (Fig. 6A), significant augmentation of 6 Gy-induced apoptosis was observed in the DMAPT treated mice at 6 h postirradiation (119.4% increase, $P = 0.0018$) compared to vehicle-treated mice. An increase in apoptosis was still present 18 hours later in the DMAPT-treated group (107.2% increase, $P = 0.048$) and apoptosis levels returned to baseline frequency by 72 h. In colorectal tissues (Fig. 6B), a reduction in 6 Gy-induced apoptosis was observed 6 and 24 h postirradiation (34.6% reduction, $P = 0.0034$ and 55.6% reduction, $P = 0.0002$), respectively, compared to the vehicle-control-treated mice. By 72 h, apoptosis returned to baseline levels. In TRAMP spleen (Fig. 6C-i), radioprotection was observed in DMAPT treated mice 6 h (40.1% reduction, $P = 0.021$) and 72 h (64.3% reduction, $P = 0.0001$) postirradiation. The apoptosis observed at 6 h was largely follicular in both the DMAPT and vehicle-control-treated groups exposed to 6 Gy, and had returned to baseline levels by 24 h. At 72 h there was an increase in apoptosis in the 6 Gy-vehicle-treated mice, but not in DMAPT-treated mice. In vehicle-control-treated spleens, this second wave of apoptosis was again largely follicular (Fig. 6C-ii), however apoptosis in DMAPT-treated spleen was mostly observed in extra-follicular red pulp regions.

Enhanced Radiosensitivity of TRAMP Prostate Tumor Tissue by DMAPT is Greater with Increasing PIN grade

TRAMP dorsolateral prostates were scored for PIN grade using the method proposed by Berman-Booty *et al.* (*48*)

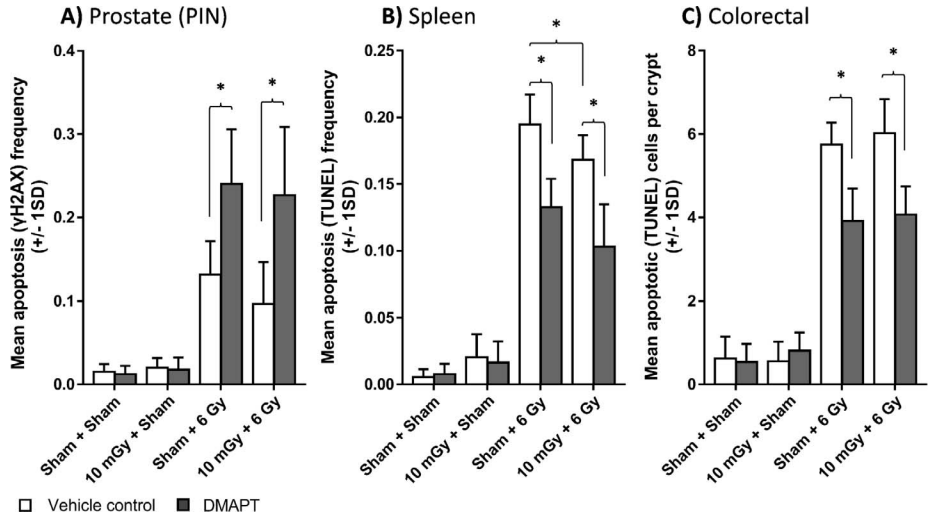

FIG. 5. Mean apoptosis (±1 SD) in TRAMP (panel A) dorsolateral prostate, (panel B) spleen and (panel C) colorectal tissues after 3× 100 mg/kg DMAPT or vehicle-control treatments over 1 week, after sham, 10 mGy or 6 Gy whole-body X irradiation (alone or in combination) 24 h after the final DMAPT treatment, with analysis at 6 h postirradiation. $*P < 0.05$, n = 11–14.

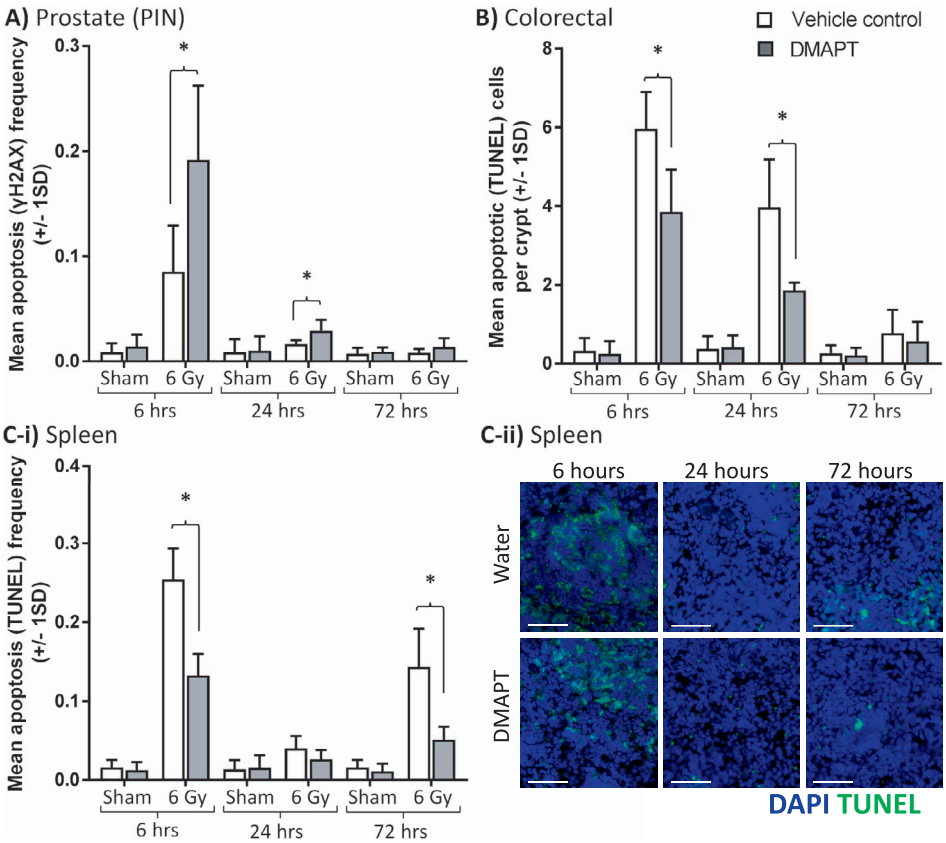

FIG. 6. Mean apoptosis (±1 SD) in TRAMP (panel A) dorsolateral prostate, (panel B) colorectal and (panel C-i) spleen tissues after 3× 100 mg/kg DMAPT treatments over 1 week, with exposure to a 6 Gy or sham irradiation, and tissues analyzed at 6, 24 and 72 h postirradiation. *$P < 0.05$, n = 5-15. Panel C-ii: Fluorescently labeled apoptotic (TUNEL) cells in normal TRAMP spleen at 6, 24 and 72 h postirradiation. Scale bars 50 μm. At 6 h postirradiation the apoptosis was largely identified in the follicles in both DMAPT and vehicle control treatment groups; at 72 h, the majority of apoptosis in vehicle-control-treated spleen was still in follicular regions, however apoptosis in DMAPT-treated spleen was mostly observed in extra-follicular red pulp regions.

(Fig. 7A–C). This method assigns tissues a score based on both the most common lesions and the most severe lesions. In TRAMP dorsolateral prostate tissues most tissues have developed moderate to high-grade PIN. Although there was no significant increase in apoptosis in the PTL group compared to the vehicle-control group (Fig 7D), there was a significant correlation between the amount of apoptosis induced by PTL in the presence of 6 Gy irradiation and increasing PIN grade ($R^2 = 0.4037$, $P = 0.015$) (Fig. 7E). There was no significant correlation in apoptosis with increasing PIN grade ($R^2 = 0.0104$, $P = 0.77$) in the vehicle-treated group. Radiation-induced apoptosis doubled in dorsolateral prostates of TRAMP mice when they were treated with the more bioavailable DMAPT (101.3% increase, $P = 0.039$) (Fig. 7F). As was the case with PTL, TRAMP dorsolateral prostates with high-grade PIN development were preferentially sensitized to radiation-induced apoptosis when mice were pre-treated with DMAPT ($R^2 = 0.7909$, $P = 0.0001$), while tissues with lower grades of PIN displayed the same apoptosis frequency as those of vehicle control-treated TRAMP mice ($R^2 = 0.0242$, $P = 0.3$) (Fig. 7G).

DISCUSSION

A major limiting factor of radiotherapy is normal tissue toxicity. Prostate cancer radiotherapy can result in short-term side effects including colorectal injury which can induce diarrhea and bleeding, while the long-term effects may include incontinence, impotence and infertility. Here we investigated the ability of the naturally occurring anti-inflammatory compound, PTL and the water soluble PTL analogue, DMAPT, to protect normal tissues and sensitize prostate tumor tissues to radiation-induced apoptosis. Previous studies have shown that the increased hydrophilicity of DMAPT provides greater bioavailability compared with PTL (*41, 43*) and that DMAPT exerts anti-cancer effects in several cancer types *in vivo* (*43, 49–52*). The increased bioavailability of DMAPT makes it the drug of choice for future human clinical trials. *In vivo*, DMAPT has been shown to selectively radiosensitize human prostate cancer PC3 cell derived tumors in nude mice (*18*); however, these preclinical investigations have been limited to xenograft studies using immune compromised animals. Studying the TRAMP model here with an intact immune

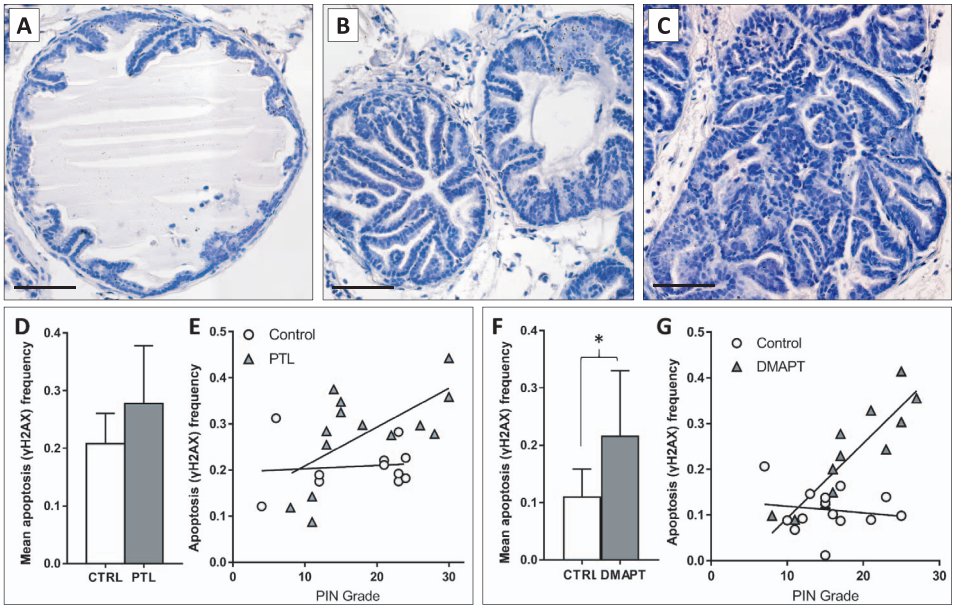

FIG. 7. Representative morphology of TRAMP-dosolaterale-prostate lobes. Panel A: Low-grade PIN, with a few short papillary proliferations of hyperplastic epithelium projecting into the lumen; panel B: moderate-grade PIN, with more prominent papillary proliferations of hyperplastic epithelial cells that project into the lumen; and panel C: high-grade PIN, where the mass of proliferating epithelial cells form a cribriform pattern completely filling the lumen of the gland. Haematoxylin stain, 40× magnification, scale bars 50 μm. Mean apoptosis (±1 SD) in irradiated-TRAMP-dorsolateral prostates after (panel D) 3× 40 mg/kg PTL or vehicle control treatments over 1 week, or (panel F) 3 × 100 mg/kg DMAPT or vehicle control. $*P < 0.05$, n = 11–15. Apoptosis in dorsolateral prostate tissue from TRAMP mice treated with (panel E) PTL or (panel G) DMAPT plotted against PIN tumor grade. TRAMP tissues scored using the method described by Berman-Booty *et al.* (*48*)

system and where the tumor progression within the prostate more closely mimics human prostate cancer progression provides the opportunity to gain a better understanding of the therapeutic efficacy of PTL. In this study, we observed simultaneous protection of normal tissues and radiosensitization of TRAMP prostate tumor tissues to 6 Gy irradiation, demonstrating the potential for DMAPT to be a therapeutic for prostate cancer, not only to decrease radiotherapy side effects but potentially to increase cure rate.

Significant radiosensitivity was observed in TRAMP dorsolateral prostate with moderate to high-grade PIN lesions, with DMAPT doubling the frequency of radiation-induced apoptosis in these tissues. Although the TRAMP mice used were born within 4 days of each other, TRAMP prostate tumor development progresses at different rates between individual mice, and there is a relatively wide range of PIN development between animals. This results in large variation in apoptosis frequency between animals, however it allows the effects of PTL to be observed in different stages of TRAMP prostate tumor development. Both PTL and DMAPT preferentially increased radiosensitivity in tissues with higher grade PIN, compared to tissues with lower grades of PIN (based on lesion severity) with DMAPT showing a stronger correlation, possibly due to the higher tissue exposure with DMAPT compared to PTL. High-oxidative-stress levels are a hallmark of prostate cancer, and ROS levels are particularly elevated in aggressive prostate tumors compared to localized disease (*53, 54*). Oxidative stress has been shown to increase with increasing PIN grade in TRAMP mice (*55*) and our data suggests that PTL/DMAPT may have the greatest effect in the presence of higher ROS levels. PIN grade in the TRAMP model does not directly correlate with Gleason grading of human prostate cancer, however the enhanced radiosensitization of high-grade-TRAMP PIN tissue may be an indicator that DMAPT could be highly effective in high-grade Gleason tumors and potentially for targeted treatment of metastatic prostate cancer, which often occurs from high-grade Gleason tumors and is incurable (*56*).

While PTL and DMAPT enhanced radiation-induced apoptosis in TRAMP prostate tumor tissue they also protected from high-dose-radiation-induced apoptosis in normal tissues with DMAPT showing superior protection in normal prostate, spleen and colorectal tissue. It was surprising that the response observed in DMAPT-treated mice was not more pronounced given both the increased bioavailability of DMAPT and that a 2.5-fold higher concentration of DMAPT was used here compared to PTL. The poor solubility of PTL restricts dosing of mice to a maximum of 40 mg/kg, providing a maximum plasma concentration of less than 1 μ*M*, which is well below ideal therapeutic plasma concentrations of 5–10 μ*M* (*57*). DMAPT dosed at 100 mg/kg results in a maximum plasma concentration above 10 μ*M* (*43*). Although the increased dose of DMAPT did not result in a proportionately greater increase in radioprotection, it still provided a greater

therapeutic effect than PTL. The ideal plasma concentration for maximum radioprotection may be somewhere between 1 and 10 μM. These results suggest that DMAPT could be a useful clinical tool for alleviating radiotherapy induced damage to normal tissue, while radiosensitizing tumor tissue. Amifostine is the only radioprotector currently approved for protection of normal tissues during radiotherapy (for treatment of head and neck cancers) (*58*), however the effects of the drug are short lived. More than 90% of amifostine is cleared within 6 min of administration and it has been shown that if radiotherapy is delivered more than 30 min after amifostine is administered, there may be little clinical benefit (*59*). The reported levels of radioprotection in response to amifostine if delivered within the restrictive timeframe (*59–61*) are similar to our results with DMAPT, however DMAPT may be a more appropriate radioprotector for clinical use, as here we show that DMAPT can be delivered at least 24 h before X-ray exposure. There have also been reported problems with amifostine-induced toxicity and lack of differential radiosensitivity between normal and tumor tissue (*61, 62*), whereas DMAPT has been shown to be highly tolerated with minimal side effects in human clinical studies (*63, 64*). The DMAPT-induced protection lasted up to 24 h postirradiation in normal colorectal tissues and to 72 h in normal spleen. If these effects can be replicated in a clinical setting it may allow particularly vulnerable tissues to be spared from damage while having the added benefit of increasing tumor killing efficacy. Further *in vivo* analysis of late-stage-radiation damage to rectum and bladder, such as fibrosis, would help to determine whether long-term protection of these particularly vulnerable tissues is possible using DMAPT. Long-term studies would also allow observation of tumor progression after DMAPT treatment and high-dose irradiation.

In all experiments, endogenous apoptosis frequencies observed in TRAMP and C57BL/6J prostate, spleen and colorectal tissues were all in the range described in the literature (*60, 65, 66*). In the absence of radiation, PTL and DMAPT did not modulate endogenous apoptosis in the normal tissues except for in one experiment with PTL where a significant reduction in apoptosis was observed in the dorsolateral prostate of C57BL/6J mice, but not in spleen or colon, 30 h after the final drug treatment was delivered. PTL may be protecting a small number of cells, which would normally proceed to apoptosis by inducing antioxidant responses. Given that apoptosis is a normal homeostatic mechanism that acts to maintain healthy cell populations, the clinical significance of this reduction below baseline apoptosis frequency is unclear. The same dose of PTL that was delivered to C57BL/6J mice in this study has previously been delivered to NOD/SCID mice thrice weekly for up to 106 days without any reported negative health effects (*20*). Further studies are required to determine if PTL is reducing endogenous apoptosis, as it would have been expected that DMAPT would induce a similar or superior reduction, and this was not observed in the experiments here.

In addition to high-therapeutic-radiation doses, low doses of radiation are commonly received by patients prior to and during radiotherapy in the form of imaging CT scans. Low-conditioning doses of radiation in the dose range of imaging CT scans have been shown to induce protection from effects of subsequent high doses of radiation for a wide range of biological endpoints including apoptosis *in vivo* (*25–27*). In the absence of PTL/DMAPT, a 10 mGy-dose induced a radioadaptive response in normal prostate and spleen in some experiments, with trends towards an adaptive response in others. A dose of 10 mGy alone induced a significant increase in apoptosis in C57BL/6J spleen but not in TRAMP spleen, although in both cases 10 mGy induced a protection from high-dose-radiation-induced apoptosis, indicating a radioadaptive response. There has only been one previous report of increased apoptosis after exposure to 10 mGy alone and that was at 6 h after *in utero* exposure of C57BL/6 embryos (*67*). When 10 mGy was combined with PTL/DMAPT, the magnitude of radioprotection from 6 Gy-induced apoptosis was greater. However, 10 mGy did not result in a significant difference in apoptosis frequency in the presence of PTL/DMAPT and 6 Gy. If there is an additive protective effect, it is small.

Beneficial radioadaptive effects in normal tissues in the context of radiotherapy have been well described in the literature, however there are very few studies describing tumor responses to low-dose radiation. Recently radioadaptive protection of tumors has been reported *in vivo* (*39*). If low doses of radiation induce a radioadaptive response in tumors, the efficacy of radiotherapy could be compromised in an image guided radiotherapy scenario. Here, a 10 mGy dose of X-irradiation did not induce an adaptive response in TRAMP prostate PIN tissue, nor did the low-conditioning dose affect the ability of DMAPT to radiosensitize the TRAMP prostate PIN tissue. Further studies are required to determine if the radiation doses and timing of the conditioning image dose and the radiotherapy dose play a role in the ability to radioprotect tumor tissue. Transgene-induced prostate pathology in the TRAMP model is driven by androgen dependent expression of SV40, which contains the large and small T-antigens. The large T-antigen in the transgene interferes with the action of p53 by directly binding its DNA binding domain, silencing p53's transcriptional activity (*42*). The radioadaptive response is known to be p53 dependent (*26*) and therefore may not be observable in TRAMP prostate tissues. Adaptive response studies in a model with functioning p53 are required to determine if PTL/DMAPT can counteract any potential radioadaptive responses in tumors which possess functional p53.

To ensure that the DMAPT-induced radioprotection from apoptosis observed 6 h postirradiation in normal tissues was not simply due to a delay in radiation-induced apoptosis, temporal studies were performed on TRAMP mice treated with DMAPT and 6 Gy of X radiation. There was no

delayed induction of apoptosis in DMAPT-treated spleen and colorectal tissue where protection compared to control-treated mice was not observed, and radioprotection was maintained up to 24 h in colorectal tissue and 72 h in spleen. This suggests that DMAPT is providing protection in the normal tissues, rather than delaying the apoptotic response. In normal TRAMP spleen, by 24 h postirradiation, apoptotic frequency was reduced to almost baseline levels both in the presence and absence of DMAPT. Unexpectedly, a second wave of apoptosis was observed at 72 h postirradiation in the vehicle-control mice, which was significantly inhibited in the DMAPT-treated mice. There are reports in the literature of delayed waves of radiation-induced apoptosis without significant investigation into the underlying mechanism; however several reports are correlated with reduced p53 expression within tissues (*68, 69*). Komarova *et al*. (*68*) showed that in gamma-irradiated spleen, DNA-damage-induced apoptosis begins in regions with high levels of p53 mRNA expression, while a slower induction of radiation-induced apoptosis was observed in regions with lower p53 mRNA expression. Regardless of the underlying mechanism of action, our results indicate that DMAPT protects normal tissues from a late induction of apoptosis. Importantly, in TRAMP dorsolateral prostate DMAPT-induced radiosensitisation was observed up to 24 h postirradiation, with apoptosis levels returning to baseline frequency by 72 h. This demonstrates that the radiosensitizing effects of DMAPT lasts for a significant period of time postirradiation, which is likely to prove useful in a clinical setting if radiosensitization of tumors continues to occur up to 24 h after a radiotherapy dose has been delivered.

In the current study, we used single whole-body doses of radiation as a proof of principle to determine the potential of PTL/DMAPT as a radioprotector of normal cells whilst radiosensitizing tumor cells. Future studies using multiple fractionated doses targeted to the region of the tumor will more closely mirror current clinical radiotherapy protocols for prostate cancer.

In summary, we have shown that DMAPT holds significant promise for use in conjunction with radiotherapy for prostate cancer. DMAPT reduced the level of radiation-induced apoptosis observed in normal tissues of C57BL/6J and TRAMP mice while doubling the efficacy of tumor cell killing. DMAPT preferentially radiosensitized regions of high-PIN grade within TRAMP prostates; this suggests that DMAPT may be particularly able to target regions of higher oxidative stress, as is often observed in high-grade-metastatic prostate cancers. We have also shown that low doses of radiation may be able to augment the radioprotective effects of DMAPT in normal tissues. Radiotherapy is used to treat a wide range of different cancers. The redox pathways involved in the action of DMAPT are not specific to prostate cancer (*70–72*) and therefore there is also the potential to utilize DMAPT as a differential radioprotector in conjunction with radiotherapy for other cancer types, as well as prostate cancer.

ACKNOWLEDGMENTS

We would like to thank Linh Tran and Mark Lawrence for help with animal work. This research was supported by a Flinders Medical Centre (FMC) Foundation Smiling for Smiddy PhD Scholarship to K. Morel, as well as Flinders Centre for Innovation in Cancer and FMC Foundation.

Received: December 7, 2016; accepted: February 3, 2017; published online: March 3, 2017

REFERENCES

1. Prasanna PGS, Stone HB, Wong RS, Capala J, Bernhard EJ, Vikram B, et al. Normal tissue protection for improving radiotherapy: Where are the Gaps? Translational Cancer Res 2012; 1(1):35–48.
2. Stone HB, Coleman CN, Anscher MS, McBride WH. Effects of radiation on normal tissue: consequences and mechanisms. Lancet Oncol 2003; 4(9):529–36.
3. Capizzi RL, Oster W. Protection of normal tissue from the cytotoxic effects of chemotherapy and radiation by amifostine: clinical experiences. Eur J Cancer 1995; 31A Suppl 1:S8–13.
4. Yuhas JM, Storer JB. Differential chemoprotection of normal and malignant tissues. J Natl Cancer Inst 1969; 42(2):331–5.
5. Mitchell JB, Anver MR, Sowers AL, Rosenberg PS, Figueroa M, Thetford A, et al. The antioxidant tempol reduces carcinogenesis and enhances survival in mice when administered after nonlethal total body radiation. Cancer Res 2012; 72(18):4846–55.
6. Blank LE, Haveman J, van Zandwijk N. The radioprotective effect of N-acetylcysteine in thorax irradiation of mice. Radiol Oncol 1987; 10(1):67–9.
7. Kim JA, Baker DG, Hahn SS, Goodchild NT, Constable WC. Topical use of N-acetylcysteine for reduction of skin reaction to radiation therapy. Seminars Oncol 1983; 10(1 Suppl 1):86–92.
8. Motoori S, Majima HJ, Ebara M, Kato H, Hirai F, Kakinuma S, et al. Overexpression of mitochondrial manganese superoxide dismutase protects against radiation-induced cell death in the human hepatocellular carcinoma cell line HLE. Cancer Res 2001; 61(14):5382–8.
9. Halperin EC, Gaspar L, George S, Darr D, Pinnell S. A double-blind, randomized, prospective trial to evaluate topical vitamin C solution for the prevention of radiation dermatitis. CNS Cancer Consortium. Int J Radiat Oncol Biol Phys 1993; 26(3):413–6.
10. Weiss JF, Landauer MR. Protection against ionizing radiation by antioxidant nutrients and phytochemicals. Toxicology 2003; 189(1-2):1–20.
11. Hassane DC, Sen S, Minhajuddin M, Rossi RM, Corbett CA, Balys M, et al. Chemical genomic screening reveals synergism between parthenolide and inhibitors of the PI-3 kinase and mTOR pathways. Blood 2010; 116(26):5983–90.
12. Raj L, Ide T, Gurkar AU, Foley M, Schenone M, Li X, et al. Selective killing of cancer cells by a small molecule targeting the stress response to ROS. Nature 2011; 475(7355):231–4.
13. Hwang DR, Wu YS, Chang CW, Lien TW, Chen WC, Tan UK, et al. Synthesis and anti-viral activity of a series of sesquiterpene lactones and analogues in the subgenomic HCV replicon system. Bioorg Med Chem 2006; 14(1):83–91.
14. Gill KK, Kaddoumi A, Nazzal S. Mixed micelles of PEG(2000)-DSPE and vitamin-E TPGS for concurrent delivery of paclitaxel and parthenolide: enhanced chemosenstization and antitumor efficacy against non-small cell lung cancer (NSCLC) cell lines. Eur J Pharm Sci 2012; 46(1-2):64–71.
15. Pajak B, Gajkowska B, Orzechowski A. Molecular basis of

parthenolide-dependent proapoptotic activity in cancer cells. Folia Histochem Cytobiol 2008; 46(2):129–35.

16. Sun Y, St Clair DK, Fang F, Warren GW, Rangnekar VM, Crooks PA, et al. The radiosensitization effect of parthenolide in prostate cancer cells is mediated by nuclear factor-kappaB inhibition and enhanced by the presence of PTEN. Mol Cancer Ther 2007; 6(9): 2477–86.
17. Sun Y, St Clair DK, Xu Y, Crooks PA, St Clair WH. A NADPH oxidase-dependent redox signaling pathway mediates the selective radiosensitization effect of parthenolide in prostate cancer cells. Cancer Res 2010; 70(7):2880–90.
18. Xu Y, Fang F, Miriyala S, Crooks PA, Oberley TD, Chaiswing L, et al. KEAP1 is a redox sensitive target that arbitrates the opposing radiosensitive effects of parthenolide in normal and cancer cells. Cancer Res 2013; 73(14):4406–17.
19. Salmeen A, Andersen JN, Myers MP, Meng TC, Hinks JA, Tonks NK, et al. Redox regulation of protein tyrosine phosphatase 1B involves a sulphenyl-amide intermediate. Nature 2003; 423(6941): 769–73.
20. Kawasaki BT, Hurt EM, Kalathur M, Duhagon MA, Milner JA, Kim YS, et al. Effects of the sesquiterpene lactone parthenolide on prostate tumor-initiating cells: An integrated molecular profiling approach. Prostate 2009; 69(8):827–37.
21. Matsumoto H, Hamada N, Takahashi A, Kobayashi Y, Ohnishi T. Vanguards of paradigm shift in radiation biology: radiation-induced adaptive and bystander responses. J Radiat Res 2007; 48(2):97–106.
22. Nenoi M, Wang B, Vares G. In vivo radioadaptive response: a review of studies relevant to radiation-induced cancer risk. Human Experiment Toxicol 2015; 34(3):272–83.
23. Day TK, Zeng G, Hooker AM, Bhat M, Scott BR, Turner DR, et al. Extremely low priming doses of X radiation induce an adaptive response for chromosomal inversions in pKZ1 mouse prostate. Radiat Res 2006; 166(5):757–66.
24. Olivieri G, Bodycote J, Wolff S. Adaptive response of human lymphocytes to low concentrations of radioactive thymidine. Science 1984; 223(4636):594–7.
25. Ito M, Shibamoto Y, Ayakawa S, Tomita N, Sugie C, Ogino H. Low-dose whole-body irradiation induced radioadaptive response in C57BL/6 mice. J Radiat Res 2007; 48(6):455–60.
26. Okazaki R, Ootsuyama A, Norimura T. TP53 and TP53-related genes associated with protection from apoptosis in the radioadaptive response. Radiat Res 2007; 167(1):51–7.
27. Yu H, Liu N, Ju B. Low dose radiation induced adaptive response of apoptosis in mouse spleen cells. Chinese-German J Clin Oncol 2010; 9(4):235–8.
28. Mitchel RE, Jackson JS, Morrison DP, Carlisle SM. Low doses of radiation increase the latency of spontaneous lymphomas and spinal osteosarcomas in cancer-prone, radiation-sensitive Trp53 heterozygous mice. Radiat Res 2003; 159(3):320–7.
29. Ina Y, Tanooka H, Yamada T, Sakai K. Suppression of thymic lymphoma induction by life-long low-dose-rate irradiation accompanied by immune activation in C57BL/6 mice. Radiat Res 2005; 163(2):153–8.
30. Sakai K, Nomura T, Ina Y. Enhancement of bio-protective functions by low dose/dose-rate radiation. Dose Resp 2006; 4(4): 327–32.
31. Tang FR, Loke WK. Molecular mechanisms of low dose ionizing radiation-induced hormesis, adaptive responses, radioresistance, bystander effects, and genomic instability. Int J Radiat Biol 2015; 91(1):13–27.
32. Lall R, Ganapathy S, Yang M, Xiao S, Xu T, Su H, et al. Low-dose radiation exposure induces a HIF-1-mediated adaptive and protective metabolic response. Cell Death Differ 2014; 21(5): 836–44.
33. Grdina DJ, Murley JS, Miller RC, Woloschak GE, Li JJ. NFkappaB and survivin-mediated radio-adaptive response. Radiat Res 2015; 183(4):391–7.
34. Ahmed KM, Li JJ. NF-kappa B-mediated adaptive resistance to ionizing radiation. Free Rad Biol Med 2008; 44(1):1–13.
35. Fan M, Ahmed KM, Coleman MC, Spitz DR, Li JJ. Nuclear factor-kappaB and manganese superoxide dismutase mediate adaptive radioresistance in low-dose irradiated mouse skin epithelial cells. Cancer Res 2007; 67(7):3220–8.
36. Liu SZ, Liu WH, Sun JB. Radiation hormesis: its expression in the immune system. Health Phys 1987; 52(5):579–83.
37. Liu SZ. Cancer control related to stimulation of immunity by low-dose radiation. Dose Resp 2006; 5(1):39–47.
38. Chen Z, Sakai K. Enhancement of radiation-induced apoptosis by preirradiation with low-dose X-rays in human leukemia MOLT-4 cells. J Radiat Res 2004; 45(2):239–43.
39. Grdina DJ, Murley JS, Miller RC, Mauceri HJ, Sutton HG, Li JJ, et al. A survivin-associated adaptive response in radiation therapy. Cancer Res 2013; 73(14):4418–28.
40. Kim YR, Eom JI, Kim SJ, Jeung HK, Cheong JW, Kim JS, et al. Myeloperoxidase expression as a potential determinant of parthenolide-induced apoptosis in leukemia bulk and leukemia stem cells. J Pharmacol Exp Ther 2010; 335(2):389–400.
41. Neelakantan S, Nasim S, Guzman ML, Jordan CT, Crooks PA. Aminoparthenolides as novel anti-leukemic agents: Discovery of the NF-kappa B inhibitor, DMAPT (LC-1). Bioorg Med Chem Let 2009; 19(15):4346–9.
42. Greenberg NM, DeMayo F, Finegold MJ, Medina D, Tilley WD, Aspinall JO, et al. Prostate cancer in a transgenic mouse. Proc Natl Acad Sci U S A 1995; 92(8):3439–43.
43. Guzman ML, Rossi RM, Neelakantan S, Li X, Corbett CA, Hassane DC, et al. An orally bioavailable parthenolide analog selectively eradicates acute myelogenous leukemia stem and progenitor cells. Blood 2007; 110(13):4427–35.
44. 44. IAEA. Absorbed Dose Determination in External Beam Radiotherapy: An international code of practice for dosimetry based on standards of absorbed dose to water. Technical Reports Series 398. Vienna: IAEA; 2000.
45. Aukett RJ, Burns JE, Greener AG, Harrison RM, Moretti C, Nahum AE, et al. Addendum to the IPEMB code of practice for the determination of absorbed dose for x-rays below 300 kV generating potential (0.035 mm Al-4 mm Cu HVL). Phys Med Biol 2005; 50(12):2739–48.
46. Aukett RJ, Thomas DW, Seaby AW, Gittins JT. Performance characteristics of the Pantak DXT-300 kilovoltage X-ray treatment machine. Br J Radiol 1996; 69(824):726–34.
47. Lawrence MD, Blyth BJ, Ormsby RJ, Tilley WD, Sykes PJ. False-positive TUNEL staining observed in SV40 based transgenic murine prostate cancer models. Transgenic Res 2013; 22(5): 1037–47.
48. Berman-Booty LD, Sargeant AM, Rosol TJ, Rengel RC, Clinton SK, Chen CS, et al. A review of the existing grading schemes and a proposal for a modified grading scheme for prostatic lesions in TRAMP mice. Toxicol Pathol 2012; 40(1):5–17.
49. Shanmugam R, Kusumanchi P, Appaiah H, Cheng L, Crooks P, Neelakantan S, et al. A water soluble parthenolide analog suppresses in vivo tumor growth of two tobacco-associated cancers, lung and bladder cancer, by targeting NF-kappaB and generating reactive oxygen species. Int J Cancer 2011; 128(10): 2481–94.
50. Shanmugam R, Kusumanchi P, Cheng L, Crooks P, Neelakantan S, Matthews W, et al. A water-soluble parthenolide analogue suppresses in vivo prostate cancer growth by targeting NFkappaB and generating reactive oxygen species. Prostate 2010; 70(10): 1074–86.
51. Yip-Schneider MT, Wu H, Njoku V, Ralstin M, Holcomb B, Crooks PA, et al. Effect of celecoxib and the novel anti-cancer

agent, dimethylamino-parthenolide, in a developmental model of pancreatic cancer. Pancreas 2008; 37(3):e45–53.

52. Estabrook NC, Chin-Sinex H, Borgmann AJ, Dhaemers RM, Shapiro RH, Gilley D, et al. Inhibition of NF-kappaB and DNA double-strand break repair by DMAPT sensitizes non-small-cell lung cancers to X-rays. Free Radic Biol Med 2011; 51(12): 2249–58.
53. Freitas M, Baldeiras I, Proenca T, Alves V, Mota-Pinto A, Sarmento-Ribeiro A. Oxidative stress adaptation in aggressive prostate cancer may be counteracted by the reduction of glutathione reductase. FEBS open bio 2012; 2:119–28.
54. Oberley TD, Zhong W, Szweda LI, Oberley LW. Localization of antioxidant enzymes and oxidative damage products in normal and malignant prostate epithelium. Prostate 2000; 44(2):144–55.
55. Tam NN, Nyska A, Maronpot RR, Kissling G, Lomnitski L, Suttie A, et al. Differential attenuation of oxidative/nitrosative injuries in early prostatic neoplastic lesions in TRAMP mice by dietary antioxidants. Prostate 2006; 66(1):57–69.
56. Humphrey PA. Gleason grading and prognostic factors in carcinoma of the prostate. Mod Pathol 2004; 17(3):292–306.
57. Sweeney CJ, Mehrotra S, Sadaria MR, Kumar S, Shortle NH, Roman Y, et al. The sesquiterpene lactone parthenolide in combination with docetaxel reduces metastasis and improves survival in a xenograft model of breast cancer. Mol Cancer Ther 2005; 4(6):1004–12.
58. Kouvaris JR, Kouloulias VE, Vlahos LJ. Amifostine: the first selective-target and broad-spectrum radioprotector. Oncologist 2007; 12(6):738–47.
59. Buentzel J, Micke O, Adamietz IA, Monnier A, Glatzel M, de Vries A. Intravenous amifostine during chemoradiotherapy for head-and-neck cancer: a randomized placebo-controlled phase III study. Int J Radiat Oncol Biol Phys 2006; 64(3):684–91.
60. Ormsby RJ, Lawrence MD, Blyth BJ, Bexis K, Bezak E, Murley JS, et al. Protection from radiation-induced apoptosis by the radioprotector amifostine (WR-2721) is radiation dose dependent. Cell Biol Toxicol 2014; 30(1):55–66.
61. Cassatt DR, Fazenbaker CA, Kifle G, Bachy CM. Effects of dose and schedule on the efficacy of ethyol: preclinical studies. Seminars Oncol 2003; 30(6 Suppl 18):31–9.
62. Gu J, Zhu S, Li X, Wu H, Li Y, Hua F. Effect of amifostine in head and neck cancer patients treated with radiotherapy: a systematic review and meta-analysis based on randomized controlled trials. PLoS One 2014; 9(5):e95968.
63. Curry EA, 3rd, Murry DJ, Yoder C, Fife K, Armstrong V, Nakshatri H, et al. Phase I dose escalation trial of feverfew with standardized doses of parthenolide in patients with cancer. Invest New Drugs 2004; 22(3):299–305.
64. Pareek A, Suthar M, Rathore GS, Bansal V. Feverfew (Tanacetum parthenium L.): A systematic review. Pharmacogn Rev 2011; 5(9): 103–10.
65. Lawrence MD, Ormsby RJ, Blyth BJ, Bezak E, England G, Newman MR, et al. Lack of high-dose radiation mediated prostate cancer promotion and low-dose radiation adaptive response in the TRAMP mouse model. Radiat Res 2013; 180(4):376–88.
66. West NJ, Courtney ED, Poullis AP, Leicester RJ. Apoptosis in the colonic crypt, colorectal adenomata, and manipulation by chemoprevention. Cancer epidemiology, biomarkers & prevention: a publication of the American Association for Cancer Research, cosponsored by the American Society of Preventive Oncology 2009; 18(6):1680–7.
67. Saha S, Woodbine L, Haines J, Coster M, Ricket N, Barazzuol L, et al. Increased apoptosis and DNA double-strand breaks in the embryonic mouse brain in response to very low-dose X-rays but not 50 Hz magnetic fields. J Royal Society, 2014; 11(100): 20140783.
68. Komarova EA, Christov K, Faerman AI, Gudkov AV. Different impact of p53 and p21 on the radiation response of mouse tissues. Oncogene 2000; 19(33):3791–8.
69. Vavrova J, Marekova-Rezacova M, Vokurkova D, Szkanderova S, Psutka J. Caffeine induces a second wave of apoptosis after low dose-rate gamma radiation of HL-60 cells. Radiat Environm Biophys 2003; 42(3):193–9.
70. Kansanen E, Kuosmanen SM, Leinonen H, Levonen AL. The Keap1-Nrf2 pathway: Mechanisms of activation and dysregulation in cancer. Redox Biol 2013; 1:45–9.
71. Leinonen HM, Kansanen E, Polonen P, Heinaniemi M, Levonen AL. Role of the Keap1-Nrf2 pathway in cancer. Adv Cancer Res 2014; 122:281–320.
72. Taguchi K, Motohashi H, Yamamoto M. Molecular mechanisms of the Keap1-Nrf2 pathway in stress response and cancer evolution. Genes Cells 2011; 16(2):123–40.

References

Abate-Shen, C, Brown, PH, Colburn, NH, Gerner, EW, Green, JE, et al. 2008, 'The Untapped Potential of Genetically Engineered Mouse Models in Chemoprevention Research: Opportunities and Challenges', *Cancer Prevention Research*, vol. 1, no. 3, pp. 161-166.

Abate-Shen, C & Shen, MM 2000, 'Molecular genetics of prostate cancer', *Genes & Development*, vol. 14, no. 19, pp. 2410-2434.

Abate-Shen, C & Shen, MM 2002, 'Mouse models of prostate carcinogenesis', *Trends in Genetics*, vol. 18, no. 5, pp. S1-S5.

ABS 2015, *Apparent Consumption of Alcohol, Australia, 2013–14*, ABo Statistics, Canberra, Australia.

Afghahi, A & Sledge, GW, Jr. 2015, 'Targeted Therapy for Cancer in the Genomic Era', *Cancer J*, vol. 21, no. 4, pp. 294-8.

Ahmad, I, Sansom, OJ & Leung, HY 2008, 'Advances in mouse models of prostate cancer', *Expert Rev Mol Med*, vol. 10, p. e16.

Ahmed, KM & Li, JJ 2008, 'NF-kappa B-mediated adaptive resistance to ionizing radiation', *Free Radic Biol Med*, vol. 44, no. 1, pp. 1-13.

Ahuja, D, Saenz-Robles, MT & Pipas, JM 2005, 'SV40 large T antigen targets multiple cellular pathways to elicit cellular transformation', *Oncogene*, vol. 24, no. 52, pp. 7729-45.

AIHW 2012, *Cancer incidence projections, Australia 2011 to 2020* in Cancer Series, vol. 66, AIHW, Canberra, Australia.

AIHW 2016, *Radiotherapy in Australia: report on the second year of a pilot collection 2014–15*, AIHW, Canberra.

AIHW & AACR 2012, *Cancer in Australia: an overview 2012* in Cancer Series, vol. 74, AIHW, Canberra.

AIHW & AACR 2014, *Cancer in Australia: an overview 2014* in Cancer Series, vol. 90, AIHW, Canberra.

Alan, Y & Daniel, P 1993, 'Cytotoxic chemotherapy for advanced hormone-resistant prostate cancer', *Cancer*, vol. 71, no. S3, pp. 1098-1109.

Ali, SH & DeCaprio, JA 2001, 'Cellular transformation by SV40 large T antigen: interaction with host proteins', *Seminars in Cancer Biology*, vol. 11, no. 1, pp. 15-23.

Allen, T & Gundrajakuppam, L 2012, 'A role of immunotherapy in metastatic malignant melanoma', *Cent Nerv Syst Agents Med Chem*, vol. 12, no. 3, pp. 182-8.

Anassi, E & Ndefo, UA 2011, 'Sipuleucel-T (provenge) injection: the first immunotherapy agent (vaccine) for hormone-refractory prostate cancer', *P T*, vol. 36, no. 4, pp. 197-202.

Anderson, LM 1988, 'Increased numbers of N-nitrosodimethylamine-initiated lung tumors in mice by chronic co-administration of ethanol', *Carcinogenesis*, vol. 9, no. 9, pp. 1717-9.

Anderson, LM, Carter, JP, Logsdon, DL, Driver, CL & Kovatch, RM 1992, 'Characterization of ethanol's enhancement of tumorigenesis by N-nitrosodimethylamine in mice', *Carcinogenesis*, vol. 13, no. 11, pp. 2107-11.

Andreas, IE, Scott, FW, Wendy, JH, Robert, AB & Norman, MG 2004, 'Steroid hormones, polypeptide growth factors, hormone refractory prostate cancer, and the neuroendocrine phenotype', *Journal of Cellular Biochemistry*, vol. 91, no. 4, pp. 671-683.

Andreoiu, M & Cheng, L 2010, 'Multifocal prostate cancer: biologic, prognostic, and therapeutic implications', *Human Pathology*, vol. 41, no. 6, pp. 781-793.

Andriole, GL, Bostwick, DG, Brawley, OW, Gomella, LG, Marberger, M, et al. 2010, 'Effect of dutasteride on the risk of prostate cancer', *N Engl J Med*, vol. 362, no. 13, pp. 1192-202.

Antonarakis, ES, Lu, C, Wang, H, Luber, B, Nakazawa, M, et al. 2014, 'AR-V7 and resistance to enzalutamide and abiraterone in prostate cancer', *N Engl J Med*, vol. 371, no. 11, pp. 1028-38.

Araujo, JC, Trudel, GC & Paliwal, P 2013, 'Long-term use of dasatinib in patients with metastatic castration-resistant prostate cancer after receiving the

combination of dasatinib and docetaxel', *Cancer Manag Res*, vol. 6, pp. 25-30.

Arima, N, Kuziel, WA, Grdina, TA & Greene, WC 1992, 'IL-2-induced signal transduction involves the activation of nuclear NF-kappa B expression', *J Immunol*, vol. 149, no. 1, pp. 83-91.

Armstrong, HK, Koay, YC, Irani, S, Das, R, Nassar, ZD, et al. 2016, 'A Novel Class of Hsp90 C-Terminal Modulators Have Pre-Clinical Efficacy in Prostate Tumor Cells Without Induction of a Heat Shock Response', *Prostate*, vol. 76, no. 16, pp. 1546-1559.

Arora, R, Koch, MO, Eble, JN, Ulbright, TM, Li, L, et al. 2004, 'Heterogeneity of Gleason grade in multifocal adenocarcinoma of the prostate', *Cancer*, vol. 100, no. 11, pp. 2362-6.

Artandi, SE & DePinho, RA 2010, 'Telomeres and telomerase in cancer', *Carcinogenesis*, vol. 31, no. 1, pp. 9-18.

Aye, MM, Ma, C, Lin, H, Bower, KA, Wiggins, RC, et al. 2004, 'Ethanol-induced in vitro invasion of breast cancer cells: the contribution of MMP-2 by fibroblasts', *Int J Cancer*, vol. 112, no. 5, pp. 738-46.

Baeuerle, PA & Henkel, T 1994, 'Function and activation of NF-kappa B in the immune system', *Annu Rev Immunol*, vol. 12, pp. 141-79.

Baldwin, AS, Jr. 1996, 'The NF-kappa B and I kappa B proteins: new discoveries and insights', *Annu Rev Immunol*, vol. 14, pp. 649-83.

Baluk, P, Morikawa, S, Haskell, A, Mancuso, M & McDonald, DM 2003, 'Abnormalities of basement membrane on blood vessels and endothelial sprouts in tumors', *Am J Pathol*, vol. 163, no. 5, pp. 1801-15.

Banan, A, Keshavarzian, A, Zhang, L, Shaikh, M, Forsyth, CB, et al. 2007, 'NF-kappaB activation as a key mechanism in ethanol-induced disruption of the F-actin cytoskeleton and monolayer barrier integrity in intestinal epithelium', *Alcohol*, vol. 41, no. 6, pp. 447-60.

Bardeesy, N & Sharpless, NE 2006, 'RAS unplugged: negative feedback and oncogene-induced senescence', *Cancer Cell*, vol. 10, no. 6, pp. 451-3.

Bargonetti, J, ReynisdÃ³ttir, I, Friedman, PN & Prives, C 1992, 'Site-specific binding of wild-type p53 to cellular DNA is inhibited by SV40 T antigen and mutant p53', *Genes & Development*, vol. 6, no. 10, pp. 1886-1898.

Barkett, M & Gilmore, TD 1999, 'Control of apoptosis by Rel/NF-kappaB transcription factors', *Oncogene*, vol. 18, no. 49, pp. 6910-24.

Barton, MB, Jacob, S, Shafiq, J, Wong, K, Thompson, SR, et al. 2014, 'Estimating the demand for radiotherapy from the evidence: a review of changes from 2003 to 2012', *Radiother Oncol*, vol. 112, no. 1, pp. 140-4.

Baskar, R, Lee, KA, Yeo, R & Yeoh, KW 2012, 'Cancer and radiation therapy: current advances and future directions', *Int J Med Sci*, vol. 9, no. 3, pp. 193-9.

Bastacky, SI, Wojno, KJ, Walsh, PC, Carmichael, MJ & Epstein, JI 1995, 'Pathological features of hereditary prostate cancer', *J Urol*, vol. 153, no. 3 Pt 2, pp. 987-92.

Batlle, E, Sancho, E, Franci, C, Dominguez, D, Monfar, M, et al. 2000, 'The transcription factor snail is a repressor of E-cadherin gene expression in epithelial tumour cells', *Nat Cell Biol*, vol. 2, no. 2, pp. 84-9.

Beaty, BT & Condeelis, J 2014, 'Digging a little deeper: the stages of invadopodium formation and maturation', *Eur J Cell Biol*, vol. 93, no. 10-12, pp. 438-44.

Berger, MF, Lawrence, MS, Demichelis, F, Drier, Y, Cibulskis, K, et al. 2011, 'The genomic complexity of primary human prostate cancer', *Nature*, vol. 470, no. 7333, pp. 214-20.

Bergers, G & Benjamin, LE 2003, 'Tumorigenesis and the angiogenic switch', *Nat Rev Cancer*, vol. 3, no. 6, pp. 401-10.

Berkey, FJ 2010, 'Managing the Adverse Effects of Radiation Therapy', *American Family Physician*, vol. 82, no. 4, pp. 381-388.

Berman-Booty, LD, Sargeant, AM, Rosol, TJ, Rengel, RC, Clinton, SK, et al. 2012, 'A review of the existing grading schemes and a proposal for a modified grading scheme for prostatic lesions in TRAMP mice', *Toxicol Pathol*, vol. 40, no. 1, pp. 5-17.

Bettuzzi, S, Brausi, M, Rizzi, F, Castagnetti, G, Peracchia, G, et al. 2006, 'Chemoprevention of human prostate cancer by oral administration of green tea catechins in volunteers with high-grade prostate intraepithelial neoplasia: a preliminary report from a one-year proof-of-principle study', *Cancer Res*, vol. 66, no. 2, pp. 1234-40.

Bhowmick, NA, Neilson, EG & Moses, HL 2004, 'Stromal fibroblasts in cancer initiation and progression', *Nature*, vol. 432, no. 7015, pp. 332-7.

Bissell, MJ, Rizki, A & Mian, IS 2003, 'Tissue architecture: the ultimate regulator of breast epithelial function - Commentary', *Current Opinion in Cell Biology*, vol. 15, no. 6, pp. 753-762.

Blankenbecler, R 2010, 'Low-dose pretreatment for radiation therapy', *Dose Response*, vol. 8, no. 4, pp. 534-42.

Bogenrieder, T & Herlyn, M 2003, 'Axis of evil: molecular mechanisms of cancer metastasis', *Oncogene*, vol. 22, no. 42, pp. 6524-36.

Bokhoven, Av, Varella-Garcia, M, Korch, C, Johannes, WU, Smith, E, et al. 2003, 'Molecular characterization of human prostate carcinoma cell lines', *The Prostate*, vol. 57, no. 3, pp. 205-225.

Bolla, M, Van Tienhoven, G, Warde, P, Dubois, JB, Mirimanoff, RO, et al. 2010, 'External irradiation with or without long-term androgen suppression for prostate cancer with high metastatic risk: 10-year results of an EORTC randomised study', *Lancet Oncology*, vol. 11, no. 11, pp. 1066-1073.

Bonizzi, G & Karin, M 2004, 'The two NF-kappa B activation pathways and their role in innate and adaptive immunity', *Trends in Immunology*, vol. 25, no. 6, pp. 280-288.

Bork, PM, Schmitz, ML, Kuhnt, M, Escher, C & Heinrich, M 1997, 'Sesquiterpene lactone containing Mexican Indian medicinal plants and pure sesquiterpene lactones as potent inhibitors of transcription factor NF-kappaB', *FEBS Lett*, vol. 402, no. 1, pp. 85-90.

Bostwick, DG, Shan, A, Qian, J, Darson, M, Maihle, NJ, et al. 1998, 'Independent origin of multiple foci of prostatic intraepithelial neoplasia: comparison with matched foci of prostate carcinoma', *Cancer*, vol. 83, no. 9, pp. 1995-2002.

Brausi, M, Rizzi, F & Bettuzzi, S 2008, 'Chemoprevention of human prostate cancer by green tea catechins: two years later. A follow-up update', *Eur Urol*, vol. 54, no. 2, pp. 472-3.

Bromberg, J 2002, 'Stat proteins and oncogenesis', *J Clin Invest*, vol. 109, no. 9, pp. 1139-42.

Buentzel, J, Micke, O, Adamietz, IA, Monnier, A, Glatzel, M, et al. 2006, 'Intravenous amifostine during chemoradiotherapy for head-and-neck cancer: a randomized placebo-controlled phase III study', *Int J Radiat Oncol Biol Phys*, vol. 64, no. 3, pp. 684-91.

Burnett, RM, Craven, KE, Krishnamurthy, P, Goswami, CP, Badve, S, et al. 2015, 'Organ-specific adaptive signaling pathway activation in metastatic breast cancer cells', *Oncotarget*, vol. 6, no. 14, pp. 12682-96.

Cabrita, MA & Christofori, G 2008, 'Sprouty proteins, masterminds of receptor tyrosine kinase signaling', *Angiogenesis*, vol. 11, no. 1, pp. 53-62.

Caldon, CE, Sutherland, RL & Musgrove, E 2010, 'Cell cycle proteins in epithelial cell differentiation: implications for breast cancer', *Cell Cycle*, vol. 9, no. 10, pp. 1918-28.

Carlisi, D, Buttitta, G, Di Fiore, R, Scerri, C, Drago-Ferrante, R, et al. 2016, 'Parthenolide and DMAPT exert cytotoxic effects on breast cancer stem-like cells by inducing oxidative stress, mitochondrial dysfunction and necrosis', *Cell Death Dis*, vol. 7, p. e2194.

Carlisi, D, D'Anneo, A, Angileri, L, Lauricella, M, Emanuele, S, et al. 2011, 'Parthenolide Sensitizes Hepatocellular Carcinoma Cells to TRAIL by Inducing the Expression of Death Receptors Through Inhibition of STAT3 Activation', *Journal of Cellular Physiology*, vol. 226, no. 6, pp. 1632-1641.

Carmeliet, P 2005, 'VEGF as a key mediator of angiogenesis in cancer', *Oncology*, vol. 69, pp. 4-10.

Carpenter, AE, Jones, TR, Lamprecht, MR, Clarke, C, Kang, IH, et al. 2006, 'CellProfiler: image analysis software for identifying and quantifying cell phenotypes', *Genome Biol*, vol. 7, no. 10, p. R100.

Cassatt, DR, Fazenbaker, CA, Kifle, G & Bachy, CM 2003, 'Effects of dose and schedule on the efficacy of ethyol: preclinical studies', *Semin Oncol*, vol. 30, no. 6 Suppl 18, pp. 31-9.

Centenera, MM, Raj, GV, Knudsen, KE, Tilley, WD & Butler, LM 2013, 'Ex vivo culture of human prostate tissue and drug development', *Nat Rev Urol*, vol. 10, no. 8, pp. 483-7.

Chen, Q, Zhao, X, Zhang, H, Yuan, H, Zhu, M, et al. 2015, 'MiR-130b suppresses prostate cancer metastasis through down-regulation of MMP2', *Mol Carcinog*, vol. 54, no. 11, pp. 1292-300.

Chen, QM & Tu, VC 2002, 'Apoptosis and heart failure: mechanisms and therapeutic implications', *Am J Cardiovasc Drugs*, vol. 2, no. 1, pp. 43-57.

Cheng, D, Xiao, JJ, Cheng, H, Liu, Z, Covey, JM, et al. 2005, 'Analytical method development and pharmacokinetics studies with parthenolide (NSC 157035) and a water-soluble analog (NSC 734325)', *AACR Meeting Abstracts*, vol. 2005, no. 1, pp. 988-.

Cheng, L, Jones, TD, Pan, CX, Barbarin, A, Eble, JN, et al. 2005a, 'Anatomic distribution and pathologic characterization of small-volume prostate cancer (<0.5 ml) in whole-mount prostatectomy specimens', *Mod Pathol*, vol. 18, no. 8, pp. 1022-6.

Cheng, L, Poulos, CK, Pan, CX, Jones, TD, Daggy, JK, et al. 2005b, 'Preoperative prediction of small volume cancer (less than 0.5 ml) in radical prostatectomy specimens', *J Urol*, vol. 174, no. 3, pp. 898-902.

Cheng, N, Chytil, A, Shyr, Y, Joly, A & Moses, HL 2008, 'Transforming growth factor-beta signaling-deficient fibroblasts enhance hepatocyte growth factor signaling in mammary carcinoma cells to promote scattering and invasion', *Mol Cancer Res*, vol. 6, no. 10, pp. 1521-33.

Chiaverotti, T, Couto, SS, Donjacour, A, Mao, J-H, Nagase, H, et al. 2008, 'Dissociation of Epithelial and Neuroendocrine Carcinoma Lineages in the Transgenic Adenocarcinoma of Mouse Prostate Model of Prostate Cancer', *American Journal of Pathology*, vol. 172, no. 1, pp. 236-246.

Chung, KW 1990, 'Effects of Chronic Ethanol Intake on Aromatization of Androgens and Concentration of Estrogen and Androgen Receptors in Rat-Liver', *Toxicology*, vol. 62, no. 3, pp. 285-295.

Chung, LWK, Baseman, A, Assikis, V & Zhau, HE 2005, 'Molecular insights into prostate cancer progression: The missing link of tumor microenvironment', *Journal of Urology*, vol. 173, no. 1, pp. 10-20.

Clark, LC, Dalkin, B, Krongrad, A, Combs, GF, Jr., Turnbull, BW, et al. 1998, 'Decreased incidence of prostate cancer with selenium supplementation: results of a double-blind cancer prevention trial', *Br J Urol*, vol. 81, no. 5, pp. 730-4.

Clevers, H 2004, 'At the Crossroads of Inflammation and Cancer', *Cell*, vol. 118, no. 6, pp. 671-674.

Colotta, F, Allavena, P, Sica, A, Garlanda, C & Mantovani, A 2009, 'Cancer-related inflammation, the seventh hallmark of cancer: links to genetic instability', *Carcinogenesis*, vol. 30, no. 7, pp. 1073-81.

Comijn, J, Berx, G, Vermassen, P, Verschueren, K, van Grunsven, L, et al. 2001, 'The two-handed E box binding zinc finger protein SIP1 downregulates E-cadherin and induces invasion', *Mol Cell*, vol. 7, no. 6, pp. 1267-78.

Corn, PG 2012, 'The tumor microenvironment in prostate cancer: elucidating molecular pathways for therapy development', *Cancer Manag Res*, vol. 4, pp. 183-93.

Coussens, LM & Werb, Z 2002, 'Inflammation and cancer', *Nature*, vol. 420, no. 6917, pp. 860-7.

Cronin, P, Kirkbride, B, Bang, A, Parkinson, B, Smith, D, et al. 2016, 'Long-term health care costs for patients with prostate cancer: A population-wide longitudinal study in New South Wales, Australia', *Asia Pac J Clin Oncol*.

Crooks, PA, Jordan, CT & Wei, X 2006, *Use of parthenolide derivatives as antileukemic and cytotoxic agents*, Google Patents.

Curry, EA, 3rd, Murry, DJ, Yoder, C, Fife, K, Armstrong, V, et al. 2004, 'Phase I dose escalation trial of feverfew with standardized doses of parthenolide in patients with cancer', *Invest New Drugs*, vol. 22, no. 3, pp. 299-305.

Czyz, M, Koprowska, K & Sztiller-Sikorska, M 2013, 'Parthenolide reduces the frequency of ABCB5-positive cells and clonogenic capacity of melanoma cells from anchorage independent melanospheres', *Cancer Biology and Therapy*, vol. 14, no. 2, pp. 135-145.

D'Anneo, A, Carlisi, D, Lauricella, M, Puleio, R, Martinez, R, et al. 2013, 'Parthenolide generates reactive oxygen species and autophagy in MDA-MB231 cells. A soluble parthenolide analogue inhibits tumour growth and

metastasis in a xenograft model of breast cancer', *Cell Death Dis*, vol. 4, p. e891.

Dai, Y, Guzman, ML, Chen, S, Wang, L, Yeung, SK, et al. 2010, 'The NF (Nuclear factor)-kappaB inhibitor parthenolide interacts with histone deacetylase inhibitors to induce MKK7/JNK1-dependent apoptosis in human acute myeloid leukaemia cells', *Br J Haematol*, vol. 151, no. 1, pp. 70-83.

David, JW, Wael, AS, David, WH, Lang, CM, LuAnn, M, et al. 1998, 'Workgroup 4: Spontaneous prostate carcinoma in dogs and nonhuman primates', *The Prostate*, vol. 36, no. 1, pp. 64-67.

Dawson, LA & Sharpe, MB 2006, 'Image-guided radiotherapy: rationale, benefits, and limitations', *Lancet Oncol*, vol. 7, no. 10, pp. 848-58.

Day, TK, Zeng, G, Hooker, AM, Bhat, M, Scott, BR, et al. 2006, 'Extremely low priming doses of X radiation induce an adaptive response for chromosomal inversions in pKZ1 mouse prostate', *Radiat Res*, vol. 166, no. 5, pp. 757-66.

De Marzo, AM, DeWeese, TL, Platz, EA, Meeker, AK, Nakayama, M, et al. 2004, 'Pathological and molecular mechanisms of prostate carcinogenesis: implications for diagnosis, detection, prevention, and treatment', *J Cell Biochem*, vol. 91, no. 3, pp. 459-77.

De Marzo, AM, Platz, EA, Sutcliffe, S, Xu, J, Gronberg, H, et al. 2007, 'Inflammation in prostate carcinogenesis', *Nat Rev Cancer*, vol. 7, no. 4, pp. 256-269.

de Visser, KE, Eichten, A & Coussens, LM 2006, 'Paradoxical roles of the immune system during cancer development', *Nat Rev Cancer*, vol. 6, no. 1, pp. 24-37.

Dean, FB, Bullock, P, Murakami, Y, Wobbe, CR, Weissbach, L, et al. 1987, 'Simian Virus 40 (SV 40) DNA Replication: SV 40 Large T Antigen Unwinds DNA Containing the SV 40 Origin of Replication', *Proceedings of the National Academy of Sciences U.S.A.*, vol. 84, no. 1, pp. 16-20.

Degroot, JM, Brundage, MD, Lam, M, Rohland, SL, Heaton, J, et al. 2013, 'Prostate cancer-specific survival differences in patients treated by radical prostatectomy versus curative radiotherapy', *Can Urol Assoc J*, vol. 7, no. 5-6, pp. E299-305.

Delbridge, AR & Strasser, A 2015, 'The BCL-2 protein family, BH3-mimetics and cancer therapy', *Cell Death Differ*, vol. 22, no. 7, pp. 1071-80.

Dell'Agli, M, Galli, GV, Bosisio, E & D'Ambrosio, M 2009, 'Inhibition of NF-kappa B and metalloproteinase-9 expression and secretion by parthenolide derivatives', *Bioorganic & Medicinal Chemistry Letters*, vol. 19, no. 7, pp. 1858-1860.

DeNardo, DG, Andreu, P & Coussens, LM 2010, 'Interactions between lymphocytes and myeloid cells regulate pro- versus anti-tumor immunity', *Cancer Metastasis Rev*, vol. 29, no. 2, pp. 309-16.

Dennis, LK & Hayes, RB 2001, 'Alcohol and prostate cancer', *Epidemiol Rev*, vol. 23, no. 1, pp. 110-4.

DeRose, YS, Wang, G, Lin, YC, Bernard, PS, Buys, SS, et al. 2011, 'Tumor grafts derived from women with breast cancer authentically reflect tumor pathology, growth, metastasis and disease outcomes', *Nat Med*, vol. 17, no. 11, pp. 1514-20.

Deshpande, A, Sicinski, P & Hinds, PW 2005, 'Cyclins and cdks in development and cancer: a perspective', *Oncogene*, vol. 24, no. 17, pp. 2909-15.

Dev, A, Iyer, S, Razani, B & Cheng, G 2011, 'NF-kappaB and innate immunity', *Curr Top Microbiol Immunol*, vol. 349, pp. 115-43.

Devarajan, E, Sahin, AA, Chen, JS, Krishnamurthy, RR, Aggarwal, N, et al. 2002, 'Down-regulation of caspase 3 in breast cancer: a possible mechanism for chemoresistance', *Oncogene*, vol. 21, no. 57, pp. 8843-51.

Dey, A, Tergaonkar, V & Lane, DP 2008, 'Double-edged swords as cancer therapeutics: Simultaneously targeting p53 and NF-κB pathways', *Nature Reviews Drug Discovery*, vol. 7, no. 12, pp. 1031-1040.

Di Fiore, R, Drago-Ferrante, R, D'Anneo, A, Augello, G, Carlisi, D, et al. 2013, 'In human retinoblastoma Y79 cells okadaic acid-parthenolide co-treatment induces synergistic apoptotic effects, with PTEN as a key player', *Cancer Biology and Therapy*, vol. 14, no. 10, pp. 922-931.

Diamanti, P, Cox, CV, Moppett, JP & Blair, A 2013, 'Parthenolide eliminates leukemia-initiating cell populations and improves survival in xenografts of childhood acute lymphoblastic leukemia', *Blood*, vol. 121, no. 8, pp. 1384-1393.

Diaz, LA, Jr., Williams, RT, Wu, J, Kinde, I, Hecht, JR, et al. 2012, 'The molecular evolution of acquired resistance to targeted EGFR blockade in colorectal cancers', *Nature*, vol. 486, no. 7404, pp. 537-40.

DiDonato, JA, Mercurio, F & Karin, M 2012, 'NF-kappaB and the link between inflammation and cancer', *Immunol Rev*, vol. 246, no. 1, pp. 379-400.

Diener, HC, Pfaffenrath, V, Schnitker, J, Friede, M & Henneicke-von Zepelin, HH 2005, 'Efficacy and safety of 6.25 mg t.i.d. feverfew CO2-extract (MIG-99) in migraine prevention--a randomized, double-blind, multicentre, placebo-controlled study', *Cephalalgia*, vol. 25, no. 11, pp. 1031-41.

Dinarello, CA 1998, 'Interleukin-1 beta, interleukin-18, and the interleukin-1 beta converting enzyme', *Molecular Mechanisms of Fever*, vol. 856, pp. 1-11.

Dittmar, T & Zänker, KS 2013, *Role of Cancer Stem Cells in Cancer Biology and Therapy*, Taylor & Francis.

Dreesen, O & Brivanlou, AH 2007, 'Signaling pathways in cancer and embryonic stem cells', *Stem Cell Reviews*, vol. 3, no. 1, pp. 7-17.

Droller, MJ 2001, 'Long-term results of intravesical bacillus Calmette-Guerin therapy for stage T1 superficial bladder cancer', *J Urol*, vol. 165, no. 2, pp. 701-2.

Dvorak, HF 1986, 'Tumors: wounds that do not heal. Similarities between tumor stroma generation and wound healing', *N Engl J Med*, vol. 315, no. 26, pp. 1650-9.

Ellis, LM & Hicklin, DJ 2008, 'VEGF-targeted therapy: mechanisms of anti-tumour activity', *Nature Reviews Cancer*, vol. 8, no. 8, pp. 579-591.

Endo, T, Toyota, M & Imai, K 2004, 'Silencing of negative regulator of JAK/STAT in colorectal cancer', *Journal of Gastroenterology*, vol. 39, no. 2, pp. 200-201.

Epstein, JI 2009, 'Precursor lesions to prostatic adenocarcinoma', *Virchows Arch*, vol. 454, no. 1, pp. 1-16.

Epstein, JI & Herawi, M 2006, 'Prostate needle biopsies containing prostatic intraepithelial neoplasia or atypical foci suspicious for carcinoma: implications for patient care', *J Urol*, vol. 175, no. 3 Pt 1, pp. 820-34.

Fang, J, Seki, T & Maeda, H 2009, 'Therapeutic strategies by modulating oxygen stress in cancer and inflammation', *Adv Drug Deliv Rev*, vol. 61, no. 4, pp. 290-302.

Fang, X, Cai, Y, Liu, J, Wang, Z, Wu, Q, et al. 2011, 'Twist2 contributes to breast cancer progression by promoting an epithelial-mesenchymal transition and cancer stem-like cell self-renewal', *Oncogene*, vol. 30, no. 47, pp. 4707-20.

Faul, F, Erdfelder, E, Lang, A-G & Buchner, A 2007, 'G*power 3: A flexible statistical power analysis program for the social, behavioral, and biomedical sciences', *Behavior Research Methods*, vol. 39, no. 2, pp. 175-191.

Feng, J, Li, L, Zhang, N, Liu, J, Zhang, L, et al. 2016, 'Androgen and AR contribute to breast cancer development and metastasis: an insight of mechanisms', *Oncogene*.

Feng, Y & Martin, P 2015, 'Imaging innate immune responses at tumour initiation: new insights from fish and flies', *Nat Rev Cancer*, vol. 15, no. 9, pp. 556-62.

Ferlay, J, Soerjomataram, I, Dikshit, R, Eser, S, Mathers, C, et al. 2015, 'Cancer incidence and mortality worldwide: sources, methods and major patterns in GLOBOCAN 2012', *Int J Cancer*, vol. 136, no. 5, pp. E359-86.

Ferrajoli, A, Faderl, S, Ravandi, F & Estrov, Z 2006, 'The JAK-STAT pathway: A therapeutic target in hematological malignancies', *Current Cancer Drug Targets*, vol. 6, no. 8, pp. 671-679.

Fidler, IJ 2003, 'Timeline - The pathogenesis of cancer metastasis: the 'seed and soil' hypothesis revisited', *Nature Reviews Cancer*, vol. 3, no. 6, pp. 453-458.

Fillmore, KM, Chikritzhs, T, Stockwell, T, Bostrom, A & Pascal, R 2009, 'Alcohol use and prostate cancer: a meta-analysis', *Mol Nutr Food Res*, vol. 53, no. 2, pp. 240-55.

Fornaro, M, Manes, T & Languino, LR 2001, 'Integrins and prostate cancer metastases', *Cancer and Metastasis Reviews*, vol. 20, no. 3-4, pp. 321-331.

Freedman, A 2012, 'Follicular lymphoma: 2012 update on diagnosis and management', *American Journal of Hematology*, vol. 87, no. 10, pp. 988-995.

Freitas, M, Baldeiras, I, Proenca, T, Alves, V, Mota-Pinto, A, et al. 2012, 'Oxidative stress adaptation in aggressive prostate cancer may be counteracted by the reduction of glutathione reductase', *FEBS Open Bio*, vol. 2, pp. 119-28.

Frese, KK & Tuveson, DA 2007, 'Maximizing mouse cancer models', *Nature Reviews Cancer*, vol. 7, no. 9, pp. 654-658.

Frohlich, MW 2012, 'Sipuleucel-T for the treatment of advanced prostate cancer', *Semin Oncol*, vol. 39, no. 3, pp. 245-52.

Galsky, MD & Vogelzang, NJ 2010, 'Docetaxel-based combination therapy for castration-resistant prostate cancer', *Annals of Oncology*.

Gambino, V, De Michele, G, Venezia, O, Migliaccio, P, Dall'Olio, V, et al. 2013, 'Oxidative stress activates a specific p53 transcriptional response that regulates cellular senescence and aging', *Aging Cell*, vol. 12, no. 3, pp. 435-45.

Ganguly, KK, Pal, S, Moulik, S & Chatterjee, A 2013, 'Integrins and metastasis', *Cell Adhesion & Migration*, vol. 7, no. 3, pp. 251-261.

Gao, ZW, Zhang, DL & Guo, CB 2010, 'Paclitaxel efficacy is increased by parthenolide via nuclear factor-kappaB pathways in in vitro and in vivo human non-small cell lung cancer models', *Curr Cancer Drug Targets*, vol. 10, no. 7, pp. 705-15.

Garcia-Pineres, AJ, Castro, V, Mora, G, Schmidt, TJ, Strunck, E, et al. 2001, 'Cysteine 38 in p65/NF-kappaB plays a crucial role in DNA binding inhibition by sesquiterpene lactones', *J Biol Chem*, vol. 276, no. 43, pp. 39713-20.

Gardenia.net, *Tanacetum parthenium 'Aureum' (Golden Feverfew)*. www.gardenia.net/plant/tanacetum-parthenium-aureum-feverfew

Gelman, IH, Peresie, J, Eng, KH & Foster, BA 2014, 'Differential requirement for Src family tyrosine kinases in the initiation, progression, and metastasis of prostate cancer', *Mol Cancer Res*, vol. 12, no. 10, pp. 1470-9.

Gerhardt, H & Semb, H 2008, 'Pericytes: gatekeepers in tumour cell metastasis?', *Journal of Molecular Medicine-Jmm*, vol. 86, no. 2, pp. 135-144.

Gerondakis, S, Grumont, R, Rourke, I & Grossmann, M 1998, 'The regulation and roles of Rel/NF-kappa B transcription factors during lymphocyte activation', *Curr Opin Immunol*, vol. 10, no. 3, pp. 353-9.

Gerweck, LE, Vijayappa, S, Kurimasa, A, Ogawa, K & Chen, DJ 2006, 'Tumor cell radiosensitivity is a major determinant of tumor response to radiation', *Cancer Research*, vol. 66, no. 17, pp. 8352-8355.

Ghantous, A, Gali-Muhtasib, H, Vuorela, H, Saliba, NA & Darwiche, N 2010, 'What made sesquiterpene lactones reach cancer clinical trials?', *Drug Discovery Today*, vol. 15, no. 15-16, pp. 668-678.

Ghantous, A, Saikali, M, Rau, T, Gali-Muhtasib, H, Schneider-Stock, R, et al. 2012, 'Inhibition of Tumor Promotion by Parthenolide: Epigenetic Modulation of p21', *Cancer Prev Res (Phila)*, vol. 5, no. 11, pp. 1298-309.

Ghantous, A, Sinjab, A, Herceg, Z & Darwiche, N 2013, 'Parthenolide: from plant shoots to cancer roots', *Drug Discovery Today*, vol. 18, no. 17-18, pp. 894-905.

Ghebranious, N & Donehower, LA 1998, 'Mouse models in tumor suppression', *Oncogene*, vol. 17, no. 25, pp. 3385-400.

Ghosh, S, May, MJ & Kopp, EB 1998, 'NF-kappa B and Rel proteins: evolutionarily conserved mediators of immune responses', *Annu Rev Immunol*, vol. 16, pp. 225-60.

Gingrich, JR, Barrios, RJ, Foster, BA & Greenberg, NM 1999, 'Pathologic progression of autochthonous prostate cancer in the TRAMP model', *Prostate Cancer Prostatic Dis*, vol. 2, no. 2, pp. 70-75.

Gingrich, JR, Barrios, RJ, Morton, RA, Boyce, BF, DeMayo, FJ, et al. 1996, 'Metastatic prostate cancer in a transgenic mouse', *Cancer Res*, vol. 56, no. 18, pp. 4096-102.

Giovannucci, E, Liu, Y, Platz, EA, Stampfer, MJ & Willett, WC 2007, 'Risk factors for prostate cancer incidence and progression in the health professionals follow-up study', *International Journal of Cancer*, vol. 121, no. 7, pp. 1571-1578.

Girinsky, T, Koumenis, C, Graeber, TG, Peehl, DM & Giaccia, AJ 1995, 'Attenuated Response of p53 and p21 in Primary Cultures of Human Prostatic Epithelial Cells Exposed to DNA-damaging Agents', *Cancer Research*, vol. 55, no. 17, pp. 3726-3731.

Gleason, DF & Mellinger, GT 1974, 'Prediction of prognosis for prostatic adenocarcinoma by combined histological grading and clinical staging', *J Urol*, vol. 111, no. 1, pp. 58-64.

Gohji, K, Fujimoto, N, Hara, I, Fujii, A, Gotoh, A, et al. 1998, 'Serum matrix metalloproteinase-2 and its density in men with prostate cancer as a new predictor of disease extension', *Int J Cancer*, vol. 79, no. 1, pp. 96-101.

Gong, Z, Kristal, AR, Schenk, JM, Tangen, CM, Goodman, PJ, et al. 2009, 'Alcohol consumption, finasteride, and prostate cancer risk: results from the Prostate Cancer Prevention Trial', *Cancer*, vol. 115, no. 16, pp. 3661-9.

Gonzalgo, ML & Isaacs, WB 2003, 'Molecular pathways to prostate cancer', *J Urol*, vol. 170, no. 6 Pt 1, pp. 2444-52.

Gopal, YN, Arora, TS & Van Dyke, MW 2007, 'Parthenolide specifically depletes histone deacetylase 1 protein and induces cell death through ataxia telangiectasia mutated', *Chem Biol*, vol. 14, no. 7, pp. 813-23.

Gopal, YNV, Chanchorn, E & Van Dyke, MW 2009, 'Parthenolide promotes the ubiquitination of MDM2 and activates p53 cellular functions', *Molecular Cancer Therapeutics*, vol. 8, no. 3, pp. 552-562.

Gore, ME & Larkin, JM 2011, 'Challenges and opportunities for converting renal cell carcinoma into a chronic disease with targeted therapies', *Br J Cancer*, vol. 104, no. 3, pp. 399-406.

Grabowska, MM, Degraff, DJ, Yu, X, Jin, RJ, Chen, Z, et al. 2014, 'Mouse models of prostate cancer: picking the best model for the question', *Cancer Metastasis Rev*.

Graham, J, Baker, M, Macbeth, F, Titshall, V & on behalf of the Guideline Development, G 2008, 'Diagnosis and treatment of prostate cancer: summary of NICE guidance', *BMJ*, vol. 336, no. 7644, pp. 610-612.

Gray, DR, Huss, WJ, Yau, JM, Durham, LE, Werdin, ES, et al. 2004, 'Short-term human prostate primary xenografts: an in vivo model of human prostate

cancer vasculature and angiogenesis', *Cancer Res*, vol. 64, no. 5, pp. 1712-21.

Grdina, DJ, Murley, JS, Miller, RC, Mauceri, HJ, Sutton, HG, et al. 2013, 'A survivin-associated adaptive response in radiation therapy', *Cancer Res*, vol. 73, no. 14, pp. 4418-28.

Grdina, DJ, Murley, JS, Miller, RC, Woloschak, GE & Li, JJ 2015, 'NFkappaB and Survivin-Mediated Radio-Adaptive Response', *Radiat Res*, vol. 183, no. 4, pp. 391-7.

Greenberg, NM, DeMayo, F, Finegold, MJ, Medina, D, Tilley, WD, et al. 1995, 'Prostate cancer in a transgenic mouse', *Proc Natl Acad Sci U S A*, vol. 92, no. 8, pp. 3439-43.

Greene, DR, Taylor, SR, Wheeler, TM & Scardino, PT 1991, 'DNA Ploidy by Image Analysis of Individual Foci of Prostate Cancer: A Preliminary Report', *Cancer Research*, vol. 51, no. 15, pp. 4084-4089.

Grivennikov, SI, Greten, FR & Karin, M 2010, 'Immunity, inflammation, and cancer', *Cell*, vol. 140, no. 6, pp. 883-99.

Gu, J, Zhu, S, Li, X, Wu, H, Li, Y, et al. 2014, 'Effect of amifostine in head and neck cancer patients treated with radiotherapy: a systematic review and meta-analysis based on randomized controlled trials', *PLoS One*, vol. 9, no. 5, p. e95968.

Gudkov, SV, Shilyagina, NY, Vodeneev, VA & Zvyagin, AV 2015, 'Targeted Radionuclide Therapy of Human Tumors', *Int J Mol Sci*, vol. 17, no. 1.

Gunn, EJ, Williams, JT, Huynh, DT, Iannotti, MJ, Han, C, et al. 2011, 'The natural products parthenolide and andrographolide exhibit anti-cancer stem cell activity in multiple myeloma', *Leuk Lymphoma*, vol. 52, no. 6, pp. 1085-97.

Gupta, S, Hastak, K, Ahmad, N, Lewin, JS & Mukhtar, H 2001, 'Inhibition of prostate carcinogenesis in TRAMP mice by oral infusion of green tea polyphenols', *Proc Natl Acad Sci U S A*, vol. 98, no. 18, pp. 10350-5.

Gupta, SC, Prasad, S, Reuter, S, Kannappan, R, Yadav, VR, et al. 2010, 'Modification of cysteine 179 of IkappaBalpha kinase by nimbolide leads to down-regulation of NF-kappaB-regulated cell survival and proliferative

proteins and sensitization of tumor cells to chemotherapeutic agents', *J Biol Chem*, vol. 285, no. 46, pp. 35406-17.

Guzman, ML & Jordan, CT 2005, 'Feverfew: weeding out the root of leukaemia', *Expert Opinion on Biological Therapy*, vol. 5, no. 9, pp. 1147-1152.

Guzman, ML, Rossi, RM, Karnischky, L, Li, X, Peterson, DR, et al. 2005, 'The sesquiterpene lactone parthenolide induces apoptosis of human acute myelogenous leukemia stem and progenitor cells', *Blood*, vol. 105, no. 11, pp. 4163-9.

Guzman, ML, Rossi, RM, Neelakantan, S, Li, X, Corbett, CA, et al. 2007, 'An orally bioavailable parthenolide analog selectively eradicates acute myelogenous leukemia stem and progenitor cells', *Blood*, vol. 110, no. 13, pp. 4427-35.

Hackney, JF, Engelman, RW & Good, RA 1992, 'Ethanol calories do not enhance breast cancer in isocalorically fed C3H/Ou mice', *Nutr Cancer*, vol. 18, no. 3, pp. 245-53.

Hallstrom, TM & Laiho, M 2008, 'Genetic changes and DNA damage responses in the prostate', *Prostate*, vol. 68, no. 8, pp. 902-18.

Hallstrom, TMK-a, Jaamaa, S, Monkkonen, M, Peltonen, K, Andersson, LC, et al. 2007, 'Human prostate epithelium lacks Wee1A-mediated DNA damage-induced checkpoint enforcement', *Proceedings of the National Academy of Sciences U.S.A.*, vol. 104, no. 17, pp. 7211-7216.

Hampton, MB & Orrenius, S 1998, 'Redox regulation of apoptotic cell death', *Biofactors*, vol. 8, no. 1-2, pp. 1-5.

Hanahan, D & Weinberg, RA 2000, 'The hallmarks of cancer', *Cell*, vol. 100, no. 1, pp. 57-70.

Hanahan, D & Weinberg, RA 2011, 'Hallmarks of cancer: the next generation', *Cell*, vol. 144, no. 5, pp. 646-74.

Harper, KL, Sosa, MS, Entenberg, D, Hosseini, H, Cheung, JF, et al. 2016, 'Mechanism of early dissemination and metastasis in Her2+ mammary cancer', *Nature*.

Hassane, DC, Sen, S, Minhajuddin, M, Rossi, RM, Corbett, CA, et al. 2010, 'Chemical genomic screening reveals synergism between parthenolide

and inhibitors of the PI-3 kinase and mTOR pathways', *Blood*, vol. 116, no. 26, pp. 5983-5990.

Hay, N 2016, 'Reprogramming glucose metabolism in cancer: can it be exploited for cancer therapy?', *Nat Rev Cancer*, vol. 16, no. 10, pp. 635-49.

Haynes, J, Srivastava, J, Madson, N, Wittmann, T & Barber, DL 2011, 'Dynamic actin remodeling during epithelial-mesenchymal transition depends on increased moesin expression', *Mol Biol Cell*, vol. 22, no. 24, pp. 4750-64.

Hehner, SP, Hofmann, TG, Droge, W & Schmitz, ML 1999, 'The antiinflammatory sesquiterpene lactone parthenolide inhibits NF-kappa B by targeting the I kappa B kinase complex', *J Immunol*, vol. 163, no. 10, pp. 5617-23.

Heidenreich, A, Bastian, PJ, Bellmunt, J, Bolla, M, Joniau, S, et al. 2014, 'EAU Guidelines on Prostate Cancer. Part 1: Screening, Diagnosis, and Local Treatment with Curative Intent-Update 2013', *European Urology*, vol. 65, no. 1, pp. 124-137.

Heinlein, CA & Chang, C 2004, 'Androgen Receptor in Prostate Cancer', *Endocrine Reviews*, vol. 25, no. 2, pp. 276-308.

Hemann, MT & Lowe, SW 2006, 'The p53-Bcl-2 connection', *Cell Death Differ*, vol. 13, no. 8, pp. 1256-9.

Henrique, R, Oliveira, AI, Costa, VL, Baptista, T, Martins, AT, et al. 2013, 'Epigenetic regulation of MDR1 gene through post-translational histone modifications in prostate cancer', *Bmc Genomics*, vol. 14.

Heptinstall, S, Awang, DV, Dawson, BA, Kindack, D, Knight, DW, et al. 1992, 'Parthenolide content and bioactivity of feverfew (Tanacetum parthenium (L.) Schultz-Bip.). Estimation of commercial and authenticated feverfew products', *J Pharm Pharmacol*, vol. 44, no. 5, pp. 391-5.

Herrera, F, Martin, V, Rodriguez-Blanco, J, Garcia-Santos, G, Antolin, I, et al. 2005, 'Intracellular redox state regulation by parthenolide', *Biochemical and Biophysical Research Communications*, vol. 332, no. 2, pp. 321-325.

Hewamana, S, Lin, TT, Jenkins, C, Burnett, AK, Jordan, CT, et al. 2008, 'The novel nuclear factor-kappaB inhibitor LC-1 is equipotent in poor prognostic subsets of chronic lymphocytic leukemia and shows strong synergy with fludarabine', *Clin Cancer Res*, vol. 14, no. 24, pp. 8102-11.

Hicklin, DJ & Ellis, LM 2005, 'Role of the vascular endothelial growth factor pathway in tumor growth and angiogenesis', *J Clin Oncol*, vol. 23, no. 5, pp. 1011-27.

Hida, J, Matsuda, T, Kitaoka, M, Machidera, N, Kubo, R, et al. 1994, 'The role of basement membrane in colorectal cancer invasion and liver metastasis', *Cancer*, vol. 74, no. 2, pp. 592-8.

Hill, DB, Barve, S, Joshi-Barve, S & McClain, C 2000, 'Increased monocyte nuclear factor-kappaB activation and tumor necrosis factor production in alcoholic hepatitis', *J Lab Clin Med*, vol. 135, no. 5, pp. 387-95.

Hoffman, RM, Koyama, T, Fan, KH, Albertsen, PC, Barry, MJ, et al. 2013, 'Mortality after radical prostatectomy or external beam radiotherapy for localized prostate cancer', *J Natl Cancer Inst*, vol. 105, no. 10, pp. 711-8.

Hoimes, CJ & Kelly, WK 2010, 'Redefining hormone resistance in prostate cancer', *Therapeutic Advances in Medical Oncology*, vol. 2, no. 2, pp. 107-123.

Hooker, AM, Bhat, M, Day, TK, Lane, JM, Swinburne, SJ, et al. 2004, 'The linear no-threshold model does not hold for low-dose ionizing radiation', *Radiation Research*, vol. 162, no. 4, pp. 447-52.

Hopkins, TG, Burns, PA & Routledge, MN 2007, 'DNA methylation of GSTP1 as biomarker in diagnosis of prostate cancer', *Urology*, vol. 69, no. 1, pp. 11-16.

Horwitz, EM, Bae, K, Hanks, GE, Porter, A, Grignon, DJ, et al. 2008, 'Ten-year follow-up of radiation therapy oncology group protocol 92-02: A phase III trial of the duration of elective androgen deprivation in locally advanced prostate cancer', *Journal of Clinical Oncology*, vol. 26, no. 15, pp. 2497-2504.

Hosseini, H, Obradovic, MM, Hoffmann, M, Harper, KL, Sosa, MS, et al. 2016, 'Early dissemination seeds metastasis in breast cancer', *Nature*.

Hsiang, CY, Wu, SL, Chen, JC, Lo, HY, Li, CC, et al. 2007, 'Acetaldehyde induces matrix metalloproteinase-9 gene expression via nuclear factor-kappaB and activator protein 1 signaling pathways in human hepatocellular carcinoma cells: Association with the invasive potential', *Toxicol Lett*, vol. 171, no. 1-2, pp. 78-86.

Hsu, CX, Ross, BD, Chrisp, CE, Derrow, SZ, Charles, LG, et al. 1998, 'Longitudinal cohort analysis of lethal prostate cancer progression in transgenic mice', *J Urol*, vol. 160, no. 4, pp. 1500-5.

Hudson, DL 2004, 'Epithelial stem cells in human prostate growth and disease', *Prostate Cancer Prostatic Dis*, vol. 7, no. 3, pp. 188-194.

Hudson, DL, Guy, AT, Fry, P, O'Hare, MJ, Watt, FM, et al. 2001, 'Epithelial Cell Differentiation Pathways in the Human Prostate: Identification of Intermediate Phenotypes by Keratin Expression', *Journal of Histochemistry and Cytochemistry*, vol. 49, no. 2, pp. 271-278.

Humphrey, PA 2004, 'Gleason grading and prognostic factors in carcinoma of the prostate', *Mod Pathol*, vol. 17, no. 3, pp. 292-306.

Hurwitz, AA, Foster, BA, Allison, JP, Greenberg, NM & Kwon, ED 2001, 'The TRAMP mouse as a model for prostate cancer', *Curr Protoc Immunol*, vol. Chapter 20, p. Unit 20 5.

Huss, WJ, Gray, DR, Tavakoli, K, Marmillion, ME, Durham, LE, et al. 2007, 'Origin of androgen-insensitive poorly differentiated tumors in the transgenic adenocarcinoma of mouse prostate model', *Neoplasia (New York, NY)*, vol. 9, no. 11, p. 938.

Huss, WJ, Maddison, LA & Greenberg, NM 2001, 'Autochthonous mouse models for prostate cancer: past, present and future', *Seminars in Cancer Biology*, vol. 11, no. 3, pp. 245-260.

IAEA 2000, *An International Code of Practice for Dosimetry Based on Standards of Absorbed Dose to Water*, International Atomic Energy Agency.

Idris, AI, Libouban, H, Nyangoga, H, Landao-Bassonga, E, Chappard, D, et al. 2009, 'Pharmacologic inhibitors of IκB kinase suppress growth and migration of mammary carcinosarcoma cells in vitro and prevent osteolytic bone metastasis in vivo', *Molecular Cancer Therapeutics*, vol. 8, no. 8, pp. 2339-2347.

Ikenouchi, J, Matsuda, M, Furuse, M & Tsukita, S 2003, 'Regulation of tight junctions during the epithelium-mesenchyme transition: direct repression of the gene expression of claudins/occludin by Snail', *J Cell Sci*, vol. 116, no. Pt 10, pp. 1959-67.

Illidge, T 2011, 'X. When should radiotherapy be used in lymphoma?', *Annals of Oncology*, vol. 22, no. suppl_4, pp. iv57-iv60.

Ito, M, Shibamoto, Y, Ayakawa, S, Tomita, N, Sugie, C, et al. 2007, 'Low-dose whole-body irradiation induced radioadaptive response in C57BL/6 mice', *J Radiat Res*, vol. 48, no. 6, pp. 455-60.

Iwata, T, Schultz, D, Hicks, J, Hubbard, GK, Mutton, LN, et al. 2010, 'MYC Overexpression Induces Prostatic Intraepithelial Neoplasia and Loss of Nkx3.1 in Mouse Luminal Epithelial Cells', *PLoS ONE*, vol. 5, no. 2, p. e9427.

Jain, NK & Kulkarni, SK 1999, 'Antinociceptive and anti-inflammatory effects of Tanacetum parthenium L. extract in mice and rats', *Journal of Ethnopharmacology*, vol. 68, no. 1-3, pp. 251-259.

Jain, RK 2005, 'Normalization of tumor vasculature: An emerging concept in antiangiogenic therapy', *Science*, vol. 307, no. 5706, pp. 58-62.

Jeet, V 2010, 'Modeling prostate cancer: a perspective on transgenic mouse models', *Cancer and Metastasis Reviews*, vol. 29, no. 1, p. 123.

Jenkins, C, Hewamana, S, Gilkes, A, Neelakantan, S, Crooks, P, et al. 2008, 'Nuclear factor-kappaB as a potential therapeutic target for the novel cytotoxic agent LC-1 in acute myeloid leukaemia', *Br J Haematol*, vol. 143, no. 5, pp. 661-71.

Jin, Z & El-Deiry, WS 2005, 'Overview of cell death signaling pathways', *Cancer Biol Ther*, vol. 4, no. 2, pp. 139-63.

Johnson, ES, Kadam, NP, Hylands, DM & Hylands, PJ 1985, 'Efficacy of feverfew as prophylactic treatment of migraine', *Br Med J (Clin Res Ed)*, vol. 291, no. 6495, pp. 569-73.

Juliana, C, Fernandes-Alnemri, T, Wu, JH, Datta, P, Solorzano, L, et al. 2010, 'Anti-inflammatory Compounds Parthenolide and Bay 11-7082 Are Direct Inhibitors of the Inflammasome', *Journal of Biological Chemistry*, vol. 285, no. 13, pp. 9792-9802.

Jung-Hynes, B, Schmit, TL, Reagan-Shaw, SR, Siddiqui, IA, Mukhtar, H, et al. 2011, 'Melatonin, a novel Sirt1 inhibitor, imparts antiproliferative effects against prostate cancer in vitro in culture and in vivo in TRAMP model', *J Pineal Res*, vol. 50, no. 2, pp. 140-9.

Kaijzel, EL, van der Pluijm, G & Lowik, CW 2007, 'Whole-body optical imaging in animal models to assess cancer development and progression', *Clin Cancer Res*, vol. 13, no. 12, pp. 3490-7.

Kamp, DW, Shacter, E & Weitzman, SA 2011, 'Chronic inflammation and cancer: the role of the mitochondria', *Oncology (Williston Park)*, vol. 25, no. 5, pp. 400-10, 413.

Kansanen, E, Kuosmanen, SM, Leinonen, H & Levonen, AL 2013, 'The Keap1-Nrf2 pathway: Mechanisms of activation and dysregulation in cancer', *Redox Biol*, vol. 1, pp. 45-9.

Kaplan-Lefko, PJ, Chen, TM, Ittmann, MM, Barrios, RJ, Ayala, GE, et al. 2003, 'Pathobiology of autochthonous prostate cancer in a pre-clinical transgenic mouse model', *Prostate*, vol. 55, no. 3, pp. 219-37.

Kaplan, RN, Riba, RD, Zacharoulis, S, Bramley, AH, Costa, C, et al. 2005, 'VEGFR1+hematopoietic bone marrow progenitors initiate the premetastatic niche', *Experimental Hematology*, vol. 33, no. 7, pp. 61-61.

Karin, M, Cao, Y, Greten, FR & Li, ZW 2002, 'NF-kappaB in cancer: from innocent bystander to major culprit', *Nat Rev Cancer*, vol. 2, no. 4, pp. 301-10.

Katsuno, Y, Lamouille, S & Derynck, R 2013, 'TGF-beta signaling and epithelial-mesenchymal transition in cancer progression', *Curr Opin Oncol*, vol. 25, no. 1, pp. 76-84.

Kawaguchi, T 2016, 'Organ Preference of Cancer Metastasis and Metastasis-Related Cell Adhesion Molecules Including Carbohydrates', *Cardiovasc Hematol Disord Drug Targets*, vol. 15, no. 3, pp. 164-86.

Kawasaki, BT, Hurt, EM, Kalathur, M, Duhagon, MA, Milner, JA, et al. 2009, 'Effects of the sesquiterpene lactone parthenolide on prostate tumor-initiating cells: An integrated molecular profiling approach', *Prostate*, vol. 69, no. 8, pp. 827-37.

Kelley, LC, Lohmer, LL, Hagedorn, EJ & Sherwood, DR 2014, 'Traversing the basement membrane in vivo: a diversity of strategies', *J Cell Biol*, vol. 204, no. 3, pp. 291-302.

Khandrika, L, Kumar, B, Koul, S, Maroni, P & Koul, HK 2009, 'Oxidative stress in prostate cancer', *Cancer Lett*, vol. 282, no. 2, pp. 125-36.

Kibel, AS, Rosenbaum, E, Kattan, MW, Picus, J, Dreicer, R, et al. 2007, 'Adjuvant weekly docetaxel for patients with high risk prostate cancer after radical prostatectomy: a multi-institutional pilot study', *J Urol*, vol. 177, no. 5, pp. 1777-81.

Killion, JJ & Fidler, IJ 1989, 'Mechanisms of cancer metastasis', *Arzneimittelforschung*, vol. 39, no. 8A, pp. 1031-4.

Kim, IH, Kim, SW, Kim, SH, Lee, SO, Lee, ST, et al. 2012, 'Parthenolide-induced apoptosis of hepatic stellate cells and anti-fibrotic effects in an in vivo rat model', *Exp Mol Med*, vol. 44, no. 7, pp. 448-56.

Kim, SL, Liu, YC, Park, YR, Seo, SY, Kim, SH, et al. 2015, 'Parthenolide enhances sensitivity of colorectal cancer cells to TRAIL by inducing death receptor 5 and promotes TRAIL-induced apoptosis', *Int J Oncol*, vol. 46, no. 3, pp. 1121-30.

Kim, SL, Trang, KT, Kim, SH, Kim, IH, Lee, SO, et al. 2013, 'Synergistic antitumor effect of 5-fluorouracil in combination with parthenolide in human colorectal cancer', *Cancer Lett*.

Kim, SL, Trang, KT, Kim, SH, Kim, IH, Lee, SO, et al. 2012, 'Parthenolide suppresses tumor growth in a xenograft model of colorectal cancer cells by inducing mitochondrial dysfunction and apoptosis', *Int J Oncol*, vol. 41, no. 4, pp. 1547-53.

Kim, YR, Eom, JI, Kim, SJ, Jeung, HK, Cheong, JW, et al. 2010, 'Myeloperoxidase expression as a potential determinant of parthenolide-induced apoptosis in leukemia bulk and leukemia stem cells', *J Pharmacol Exp Ther*, vol. 335, no. 2, pp. 389-400.

Kishi, H, Nakagawa, K, Matsumoto, M, Suga, M, Ando, M, et al. 2001, 'Osmotic shock induces G1 arrest through p53 phosphorylation at Ser33 by activated p38MAPK without phosphorylation at Ser15 and Ser20', *J Biol Chem*, vol. 276, no. 42, pp. 39115-22.

Kishida, Y, Yoshikawa, H & Myoui, A 2007, 'Parthenolide, a natural inhibitor of Nuclear Factor-kappaB, inhibits lung colonization of murine osteosarcoma cells', *Clin Cancer Res*, vol. 13, no. 1, pp. 59-67.

Klatte, T, Patard, JJ, de Martino, M, Bensalah, K, Verhoest, G, et al. 2008, 'Tumor size does not predict risk of metastatic disease or prognosis of small renal cell carcinomas', *J Urol*, vol. 179, no. 5, pp. 1719-26.

Klein, EA, Thompson, IM, Jr., Tangen, CM, Crowley, JJ, Lucia, MS, et al. 2011, 'Vitamin E and the risk of prostate cancer: the Selenium and Vitamin E Cancer Prevention Trial (SELECT)', *JAMA*, vol. 306, no. 14, pp. 1549-56.

Kleinman, HK, Koblinski, J, Lee, S & Engbring, J 2001, 'Role of basement membrane in tumor growth and metastasis', *Surg Oncol Clin N Am*, vol. 10, no. 2, pp. 329-38, ix.

Knight, DW 1995, 'Feverfew: chemistry and biological activity', *Nat Prod Rep*, vol. 12, no. 3, pp. 271-6.

Kolodziej, M 2014, 'Management of biochemically recurrent prostate cancer following local therapy', *Am J Manag Care*, vol. 20, no. 12 Suppl, pp. S273-81.

Komarova, EA, Christov, K, Faerman, AI & Gudkov, AV 2000, 'Different impact of p53 and p21 on the radiation response of mouse tissues', *Oncogene*, vol. 19, no. 33, pp. 3791-8.

Koreckij, T, Nguyen, H, Brown, LG, Yu, EY, Vessella, RL, et al. 2009, 'Dasatinib inhibits the growth of prostate cancer in bone and provides additional protection from osteolysis', *Br J Cancer*, vol. 101, no. 2, pp. 263-8.

Kouvaris, JR, Kouloulias, VE & Vlahos, LJ 2007, 'Amifostine: the first selective-target and broad-spectrum radioprotector', *Oncologist*, vol. 12, no. 6, pp. 738-47.

Koya, MP, Simon, MA & Soloway, MS 2006, 'Complications of intravesical therapy for urothelial cancer of the bladder', *J Urol*, vol. 175, no. 6, pp. 2004-10.

Kreuger, MR, Grootjans, S, Biavatti, MW, Vandenabeele, P & D'Herde, K 2012, 'Sesquiterpene lactones as drugs with multiple targets in cancer treatment: focus on parthenolide', *Anticancer Drugs*, vol. 23, no. 9, pp. 883-96.

Kristiansen, E, Clemmensen, S & Meyer, O 1990, 'Chronic ethanol intake and reduction of lung tumours from urethane in strain A mice', *Food Chem Toxicol*, vol. 28, no. 1, pp. 35-8.

Kroon, J, Kooijman, S, Cho, NJ, Storm, G & van der Pluijm, G 2016, 'Improving Taxane-Based Chemotherapy in Castration-Resistant Prostate Cancer', *Trends Pharmacol Sci*, vol. 37, no. 6, pp. 451-62.

Kwok, BH, Koh, B, Ndubuisi, MI, Elofsson, M & Crews, CM 2001, 'The anti-inflammatory natural product parthenolide from the medicinal herb Feverfew directly binds to and inhibits IkappaB kinase', *Chem Biol*, vol. 8, no. 8, pp. 759-66.

Lakin, ND & Jackson, SP 1999, 'Regulation of p53 in response to DNA damage', *Oncogene*, vol. 18, no. 53, pp. 7644-55.

Lall, R, Ganapathy, S, Yang, M, Xiao, S, Xu, T, et al. 2014, 'Low-dose radiation exposure induces a HIF-1-mediated adaptive and protective metabolic response', *Cell Death Differ*, vol. 21, no. 5, pp. 836-44.

Landen, NX, Li, D & Stahle, M 2016, 'Transition from inflammation to proliferation: a critical step during wound healing', *Cell Mol Life Sci*, vol. 73, no. 20, pp. 3861-85.

Lawrence, MD, Blyth, BJ, Ormsby, RJ, Tilley, WD & Sykes, PJ 2013a, 'False-positive TUNEL staining observed in SV40 based transgenic murine prostate cancer models', *Transgenic Res*, vol. 22, no. 5, pp. 1037-47.

Lawrence, MD, Ormsby, RJ, Blyth, BJ, Bezak, E, England, G, et al. 2013b, 'Lack of high-dose radiation mediated prostate cancer promotion and low-dose radiation adaptive response in the TRAMP mouse model', *Radiat Res*, vol. 180, no. 4, pp. 376-88.

Lee, HY, Cha, MK & Kim, IH 2000, 'Activation of thiol-dependent antioxidant activity of human serum albumin by alkaline pH is due to the B-like conformational change', *Archives of Biochemistry and Biophysics*, vol. 380, no. 2, pp. 309-318.

Lee, JU, Hosotani, R, Wada, M, Doi, R, Kosiba, T, et al. 1999, 'Role of Bcl-2 family proteins (Bax, Bcl-2 and Bcl-X) on cellular susceptibility to radiation in pancreatic cancer cells', *Eur J Cancer*, vol. 35, no. 9, pp. 1374-80.

Lee, LF, Louie, MC, Desai, SJ, Yang, J, Chen, HW, et al. 2004, 'Interleukin-8 confers androgen-independent growth and migration of LNCaP: differential effects of tyrosine kinases Src and FAK', *Oncogene*, vol. 23, no. 12, pp. 2197-205.

Lee, YC, Jin, JK, Cheng, CJ, Huang, CF, Song, JH, et al. 2013, 'Targeting Constitutively Activated beta(1) Integrins Inhibits Prostate Cancer Metastasis', *Molecular Cancer Research*, vol. 11, no. 4, pp. 405-417.

Leibovitz, A, Baumoehl, Y & Segal, R 2004, 'Increased incidence of pathological and clinical prostate cancer with age: age related alterations of local immune surveillance', *The Journal of Urology*, vol. 172, no. 2, pp. 435-437.

Leinonen, HM, Kansanen, E, Polonen, P, Heinaniemi, M & Levonen, AL 2014, 'Role of the Keap1-Nrf2 pathway in cancer', *Adv Cancer Res*, vol. 122, pp. 281-320.

Leman, ES & Getzenberg, RH 2009, 'Biomarkers for Prostate Cancer', *Journal of Cellular Biochemistry*, vol. 108, no. 1, pp. 3-9.

Leong, HS, Robertson, AE, Stoletov, K, Leith, SJ, Chin, CA, et al. 2014, 'Invadopodia are required for cancer cell extravasation and are a therapeutic target for metastasis', *Cell Rep*, vol. 8, no. 5, pp. 1558-70.

Letai, AG 2008, 'Diagnosing and exploiting cancer's addiction to blocks in apoptosis', *Nat Rev Cancer*, vol. 8, no. 2, pp. 121-32.

Levesque, MH, El-Alfy, M, Cusan, L & Labrie, F 2009, 'Androgen receptor as a potential sign of prostate cancer metastasis', *Prostate*, vol. 69, no. 15, pp. 1704-11.

Levitt, NC & Hickson, ID 2002, 'Caretaker tumour suppressor genes that defend genorne integrity', *Trends in Molecular Medicine*, vol. 8, no. 4, pp. 179-186.

Lilyestrom, W, Klein, MG, Zhang, R, Joachimiak, A & Chen, XS 2006, 'Crystal structure of SV40 large T-antigen bound to p53: interplay between a viral oncoprotein and a cellular tumor suppressor', *Genes & Development*, vol. 20, no. 17, pp. 2373-2382.

Lin, D, Wyatt, AW, Xue, H, Wang, Y, Dong, X, et al. 2014, 'High fidelity patient-derived xenografts for accelerating prostate cancer discovery and drug development', *Cancer Res*, vol. 74, no. 4, pp. 1272-83.

Lipinski, MM & Jacks, T 1999, 'The retinoblastoma gene family in differentiation and development', *Oncogene*, vol. 18, no. 55, pp. 7873-82.

Liu, D & Xu, Y 2011, 'p53, oxidative stress, and aging', *Antioxid Redox Signal*, vol. 15, no. 6, pp. 1669-78.

Liu, Y, Lu, WL, Guo, J, Du, J, Li, T, et al. 2008, 'A potential target associated with both cancer and cancer stem cells: a combination therapy for eradication of breast cancer using vinorelbine stealthy liposomes plus parthenolide stealthy liposomes', *J Control Release*, vol. 129, no. 1, pp. 18-25.

Liu, YN, Liu, Y, Lee, HJ, Hsu, YH & Chen, JH 2008, 'Activated androgen receptor downregulates E-cadherin gene expression and promotes tumor metastasis', *Mol Cell Biol*, vol. 28, no. 23, pp. 7096-108.

Liu, Z, Liu, S, Xie, Z, Pavlovicz, RE, Wu, J, et al. 2009, 'Modulation of DNA methylation by a sesquiterpene lactone parthenolide', *J Pharmacol Exp Ther*, vol. 329, no. 2, pp. 505-14.

Livingston, M & Dietze, P 2016, 'National survey data can be used to measure trends in population alcohol consumption in Australia', *Aust N Z J Public Health*, vol. 40, no. 3, pp. 233-5.

Lizee, G, Radvanyi, LG, Overwijk, WW & Hwu, P 2006, 'Immunosuppression in melanoma immunotherapy: potential opportunities for intervention', *Clin Cancer Res*, vol. 12, no. 7 Pt 2, pp. 2359s-2365s.

Lo, HW, Hsu, SC, Xia, W, Cao, X, Shih, JY, et al. 2007, 'Epidermal growth factor receptor cooperates with signal transducer and activator of transcription 3 to induce epithelial-mesenchymal transition in cancer cells via up-regulation of TWIST gene expression', *Cancer Res*, vol. 67, no. 19, pp. 9066-76.

Lokeshwar, BL 1999, 'MMP inhibition in prostate cancer', *Ann N Y Acad Sci*, vol. 878, pp. 271-89.

Long, RM, Morrissey, C, Fitzpatrick, JM & Watson, RW 2005, 'Prostate epithelial cell differentiation and its relevance to the understanding of prostate cancer therapies', *Clin Sci (Lond)*, vol. 108, no. 1, pp. 1-11.

Lucas, PC, McAllister-Lucas, LM & Nunez, G 2004, 'NF-kappaB signaling in lymphocytes: a new cast of characters', *J Cell Sci*, vol. 117, no. Pt 1, pp. 31-9.

Mantovani, A, Allavena, P, Sica, A & Balkwill, F 2008, 'Cancer-related inflammation', *Nature*, vol. 454, no. 7203, pp. 436-44.

Mariotto, AB, Yabroff, KR, Shao, Y, Feuer, EJ & Brown, ML 2011, 'Projections of the cost of cancer care in the United States: 2010-2020', *J Natl Cancer Inst*, vol. 103, no. 2, pp. 117-28.

Marks, LB, Carroll, PR, Dugan, TC & Anscher, MS 1995, 'The Response of the Urinary-Bladder, Urethra, and Ureter to Radiation and Chemotherapy', *International Journal of Radiation Oncology Biology Physics*, vol. 31, no. 5, pp. 1257-1280.

Marles, RJ, Pazossanou, L, Compadre, CM, Pezzuto, JM, Bloszyk, E, et al. 1995, 'Sesquiterpene lactones revisited - Recent developments in the assessment of biological activities and structure relationships', *Phytochemistry of Medicinal Plants*, vol. 29, pp. 333-356.

Maroulakou, IG, Anver, M, Garrett, L & Green, JE 1994, 'Prostate and mammary adenocarcinoma in transgenic mice carrying a rat C3 (1) simian virus 40 large tumor antigen fusion gene', *Proceedings of the National Academy of Sciences of the United States of America*, vol. 91, no. 23, p. 11236.

Marshall, DT, Ramey, S, Golshayan, AR, Keane, TE, Kraft, AS, et al. 2014, 'Phase I trial of weekly docetaxel, total androgen blockade, and image-guided intensity-modulated radiotherapy for localized high-risk prostate adenocarcinoma', *Clin Genitourin Cancer*, vol. 12, no. 2, pp. 80-6.

Mathema, VB, Koh, YS, Thakuri, BC & Sillanpaa, M 2012, 'Parthenolide, a sesquiterpene lactone, expresses multiple anti-cancer and anti-inflammatory activities', *Inflammation*, vol. 35, no. 2, pp. 560-5.

Mazaris, E & Tsiotras, A 2013, 'Molecular pathways in prostate cancer', *Nephrourol Mon*, vol. 5, no. 3, pp. 792-800.

McConnell, JD, Bruskewitz, R, Walsh, P, Andriole, G, Lieber, M, et al. 1998, 'The effect of finasteride on the risk of acute urinary retention and the need for surgical treatment among men with benign prostatic hyperplasia. Finasteride Long-Term Efficacy and Safety Study Group', *N Engl J Med*, vol. 338, no. 9, pp. 557-63.

McNeal, JE 1968, 'Regional morphology and pathology of the prostate', *American journal of clinical pathology*, vol. 49, no. 3, pp. 347-357.

McNeal, JE & Bostwick, DG 1986, 'Intraductal dysplasia: A premalignant lesion of the prostate', *Human Pathology*, vol. 17, no. 1, pp. 64-71.

McNeal, JE, Redwine, EA, Freiha, FS & Stamey, TA 1988, 'Zonal distribution of prostatic adenocarcinoma. Correlation with histologic pattern and direction of spread', *Am J Surg Pathol*, vol. 12, no. 12, pp. 897-906.

Meadows, GG & Zhang, H 2015, 'Effects of Alcohol on Tumor Growth, Metastasis, Immune Response, and Host Survival', *Alcohol Res*, vol. 37, no. 2, pp. 311-22.

Mendes, O, Kim, HT, Lungu, G & Stoica, G 2007, 'MMP2 role in breast cancer brain metastasis development and its regulation by TIMP2 and ERK1/2', *Clin Exp Metastasis*, vol. 24, no. 5, pp. 341-51.

Mendes, O, Kim, HT & Stoica, G 2005, 'Expression of MMP2, MMP9 and MMP3 in breast cancer brain metastasis in a rat model', *Clin Exp Metastasis*, vol. 22, no. 3, pp. 237-46.

Mendonca, MS, Chin-Sinex, H, Gomez-Millan, J, Datzman, N, Hardacre, M, et al. 2007, 'Parthenolide sensitizes cells to X-ray-induced cell killing through inhibition of NF-κB and split-dose repair', *Radiation Research*, vol. 168, no. 6, pp. 689-697.

Meyer, T & Vinkemeier, U 2007, 'STAT nuclear translocation: potential for pharmacological intervention', *Expert Opinion on Therapeutic Targets*, vol. 11, no. 10, pp. 1355-1365.

Miller, GJ & Cygan, JM 1994, 'Morphology of prostate cancer: the effects of multifocality on histological grade, tumor volume and capsule penetration', *J Urol*, vol. 152, no. 5 Pt 2, pp. 1709-13.

Mitchel, RE, Dolling, JA, Misonoh, J & Boreham, DR 2002, 'Influence of prior exposure to low-dose adapting radiation on radiation-induced teratogenic effects in fetal mice with varying Trp53 function', *Radiat Res*, vol. 158, no. 4, pp. 458-63.

Mitchel, RE, Jackson, JS, Morrison, DP & Carlisle, SM 2003, 'Low doses of radiation increase the latency of spontaneous lymphomas and spinal osteosarcomas in cancer-prone, radiation-sensitive Trp53 heterozygous mice', *Radiat Res*, vol. 159, no. 3, pp. 320-7.

Moding, EJ, Kastan, MB & Kirsch, DG 2013, 'Strategies for optimizing the response of cancer and normal tissues to radiation', *Nat Rev Drug Discov*, vol. 12, no. 7, pp. 526-42.

Molina, PE, Happel, KI, Zhang, P, Kolls, JK & Nelson, S 2010, 'Focus on: Alcohol and the immune system', *Alcohol Res Health*, vol. 33, no. 1-2, pp. 97-108.

Moroz, A, Delella, FK, Lacorte, LM, Deffune, E & Felisbino, SL 2013, 'Fibronectin induces MMP2 expression in human prostate cancer cells', *Biochemical and Biophysical Research Communications*, vol. 430, no. 4, pp. 1319-1321.

Mosesson, Y, Mills, GB & Yarden, Y 2008, 'Derailed endocytosis: an emerging feature of cancer', *Nat Rev Cancer*, vol. 8, no. 11, pp. 835-50.

Motzer, RJ, Mazumdar, M, Bacik, J, Berg, W, Amsterdam, A, et al. 1999, 'Survival and prognostic stratification of 670 patients with advanced renal cell carcinoma', *J Clin Oncol*, vol. 17, no. 8, pp. 2530-40.

Msaouel, P, Pissimissis, N, Halapas, A & Koutsilieris, M 2008, 'Mechanisms of bone metastasis in prostate cancer: clinical implications', *Best Pract Res Clin Endocrinol Metab*, vol. 22, no. 2, pp. 341-55.

Murphy, JJ, Heptinstall, S & Mitchell, JR 1988, 'Randomised double-blind placebo-controlled trial of feverfew in migraine prevention', *Lancet*, vol. 2, no. 8604, pp. 189-92.

Murray, NP, Reyes, E, Tapia, P, Badinez, L & Orellana, N 2012, 'Differential expression of matrix metalloproteinase-2 expression in disseminated tumor cells and micrometastasis in bone marrow of patients with nonmetastatic and metastatic prostate cancer: theoretical considerations and clinical implications-an immunocytochemical study', *Bone Marrow Res*, vol. 2012, p. 259351.

Murugan, S, Zhang, C, Mojtahedzadeh, S & Sarkar, DK 2013, 'Alcohol exposure in utero increases susceptibility to prostate tumorigenesis in rat offspring', *Alcohol Clin Exp Res*, vol. 37, no. 11, pp. 1901-9.

Nagy, JA, Chang, SH, Dvorak, AM & Dvorak, HF 2009, 'Why are tumour blood vessels abnormal and why is it important to know?', *British Journal of Cancer*, vol. 100, no. 6, pp. 865-869.

Nakabayashi, H & Shimizu, K 2012, 'Involvement of Akt/NF-kappaB pathway in antitumor effects of parthenolide on glioblastoma cells in vitro and in vivo', *BMC Cancer*, vol. 12, no. 1, p. 453.

Nakshatri, H, Rice, SE & Bhat-Nakshatri, P 2004, 'Antitumor agent parthenolide reverses resistance of breast cancer cells to tumor necrosis factor-related apoptosis-inducing ligand through sustained activation of c-Jun N-terminal kinase', *Oncogene*, vol. 23, no. 44, pp. 7330-7344.

Nakshatri, H & Sweeney, CJ 2005, *Use of parthenolide to inhibit cancer*, Google Patents.

Nam, S, Kim, D, Cheng, JQ, Zhang, S, Lee, JH, et al. 2005, 'Action of the Src family kinase inhibitor, dasatinib (BMS-354825), on human prostate cancer cells', *Cancer Res*, vol. 65, no. 20, pp. 9185-9.

Nanji, AA, Jokelainen, K, Rahemtulla, A, Miao, L, Fogt, F, et al. 1999, 'Activation of nuclear factor kappa B and cytokine imbalance in experimental alcoholic liver disease in the rat', *Hepatology*, vol. 30, no. 4, pp. 934-43.

Nasim, S & Crooks, PA 2008, 'Antileukemic activity of aminoparthenolide analogs', *Bioorganic & Medicinal Chemistry Letters*, vol. 18, no. 14, pp. 3870-3873.

Natoli, C, Perrucci, B, Perrotti, F, Falchi, L, Iacobelli, S, et al. 2010, 'Tyrosine Kinase Inhibitors', *Current Cancer Drug Targets*, vol. 10, no. 5, pp. 462-483.

Navone, NM, Logothetis, CJ, von Eschenbach, AC & Troncoso, P 1998, 'Model Systems of Prostate Cancer: Uses and Limitations', *Cancer and Metastasis Reviews*, vol. 17, no. 4, pp. 361-371.

Neelakantan, S, Nasim, S, Guzman, ML, Jordan, CT & Crooks, PA 2009, 'Aminoparthenolides as novel anti-leukemic agents: Discovery of the NF-kappa B inhibitor, DMAPT (LC-1)', *Bioorganic & Medicinal Chemistry Letters*, vol. 19, no. 15, pp. 4346-4349.

Negrini, S, Gorgoulis, VG & Halazonetis, TD 2010, 'Genomic instability--an evolving hallmark of cancer', *Nat Rev Mol Cell Biol*, vol. 11, no. 3, pp. 220-8.

Nelson, WG, De Marzo, AM & Yegnasubramanian, S 2009, 'Epigenetic Alterations in Human Prostate Cancers', *Endocrinology*, vol. 150, no. 9, pp. 3991-4002.

Neville, JA, Welch, E & Leffell, DJ 2007, 'Management of nonmelanoma skin cancer in 2007', *Nat Clin Pract Oncol*, vol. 4, no. 8, pp. 462-9.

Nieto, MA 2013, 'Epithelial plasticity: a common theme in embryonic and cancer cells', *Science*, vol. 342, no. 6159, p. 1234850.

Nilsson, S, Norlen, BJ & Widmark, A 2004, 'A systematic overview of radiation therapy effects in prostate cancer', *Acta Oncol*, vol. 43, no. 4, pp. 316-81.

O'Brien, PC, Franklin, CI, Poulsen, MG, Joseph, DJ, Spry, NS, et al. 2002, 'Acute symptoms, not rectally administered sucralfate, predict for late radiation proctitis: longer term follow-up of a phase III trial--Trans-Tasman Radiation Oncology Group', *Int J Radiat Oncol Biol Phys*, vol. 54, no. 2, pp. 442-9.

Oberley, TD, Zhong, W, Szweda, LI & Oberley, LW 2000, 'Localization of antioxidant enzymes and oxidative damage products in normal and malignant prostate epithelium', *Prostate*, vol. 44, no. 2, pp. 144-55.

Oka, D, Nishimura, K, Shiba, M, Nakai, Y, Arai, Y, et al. 2007, 'Sesquiterpene lactone parthenolide suppresses tumor growth in a xenograft model of renal cell carcinoma by inhibiting the activation of NF-kappaB', *Int J Cancer*, vol. 120, no. 12, pp. 2576-81.

Okazaki, R, Ootsuyama, A & Norimura, T 2007, 'TP53 and TP53-related genes associated with protection from apoptosis in the radioadaptive response', *Radiat Res*, vol. 167, no. 1, pp. 51-7.

Olivieri, G, Bodycote, J & Wolff, S 1984, 'Adaptive response of human lymphocytes to low concentrations of radioactive thymidine', *Science*, vol. 223, no. 4636, pp. 594-7.

Ormsby, RJ, Lawrence, MD, Blyth, BJ, Bexis, K, Bezak, E, et al. 2014, 'Protection from radiation-induced apoptosis by the radioprotector amifostine (WR-2721) is radiation dose dependent', *Cell Biol Toxicol*, vol. 30, no. 1, pp. 55-66.

Oskarsson, T, Batlle, E & Massague, J 2014, 'Metastatic stem cells: sources, niches, and vital pathways', *Cell Stem Cell*, vol. 14, no. 3, pp. 306-21.

Pages, F, Galon, J, Dieu-Nosjean, MC, Tartour, E, Sautes-Fridman, C, et al. 2010, 'Immune infiltration in human tumors: a prognostic factor that should not be ignored', *Oncogene*, vol. 29, no. 8, pp. 1093-102.

Pahl, HL 1999, 'Activators and target genes of Rel/NF-kappaB transcription factors', *Oncogene*, vol. 18, no. 49, pp. 6853-66.

Pajak, B, Orzechowski, A & Gajkowska, B 2008, 'Molecular basis of parthenolide-dependent proapoptotic activity in cancer cells', *Folia Histochemica Et Cytobiologica*, vol. 46, no. 2, pp. 129-135.

Pareek, A, Suthar, M, Rathore, GS & Bansal, V 2011, 'Feverfew (Tanacetum parthenium L.): A systematic review', *Pharmacogn Rev*, vol. 5, no. 9, pp. 103-10.

Parisotto, M & Metzger, D 2013, 'Genetically engineered mouse models of prostate cancer', *Mol Oncol*, vol. 7, no. 2, pp. 190-205.

Park, SI, Zhang, J, Phillips, KA, Araujo, JC, Najjar, AM, et al. 2008, 'Targeting SRC family kinases inhibits growth and lymph node metastases of prostate cancer in an orthotopic nude mouse model', *Cancer Res*, vol. 68, no. 9, pp. 3323-33.

Parks, WC, Wilson, CL & Lopez-Boado, YS 2004, 'Matrix metalloproteinases as modulators of inflammation and innate immunity', *Nature Reviews Immunology*, vol. 4, no. 8, pp. 617-629.

Parsons, SJ & Parsons, JT 2004, 'Src family kinases, key regulators of signal transduction', *Oncogene*, vol. 23, no. 48, pp. 7906-9.

Pedraza-Farina, LG 2006, 'Mechanisms of oncogenic cooperation in cancer initiation and metastasis', *Yale J Biol Med*, vol. 79, no. 3-4, pp. 95-103.

Peese, K 2010, 'New agents for the treatment of leukemia: discovery of DMAPT (LC-1)', *Drug Discovery Today*, vol. 15, no. 7-8, pp. 322-322.

Pesic, M & Greten, FR 2016, 'Inflammation and cancer: tissue regeneration gone awry', *Curr Opin Cell Biol*, vol. 43, pp. 55-61.

Peto, J 2001, 'Cancer epidemiology in the last century and the next decade', *Nature*, vol. 411, no. 6835, pp. 390-395.

Pfaffenrath, V, Diener, HC, Fischer, M, Friede, M & Henneicke-von Zepelin, HH 2002, 'The efficacy and safety of Tanacetum parthenium (feverfew) in migraine prophylaxis--a double-blind, multicentre, randomized placebo-controlled dose-response study', *Cephalalgia*, vol. 22, no. 7, pp. 523-32.

Phan, LM, Yeung, SC & Lee, MH 2014, 'Cancer metabolic reprogramming: importance, main features, and potentials for precise targeted anti-cancer therapies', *Cancer Biol Med*, vol. 11, no. 1, pp. 1-19.

Pilepich, MV, Winter, K, Lawton, CA, Krisch, RE, Wolkov, HB, et al. 2005, 'Androgen suppression adjuvant to definitive radiotherapy in prostate carcinoma - Long-term results of Phase III RTOG 85-31', *International Journal of Radiation Oncology Biology Physics*, vol. 61, no. 5, pp. 1285-1290.

Pinkawa, M, Holy, R, Piroth, MD, Fischedick, K, Schaar, S, et al. 2010, 'Consequential late effects after radiotherapy for prostate cancer - a prospective longitudinal quality of life study', *Radiation Oncology*, vol. 5.

Porta-de-la-Riva, M, Stanisavljevic, J, Curto, J, Franci, C, Diaz, VM, et al. 2011, 'TFCP2c/LSF/LBP-1c is required for Snail1-induced fibronectin gene expression', *Biochem J*, vol. 435, no. 3, pp. 563-8.

Powell, IJ, Bock, CH, Ruterbusch, JJ & Sakr, W 2010, 'Evidence supports a faster growth rate and/or earlier transformation to clinically significant prostate cancer in black than in white American men, and influences racial progression and mortality disparity', *J Urol*, vol. 183, no. 5, pp. 1792-6.

Quintavalle, C, Donnarumma, E, Iaboni, M, Roscigno, G, Garofalo, M, et al. 2013, 'Effect of miR-21 and miR-30b/c on TRAIL-induced apoptosis in glioma cells', *Oncogene*, vol. 32, no. 34, pp. 4001-8.

Raheem, O, Kulidjian, AA, Wu, C, Jeong, YB, Yamaguchi, T, et al. 2011, 'A novel patient-derived intra-femoral xenograft model of bone metastatic prostate cancer that recapitulates mixed osteolytic and osteoblastic lesions', *J Transl Med*, vol. 9, p. 185.

Raina, K, Rajamanickam, S, Singh, RP, Deep, G, Chittezhath, M, et al. 2008, 'Stage-specific inhibitory effects and associated mechanisms of silibinin on tumor progression and metastasis in transgenic adenocarcinoma of the mouse prostate model', *Cancer Res*, vol. 68, no. 16, pp. 6822-30.

Rampling, R, James, A & Papanastassiou, V 2004, 'The present and future management of malignant brain tumours: Surgery, radiotherapy, chemotherapy', *Journal of Neurology Neurosurgery and Psychiatry*, vol. 75, pp. 24-30.

Rayet, B & Gelinas, C 1999, 'Aberrant rel/nfkb genes and activity in human cancer', *Oncogene*, vol. 18, no. 49, pp. 6938-47.

Resnick, MJ, Koyama, T, Fan, KH, Albertsen, PC, Goodman, M, et al. 2013, 'Long-term functional outcomes after treatment for localized prostate cancer', *N Engl J Med*, vol. 368, no. 5, pp. 436-45.

Reuter, S, Gupta, SC, Chaturvedi, MM & Aggarwal, BB 2010, 'Oxidative stress, inflammation, and cancer: how are they linked?', *Free Radic Biol Med*, vol. 49, no. 11, pp. 1603-16.

Reya, T, Morrison, SJ, Clarke, MF & Weissman, IL 2001, 'Stem cells, cancer, and cancer stem cells', *Nature*, vol. 414, no. 6859, pp. 105-111.

Ricciardi, M, Zanotto, M, Malpeli, G, Bassi, G, Perbellini, O, et al. 2015, 'Epithelial-to-mesenchymal transition (EMT) induced by inflammatory priming elicits mesenchymal stromal cell-like immune-modulatory properties in cancer cells', *Br J Cancer*, vol. 112, no. 6, pp. 1067-75.

Riley, T, Sontag, E, Chen, P & Levine, A 2008, 'Transcriptional control of human p53-regulated genes', *Nat Rev Mol Cell Biol*, vol. 9, no. 5, pp. 402-12.

Ringshausen, I, Peschel, C & Decker, T 2006, 'Cell cycle inhibition in malignant lymphoma: disease control by attacking the cellular proliferation machinery', *Curr Drug Targets*, vol. 7, no. 10, pp. 1349-59.

Rogakou, EP, Nieves-Neira, W, Boon, C, Pommier, Y & Bonner, WM 2000, 'Initiation of DNA fragmentation during apoptosis induces phosphorylation of H2AX histone at serine 139', *J Biol Chem*, vol. 275, no. 13, pp. 9390-5.

Roman, J, Ritzenthaler, JD, Bechara, R, Brown, LA & Guidot, D 2005, 'Ethanol stimulates the expression of fibronectin in lung fibroblasts via kinase-dependent signals that activate CREB', *American Journal of Physiology-Lung Cellular and Molecular Physiology*, vol. 288, no. 5, pp. L975-L987.

Rubio-Viqueira, B & Hidalgo, M 2009, 'Direct in vivo xenograft tumor model for predicting chemotherapeutic drug response in cancer patients', *Clin Pharmacol Ther*, vol. 85, no. 2, pp. 217-21.

Saha, S, Woodbine, L, Haines, J, Coster, M, Ricket, N, et al. 2014, 'Increased apoptosis and DNA double-strand breaks in the embryonic mouse brain in response to very low-dose X-rays but not 50 Hz magnetic fields', *J R Soc Interface*, vol. 11, no. 100, p. 20140783.

Sakr, WA, Grignon, DJ, Haas, GP, Heilbrun, LK, Pontes, JE, et al. 1996, 'Age and racial distribution of prostatic intraepithelial neoplasia', *Eur Urol*, vol. 30, no. 2, pp. 138-44.

Sakr, WA, Haas, GP, Cassin, BF, Pontes, JE & Crissman, JD 1993, 'The frequency of carcinoma and intraepithelial neoplasia of the prostate in young male patients', *J Urol*, vol. 150, no. 2 Pt 1, pp. 379-85.

Sakurai, T & Kudo, M 2011, 'Signaling pathways governing tumor angiogenesis', *Oncology*, vol. 81 Suppl 1, pp. 24-9.

Salisbury, CM & Cravatt, BF 2008, 'Optimization of activity-based probes for proteomic profiling of histone deacetylase complexes', *J Am Chem Soc*, vol. 130, no. 7, pp. 2184-94.

Sanda, MG, Dunn, RL, Michalski, J, Sandler, HM, Northouse, L, et al. 2008, 'Quality of life and satisfaction with outcome among prostate-cancer survivors', *N Engl J Med*, vol. 358, no. 12, pp. 1250-61.

Sandhu, GS, Nepple, KG, Tanagho, YS & Andriole, GL 2013, 'Prostate cancer chemoprevention', *Semin Oncol*, vol. 40, no. 3, pp. 276-85.

Sankaranarayanan, K & Chakraborty, R 1995, 'Cancer predisposition, radiosensitivity and the risk of radiation-induced cancers. I. Background', *Radiat Res*, vol. 143, no. 2, pp. 121-43.

Sarkar, DK 2015, 'Fetal alcohol exposure increases susceptibility to carcinogenesis and promotes tumor progression in prostate gland', *Adv Exp Med Biol*, vol. 815, pp. 389-402.

Schaffert, CS, Sorrell, MF & Tuma, DJ 2001, 'Expression and cytoskeletal association of integrin subunits is selectively increased in rat perivenous hepatocytes after chronic ethanol administration', *Alcohol Clin Exp Res*, vol. 25, no. 12, pp. 1749-57.

Schalken, JA & van Leenders, G 2003, 'Cellular and molecular biology of the prostate: stem cell biology', *Urology*, vol. 62, no. 5 Suppl 1, pp. 11-20.

Schatton, T, Murphy, GF, Frank, NY, Yamaura, K, Waaga-Gasser, AM, et al. 2008, 'Identification of cells initiating human melanomas', *Nature*, vol. 451, no. 7176, pp. 345-349.

Schneider-Stock, R, Ghantous, A, Bajbouj, K, Saikali, M & Darwiche, N 2012, 'Epigenetic mechanisms of plant-derived anticancer drugs', *Front Biosci*, vol. 17, pp. 129-73.

Schoonen, WM, Salinas, CA, Kiemeney, LA & Stanford, JL 2005, 'Alcohol consumption and risk of prostate cancer in middle-aged men', *Int J Cancer*, vol. 113, no. 1, pp. 133-40.

Schrecengost, R & Knudsen, KE 2013, 'Molecular Pathogenesis and Progression of Prostate Cancer', *Seminars in Oncology*, vol. 40, no. 3, pp. 244-258.

Sen, R 2006, 'Control of B lymphocyte apoptosis by the transcription factor NF-kappaB', *Immunity*, vol. 25, no. 6, pp. 871-83.

Shafik, A, Shafik, AA, El Sibai, O & Shafik, IA 2006, 'Contractile activity of the prostate at ejaculation: An electrophysiologic study', *Urology*, vol. 67, no. 4, pp. 793-796.

Shanmugam, R, Jayaprakasan, V, Gokmen-Polar, Y, Kelich, S, Miller, KD, et al. 2006, 'Restoring chemotherapy and hormone therapy sensitivity by parthenolide in a xenograft hormone refractory prostate cancer model', *Prostate*, vol. 66, no. 14, pp. 1498-511.

Shanmugam, R, Kusumanchi, P, Appaiah, H, Cheng, L, Crooks, P, et al. 2011, 'A water soluble parthenolide analog suppresses in vivo tumor growth of two tobacco-associated cancers, lung and bladder cancer, by targeting NF-kappaB and generating reactive oxygen species', *Int J Cancer*, vol. 128, no. 10, pp. 2481-94.

Shanmugam, R, Kusumanchi, P, Cheng, L, Crooks, P, Neelakantan, S, et al. 2010, 'A water-soluble parthenolide analogue suppresses in vivo prostate cancer growth by targeting NFkappaB and generating reactive oxygen species', *Prostate*, vol. 70, no. 10, pp. 1074-86.

Shappell, SB, Thomas, GV, Roberts, RL, Herbert, R, Ittmann, MM, et al. 2004, 'Prostate Pathology of Genetically Engineered Mice: Definitions and Classification. The Consensus Report from the Bar Harbor Meeting of the Mouse Models of Human Cancer Consortium Prostate Pathology Committee', *Cancer Research*, vol. 64, no. 6, pp. 2270-2305.

Shaverdashvili, K, Wong, P, Ma, J, Zhang, K, Osman, I, et al. 2014, 'MT1-MMP modulates melanoma cell dissemination and metastasis through activation of MMP2 and RAC1', *Pigment Cell Melanoma Res*, vol. 27, no. 2, pp. 287-96.

Shay, G, Lynch, CC & Fingleton, B 2015, 'Moving targets: Emerging roles for MMPs in cancer progression and metastasis', *Matrix Biol*, vol. 44-46, pp. 200-6.

Sheen-Chen, SM, Huang, CC, Tang, RP, Yang, CH, Chou, FF, et al. 2007, 'Signal transducer and activator of transcription 1 in breast cancer: Analysis with tissue microarray', *Anticancer Research*, vol. 27, no. 4B, pp. 2481-2486.

Shekhar, MP, Pauley, R & Heppner, G 2003, 'Host microenvironment in breast cancer development: extracellular matrix-stromal cell contribution to neoplastic phenotype of epithelial cells in the breast', *Breast Cancer Res*, vol. 5, no. 3, pp. 130-5.

Shelley, M, Harrison, C, Coles, B, Stafforth, J, Wilt, T, et al. 2008, 'Chemotherapy for hormone-refractory prostate cancer', *The Cochrane Library*, vol. 4.

Sherr, CJ 2004, 'Principles of tumor suppression', *Cell*, vol. 116, no. 2, pp. 235-46.

Sherr, CJ & McCormick, F 2002, 'The RB and p53 pathways in cancer', *Cancer Cell*, vol. 2, no. 2, pp. 103-12.

Siedle, B, Garcia-Pineres, AJ, Murillo, R, Schulte-Monting, J, Castro, V, et al. 2004, 'Quantitative structure - Activity relationship of sesquiterpene lactones as inhibitors of the transcription factor NF-kappa B', *Journal of Medicinal Chemistry*, vol. 47, no. 24, pp. 6042-6054.

Siegel, RL, Miller, KD & Jemal, A 2016, 'Cancer statistics, 2016', *CA Cancer J Clin*, vol. 66, no. 1, pp. 7-30.

Simonsson, M, Qvarnstrom, F, Nyman, J, Johansson, KA, Garmo, H, et al. 2008, 'Low-dose hypersensitive gammaH2AX response and infrequent

apoptosis in epidermis from radiotherapy patients', *Radiother Oncol*, vol. 88, no. 3, pp. 388-97.

Singh, RP, Raina, K, Sharma, G & Agarwal, R 2008, 'Silibinin inhibits established prostate tumor growth, progression, invasion, and metastasis and suppresses tumor angiogenesis and epithelial-mesenchymal transition in transgenic adenocarcinoma of the mouse prostate model mice', *Clin Cancer Res*, vol. 14, no. 23, pp. 7773-80.

Slack-Davis, JK, Hershey, ED, Theodorescu, D, Frierson, HF & Parsons, JT 2009, 'Differential requirement for focal adhesion kinase signaling in cancer progression in the transgenic adenocarcinoma of mouse prostate model', *Molecular Cancer Therapeutics*.

Smaldone, MC, Kutikov, A, Egleston, BL, Canter, DJ, Viterbo, R, et al. 2012, 'Small renal masses progressing to metastases under active surveillance', *Cancer*, vol. 118, no. 4, pp. 997-1006.

Smith, DP, King, MT, Egger, S, Berry, MP, Stricker, PD, et al. 2009, 'Quality of life three years after diagnosis of localised prostate cancer: population based cohort study', *British Medical Journal*, vol. 339.

Sobel, RE & Sadar, MD 2005, 'CELL LINES USED IN PROSTATE CANCER RESEARCH: A COMPENDIUM OF OLD AND NEW LINES--PART 1', *The Journal of Urology*, vol. 173, no. 2, pp. 342-359.

Sobota, R, Szwed, M, Kasza, A, Bugno, M & Kordula, T 2000, 'Parthenolide inhibits activation of signal transducers and activators of transcription (STATs) induced by cytokines of the IL-6 family', *Biochemical and Biophysical Research Communications*, vol. 267, no. 1, pp. 329-333.

Sohma, I, Fujiwara, Y, Sugita, Y, Yoshioka, A, Shirakawa, M, et al. 2011, 'Parthenolide, an NF-kappaB inhibitor, suppresses tumor growth and enhances response to chemotherapy in gastric cancer', *Cancer Genomics Proteomics*, vol. 8, no. 1, pp. 39-47.

Song, JM, Qian, X, Upadhyayya, P, Hong, KH & Kassie, F 2014, 'Dimethylaminoparthenolide, a water soluble parthenolide, suppresses lung tumorigenesis through down-regulating the STAT3 signaling pathway', *Curr Cancer Drug Targets*, vol. 14, no. 1, pp. 59-69.

Sosa, MS, Bragado, P & Aguirre-Ghiso, JA 2014, 'Mechanisms of disseminated cancer cell dormancy: an awakening field', *Nat Rev Cancer*, vol. 14, no. 9, pp. 611-22.

Sottnik, JL, Dalgnault-Newton, S, Zhang, XT, Colm, M, Hussain, MH, et al. 2013, 'Integrin alpha2beta1 (alpha 2 beta 1) promotes prostate cancer skeletal metastasis', *Cancer Research*, vol. 73.

Spagnuolo, PA, Hurren, R, Gronda, M, MacLean, N, Datti, A, et al. 2013, 'Inhibition of intracellular dipeptidyl peptidases 8 and 9 enhances parthenolide's anti-leukemic activity', *Leukemia*, vol. 27, no. 6, pp. 1236-1244.

Stamatiou, K, Alevizos, A, Agapitos, E & Sofras, F 2006, 'Incidence of impalpable carcinoma of the prostate and of non-malignant and precarcinomatous lesions in Greek male population: an autopsy study', *Prostate*, vol. 66, no. 12, pp. 1319-28.

Standring, S 2008, *Gray's Anatomy: The Anatomical Basis of Clinical Practice*, 40 edn, Churchill Livingstone.

Staudt, LM 2010, 'Oncogenic activation of NF-kappaB', *Cold Spring Harb Perspect Biol*, vol. 2, no. 6, p. a000109.

Steeg, PS 2016, 'Targeting metastasis', *Nat Rev Cancer*, vol. 16, no. 4, pp. 201-18.

Steele, AJ, Jones, DT, Ganeshaguru, K, Duke, VM, Yogashangary, BC, et al. 2006, 'The sesquiterpene lactone parthenolide induces selective apoptosis of B-chronic lymphocytic leukemia cells in vitro', *Leukemia*, vol. 20, no. 6, pp. 1073-1079.

Sterzing, F, Engenhart-Cabillic, R, Flentje, M & Debus, J 2011, 'Image-guided radiotherapy: a new dimension in radiation oncology', *Dtsch Arztebl Int*, vol. 108, no. 16, pp. 274-80.

Stewart, B & Wild, CP 2014, *World Cancer Report 2014*, International Agency for Research on Cancer, WHO.

Still, K, Robson, CN, Autzen, P, Robinson, MC & Hamdy, FC 2000, 'Localization and quantification of mRNA for matrix metalloproteinase-2 (MMP-2) and tissue inhibitor of matrix metalloproteinase-2 (TIMP-2) in human benign and malignant prostatic tissue', *Prostate*, vol. 42, no. 1, pp. 18-25.

Stone, CA, May, FW, Pinnock, CB, Elwood, M & Rowett, DS 2005, 'Prostate cancer, the PSA test and academic detailing in Australian general practice: an economic evaluation', *Aust N Z J Public Health*, vol. 29, no. 4, pp. 349-57.

Strom, TJ, Hutchinson, SZ, Shrinath, K, Cruz, AA, Figura, NB, et al. 2014, 'External beam radiation therapy and a low-dose-rate brachytherapy boost without or with androgen deprivation therapy for prostate cancer', *Int Braz J Urol*, vol. 40, no. 4, pp. 474-83.

Summy, JM & Gallick, GE 2003, 'Src family kinases in tumor progression and metastasis', *Cancer Metastasis Rev*, vol. 22, no. 4, pp. 337-58.

Sun, Y, St Clair, DK, Fang, F, Warren, GW, Rangnekar, VM, et al. 2007, 'The radiosensitization effect of parthenolide in prostate cancer cells is mediated by nuclear factor-kappaB inhibition and enhanced by the presence of PTEN', *Mol Cancer Ther*, vol. 6, no. 9, pp. 2477-86.

Sun, Y, St Clair, DK, Xu, Y, Crooks, PA & St Clair, WH 2010, 'A NADPH oxidase-dependent redox signaling pathway mediates the selective radiosensitization effect of parthenolide in prostate cancer cells', *Cancer Res*, vol. 70, no. 7, pp. 2880-90.

Suttie, A, Nyska, A, Haseman, JK, Moser, GJ, Hackett, TR, et al. 2003, 'A grading scheme for the assessment of proliferative lesions of the mouse prostate in the TRAMP model', *Toxicologic Pathology*, vol. 31, no. 1, pp. 31-38.

Sweeney, CJ, Mehrotra, S, Sadaria, MR, Kumar, S, Shortle, NH, et al. 2005, 'The sesquiterpene lactone parthenolide in combination with docetaxel reduces metastasis and improves survival in a xenograft model of breast cancer', *Mol Cancer Ther*, vol. 4, no. 6, pp. 1004-12.

Taguchi, K, Motohashi, H & Yamamoto, M 2011, 'Molecular mechanisms of the Keap1-Nrf2 pathway in stress response and cancer evolution', *Genes Cells*, vol. 16, no. 2, pp. 123-40.

Taguchi, T, Takao, T, Iwasaki, Y, Nishiyama, M, Asaba, K, et al. 2006, 'Suppressive effects of dehydroepiandrosterone and the nuclear factor-kappaB inhibitor parthenolide on corticotroph tumor cell growth and function in vitro and in vivo', *J Endocrinol*, vol. 188, no. 2, pp. 321-31.

Tak, PP & Firestein, GS 2001, 'NF-kappa B: a key role in inflammatory diseases', *Journal of Clinical Investigation*, vol. 107, no. 1, pp. 7-11.

Tam, L, McGlynn, LM, Traynor, P, Mukherjee, R, Bartlett, JMS, et al. 2007, 'Expression levels of the JAK/STAT pathway in the transition from hormone-sensitive to hormone-refractory prostate cancer', *British Journal of Cancer*, vol. 97, no. 3, pp. 378-383.

Tam, NN, Nyska, A, Maronpot, RR, Kissling, G, Lomnitski, L, et al. 2006, 'Differential attenuation of oxidative/nitrosative injuries in early prostatic neoplastic lesions in TRAMP mice by dietary antioxidants', *Prostate*, vol. 66, no. 1, pp. 57-69.

Tanaka, H, Arakawa, H, Yamaguchi, T, Shiraishi, K, Fukuda, S, et al. 2000, 'A ribonucleotide reductase gene involved in a p53-dependent cell-cycle checkpoint for DNA damage', *Nature*, vol. 404, no. 6773, pp. 42-9.

Tanaka, K, Hasegawa, J, Asamitsu, K & Okamoto, T 2005, 'Prevention of the ultraviolet B-mediated skin photoaging by a nuclear factor kappaB inhibitor, parthenolide', *J Pharmacol Exp Ther*, vol. 315, no. 2, pp. 624-30.

Tang, FR & Loke, WK 2015, 'Molecular mechanisms of low dose ionizing radiation-induced hormesis, adaptive responses, radioresistance, bystander effects, and genomic instability', *Int J Radiat Biol*, vol. 91, no. 1, pp. 13-27.

Tapia, PC 2006, 'Sublethal mitochondrial stress with an attendant stoichiometric augmentation of reactive oxygen species may precipitate many of the beneficial alterations in cellular physiology produced by caloric restriction, intermittent fasting, exercise and dietary phytonutrients: "Mitohormesis" for health and vitality', *Medical Hypotheses*, vol. 66, no. 4, pp. 832-843.

Taylor, RA, Toivanen, R & Risbridger, GP 2010, 'Stem cells in prostate cancer: treating the root of the problem', *Endocr Relat Cancer*, vol. 17, no. 4, pp. R273-85.

Teng, MW, Swann, JB, Koebel, CM, Schreiber, RD & Smyth, MJ 2008, 'Immune-mediated dormancy: an equilibrium with cancer', *J Leukoc Biol*, vol. 84, no. 4, pp. 988-93.

Thompson, IM, Goodman, PJ, Tangen, CM, Lucia, MS, Miller, GJ, et al. 2003, 'The influence of finasteride on the development of prostate cancer', *N Engl J Med*, vol. 349, no. 3, pp. 215-24.

Toivanen, R, Frydenberg, M, Murphy, D, Pedersen, J, Ryan, A, et al. 2013, 'A preclinical xenograft model identifies castration-tolerant cancer-repopulating cells in localized prostate tumors', *Sci Transl Med*, vol. 5, no. 187, p. 187ra71.

Twardowski, PW, Beumer, JH, Chen, CS, Kraft, AS, Chatta, GS, et al. 2013, 'A phase II trial of dasatinib in patients with metastatic castration-resistant prostate cancer treated previously with chemotherapy', *Anticancer Drugs*, vol. 24, no. 7, pp. 743-53.

Uchibori, R, Tsukahara, T, Mizuguchi, H, Saga, Y, Urabe, M, et al. 2013, 'NF-kappaB activity regulates mesenchymal stem cell accumulation at tumor sites', *Cancer Res*, vol. 73, no. 1, pp. 364-72.

Vajdic, CM & van Leeuwen, MT 2009, 'Cancer incidence and risk factors after solid organ transplantation', *Int J Cancer*, vol. 125, no. 8, pp. 1747-54.

Valastyan, S & Weinberg, RA 2011, 'Tumor metastasis: molecular insights and evolving paradigms', *Cell*, vol. 147, no. 2, pp. 275-92.

Valent, P, Bonnet, D, De Maria, R, Lapidot, T, Copland, M, et al. 2012, 'Cancer stem cell definitions and terminology: the devil is in the details', *Nature Reviews Cancer*, vol. 12, no. 11, pp. 767-775.

Van Waes, C 2007, 'Nuclear factor-kappaB in development, prevention, and therapy of cancer', *Clin Cancer Res*, vol. 13, no. 4, pp. 1076-82.

Vavrova, J, Marekova-Rezacova, M, Vokurkova, D, Szkanderova, S & Psutka, J 2003, 'Caffeine induces a second wave of apoptosis after low dose-rate gamma radiation of HL-60 cells', *Radiat Environ Biophys*, vol. 42, no. 3, pp. 193-9.

Vegeler, RC, Yip-Schneider, MT, Ralstin, M, Wu, H, Crooks, PA, et al. 2007, 'Effect of celecoxib and novel agent LC-1 in a hamster model of lung cancer', *J Surg Res*, vol. 143, no. 1, pp. 169-76.

Vemana, G, Hamilton, RJ, Andriole, GL & Freedland, SJ 2014, 'Chemoprevention of prostate cancer', *Annu Rev Med*, vol. 65, pp. 111-23.

Venkitaraman, AR 2001, 'Functions of BRCA1 and BRCA2 in the biological response to DNA damage', *J Cell Sci*, vol. 114, no. Pt 20, pp. 3591-8.

Viatour, P, Bentires-Alj, M, Chariot, A, Deregowski, V, de Leval, L, et al. 2003, 'NF-kappa B2/p100 induces Bcl-2 expression', *Leukemia*, vol. 17, no. 7, pp. 1349-56.

Visconti, R & Grieco, D 2009, 'New insights on oxidative stress in cancer', *Curr Opin Drug Discov Devel*, vol. 12, no. 2, pp. 240-5.

Vogel, CL, Cobleigh, MA, Tripathy, D, Gutheil, JC, Harris, LN, et al. 2002, 'Efficacy and safety of trastuzumab as a single agent in first-line treatment of HER2-overexpressing metastatic breast cancer', *Journal of Clinical Oncology*, vol. 20, no. 3, pp. 719-726.

Vogler, BK, Pittler, MH & Ernst, E 1998, 'Feverfew as a preventive treatment for migraine: a systematic review', *Cephalalgia*, vol. 18, no. 10, pp. 704-708.

Wallace, TJ, Torre, T, Grob, M, Yu, J, Avital, I, et al. 2014, 'Current Approaches, Challenges and Future Directions for Monitoring Treatment Response in Prostate Cancer', *J Cancer*, vol. 5, no. 1, pp. 3-24.

Walsh, JH, Karnes, WE, Cuttitta, F & Walker, A 1991, 'Autocrine growth factors and solid tumor malignancy', *West J Med*, vol. 155, no. 2, pp. 152-63.

Wang, CM, Lu, J, Wang, YM, Bai, ST, Wang, YC, et al. 2012, 'Combined effects of FLT3 and NF-kappa B selective inhibitors on acute myeloid leukemia in vivo', *Journal of Biochemical and Molecular Toxicology*, vol. 26, no. 1, pp. 35-43.

Wang, CY, Mayo, MW, Korneluk, RG, Goeddel, DV & Baldwin, AS, Jr. 1998, 'NF-kappaB antiapoptosis: induction of TRAF1 and TRAF2 and c-IAP1 and c-IAP2 to suppress caspase-8 activation', *Science*, vol. 281, no. 5383, pp. 1680-3.

Wang, F, Yang, JL, Yu, KK, Xu, M, Xu, YZ, et al. 2015, 'Activation of the NF-kappaB pathway as a mechanism of alcohol enhanced progression and metastasis of human hepatocellular carcinoma', *Mol Cancer*, vol. 14, p. 10.

Wang, R, Xu, J, Juliette, L, Castilleja, A, Love, J, et al. 2005, 'Three-dimensional co-culture models to study prostate cancer growth, progression, and metastasis to bone', *Semin Cancer Biol*, vol. 15, no. 5, pp. 353-64.

Wang, W, Adachi, M, Zhang, R, Zhou, J & Zhu, D 2009, 'A novel combination therapy with arsenic trioxide and parthenolide against pancreatic cancer cells', *Pancreas*, vol. 38, no. 4, pp. e114-23.

Ward, MC, Tendulkar, RD, Ciezki, JP & Klein, EA 2014, 'Future Directions From Past Experience: A Century of Prostate Radiotherapy', *Clinical Genitourinary Cancer*, vol. 12, no. 1, pp. 13-20.

Waris, G & Ahsan, H 2006, 'Reactive oxygen species: role in the development of cancer and various chronic conditions', *Journal of Carcinogenesis*, vol. 5, pp. 14-14. Available from: PMC.

Watanabe, A, Hoshino, D, Koshikawa, N, Seiki, M, Suzuki, T, et al. 2013, 'Critical role of transient activity of MT1-MMP for ECM degradation in invadopodia', *PLoS Comput Biol*, vol. 9, no. 5, p. e1003086.

Watson, C, Miller, DA, Chin-Sinex, H, Losch, A, Hughes, W, et al. 2009, 'Suppression of NF-κB activity by parthenolide induces x-ray sensitivity through inhibition of split-dose repair in TP53 null prostate cancer Cells', *Radiation Research*, vol. 171, no. 4, pp. 389-396.

WCRF 2007, *Food, Nutrition, Physical Activity, and the Prevention of Cancer: A Global Perspective* American Institute for Cancer Research, Washington, DC.

Webber, MM, Bello, D & Quader, S 1996, 'Immortalized and tumorigenic adult human prostatic epithelial cell lines: Characteristics and applications part I. Cell markers and immortalized nontumorigenic cell lines', *The Prostate*, vol. 29, no. 6, pp. 386-394.

Wei, SC, Fattet, L, Tsai, JH, Guo, Y, Pai, VH, et al. 2015, 'Matrix stiffness drives epithelial-mesenchymal transition and tumour metastasis through a TWIST1-G3BP2 mechanotransduction pathway', *Nat Cell Biol*, vol. 17, no. 5, pp. 678-88.

Weiber, H, Andersson, C, Murne, A, Rannevik, G, Lindstrom, C, et al. 1990, 'Beta microseminoprotein is not a prostate-specific protein. Its identification in mucous glands and secretions', *American Journal of Pathology*, vol. 137, no. 3, pp. 593-603.

Wendell-Smith, C 2000, 'Terminology of the prostate and related structures', *Clin Anat*, vol. 13, no. 3, pp. 207-13.

Wertz, IE & Dixit, VM 2010, 'Regulation of death receptor signaling by the ubiquitin system', *Cell Death Differ*, vol. 17, no. 1, pp. 14-24.

West, NJ, Courtney, ED, Poullis, AP & Leicester, RJ 2009, 'Apoptosis in the colonic crypt, colorectal adenomata, and manipulation by chemoprevention', *Cancer Epidemiol Biomarkers Prev*, vol. 18, no. 6, pp. 1680-7.

Wiedhopf, RM, Young, M, Bianchi, E & Cole, JR 1973, 'Tumor inhibitory agent from Magnolia grandiflora (Magnoliaceae). I. Parthenolide', *J Pharm Sci*, vol. 62, no. 2, p. 345.

Wilt, TJ, MacDonald, R, Rutks, I, Shamliyan, TA, Taylor, BC, et al. 2008, 'Systematic Review: Comparative Effectiveness and Harms of Treatments for Clinically Localized Prostate Cancer', *Annals of Internal Medicine*, vol. 148, no. 6, pp. 435-448.

Winter, SF, Cooper, AB & Greenberg, NM 2003, 'Models of metastatic prostate cancer: a transgenic perspective', *Prostate Cancer Prostatic Dis*, vol. 6, no. 3, pp. 204-211.

Winterbourn, CC & Hampton, MB 2008, 'Thiol chemistry and specificity in redox signaling', *Free Radical Biology and Medicine*, vol. 45, no. 5, pp. 549-561.

Wolf, AMD, Wender, RC, Etzioni, RB, Thompson, IM, D'Amico, AV, et al. 2010, 'American Cancer Society Guideline for the Early Detection of Prostate Cancer: Update 2010', *CA: A Cancer Journal for Clinicians*, vol. 60, no. 2, pp. 70-98.

Won, YK, Ong, CN, Shi, X & Shen, HM 2004, 'Chemopreventive activity of parthenolide against UVB-induced skin cancer and its mechanisms', *Carcinogenesis*, vol. 25, no. 8, pp. 1449-58.

Wood, M, Fudge, K, Mohler, JL, Frost, AR, Garcia, F, et al. 1997, 'In situ hybridization studies of metalloproteinases 2 and 9 and TIMP-1 and TIMP-2 expression in human prostate cancer', *Clin Exp Metastasis*, vol. 15, no. 3, pp. 246-58.

Wozniak, M, Szulawska-Mroczek, A, Hartman, ML, Nejc, D & Czyz, M 2013, 'Parthenolide complements the cell death-inducing activity of doxorubicin in melanoma cells', *Anticancer Research*, vol. 33, no. 8, pp. 3205-3212.

Wu, B, Ricchetti, F, Sanguineti, G, Kazhdan, M, Simari, P, et al. 2009, 'Patient geometry-driven information retrieval for IMRT treatment plan quality control', *Med Phys*, vol. 36, no. 12, pp. 5497-505.

Wu, D, Wu, P, Zhao, L, Huang, L, Zhang, Z, et al. 2015, 'NF-kappaB Expression and Outcomes in Solid Tumors: A Systematic Review and Meta-Analysis', *Medicine (Baltimore)*, vol. 94, no. 40, p. e1687.

Wu, XY, Gong, SC, Roy-Burman, P, Lee, P & Culig, Z 2013, 'Current mouse and cell models in prostate cancer research', *Endocrine-Related Cancer*, vol. 20, no. 4, pp. R155-R170.

Wu, Y, Deng, J, Rychahou, PG, Qiu, S, Evers, BM, et al. 2009, 'Stabilization of snail by NF-kappaB is required for inflammation-induced cell migration and invasion', *Cancer Cell*, vol. 15, no. 5, pp. 416-28.

Xian, XJ, Hakansson, J, Stahlberg, A, Lindblom, P, Betsholtz, C, et al. 2006, 'Pericytes limit tumor cell metastasis', *Journal of Clinical Investigation*, vol. 116, no. 3, pp. 642-651.

Xu, M, Bower, KA, Chen, G, Shi, XL, Dong, Z, et al. 2010, 'Ethanol Enhances the Interaction of Breast Cancer Cells Over-Expressing ErbB2 With Fibronectin', *Alcoholism-Clinical and Experimental Research*, vol. 34, no. 5, pp. 751-760.

Xu, Y, Fang, F, Miriyala, S, Crooks, PA, Oberley, TD, et al. 2013, 'KEAP1 is a redox sensitive target that arbitrates the opposing radiosensitive effects of parthenolide in normal and cancer cells', *Cancer Res*, vol. 73, no. 14, pp. 4406-17.

Yang, J, Mani, SA, Donaher, JL, Ramaswamy, S, Itzykson, RA, et al. 2004, 'Twist, a master regulator of morphogenesis, plays an essential role in tumor metastasis', *Cell*, vol. 117, no. 7, pp. 927-39.

Yang, JC, Bai, L, Yap, S, Gao, AC, Kung, HJ, et al. 2010, 'Effect of the specific Src family kinase inhibitor saracatinib on osteolytic lesions using the PC-3 bone model', *Mol Cancer Ther*, vol. 9, no. 6, pp. 1629-37.

Yang, YL & Li, XM 2000, 'The IAP family: endogenous caspase inhibitors with multiple biological activities', *Cell Res*, vol. 10, no. 3, pp. 169-77.

Yao, T, Linbo, W, Olga, G, Mohammad Afnan, K, DongIk, L, et al. 2009, 'The relationship of neuroendocrine carcinomas to anti-tumor therapies in TRAMP mice', *The Prostate*, vol. 69, no. 16, pp. 1763-1773.

Yeoh, EK, Holloway, RH, Fraser, RJ, Botten, RJ, Di Matteo, AC, et al. 2012, 'Pathophysiology and natural history of anorectal sequelae following radiation therapy for carcinoma of the prostate', *Int J Radiat Oncol Biol Phys*, vol. 84, no. 5, pp. e593-9.

Yeung, KT & Yang, J 2017, 'Epithelial-mesenchymal transition in tumor metastasis', *Mol Oncol*, vol. 11, no. 1, pp. 28-39.

Yip-Schneider, MT, Wu, H, Hruban, RH, Lowy, AM, Crooks, PA, et al. 2013a, 'Efficacy of dimethylaminoparthenolide and sulindac in combination with gemcitabine in a genetically engineered mouse model of pancreatic cancer', *Pancreas*, vol. 42, no. 1, pp. 160-7.

Yip-Schneider, MT, Wu, H, Njoku, V, Ralstin, M, Holcomb, B, et al. 2008, 'Effect of celecoxib and the novel anti-cancer agent, dimethylamino-parthenolide, in a developmental model of pancreatic cancer', *Pancreas*, vol. 37, no. 3, pp. e45-53.

Yip-Schneider, MT, Wu, H, Stantz, K, Agaram, N, Crooks, PA, et al. 2013b, 'Dimethylaminoparthenolide and gemcitabine: a survival study using a genetically engineered mouse model of pancreatic cancer', *BMC Cancer*, vol. 13, p. 194.

Yoshimura, K & Uemura, H 2013, 'Role of vaccine therapy for renal cell carcinoma in the era of targeted therapy', *Int J Urol*, vol. 20, no. 8, pp. 744-55.

Yu, EY, Massard, C, Gross, ME, Carducci, MA, Culine, S, et al. 2011, 'Once-daily dasatinib: expansion of phase II study evaluating safety and efficacy of dasatinib in patients with metastatic castration-resistant prostate cancer', *Urology*, vol. 77, no. 5, pp. 1166-71.

Yu, EY, Wilding, G, Posadas, E, Gross, M, Culine, S, et al. 2009, 'Phase II study of dasatinib in patients with metastatic castration-resistant prostate cancer', *Clin Cancer Res*, vol. 15, no. 23, pp. 7421-8.

Yu, H, Liu, N & Ju, B 2010, 'Low dose radiation induced adaptive response of apoptosis in mouse spleen cells', *The Chinese-German Journal of Clinical Oncology*, vol. 9, no. 4, pp. 235-238.

Yucel, B, Akkas, EA, Okur, Y, Eren, AA, Eren, MF, et al. 2014, 'The impact of radiotherapy on quality of life for cancer patients: a longitudinal study', *Supportive Care in Cancer*, vol. 22, no. 9, pp. 2479-2487.

Zariwala, MB, Lalitha, VS & Bhide, SV 1991, 'Carcinogenic potential of Indian alcoholic beverage (country liquor)', *Indian J Exp Biol*, vol. 29, no. 8, pp. 738-43.

Zelefsky, MJ, Leibel, SA, Gaudin, PB, Kutcher, GJ, Fleshner, NE, et al. 1998, 'Dose escalation with three-dimensional conformal radiation therapy affects the outcome in prostate cancer', *Int J Radiat Oncol Biol Phys*, vol. 41, no. 3, pp. 491-500.

Zhang, D, Qiu, L, Jin, X, Guo, Z & Guo, C 2009, 'Nuclear factor-kappaB inhibition by parthenolide potentiates the efficacy of Taxol in non-small cell lung cancer in vitro and in vivo', *Mol Cancer Res*, vol. 7, no. 7, pp. 1139-49.

Zhang, S, Won, YK, Ong, CN & Shen, HM 2005, 'Anti-cancer potential of sesquiterpene lactones: bioactivity and molecular mechanisms', *Curr Med Chem Anticancer Agents*, vol. 5, no. 3, pp. 239-49.

Zhang, SY, Ong, CN & Shen, HM 2004, 'Involvement of proapoptotic Bcl-2 family members in parthenolide-induced mitochondrial dysfunction and apoptosis', *Cancer Letters*, vol. 211, no. 2, pp. 175-188.

Zhao, LJ, Xu, YH & Li, Y 2009, 'Effect of parthenolide on proliferation and apoptosis in gastric cancer cell line SGC7901', *Journal of Digestive Diseases*, vol. 10, no. 3, pp. 172-180.

Zhou, J, Zhang, H, Gu, P, Bai, J, Margolick, JB, et al. 2008, 'NF-kappaB pathway inhibitors preferentially inhibit breast cancer stem-like cells', *Breast Cancer Res Treat*, vol. 111, no. 3, pp. 419-27.

Zhou, J & Zhang, Y 2008, 'Cancer stem cells: Models, mechanisms and implications for improved treatment', *Cell Cycle*, vol. 7, no. 10, pp. 1360-1370.

Zhou, Z, Flesken-Nikitin, A & Nikitin, AY 2007, 'Prostate Cancer Associated with p53 and Rb Deficiency Arises from the Stem/Progenitor Cell-Enriched Proximal Region of Prostatic Ducts', *Cancer Research*, vol. 67, no. 12, pp. 5683-5690.

Zietman, AL, DeSilvio, ML, Slater, JD, Rossi, CJ, Jr., Miller, DW, et al. 2005, 'Comparison of conventional-dose vs high-dose conformal radiation therapy in clinically localized adenocarcinoma of the prostate: a randomized controlled trial', *JAMA*, vol. 294, no. 10, pp. 1233-9.

Zunino, SJ, Ducore, JM & Storms, DH 2007, 'Parthenolide induces significant apoptosis and production of reactive oxygen species in high-risk pre-B leukemia cells', *Cancer Letters*, vol. 254, no. 1, pp. 119-127.